



Calhoun: The NPS Institutional Archive
DSpace Repository

Theses and Dissertations

1. Thesis and Dissertation Collection, all items

1975-06

Hybrid mode analysis of coplanar transmission lines

Kuchler, Klaus-Dieter

Monterey, California. Naval Postgraduate School

<http://hdl.handle.net/10945/26579>

Copyright is reserved by the copyright owner

Downloaded from NPS Archive: Calhoun



Calhoun is the Naval Postgraduate School's public access digital repository for research materials and institutional publications created by the NPS community. Calhoun is named for Professor of Mathematics Guy K. Calhoun, NPS's first appointed -- and published -- scholarly author.

Dudley Knox Library / Naval Postgraduate School
411 Dyer Road / 1 University Circle
Monterey, California USA 93943

<http://www.nps.edu/library>

HYBRID MODE ANALYSIS
OF COPLANAR TRANSMISSION LINES

Klaus-Dieter Kuchler

NAVAL POSTGRADUATE SCHOOL

Monterey, California



THESIS

HYBRID MODE ANALYSIS
OF COPLANAR TRANSMISSION LINES

by

Klaus-Dieter Kuchler

June 1975

Thesis Advisor:

J. B. Knorr

Approved for public release; distribution unlimited.

T168328

REPORT DOCUMENTATION PAGE		READ INSTRUCTIONS BEFORE COMPLETING FORM
1. REPORT NUMBER	2. GOVT ACCESSION NO.	3. RECIPIENT'S CATALOG NUMBER
4. TITLE (and Subtitle) Hybrid Mode Analysis of Coplanar Transmission Lines		5. TYPE OF REPORT & PERIOD COVERED Ph.D. Thesis June 1975
		6. PERFORMING ORG. REPORT NUMBER
7. AUTHOR(s) Klaus-Dieter Kuchler		8. CONTRACT OR GRANT NUMBER(s)
9. PERFORMING ORGANIZATION NAME AND ADDRESS Naval Postgraduate School Monterey, California 93940		10. PROGRAM ELEMENT, PROJECT, TASK AREA & WORK UNIT NUMBERS
11. CONTROLLING OFFICE NAME AND ADDRESS Naval Postgraduate School Monterey, California 93940		12. REPORT DATE June 1975
		13. NUMBER OF PAGES 284
14. MONITORING AGENCY NAME & ADDRESS (if different from Controlling Office)		15. SECURITY CLASS. (of this report) Unclassified
		15a. DECLASSIFICATION/DOWNGRADING SCHEDULE
16. DISTRIBUTION STATEMENT (of this Report) Approved for public release; distribution unlimited.		
17. DISTRIBUTION STATEMENT (of the abstract entered in Block 20, if different from Report)		
18. SUPPLEMENTARY NOTES		
19. KEY WORDS (Continue on reverse side if necessary and identify by block number) slotline, coplanar stripline slotlines on ferrite slotline resonator coupled slotlines		
20. ABSTRACT (Continue on reverse side if necessary and identify by block number) A frequency dependent hybrid mode analysis of general coplanar transmission lines is presented. A Fourier transform technique is applied and the resulting expressions are evaluated numerically using the method of moments. Shielded slot line resonators as well as dispersion characteristic and characteristic impedance of open and closed boundary slot		

(20. ABSTRACT Continued)

lines, coupled slot lines and coplanar strip lines are obtained. An extension of this technique is used in a perturbational analysis of slot lines on a ferrite substrate.

The theoretical performances of various slot line directional couplers are predicted. Numerical results are compared with experiments in various cases, where excellent agreement has been obtained.

Hybrid Mode Analysis
of Coplanar Transmission Lines

by

Klaus-Dieter Kuchler

Kapitänleutnant, Federal German Navy

Ing.(grad.), Technische Akademie der Luftwaffe, 1968

M.S.E.E.(with distinct.), Naval Postgraduate School, 1973

Submitted in partial fulfillment of the
requirements for the degree of

DOCTOR OF PHILOSOPHY

from the

NAVAL POSTGRADUATE SCHOOL

June 1975

TABLE OF CONTENTS

1.0	<u>INTRODUCTION</u> -----	14
1.1	TRANSMISSION LINES FOR INTEGRATED CIRCUIT APPLICATIONS -----	14
1.2	MATHEMATICAL ANALYSES OF COPLANAR TRANSMISSION LINES -----	20
1.3	UNSOLVED COPLANAR TRANSMISSION LINE PROBLEMS -----	24
1.4	CONTENTS AND SUMMARY -----	25
2.0	<u>OPEN BOUNDARY STRUCTURES</u> -----	28
2.1	SINGLE SLOT-LINE -----	29
2.1.1	Dispersion Characteristic -----	30
2.1.2	Characteristic Impedance -----	42
2.2	COUPLED SLOT LINES -----	50
2.3	COPLANAR STRIP LINE -----	61
2.4	PERTURBATIONAL ANALYSIS OF A SINGLE SLOT LINE ON A FERRITE SUBSTRATE -----	68
2.4.1	Perturbation Expression for the Propagation Constant -----	71
2.4.2	Computation of Perturbation Expression in the Spectral Domain -----	72
2.5	SUMMARY -----	78
3.0	<u>CLOSED BOUNDARY STRUCTURES</u> -----	81
3.1	SINGLE RESONANT SLOT LINE -----	85
3.2	DISPERSION CHARACTERISTIC AND CHARACTERISTIC IMPEDANCE -----	97
3.3	END EFFECT OF SHORTED SLOT LINE -----	105
3.4	END COUPLED SLOT-LINES -----	109
3.5	SUMMARY -----	116

4.0	<u>SLOT LINE DIRECTIONAL COUPLER DESIGN</u> -----	121
4.1	THEORETICAL METHODS FOR ANALYSIS -----	122
4.1.1	Impedance Matrix Formulation -----	124
4.1.2	Explicit Coupler Equations -----	126
4.2	THEORETICAL RESPONSE OF SEVERAL COUPLERS -----	128
4.3	DESIGN OF TWO COUPLERS -----	132
4.4	SUMMARY -----	139
5.0	<u>COMPUTER PROGRAMMING</u> -----	140
5.1	REMARKS ON NUMERICAL ANALYSIS -----	140
5.2	COMPUTER PROGRAM 'COPLAN' FOR OPEN BOUNDARY COPLANAR TRANSMISSION LINES -----	157
5.3	COMPUTER PROGRAM 'RESO' FOR RESONATING SLOT LINE AND TRANSMISSION LINE PARAMETERS FOR SHIELDED CONFIGURATIONS -----	167
6.0	<u>SUGGESTIONS FOR FURTHER RESEARCH</u> -----	173
7.0	<u>CONCLUSION</u> -----	176
APPENDIX A:	DERIVATION OF SPECTRAL DOMAIN DYADIC GREEN'S FUNCTION COMPONENTS (OPEN BOUNDARY) -----	178
APPENDIX B:	TIME AVERAGE POWER FLOW IN THE SPECTRAL DOMAIN (OPEN BOUNDARY) -----	186
APPENDIX C:	PERTURBATION THEORY FOR OPEN BOUNDARY WAVEGUIDES -----	190
APPENDIX D:	PERTURBATION EXPRESSION FOR THE PROPAGATION CONSTANT IN THE SPECTRAL DOMAIN -----	196
APPENDIX E:	DERIVATION OF SPECTRAL DOMAIN DYADIC GREEN'S FUNCTION COMPONENTS (CLOSED BOUNDARY) -----	201
APPENDIX F:	TIME AVERAGE POWER FLOW IN THE SPECTRAL DOMAIN (CLOSED BOUNDARY) -----	207
APPENDIX G:	NORMALIZED EQUATIONS FOR OPEN BOUNDARY LINES -----	210

APPENDIX H:	NORMALIZED POWER FLOW EQUATIONS -----	219
APPENDIX J:	NORMALIZED EQUATIONS FOR CLOSED BOUNDARY LINES -----	227
APPENDIX K:	CIRCULAR RESONATING APERTURE ON A DIELECTRIC SUBSTRATE -----	235
APPENDIX L:	DESIGN CURVES -----	242
APPENDIX M:	COMPUTER PROGRAM 'COPLAN' -----	252
APPENDIX N:	COMPUTER PROGRAM 'RESO' -----	269
LIST OF REFERENCES	-----	281
INITIAL DISTRIBUTION LIST	-----	284

LIST OF TABLES

TABLE I	SINGLE SLOT LINE ON A DIELECTRIC SUBSTRATE -----	162
TABLE II	COUPLED SLOT LINES ON A DIELECTRIC SUBSTRATE -----	162
TABLE III	COPLANAR WAVEGUIDE ON A DIELECTRIC SUBSTRATE -----	163
TABLE IV	COPLANAR STRIP LINE ON A DIELECTRIC SUBSTRATE -----	163
TABLE V	SINGLE SLOT LINE ON A FERRITE SUBSTRATE ----	164
TABLE VI	COUPLED SLOT LINES ON A FERRITE SUBSTRATE --	165
TABLE VII	COPLANAR WAVEGUIDE ON A FERRITE SUBSTRATE --	166
TABLE VIII	SHIELDED SLOT LINE, HALFWAVE RESONATOR AND END COUPLED SLOT LINES ON A DIELECTRIC SUBSTRATE -----	172

LIST OF FIGURES

FIGURE 1.1/1	Microstrip Transmission Line -----	16
FIGURE 1.1/2	Slot Transmission Line -----	17
FIGURE 1.1/3	Parallel Coupled Slot Transmission Line --	18
FIGURE 1.1/4	Parallel Coplanar Strip Transmission Line -----	19
FIGURE 2.1/1	Comparison of Approximations for Dispersion Characteristic of a Single Slot Line -----	40
FIGURE 2.1/2	Comparison for Characteristic Impedances of a Single Slot Line -----	46
FIGURE 2.1/3	Time Average Power Ratio in Regions 1,2 and 3 vs. Normalized Frequency for a Single Slot Line with $W/D = 1.0$ -----	47
FIGURE 2.1/4	Power Density Distribution in a) Spectral, b) Space Domain for Region 1 of a Single Slot Line with $\epsilon_r = 20$, $W/D = 1.0$ and $D/\lambda = 0.02$ -----	49
FIGURE 2.2/1	Assumed Electric Field Component in x- Direction vs x for Even and Odd Mode on Coupled Slot Lines -----	52
FIGURE 2.2/2a	Even and Odd Mode Dispersion Character- istics for Coupled Slots with $W/D = 0.4$ and $\epsilon_r = 16$ -----	55
FIGURE 2.2/2b	Even and Odd Mode Characteristic Impedances for Coupled Slots with $W/D = 0.4$ and $\epsilon_r = 16$ -----	56
FIGURE 2.2/3	Dispersion Characteristic and Characteristic Impedance for Coplanar Waveguide with $W/D = 1$ and $\epsilon_r = 10$ -----	57
FIGURE 2.2/4	Even and Odd Mode Characteristic Impedance vs Separation for $D/\lambda = 0.03$, $W/D = 0.4$ and $\epsilon_r = 16$ -----	60

FIGURE 2.3/1	Assumed Current Density Component in z-Direction vs x for Coplanar Strip Line a) Equation (2-33a) b) Equation (2-34a) c) Equation (2-35a) -----	64
FIGURE 2.3/2	a) Dispersion Characteristic and b) Characteristic Impedance for Coplanar Strip Line with S/D = W/D = 1.0 and $\epsilon_r = 12$ -----	67
FIGURE 2.4/1	Field Configurations on Slot Line -----	70
FIGURE 2.4/2	a) Propagation Constant Ratio and b) Attenuation for Waves Travelling on a Slot Line with Ferrite Substrate in +z and -z (dashed) Direction -----	77
FIGURE 3.1/1	Shielded Slot Line Resonator -----	84
FIGURE 3.1/2	Resonant Slot Length vs Normalized Frequency for a Halfwave Slot Line Resonator with $a/D = 5.5$, $h_1/D = h_2/D =$ 8.0 and $\epsilon_r = 20$ -----	96
FIGURE 3.2/1	a) Dispersion Characteristic and b) Characteristic Impedance of a Shielded Slot Line vs Normalized Frequency with $a/D = 5.5$, $h_1/D = h_2/D = 8.0$ and $\epsilon_r = 20$ -----	103
FIGURE 3.3/1	Short-circuit Reactance Referred to a Plane Coincident with End of Slot Line for a) $\epsilon_r = 12$, b) $\epsilon_r = 20$ with $a/D = 5.5$ and $h_1/D = h_2/D = 8.0$ -----	108
FIGURE 3.4/1	End Coupled Slot Line Resonators a) Physical Layout and Dimensions b) Electric Field Component in x- Direction vs z for Even and Odd Mode of Excitation -----	111
FIGURE 3.4/2	Circuit Model for End Coupled Slot Resonator -----	113
FIGURE 3.4/3	Reactances x_c and m for two End Coupled Slot Lines vs Varying Separation with $a/D = 5.5$, $h_1/D = h_2/D = 8.0$, $W/D = 0.5$, $D/\lambda = 0.0159$ and $\epsilon_r = 20$ -----	117
FIGURE 4.1/1	Schematic of Directional Coupler -----	123

FIGURE 4.2/1	Theoretical Response of Coupler with $\theta_o = \theta + \pi$, $W/D = 0.5$, $S/D = 0.3$ and $\epsilon_r = 16$ -----	130
FIGURE 4.2/2	Theoretical Response of Contradirectional Coupler with $S/D = 0.3$, $W/D = 0.5$ and $\epsilon_r = 16$ -----	131
FIGURE 4.3/1	Geometry of Experimental Slot Line Coupler with Microstrip-Slot Transitions --	133
FIGURE 4.3/2	Theoretical and Experimental Response of Codirectional Coupler with $S/D = 1.08$, $W/D = 0.5$ and $\epsilon_r = 16$ -----	136
FIGURE 4.3/3	Theoretical and Experimental Response of a Coupler with $S/D = 0.3$, $W/D = 0.5$ and $\epsilon_r = 16$ -----	138
FIGURE 5.1/1	$M''(\alpha D, \lambda'/\lambda)$ vs αD with $\epsilon_r = 12$ and $D/\lambda = 0.03$ for five arbitrary values λ'/λ -----	145
FIGURE 5.1/2	$N_1''(\alpha D, \lambda'/\lambda)$ vs αD with $\epsilon_r = 16$ and $D/\lambda = 0.03$ for five arbitrary values λ'/λ -----	146
FIGURE 5.1/3	$N_1''(\alpha D, \lambda'/\lambda) \cdot E_x(\alpha D) ^2$ vs αD with $W/D = 0.5$, $D/\lambda \cong 0.03$ and $\epsilon_r = 16$ (single slot) -----	148
FIGURE 5.1/4	$N_1''(\alpha D, \lambda'/\lambda) \cdot E_x(\alpha D) ^2$ vs αD with $W/D = 0.5$, $D/\lambda \cong 0.03$, $S/D = 1.0$ and $\epsilon_r = 16$ (coupled slots, even mode) -----	149
FIGURE 5.1/5	$N_1''(\alpha D, \lambda'/\lambda) \cdot E_x(\alpha D) ^2$ vs αD with $W/D = 0.5$, $D/\lambda \cong 0.03$, $S/D = 1.0$ and $\epsilon_r = 16$ (coupled slots, odd mode) -----	150
FIGURE 5.1/6	$M_4''(\alpha D, \lambda'/\lambda) \cdot J_z(\alpha D) ^2$ vs αD with $W/D = S/D = 1.0$, $D/\lambda = 0.03$ and $\epsilon_r = 12$ (coplanar strip line) -----	151
FIGURE K/1	Circular Resonant Aperture on a Dielectric in a Closed Cylinder -----	236
FIGURE L/1	Dispersion Characteristic and Characteristic Impedance of Single Slot Line with $\epsilon_r = 12$ -----	243

FIGURE L/2	Dispersion Characteristic and Characteristic Impedance of Single Slot Line with $\epsilon_r = 16$ -----	244
FIGURE L/3	Dispersion Characteristic and Characteristic Impedance of Single Slot Line with $\epsilon_r = 20$ -----	245
FIGURE L/4a	Dispersion Characteristic of Coplanar Stripline with $W/D = 1.5$ and $\epsilon_r = 2.5$ ----	246
FIGURE L/4b	Characteristic Impedance of Coplanar Stripline with $W/D = 1.5$ and $\epsilon_r = 2.5$ ----	247
FIGURE L/5a	Dispersion Characteristic of Coplanar Stripline with $W/D = 1.5$ and $\epsilon_r = 9.0$ ----	248
FIGURE L/5b	Characteristic Impedance of Coplanar Stripline with $W/D = 1.5$ and $\epsilon_r = 9.0$ ----	249
FIGURE L/6a	Dispersion Characteristic of Coplanar Stripline with $W/D = 1.5$ and $\epsilon_r = 20$ -----	250
FIGURE L/6b	Characteristic Impedance of Coplanar Stripline with $W/D = 1.5$ and $\epsilon_r = 20$ -----	251

ACKNOWLEDGMENT

I am very much obliged to the Federal German Navy who gave me the opportunity to pursue this graduate education.

I gratefully acknowledge my indebtedness to my thesis advisor for his continuous aid and encouragement throughout the development of this work.

My thanks are due also to the members of my committee and various members of the faculty of the Naval Postgraduate School for their valuable help.

1.0 INTRODUCTION

The study of electromagnetic energy transmission is but one important area in microwave engineering, where the electromagnetic waves are travelling through some transmission medium, which provides the link between the transmitting and the receiving part of a transmission system. The transmission medium may be the free space or it may be a guidance structure which will direct the energy flow into a certain prescribed direction. This structure will be in general a boundary where the surrounding fields interface with the surface currents and charges on this boundary which will be in most cases an electric conductor, although in some cases a dielectric material may be used instead. Some standard examples for guided wave structures for microwave applications are the open wire transmission lines, coaxial cables and rectangular or circular waveguides.

1.1 TRANSMISSION LINES FOR INTEGRATED CIRCUIT APPLICATIONS

In most cases of designing a transmission link the decision of which guidance structure should be used will be based upon various determining factors which are sought to be optimal in some sense. Some examples of these factors are the cost of design and maintenance, the transmitted power level and the frequency band of operation, to name only a few. While most of these examples given so far apply mainly to

large scale transmission systems, recent advances and increasing use of integrated circuit technology at microwave frequencies set different standards where new transmission lines are required that are planar in nature. Several reasons may have led to this ever increased interest in planar transmission lines; e.g. the use of microwave circuits in satellite communications requires light weight and small sizes; another reason is that the etching of a planar transmission line on a dielectric or ferrite substrate is just another production step within the fabrication of a wholly automatically fabricated integrated circuit module. The most commonly used transmission line to date in microwave IC's is the microstrip line shown in Figure 1.1/1. It was first proposed in 1955 by M. Arđiti [Ref. 1] and has since then received considerable attention by innumerable investigators.

Although the investigations of single and coupled microstrip lines continue to be the subject of more sophisticated research today only recently the interest shifted towards investigations of coplanar transmission lines. Some examples of these lines are shown in Figures 1.1/2-4. These lines offer the advantage of being more easily adaptable to shunt element connections without the need to penetrate the dielectric substrate as in the case of microstrip lines. Active devices as well as passive elements may be fabricated in either series or shunt configuration directly on to these lines in either hybrid or monolithic fabrication techniques [Ref. 2].

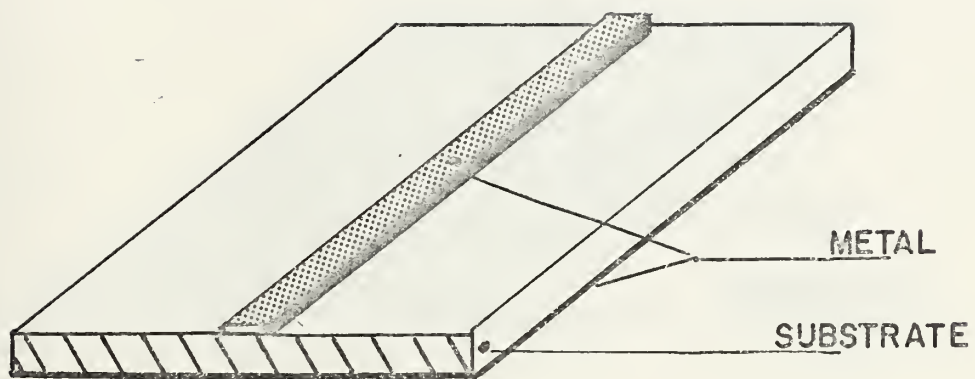


Figure 1.1/1 Microstrip Transmission Line

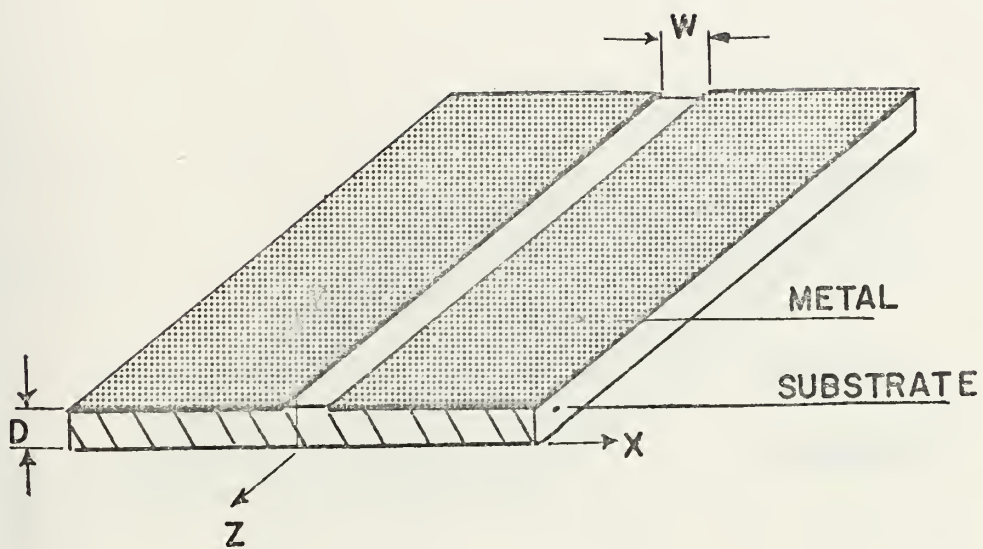


Figure 1.1/2 Slot Transmission Line

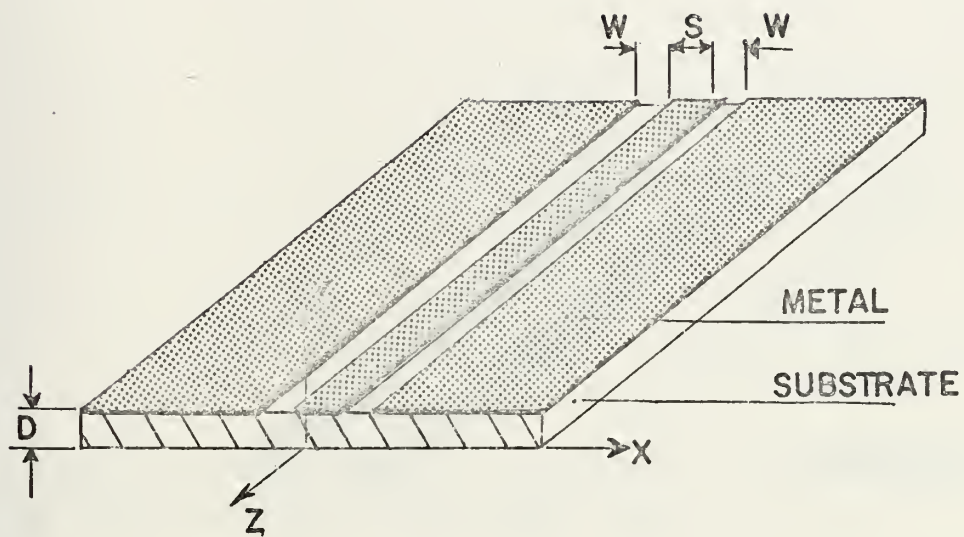


Figure 1.1/3 Parallel Coupled Slot Transmission Line

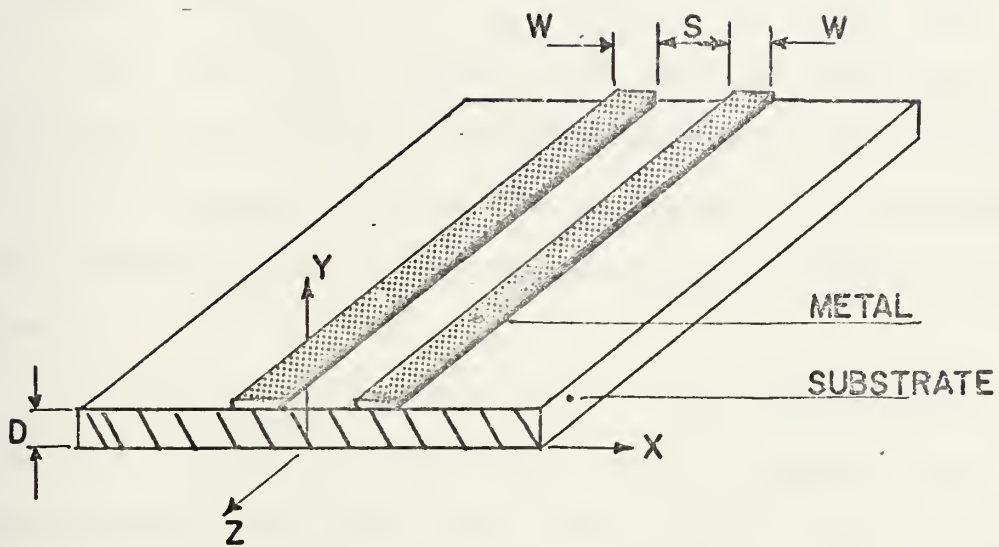


Figure 1.1/4 Parallel Coplanar Strip Transmission Line

The slot line in Figure 1.1/2 consists of a narrow gap between two conducting surfaces which are on one side of a dielectric substrate. A fairly high permittivity of this substrate confines the waves travelling on this structure to the region of this slot such that the main mode of propagation is similar to a TE_{10} rectangular waveguide mode [Ref. 3].

Figure 1.1/3 shows two adjacent slot lines parallel to each other and of equal width, where the coupling effect between these lines may be advantageous in the design of microwave filters and couplers. If this configuration is used as a single transmission line such that both outer conductors are the ground electrodes, this line is called a coplanar waveguide (CPW) according to Wen [Ref. 4].

Both lines use a fairly broad area of conductor surface which may serve as the ground plane for a microstrip placed onto the opposite side of the substrate, thus coupling from one transmission line to the other can be easily achieved [Ref. 5].

Another promising property of these two lines is the fact that both provide an area where the RF magnetic field is elliptically polarized which makes these lines suitable for nonreciprocal applications when the dielectric is replaced by a ferrite substrate. This elliptic polarization is in contrast to microstrip lines where a similar effect can be achieved only by using meander type lines [Ref. 2]. The coplanar strip line shown in Fig. 1.1/4 consists of two strip conductors on

a dielectric substrate with no ground plane and can be thought of as a dual to the coplanar waveguide [Ref. 4].

1.2 MATHEMATICAL ANALYSES OF COPLANAR TRANSMISSION LINES

In the design of a transmission line the two important line parameters are the characteristic impedance and the propagation or phase velocity.

A standard approach in the analysis of these lines is to consider the line as having distributed parameters of capacitance and inductance and to solve for these in terms of the physical dimensions. This solution assumes a TEM mode of propagation since static fields are assumed for the calculation of the line reactances. However it can be easily proved that the inhomogeneous guidance structures shown in Figures 1.1/1-4 strictly cannot support a TEM mode. Assume waves are propagating along a non homogeneous guiding system such as a microstrip or a slot line with a propagating term $e^{(j\omega t - \gamma z)}$ where ω is the radian frequency, t the time and $\gamma = \alpha + j\beta$ the propagation constant assumed from now on to be pure imaginary (lossless case, $\alpha=0$), $j = \sqrt{-1}$.

The transverse field components can be related to the longitudinal field components through an algebraic manipulation of Maxwell's curl equations to yield

$$H_{xi} = \frac{1}{k_i^2 - \beta^2} (j\omega\epsilon_i \frac{\partial E_{zi}}{\partial y} - j\beta \frac{\partial H_{zi}}{\partial x})$$

$$H_{yi} = \frac{-1}{k_i^2 - \beta^2} (j\omega\epsilon_i \frac{\partial E_{zi}}{\partial x} + j\beta \frac{\partial H_{zi}}{\partial y})$$

$$E_{xi} = \frac{-1}{k_i^2 - \beta^2} (j\beta \frac{\partial E_{zi}}{\partial x} + j\omega\mu_i \frac{\partial H_{zi}}{\partial y})$$

$$E_{yi} = \frac{1}{k_i^2 - \beta^2} (-j\beta \frac{\partial E_{zi}}{\partial y} + j\omega\mu_i \frac{\partial H_{zi}}{\partial x})$$

where $k_i^2 = \omega^2 \epsilon_i \mu_i$ $i = 1, 2, 3, \dots$ defining the spatial region.

If the TEM mode is assumed E_z and H_z are non existing throughout the guidance structure. A solution other than the trivial solution clearly can only exist if $k_i^2 - \beta^2 = 0$. Since for the inhomogeneous guidance system β is the same for all regions but for certain $i \neq j$, $k_i \neq k_j$ the TEM mode condition cannot be met.

But although a planar transmission line such as the microstrip line has an inhomogeneous cross-section a TEM or often called "quasi-static" mode approximation can be used since most of the fields are confined to the dielectric between the two conductors. Recent investigations show however that this is only valid for frequencies up to approximately 5 GHz [Ref. 6]. For coplanar transmission lines a quasi-static approximation seems no longer suitable for microwave frequencies in the GHz region since the waves are not as closely bound in the dielectric. Investigations of coplanar transmission lines thus should start from the general field theory to include the hybrid mode which provides a frequency

dependent analysis. This means that in general a solution to Helmholtz's equation rather than Poisson's equation is to be found with inhomogeneous boundary conditions due to the interaction between fields and guiding structure. This is not an easy task in a mathematical sense. A Green's function solution e.g. should be feasible at least theoretically but has not been reported in the literature so far, probably due to the immense complexity of the problem.

In his analysis of the slot line Cohn [Ref. 3] introduced electric and magnetic boundary walls which permitted the slot line configuration to be treated as a rectangular waveguide problem. The set of rectangular waveguide modes was used as a set of orthogonal functions; in the final analysis the fields were approximated by the TE_{10} rectangular waveguide mode.

Wen [Ref. 4] investigated the coplanar waveguide and the coplanar strips with the assumption that the dielectric substrate is thick enough to be considered infinite for conformal mapping purposes. For large values of the permittivity this may be a practical assumption but it appears to be impractical for relatively small values or for thin substrates. An alteration of this method used by Wen is given by Davis et al. [Ref. 7] and takes the finite thickness of the substrate into account. The coplanar strip line, however, is not treated. Furthermore, both methods lack any frequency dependent information on the behavior of the line parameters since a quasi-static approximation is used.

Recently, Itoh and Mittra [Ref. 8] proposed a new method for calculating the dispersion characteristic of a single slot line. Here Helmholtz's equations for the scalar potential functions [Ref. 9] are transformed into the Fourier domain and are solved for in accordance with the given boundary conditions. The method of moments is then used to solve for the propagation constant. This approach showed good agreement with results from Cohn [Ref. 3]. However no analysis of the characteristic impedance has been reported in Reference 8.

This spectral domain approach was used by Luna [Ref. 10] to compute the dispersion characteristic of coplanar strips. No further analysis of this transmission line has appeared in the literature.

1.3 UNSOLVED COPLANAR TRANSMISSION LINE PROBLEMS

Besides the known parameters of coplanar transmission lines given in Section 1.2 there remain several problems open for analysis which will be shortly listed here and are the subject of this thesis. Although the slot line was studied in 1968 by Cohn [Ref. 3] with a frequency dependent analysis and the coplanar waveguide structure was analyzed by Wen and Davis et al. [Refs. 4,7] by a quasi-static method, no complete analysis of two coupled slot lines has appeared yet, although originally planned by Cohn. Line parameters which describe the coupling effect between these lines are important in the design of directional couplers and in filter design.

Moreover, in the design of slot line filters, the application of resonant slot structures may be desirable and these have not yet been studied analytically at all.

Another unsolved problem is the shielded slot line structure. Since waves traveling on a slot line are not closely bound to the dielectric next to the slot but extend somewhat into the air regions it seems important to study the behavior of the line parameters under the influence of nearby obstacles such as an enclosing or shielding structure. These results could be of some significance in the design of microwave IC modules.

A further investigation is needed for a slot line on a ferrite substrate. Although recently a publication by Kitasawa et al. [Ref. 11] discussed this problem, the analysis presented is restricted since the operating frequency is assumed to be far above the resonance frequency of the ferrite. No analysis about attenuation of the waves on the ferrite is mentioned.

Finally, although the frequency dependent dispersion characteristics of coplanar strips were analyzed by Luna [Ref. 10] a frequency dependent formulation of the characteristic impedance is still missing.

1.4 CONTENTS AND SUMMARY

Inhomogeneous waveguide structures such as coplanar transmission lines will not support a TEM-mode of propagation at high frequencies. Therefore any analysis will assume a

full or hybrid mode which may be thought of as being a superposition of TE and TM modes. This formulation will yield a frequency dependent phase velocity and characteristic impedance.

This thesis is devoted to a hybrid mode analysis of coplanar transmission lines. In Section 2.0 open boundary structures are analyzed. Following the proposed method of Itoh and Mittra [Ref. 8] the dispersion characteristic of a single slot line is formulated. The investigations are extended by comparing various possible approximations. Using Parseval's relation it is shown that the power flow on this waveguide structure can be computed in the spectral domain.

The resultant calculations for the characteristic impedance are compared with results from Reference 12. This is the first verification of Cohn's method by an entirely different numerical analysis and shows very close agreement. The theory is extended for an analysis of two coupled slot lines of equal width, the results are new and very important for the microwave industry in the design of slot line couplers and filters. A frequency dependent analysis of coplanar waveguide is included.

An easy extension of the theory is then used to analyze the line parameters of a coplanar strip transmission line. The final part of Section 2.0 shows a perturbational expression for the propagation constant of slot lines on a ferrite substrate.

In Section 3.0 various closed boundary structures are analyzed. The shielded slot transmission line is compared with the open boundary structure. Resonating slot configurations are investigated such as a single resonant slot and two end coupled resonating slots. A byproduct of the resonant slot investigation is the end effect analysis of slot lines. Theoretical results are compared with experimental data from open boundary experiments and show good agreement.

Section 4.0 is devoted to an experimental verification of the numerical data for coupled slot line parameters. Using basic network theory the theoretical response of a slot line directional coupler can be computed. Due to the non-equal phase velocities in the two natural modes co- or contra-directional coupling can be achieved. Two slot line couplers, a co- and a contra-directional, were built and their performance measured.

In Section 5.0 remarks are made about the numerical analysis and the computer programs. It is believed that results of this thesis are of interest to the microwave industry. Hence two of the most important computer programs used in this work are attached to the thesis and their use explained in this section.

Section 6.0 shortly outlines an attempt to analyze a circular resonating aperture on a dielectric substrate and shows the difficulties encountered there. Suggestions for expansions of the presented work conclude this section.

2.0 OPEN BOUNDARY STRUCTURES

In this section open boundary coplanar transmission lines are analysed where it is assumed that the lines extend infinitely in the z -direction in an infinite x - z plane. It is further assumed that conductors are negligibly thick and that dielectric and conductor are perfect.

The electromagnetic fields surrounding the guidance structure are derived in a most general way from hybrid modes where use is made of the fact that any hybrid mode can be thought of being a superposition of TE and TM modes by the orthogonality properties of open boundary waveguide modes, proved by Collins [Ref. 13]. The derivation of all equations is general and not limited to any specific mode of propagation. Approximations for the lowest order mode are made in the very end and can be easily modified to yield results for higher order modes.

It is further assumed that the operating frequency is kept below the frequency for the onset of surface wave modes which could propagate in the dielectric-air medium for $y < D$ (see Figure 1.1/2-4).

This onset of surface wave modes for the slot line configuration e.g. can approximately be determined. Consider the region $y < D$ and assume that the dielectric has the permittivity ϵ_2 while for $y < 0$ the permittivity is that of free space ϵ_0 . All further assumptions stated above hold and the

existence of a slot in the metal is irrelevant. Attwood in Reference 14 has derived the determinantal equation for TM surface wave modes which yield the lowest order mode.

This equation is given as $k_{c2} \tan(k_{c2}D) = -\frac{\epsilon_2}{\epsilon_0} k_{co}$ where $k_{c2} = \sqrt{k_2^2 - \beta^2}$ and $k_{co} = \sqrt{\beta^2 - k_o^2}$, $k_o^2 = \omega^2 \epsilon_0 \mu_o$ and $k_2^2 = \omega^2 \epsilon_2 \mu_o$. A bound for the lowest order cutoff wave-

length can be found by approximating this transcendental equation. For $k_{c2} \tan(k_{c2}D) < 0$, $\tan(k_{c2}D) < 0$ or $k_{c2}D > \frac{\pi}{2}$. But $k_{c2} = \sqrt{k_2^2 - \beta^2}$ so that the following

inequality holds $k_2D > \sqrt{k_2^2 - \beta^2} D > \frac{\pi}{2}$. If $\lambda_2 = \frac{2\pi}{\sqrt{\epsilon_2 \mu_o} \omega}$

the bound for the onset of surface waves is

$$\lambda_2 < 4 \cdot D$$

2.1 SINGLE SLOT-LINE

The schematic of a single slot line and its orientation with respect to a three-dimensional rectangular coordinate system is shown in Figure 1.1/2. The substrate is assumed to be dielectric. Let this transmission line be divided into three regions in space and define these regions as

region 1	for	$D < y$
2		$0 \leq y \leq D$
3		$y < 0$

Since the lossless case is assumed, the propagation constant $\gamma = \alpha + j\beta$ is pure imaginary with $\alpha = 0$. The following derivation, however, is perfectly general and the above simplification is made only at the end.

2.1.1 Dispersion Characteristic

In the construction of solutions to Maxwell's field equations for a transmission line problem it is sufficient to assume two scalar potential functions, a scalar electric potential ϕ and a scalar magnetic potential ψ which may be both related to TM and TE modes respectively [Refs. 9,13]. The axial components of TM and TE modes are then

$$E_z = k_{ci}^2 \phi(x,y) e^{\pm \gamma z} \quad (2-1)$$

$$\text{and } H_z = k_{ci}^2 \psi(x,y) e^{\pm \gamma z} \quad (2-2)$$

where $k_{ci}^2 = k_i^2 + \gamma^2$, $i=1,2,3$ defining the spatial region of the transmission line as stated in Section 2.1.

Through Maxwell's curl equations the transverse field components are then determined by these axial components and can be given as

$$E_{xi} = \left(\gamma \frac{\partial \phi_i}{\partial x} - j\omega\mu \frac{\partial \psi_i}{\partial y} \right) e^{\gamma z} \quad (2-3)$$

$$E_{yi} = \left(\gamma \frac{\partial \phi_i}{\partial y} + j\omega\mu \frac{\partial \psi_i}{\partial x} \right) e^{\gamma z} \quad (2-4)$$

$$H_{xi} = \left(\gamma \frac{\partial \psi_i}{\partial x} + j\omega \epsilon_i \frac{\partial \phi_i}{\partial y} \right) e^{\gamma z} \quad (2-5)$$

$$H_{yi} = \left(\gamma \frac{\partial \psi_i}{\partial y} - j\omega \epsilon_i \frac{\partial \phi_i}{\partial x} \right) e^{\gamma z} \quad (2-6)$$

$$i=1,2,3$$

where propagation in the z direction is assumed and the dependence of the scalar potentials on the variables x and y is understood.

The scalar potential functions satisfy Helmholtz's equations in the three spatial regions, thus

$$(\nabla_{xy}^2 + k_{ci}^2) \phi_i = 0 \quad (2-7)$$

$$\text{and } (\nabla_{xy}^2 + k_{ci}^2) \psi_i = 0 \quad (2-8)$$

where ∇_{xy}^2 denotes the two-dimensional Laplacian operator in the transverse (x,y) direction. So equations (2-7) and (2-8) are second order partial differential equations (P.D.E.). A common practice in solving these P.D.E. which essentially present a boundary value problem is to transform these into ordinary differential equations (O.D.E.) by an integral transform technique [e.g. Ref. 15] which may then be solved analytically. The boundary conditions for (2-7) and (2-8) are intuitively obvious, for instance $\phi_i(x,y) \rightarrow 0$ for $x,y \rightarrow \pm\infty$ and furthermore $\int_{-\infty}^{\infty} |\phi_i(x,y)|^2 dx$ is bounded for finite energy reasons — the same holds if ϕ is replaced by ψ — since the time average power flow is related to the scalar

potentials as shown in Reference 13 and is assumed to be finite. Although no rigorous proof will be given it is therefore assumed that the scalar potential functions can be transformed into the Fourier domain via a Fourier transformation defined as

$$F\{\phi(x,y)\} = \phi(\alpha,y) = \int_{-\infty}^{\infty} \phi(x,y) e^{j\alpha x} dx \quad (2-9)$$

If this transform is applied to equations (2-7) and (2-8) the following O.D.E. are obtained:

$$\frac{\partial^2}{\partial y^2} \phi_i(\alpha,y) = \gamma_i^2 \phi_i(\alpha,y) \quad (2-10)$$

$$\frac{\partial^2}{\partial y^2} \psi_i(\alpha,y) = \gamma_i^2 \psi_i(\alpha,y) \quad (2-11)$$

where $\gamma_i^2 = \alpha^2 - \gamma^2 - k_i^2$.

Again for energy reasons certain solutions to these O.D.E. may be eliminated by boundary conditions in the three spatial regions since for $y \rightarrow \infty$, $\phi(x,y) \rightarrow 0$ and so $\phi(\alpha,y) \rightarrow 0$.

The solutions to (2-10) and (2-11) may then be given as

$$\begin{aligned} \phi_1(\alpha,y) &= A^e(\alpha) e^{-\gamma_1(y-D)} \\ \phi_2(\alpha,y) &= B^e(\alpha) \sinh \gamma_2 y + C^e(\alpha) \cosh \gamma_2 y \\ \phi_3(\alpha,y) &= D^e(\alpha) e^{\gamma_1 y} \end{aligned} \quad (2-12)$$

and

$$\begin{aligned}\Psi_1(\alpha, Y) &= A^h(\alpha) e^{-\gamma_1(Y-D)} \\ \Psi_2(\alpha, Y) &= B^h(\alpha) \sinh \gamma_2 Y + C^h(\alpha) \cosh \gamma_2 Y \\ \Psi_3(\alpha, Y) &= D^h e^{\gamma_1 Y}\end{aligned}\quad (2-13)$$

The following observation about the solutions in region 2 must be emphasized. Any wave on this inhomogeneous waveguide structure will partly travel through air and partly through the dielectric slab. It is then obvious that $k_0 < \beta < k_2$ in the lossless case where $k_1 = k_3 = k_0$. Since $-\infty < \alpha < \infty$, for $|\alpha| < \sqrt{k_2^2 - \beta^2}$ then $\gamma_2^2 < 0$. For these values of the transform variable α the solutions in (2-12) and (2-13) for region 2 will change from hyperbolic to trigonometric functions since $\gamma_2 = j\gamma_2''$, $\gamma_2'' = \sqrt{k_{c2}^2 - \alpha^2}$.

The eight unknown coefficients $A^e(\alpha)$ through $D^h(\alpha)$ are not independent but can be related to each other through the continuity conditions of the field components at the interfaces between the three spatial regions. These continuity conditions in the spatial domain are for

$$\underline{y = 0}$$

$$\begin{aligned}\vec{E}_{t2}(x, 0, z) &= \vec{E}_{t3}(x, 0, z) \\ \vec{H}_{t2}(x, 0, z) &= \vec{H}_{t3}(x, 0, z)\end{aligned}\quad (2-14)$$

and for $y = D$

$$\vec{E}_{t1}(x, D, z) = \vec{E}_{t2}(x, D, z)$$

$$E_{z1}(x, D, z) = \begin{cases} E_z(x) e^{\gamma z} & |x| < \frac{W}{2} \\ 0 & \text{elsewhere} \end{cases} \quad (2-15)$$

$$E_{x1}(x, D, z) = \begin{cases} E_x(x) e^{\gamma z} & |x| < \frac{W}{2} \\ 0 & \text{elsewhere} \end{cases}$$

$$H_{z1}(x, D, z) - H_{z2}(x, D, z) = \begin{cases} j_x(x) e^{\gamma z} & |x| > \frac{W}{2} \\ 0 & \text{elsewhere} \end{cases}$$

$$H_{x1}(x, D, z) - H_{x2}(x, D, z) = \begin{cases} j_z(x) e^{\gamma z} & |x| > \frac{W}{2} \\ 0 & \text{elsewhere} \end{cases}$$

The subscript t is an abbreviation for tangential x and z components to avoid writing essentially identical equations twice. $E_{x,z}(x)$ and $j_{x,z}(x)$ are the electric field components and the current densities in the x - z plane at $y = D$ in region 1.

Denoting the Fourier transforms of the x - and z -directed current density and electric field components by

$$E_x(\alpha) = F\{E_x(x)\}$$

$$E_z(\alpha) = F\{E_z(x)\}$$

$$J_x(\alpha) = F\{j_x(x)\}$$

$$J_z(\alpha) = F\{j_z(x)\}$$

and applying these transforms and the transforms of the continuity conditions to equations (2-12) and (2-13) an elimination of the unknown coefficients A^e through D^h by substitution is possible. The details of this lengthy algebraic manipulation are given in Appendix A. The results yield a set of coupled equations of the form

$$\begin{bmatrix} N_1(\alpha, \beta) & N_2(\alpha, \beta) \\ N_3(\alpha, \beta) & N_4(\alpha, \beta) \end{bmatrix} \begin{bmatrix} E_x(\alpha) \\ E_z(\alpha) \end{bmatrix} = \begin{bmatrix} J_x(\alpha) \\ J_z(\alpha) \end{bmatrix} \quad (2-16)$$

where the elements of the N matrix can be thought of being the Fourier transforms of dyadic Green's function components [Ref. 13] by an application of the convolution integral in the space domain. The lossless case $\gamma = j\beta$ is assumed in (2-16).

Nothing seems to be gained so far since neither the electric field and current density components nor their transforms are known. The coupled equations in (2-16) can however be further simplified by the methods of moments [Ref. 16], applied in the spectral domain. Define the scalar product on the space of complex-valued functions of the real variable α over the domain $-\infty < \alpha < \infty$ according to Reference 15 as

$$\langle f(\alpha), g(\alpha) \rangle = \int_{-\infty}^{\infty} f(\alpha) g^*(\alpha) d\alpha$$

and choose as a suitable set of weighting functions the Fourier transforms of the electric field components, which means Galerkin's method [Refs. 9,16]. The moment method applied to equation (2-16) leads to

$$\langle N_1(\alpha, \beta) E_x(\alpha), E_x(\alpha) \rangle + \langle N_2(\alpha, \beta) E_z(\alpha), E_x(\alpha) \rangle = 0 \quad (2-17)$$

$$\langle N_3(\alpha, \beta) E_x(\alpha), E_z(\alpha) \rangle + \langle N_4(\alpha, \beta) E_z(\alpha), E_z(\alpha) \rangle = 0$$

That the right hand side is zero can be easily verified by Parseval's relation [Ref. 15], observing that at $y = D$ the presence of an electric field component excludes the presence of a current density component and vice versa, thus electric field and current density are orthogonal to each other.

Up to this point the formulation of the problem is exact since no approximation has been made yet. Note that the electric field components and their transform although unknown can be expanded in a set of complete basis functions so that in general

$$E_x(x) = \sum_{n=1}^{\infty} a_n e_{xn}(x) \quad (2-18)$$

and
$$E_z(x) = \sum_{n=1}^{\infty} b_n e_{zn}(x)$$

The following analysis is restricted to a one term approximation for each of the series in (2-18) since it was found that

sufficient accuracy could be obtained for all practical purposes. So $n = 1$ in equation (2-18) and this subscript will be omitted from here on.

With $E_x(\alpha) \approx F\{e_x(x)\}$ and $E_z(\alpha) \approx F\{e_z(x)\}$
 (2-17) then becomes

$$\begin{aligned}
 a \int_{-\infty}^{\infty} N_1(\alpha, \beta) |E_x(\alpha)|^2 d\alpha + b \int_{-\infty}^{\infty} N_2(\alpha, \beta) E_z(\alpha) E_x^*(\alpha) d\alpha &= 0 \\
 a \int_{-\infty}^{\infty} N_3(\alpha, \beta) E_x(\alpha) E_z^*(\alpha) d\alpha + b \int_{-\infty}^{\infty} N_4(\alpha, \beta) |E_z(\alpha)|^2 d\alpha &= 0
 \end{aligned}
 \tag{2-19}$$

The dispersion characteristic of the slot line can now be found by varying β such that the determinant of the coefficient matrix of (2-19) is zero for a given set of physical parameters at a desired frequency of operation.

The remaining question is what kind of basis functions to choose. The choice of this complete set of basis functions is arbitrary in a mathematical sense, since as long as this set is complete, any closed form of the field components can be represented by it. However, the rate of convergence of the series representation will depend on how well the first few terms approximate the closed form. This in general requires some a priori knowledge of the true distribution.

In order to determine the sensitivity of this analysis to the choice of basis functions, an investigation of various one term approximations was made. One choice for the electric

field components which requires almost no insight into the field problem is of the form

$$e_x^{(1)}(x) = \begin{cases} 1 & |x| < \frac{W}{2} \\ 0 & \text{elsewhere} \end{cases} \quad (2-20a)$$

$$e_z^{(1)}(x) = \begin{cases} -1 & -\frac{W}{2} < x < 0 \\ 1 & 0 < x < \frac{W}{2} \\ 0 & \text{elsewhere} \end{cases} \quad (2-20b)$$

The Fourier transforms of these basis functions are then

$$E_x^{(1)}(\alpha) = \frac{2}{\alpha} \sin\left(\frac{\alpha W}{2}\right) \quad (2-21a)$$

$$E_z^{(1)}(\alpha) = j \frac{2}{\alpha} [1 - \cos\left(\frac{\alpha W}{2}\right)] \quad (2-21b)$$

Another choice which certainly approximates the field more closely is

$$e_x^{(2)}(x) = \begin{cases} \frac{1}{\sqrt{\left(\frac{W}{2}\right)^2 - x^2}} & |x| < \frac{W}{2} \\ 0 & \text{elsewhere} \end{cases} \quad (2-22a)$$

$$e_z^{(2)}(x) = \begin{cases} x \sqrt{\left(\frac{W}{2}\right)^2 - x^2} & |x| < \frac{W}{2} \\ 0 & \text{elsewhere} \end{cases} \quad (2-22b)$$

The reason that (2-22) are superior basis functions to (2-20) is that (2-22b) approaches zero smoothly as $|x| \rightarrow \frac{W}{2}$ and $|x| \rightarrow 0$. Furthermore (2-22a) approximates the fields more closely near the edge of the slot than (2-20a).

The Fourier transform of (2-22) can now be found in a standard table of Fourier transforms (e.g. Ref. 17],

$$E_x^{(2)}(\alpha) = \pi B_0\left(\frac{\alpha W}{2}\right) \quad (2-23a)$$

$$E_z^{(2)}(\alpha) = j \frac{\sqrt{2}}{4} \pi \frac{W}{\alpha} B_2\left(\frac{\alpha W}{2}\right) \quad (2-23b)$$

where B_0 and B_2 are Bessel functions of the first kind of order zero and two respectively.

Call the use of x and z directed field components the second order approximation while the use of an x directed component only is called a first order approximation. Then a reduction in computation time is possible using this first order approximation since only one integral in (2-18) has to be evaluated instead of four for the second order approximation. These two formulations of the dispersion problem were programmed into a digital computer language and the root β which rendered the determinant of the coefficient matrix to zero was found numerically by an iteration scheme. Details of the programming are given in Section 5. First and second order approximations using equations (2-21) and (2-23) are compared in Figure 2.1/1 with results from Cohn's method in Reference 12. Although no indication about the rate of

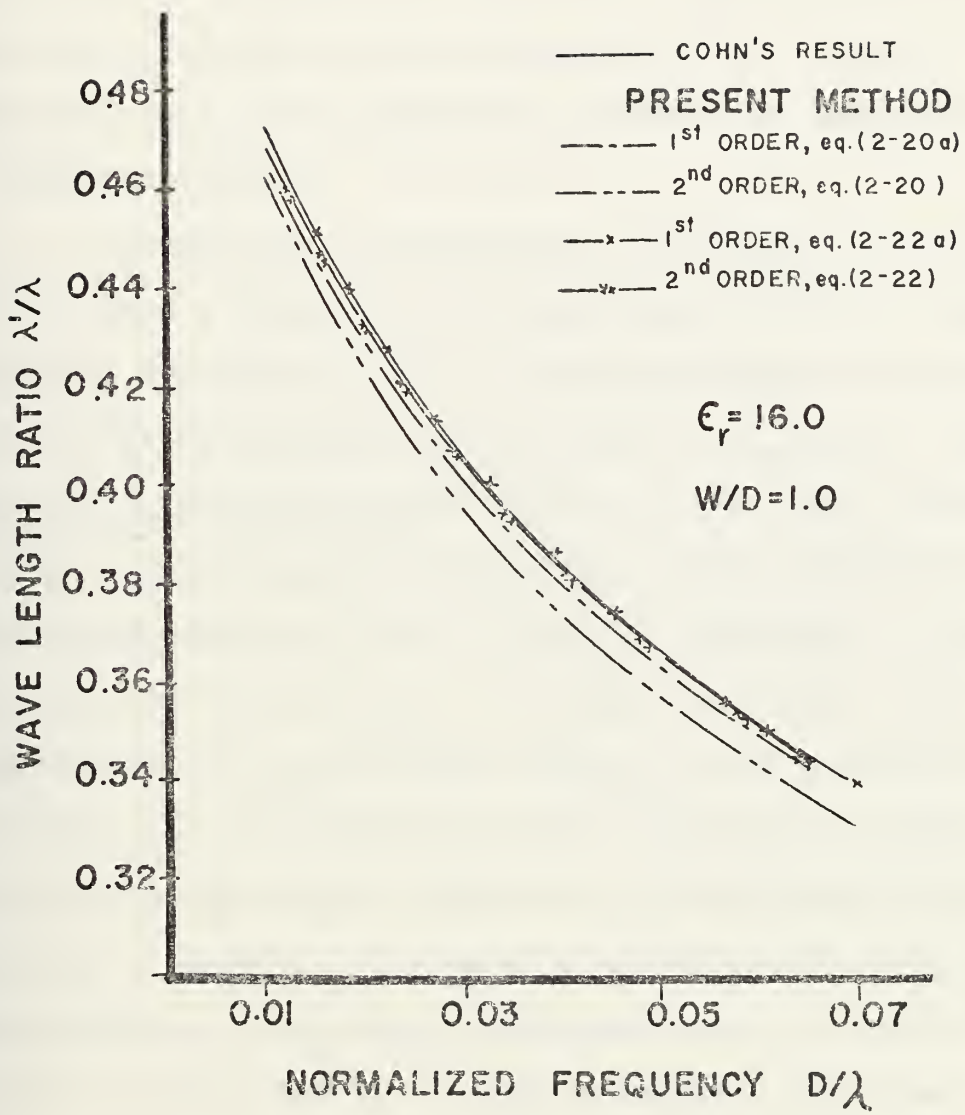


Figure 2.1/1 Comparison of Approximations for Dispersion Characteristic of a Single Slot Line

convergence and hence the accuracy of the two series for a general problem can be obtained, a comparison for this particular example shows that the largest deviation between the different approximations is less than 4%. As already noted above, the basis set (2-22) is vastly superior to basis set (2-20) in a one term approximation for the field components due to the physically impossible discontinuities of equation (2-20b).

A numerical investigation with regard to the magnitude of the x and z components of the electric field was made, using the field equations (2-23) in the second order approximation for an arbitrary choice of $W/D = 0.2$ and $\epsilon_r = 20$. Up to a value of normalized frequency $D/\lambda = 0.03$ the x directed electric field component was found to have a magnitude greater than ten times that of the z directed component. This provides justification for the use of the more efficient first order approximation. As one might expect, the magnitude of the z component of the electric field increases for larger values of normalized frequency. However, the agreement between this and Cohn's [Refs. 3,12] method is excellent for a first order approximation. The theory presented here is a verification of Cohn's theory and in a sense a check on the numerical analysis by Itoh and Mittra [Ref. 8] since it was derived independently with only their very brief letter for guidance.

2.1.2 Characteristic Impedance

The definition of the characteristic impedance for an ideal transmission line is uniquely given by static quantities because these lines support a TEM mode wave. On the other hand, in investigations of pipe-like waveguides the wave impedance is widely used [Ref. 13], however the impedances are different for TM and TE waves. Since the slot line is neither a TEM transmission line nor does it support a pure TE or TM waveguide mode but rather supports hybrid modes, no unique definition of the characteristic impedance can be found.

Since the choice of definition is arbitrary Cohn's very practical definition in Reference 3 is used in the following derivation of the characteristic impedance for a slot line. Define

$$Z_0 = \frac{V_0^2}{2 P_{avg}} \quad (2-24)$$

where V_0 is the slot voltage and P_{avg} is the time average power flow on the slot line which according to Reference 13 may be computed as

$$P_{avg} = \frac{1}{2} \operatorname{Re} \left\{ \iint_S \vec{E}_t \times \vec{H}_t^* \cdot \vec{a}_z \, dx dy \right\} \quad (2-25)$$

Observe that although the hybrid mode can be fully described as a superposition of TE and TM modes, the evaluation of the time average power flow is not just a superposition of the

single time average power flow carried by each single mode. A simple manipulation unveils that in addition to the single TE and TM power terms there are cross terms as shown below in (2-26). Assume $\gamma = j\beta$, which means for z dependence $e^{j\beta z}$ a wave traveling in the $-z$ direction.

The transverse field components of the integrand in (2-25) can be expressed in terms of the scalar potential functions as shown in equations (2-3) through (2-6). Equation (2-25) becomes with this substitution and dependence of the scalar potentials on x and y understood

$$P_{avg} = \frac{1}{2} \operatorname{Re} \int_{-\infty}^{\infty} \int_{-\infty}^{\infty} \{ \omega \mu \beta [(\frac{\partial \psi}{\partial x})^2 + (\frac{\partial \psi}{\partial y})^2] + \omega \epsilon \beta [(\frac{\partial \phi}{\partial x})^2 + (\frac{\partial \phi}{\partial y})^2] + (\beta^2 + k^2) (\frac{\partial \phi}{\partial y} \frac{\partial \psi}{\partial x} - \frac{\partial \phi}{\partial x} \frac{\partial \psi}{\partial y}) \} dy dx \quad (2-26)$$

The limits of integration are infinite since the slot line is an open boundary structure, which makes the use of Parseval's relation [Ref. 15] feasible. By this method (2-26) is transformed into the spectral domain where again a double integral is obtained with the variables of integration α and y instead of x and y .

$$P_{avg} = \frac{1}{4\pi} \operatorname{Re} \int_{-\infty}^{\infty} \int_{-\infty}^{\infty} [-\alpha^2 \beta \omega \epsilon |\phi|^2 - \beta \omega \mu |\frac{\partial \psi}{\partial y}|^2 - \beta \omega \epsilon |\frac{\partial \phi}{\partial y}|^2 - \alpha^2 \beta \omega \mu |\psi|^2 - j\alpha \beta^2 (\phi \frac{\partial \psi^*}{\partial y} + \frac{\partial \phi}{\partial y} \psi^*) + j\alpha k^2 (\phi^* \frac{\partial \psi}{\partial y} + \frac{\partial \phi^*}{\partial y} \psi)] d\alpha dy \quad (2-27)$$

where the dependence of the scalar potentials on variables α and y is implicitly understood. Besides any dependence on physical parameters and the frequency of operations, these scalar potentials are furthermore dependent on the propagation constant β , which is known from Section 2.1.1, and on the assumed field distributions as given by equations (2-12), (2-13) and the detailed derivation in Appendix A. Note that the functional dependence on the variable y may be removed by analytical integration, which changes the double integral to a single integral. For a numerical integration on a digital computer the integral (2-27) has to be evaluated separately for the three spatial regions since according to equations (2-12) and (2-13) the integrand assumes different forms there. The integrands for the three regions are given in Appendix B in equations (B-1) through (B-4).

It should be noted that the amount of algebraic complexity in these equations although still quite large could be decreased for numerical purposes by neglecting the z -directed electric field component which means that the spatial phase shift between E_x and E_z required no attention in this algebraic derivation. It is shown in the comparison with Cohn's method [Refs. 3,12] that this use of a first order solution results in good agreement.

A computer program was developed which first computes the dispersion characteristic and then the average power flow where the electric field was approximated by (2-22a). To solve for the characteristic impedance in equation (2-24),

the slot voltage has to be computed. Since the slot voltage

$$V_0 = \int_{-\frac{W}{2}}^{\frac{W}{2}} E_x(x) dx, \text{ this integration may be accomplished}$$

analytically; depending on the assumed electric field approximations $V_0 = \pi$ for (2-22a) for instance. A comparison of results obtained by this formulation of the characteristic impedance with values obtained by Cohn's method in Reference 12 is given in Figure 2.1/2. The very close agreement for the two arbitrarily chosen sets of parameters substantiates the accuracy of both methods and is the first known verification of Cohn's method.

For comparative purposes it is noted that the field distribution (2-20a) resulted in lower values for the characteristic impedance by not more than 10% from those obtained from (2-22a).

A byproduct of this analysis is a consideration of the power distribution. The spatial division of the slot line in this numerical formulation allows an analysis of the amount of power flowing in each of these three regions. In Figure 2.1/3 the ratio of the power in each region over the total power carried on the structure is shown as a function of normalized frequency for two different permittivities.

Several facts can be learned from these graphs:

- a) The amount of power carried in each region is frequency dependent. As the frequency increases more power is carried through region 2, the dielectric region.
- b) Only a small amount of the total power is found in region 3.
- c) More power is carried through the air regions if the permittivity is lowered.

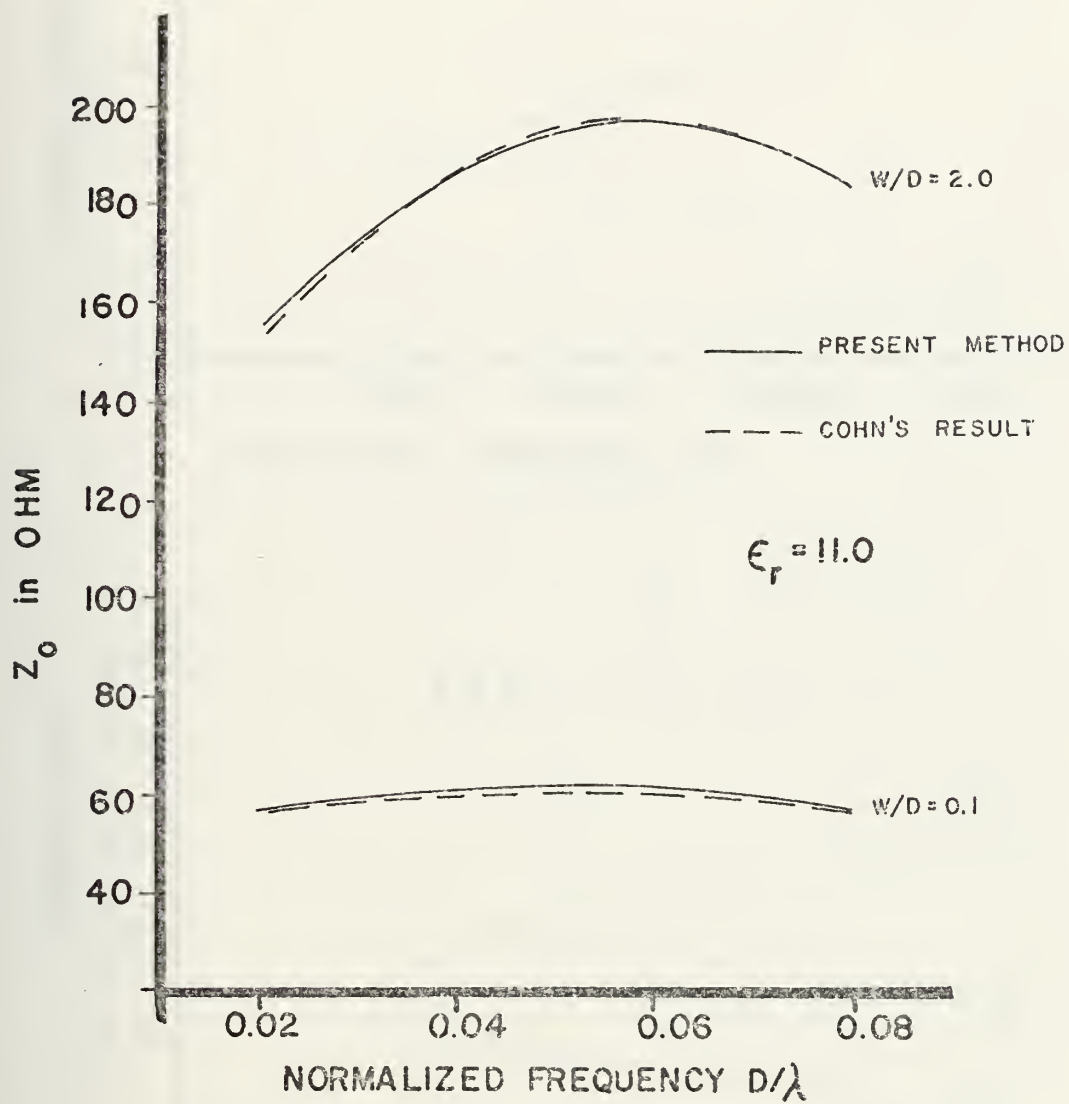


Figure 2.1/2 Comparison for Characteristic Impedances of a Single Slot Line

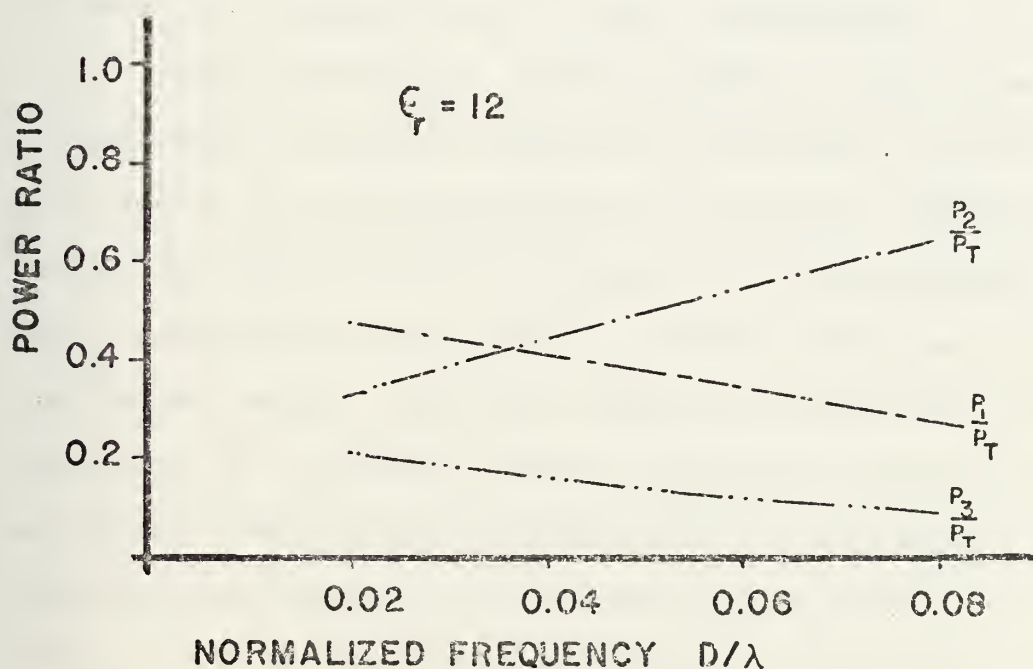
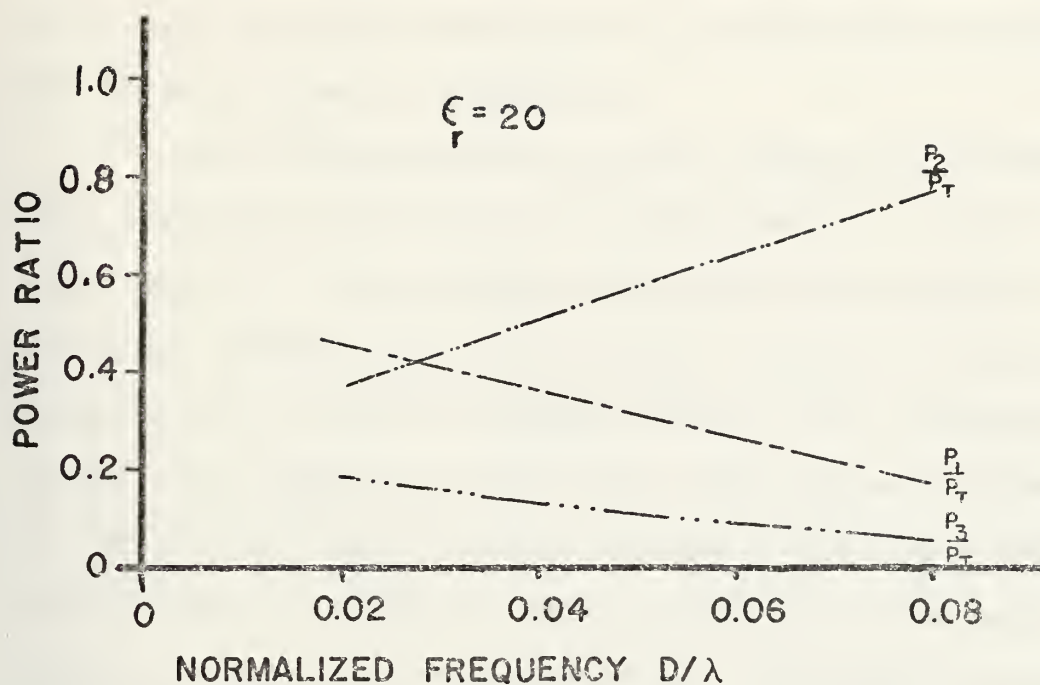


Figure 2.1/3 Time Average Power Ratio in Region 1, 2 and 3 vs. Normalized Frequency for a Single Slot Line with $W/D = 1.0$.

These results may have been known previously but for the first time are here quantitatively analyzed by the means of the spectral domain formulation.

The following investigation indicates, however, that a slight error due to the approximation in the first order exists. This example serves more illustrative purposes but might perhaps stimulate further research. With the above formulation of the time average power flow a graphical display of the power density for the slot line may be obtained. For an arbitrarily chosen set of parameters the power density in the spectral domain is shown in Figure 2.1/4a versus the normalized transform variable αD for the spatial region 1 above the substrate. The unit on the ordinate is omitted since it is insignificant in this illustration.

From Cohn's zero order analysis in Reference 3 it is obvious that the power density is the largest close to the slot and it is also obvious that it does not change its sign. To verify this the Fourier inversion of the spectral domain power density has to be taken to obtain the power density in the space domain. Since the analysis is numerical in nature inversion by a discrete Fourier transform technique (DFT) on a digital computer seemed appropriate. The result is displayed in Figure 2.1/4b. Clearly the power is the largest close to the slot and decays rapidly but contrary to any expectation changes its sign. It can be easily verified that this behavior is due to the small dip at $\alpha D = 0$ for the power

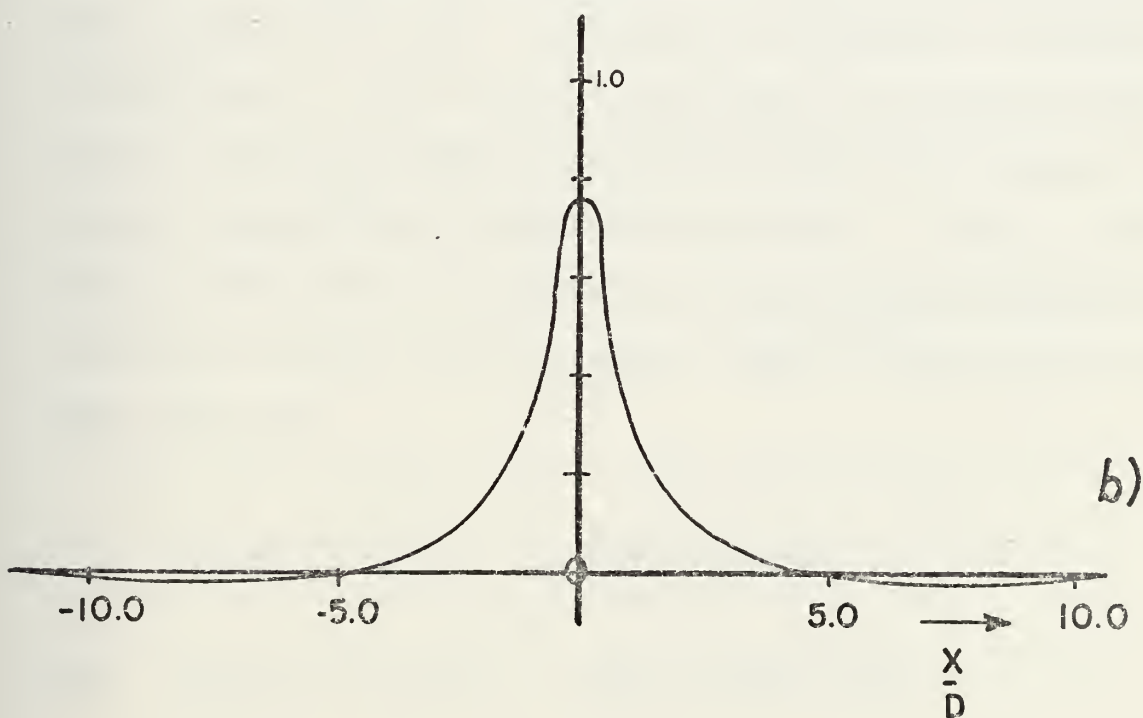
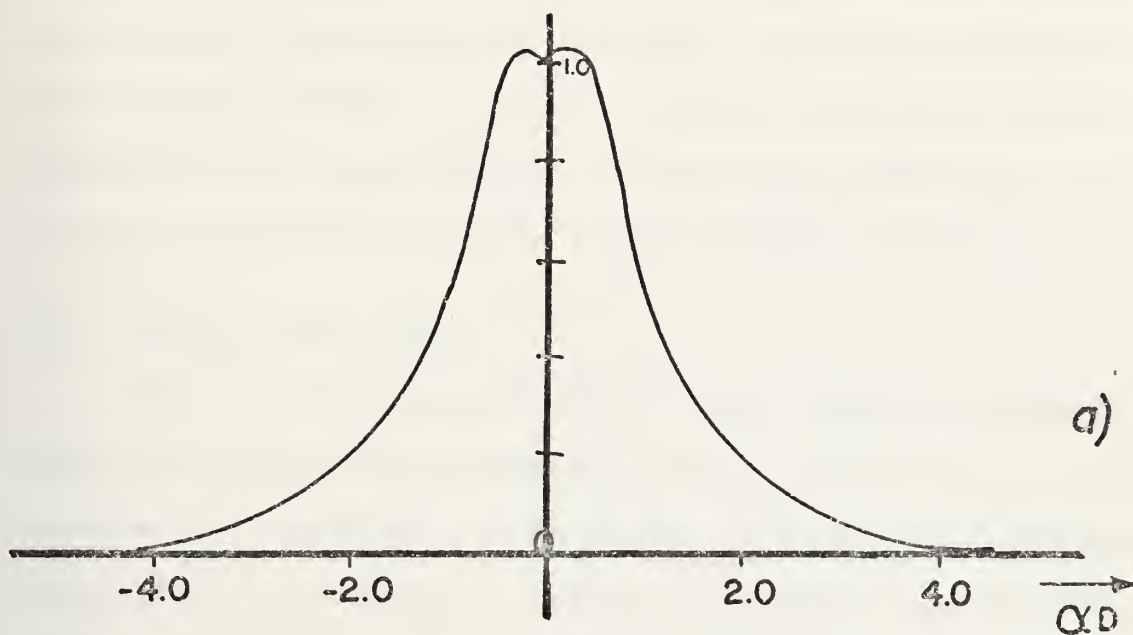


Figure 2.1/4 Power Density Distribution in a) Spectral,
b) Space Domain for Region 1 of a Single Slot
Line with $\epsilon_r = 20$, $W/D = 1.0$ and $D/\lambda = 0.02$

density distribution in the spectral domain. This dip is believed to originate from the first order approximation of the electric field. Although a similar phenomenon can be observed in an investigation of the power densities in regions 2 and 3 it is seen that the error introduced is quite small.

2.2 COUPLED SLOT LINES

With two transmission lines placed adjacent to each other such that electromagnetic coupling effects the fields on both line structures, the design of directional couplers and filters is possible. Figure 1.1/2 shows two parallel slot lines whose analysis is the subject of this section. There are many ways to describe the coupling effect between two transmission lines. According to Reference 18, which is a compilation of some twenty-nine papers on coupled transmission lines, the most common formulation is to define the natural modes of the guided wave structure. Since in this analysis two slots of equal width and constant separation are considered, define the two natural modes as the even and odd mode such that

$$E_x(x) = E_x(-x) \quad \text{for the even}$$

and
$$E_x(x) = -E_x(-x) \quad \text{for the odd mode.}$$

The existing theory developed so far in Sections 2.1.1 and 2.1.2 can now be easily extended for the analysis of line parameters for these two modes of the coupled slot lines.

It is observed that the dyadic Green's function transforms in equation (2-16) are functions of α , β , ϵ_r , D and the operating frequency but are independent of the slot configuration. The physical dimensions of the slot enter into the calculation only through the assumed field distributions or basis functions. Thus, it is only necessary to modify equations (2-20) and (2-22) such that the mathematical formulation of the basis functions corresponds to the physical configuration and field distributions of the coupled slots. As an example Figure 2.2/1 shows the assumed electric field distribution

$$e_x^{(2)}(x) = \begin{cases} \frac{1}{\sqrt{(\frac{W}{2})^2 - (x - \frac{S+W}{2})^2}} & \frac{S}{2} < x < \frac{S}{2} + W \\ \frac{\pm 1}{\sqrt{(\frac{W}{2})^2 - (x + \frac{S+W}{2})^2}} & -\frac{S}{2} - W < x < -\frac{S}{2} \\ 0 & \text{elsewhere} \end{cases} \quad (2-28)$$

The modification for the z-directed electric field component is similar. The following short manipulation leads to the Fourier transform of this distribution:

The shifting property of Fourier transforms states that if

$$F\{\phi(x)\} = \phi(\alpha) = \int_{-\infty}^{\infty} \phi(x) e^{j\alpha x} dx \quad \text{then} \quad F\{\phi(x-x_0)\} = e^{j\alpha x_0} \phi(\alpha)$$

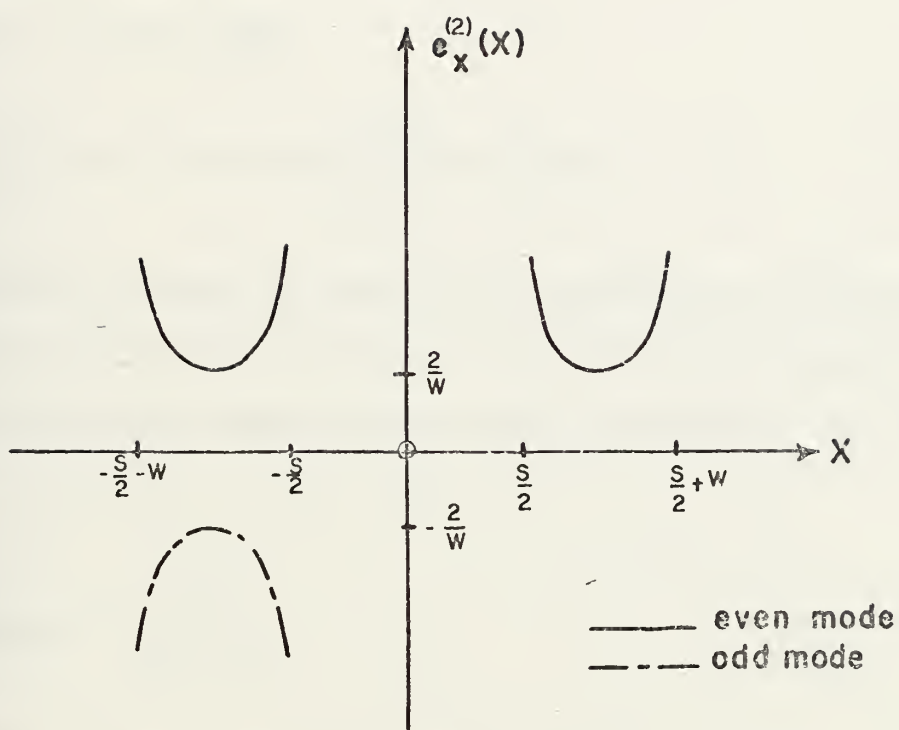


Figure 2.2/1 Assumed Electric Field Component in x-direction vs. x for Even and Odd Mode on Coupled Slot Lines

The Fourier transform of (2-22a) is given in (2-23a) as $E_x^{(2)}(\alpha)$. Then the Fourier transforms of the electric field in (2-28) become for the even mode

$$\begin{aligned} E_{xe}^{(2)}(\alpha) &= \left(e^{j\alpha \frac{S+W}{2}} + e^{-j\alpha \frac{S+W}{2}} \right) E_x^{(2)}(\alpha) \\ &= 2 \cos\left(\alpha \frac{S+W}{2}\right) \cdot E_x^{(2)}(\alpha) \end{aligned} \quad (2-28a)$$

and for the odd mode

$$E_{xo}^{(2)}(\alpha) = +j2 \sin\left(\alpha \frac{S+W}{2}\right) \cdot E_x^{(2)}(\alpha) \quad (2-28b)$$

Another change to adapt the formulation of Section 2.1 for the coupled line analysis is necessary in equation (2-24); since the total time average power surrounding the transmission lines is now due to two lines

$$Z_{0o,e} = \frac{V_0^2}{P_{avg\ o,e}} \quad (2-29)$$

for the odd and even mode respectively.

Beyond these no further major modifications are necessary to use the previously developed theory and computer programs. In the following discussion only results using a field approximation (2-28a) and (2-28b) are presented. There are two reasons for this: a) the approximation of equations (2-22) was found to be superior to (2-20) in Section 2.1

b) the use of a second order approximation became prohibitive for the dispersion characteristic of coupled slots since the amount of computer time increased tremendously due to the necessity of using a more sophisticated numerical integration scheme (details in Section 5). Besides, the time average power computation uses only a first order approximation anyway.

Figures 2.2/2a-b show now an example of the numerical results for the dispersion characteristics and the characteristic impedances. These results are basically new in the literature and only a partial comparison with other results is possible. A quantitative comparison e.g. between these odd mode line parameters and the quasi-static parameters calculated by Davis et al. in Reference 7 was made and is shown in Figure 2.2/3 for $W/D = 1.0$ — or in the notation of Reference 7, $t = S$ — at frequencies of 1, 3 and 5 GHz. Good agreement is found for the lower frequency range. Note that the characteristic impedance of a CPW is one half of Z_{0o} (odd mode characteristic impedance) for equal slot widths.

A qualitative check on these results can be made by investigating the even mode characteristic impedance in the limiting case as the separation between the slots becomes very small. One expects that the even mode characteristic impedance Z_{0e} will be close to one half of Z_0 , where Z_0 is the characteristic impedance of a single slot whose width is twice the width of the slot in the coupled structure.

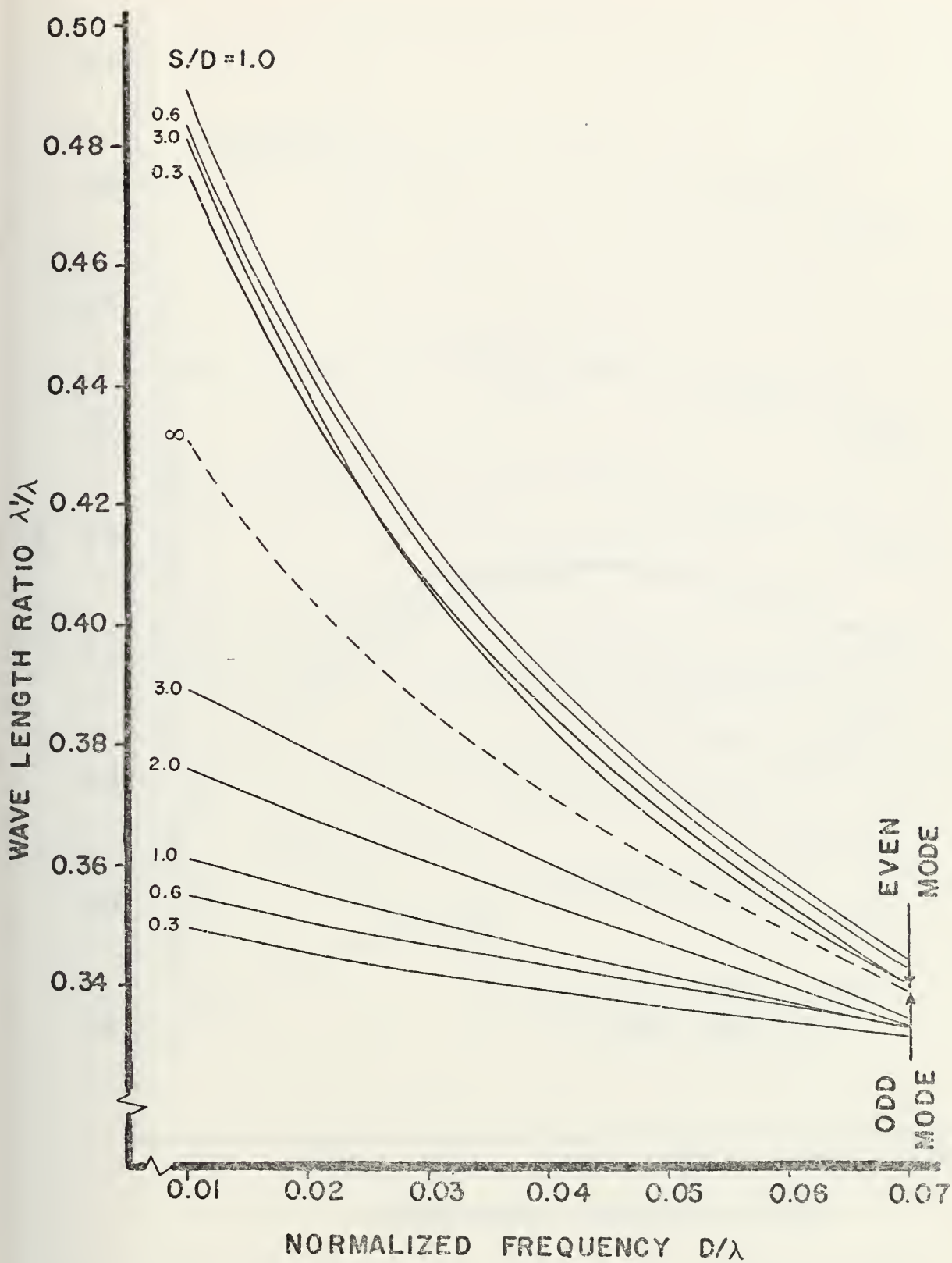


Figure 2.2/2a Even and Odd Mode Dispersion Characteristics for Coupled Slots with $W/D = 0.4$ and $\epsilon_r = 16$

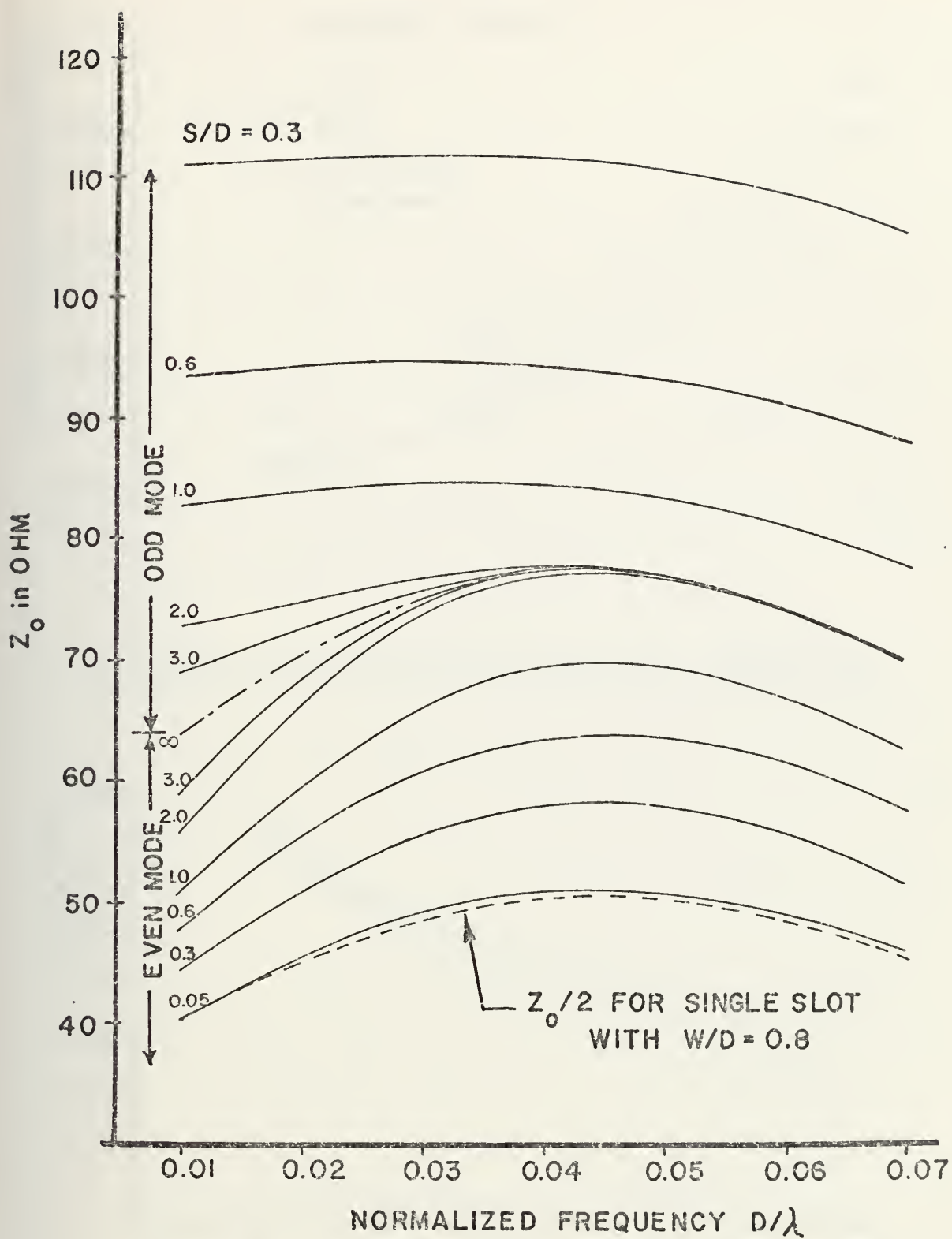


Figure 2.2/2b Even and Odd Mode Characteristic Impedances for Coupled Slots with $W/D = 0.4$ and $\epsilon_r = 16$

PRESENT METHOD

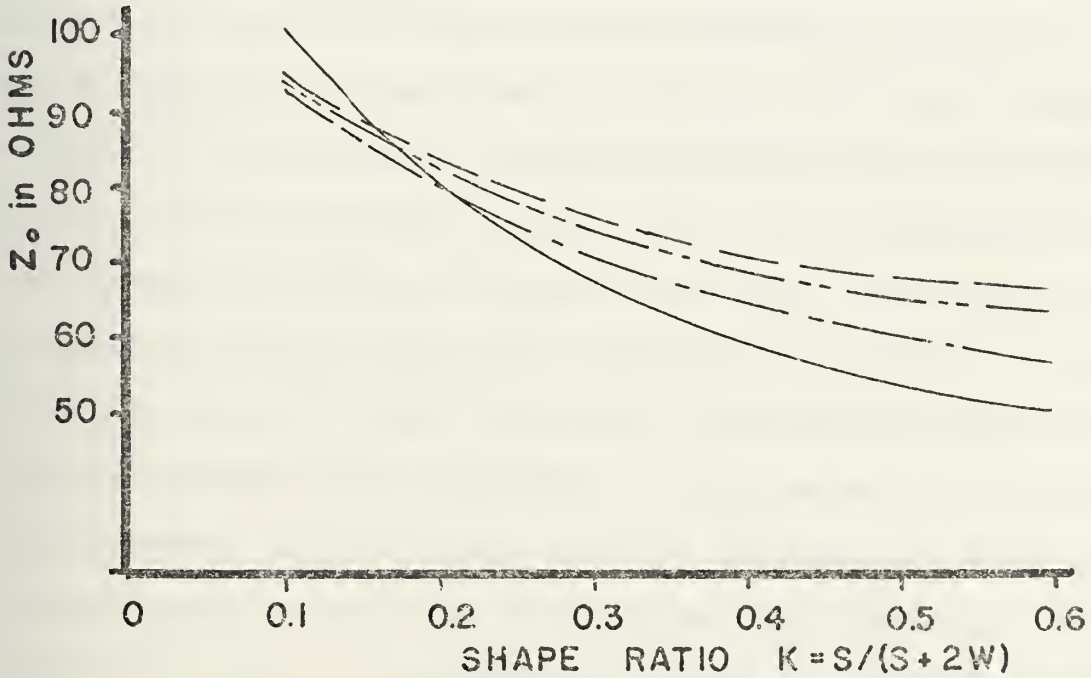
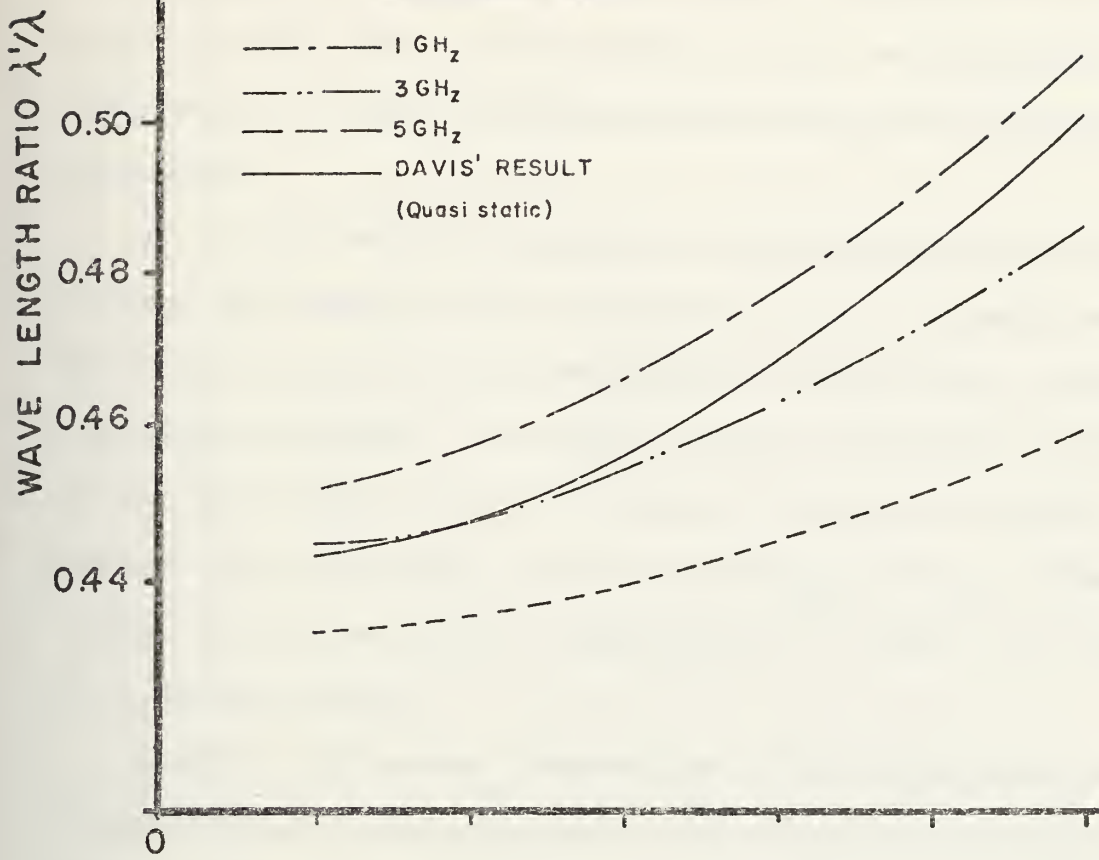


Figure 2.2/3 Dispersion Characteristics and Characteristic Impedance for Coplanar Waveguide with $W/D = 1$ and $\epsilon_r = 10$

The dispersion characteristic for both structures, however, should be the same. This comparison for the impedances is indicated in Figure 2.2/2b and again shows an excellent agreement.

It is interesting to observe the coupling and decoupling between the waves in the two slots as the frequency varies for larger values of the separation constant S/D . With increasing frequency the waves become more closely bound to the slot which means that there is less interaction between the two waves. In this case Z_{0e} and Z_{0o} converge to Z_0 , the characteristic impedance of a single slot with no coupling effect.

Another interesting phenomenon is the fact that for a fixed frequency the wavelength ratio λ'/λ in the even mode first increases and then decreases as S/D is increased from very small to larger values as shown in Figure 2.2/2a. An explanation may be given as follows. For small enough values of S/D the metal strip between the slots has little effect on the propagating wave and the wave propagates as if it were in a slot of width $2 \cdot W/D + S/D$. Increasing the separation between the slots effectively increases the slot width so that the metal strip still has little effect and the wavelength ratio increases. As the separation continues to increase, the two waves start to decouple and behave more as two waves on two slot lines which will finally be totally decoupled. Each wave then propagates on a slot line with width W/D , hence λ'/λ decreases.

However, again an error due to the first order approximation can be observed. Note that for larger values of S/D the wavelength ratios and the characteristic impedances for the two natural modes should merge evenly together towards the respective line parameters for a single slot line. It is observed, however, that for still distinct wavelength ratios for the two modes the characteristic impedances for these modes merge not only together but overcross each other by a small amount. This fact is not shown in Figures 2.2/2a-b for clarity purposes but is presented in Figure 2.2/4 where for one arbitrarily chosen value of normalized frequency and slot width the two impedances for the two modes are displayed as a function of separation. Obviously the error introduced is not very large in this example but tends to increase somewhat for higher frequencies. Since the numerical methods used in this analysis were carefully checked it is believed that this error is caused by neglecting the z -directed component of the electric field in the power calculation. As noted in Section 2.1.1 this component increases with frequency and the approximation caused a slight error in the power calculation on a single slot line in Section 2.1.2.

However the partial comparison of the results with other data given above and an experimental verification described in Section 4 confirms the accuracy of the first order approximation for the frequency ranges considered here.

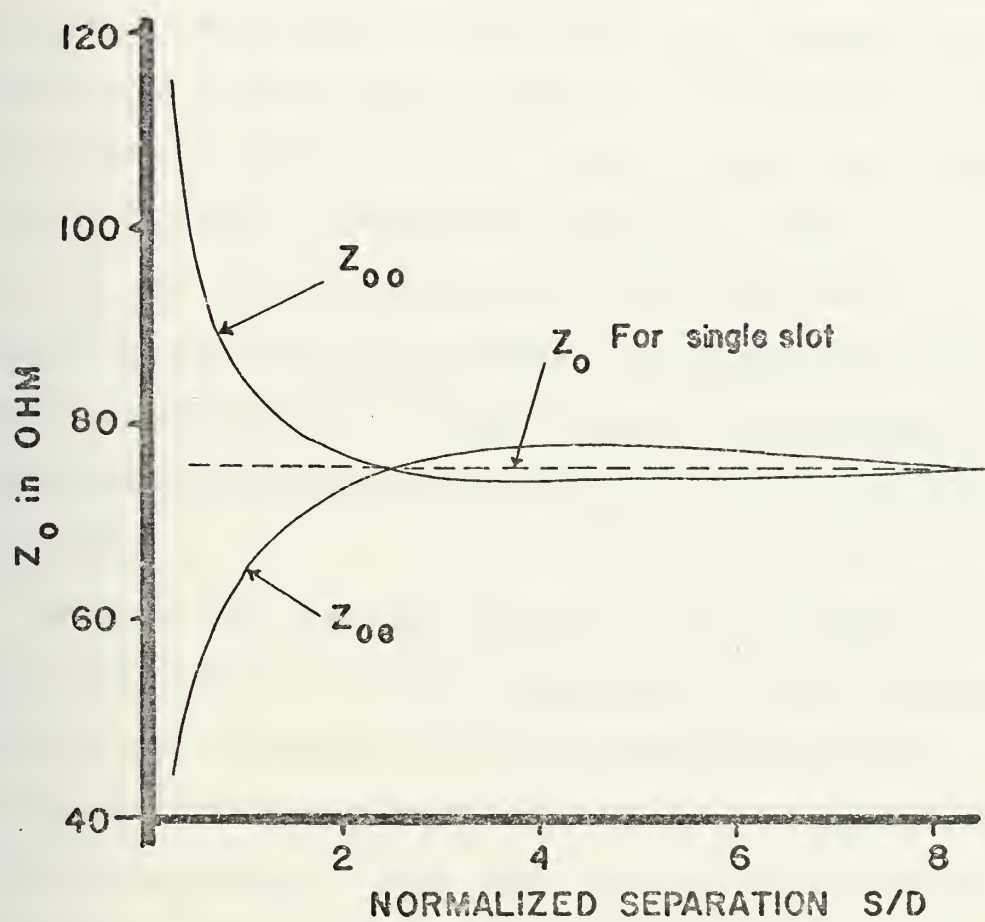


Figure 2.2/4 Even and Odd Mode Characteristic Impedance vs. Separation for $D/\lambda = 0.03$, $W/D = 0.4$ and $\epsilon_r = 16$

2.3 COPLANAR STRIP LINE

The configuration of a coplanar strip line is shown in Figure 1.1/4 and consists of two metal strip conductors placed on one side of the dielectric substrate. The spacing between these two strips is assumed to be constant in the z direction. The permittivity of the substrate confines the fields to regions around the conductors to minimize radiation losses and to make this line suitable for integrated circuit applications. A hybrid mode analysis in the spectral domain is again used to obtain the two important line parameters. However the key for a solution by this method is that the investigator has to have some idea of how the fields on this structure behave. In the study of the slot line an approximation of the electric field across the slot was required and was not difficult to obtain by physical reasoning.

However for the coplanar strip line an approximation of the current density across each strip is more feasible. Hence a set of coupled equations similar to (2-16) is desirable with the roles of current density and electric field interchanged. Note that this inversion was already obtained in the development of (2-16) and is the equation (A-22) in Appendix A give here as

$$\begin{bmatrix} M_1(\alpha, \beta) & M_2(\alpha, \beta) \\ M_3(\alpha, \beta) & M_4(\alpha, \beta) \end{bmatrix} \begin{bmatrix} J_x(\alpha) \\ J_z(\alpha) \end{bmatrix} = \begin{bmatrix} E_x(\alpha) \\ E_z(\alpha) \end{bmatrix} \quad (2-30)$$

According to the scalar product definition and Galerkin's method given in Section 2.1.1 a suitable set of weighting functions are the transforms of the current density distributions. The methods of moments applied to (2-30) and an expansion of the current densities in basis functions yields the second order approximations similar to (2-19)

$$c \int_{-\infty}^{\infty} M_1(\alpha, \beta) |J_x(\alpha)|^2 d\alpha + d \int_{-\infty}^{\infty} M_2(\alpha, \beta) J_z(\alpha) J_x^*(\alpha) d\alpha = 0 \quad (2-31)$$

$$c \int_{-\infty}^{\infty} M_3(\alpha, \beta) J_x(\alpha) J_z^*(\alpha) d\alpha + d \int_{-\infty}^{\infty} M_4(\alpha, \beta) |J_z(\alpha)|^2 d\alpha = 0$$

In the detailed analysis of different approximations in Section 2.1.1 it was found that a first order approximation using only $E_x(\alpha)$ was sufficient. Since the necessary power calculation for the computation of the characteristic impedance will only use a first order approximation, this approach is used throughout the analysis of coplanar strips. Thus $J_x(x) \approx 0$ and (2-31) reduces to the problem of finding a propagation constant β such that

$$\int_{-\infty}^{\infty} M_4(\alpha, \beta) |J_z(\alpha)|^2 d\alpha = 0 \quad (2-32)$$

Again one has the task here to choose a proper basis function. The following functions are reasonable basis functions for the current density component $j_z(x)$ over the strip conductors and have been used extensively in the

analysis of microstrip transmission lines. According to Figure 1.1/4 the left strip extends for x such that $-S/2 - W < x < -S/2$ and the right strip for $S/2 < x < S/2 + W$ respectively. Then the three possible basis functions are

$$j_z^{(1)}(x) = \begin{cases} -1 & \text{left} \\ +1 & \text{right} \\ 0 & \text{elsewhere} \end{cases} \quad (2-33a)$$

$$j_z^{(2)}(x) = \begin{cases} \frac{-1}{\left(\frac{W}{2}\right)^2 - \left(x + \frac{S+W}{2}\right)^2} & \text{left} \\ \frac{1}{\left(\frac{W}{2}\right)^2 - \left(x - \frac{S+W}{2}\right)^2} & \text{right} \\ 0 & \text{elsewhere} \end{cases} \quad (2-34a)$$

$$j_z^{(3)}(x) = \begin{cases} -1 - \left| \frac{x + \frac{S+W}{2}}{\frac{W}{2}} \right| & \text{left} \\ 1 + \left| \frac{x - \frac{S+W}{2}}{\frac{W}{2}} \right| & \text{right} \\ 0 & \text{elsewhere} \end{cases} \quad (2-35a)$$

A schematic presentation of these basis functions is given in Figure 2.3/1.

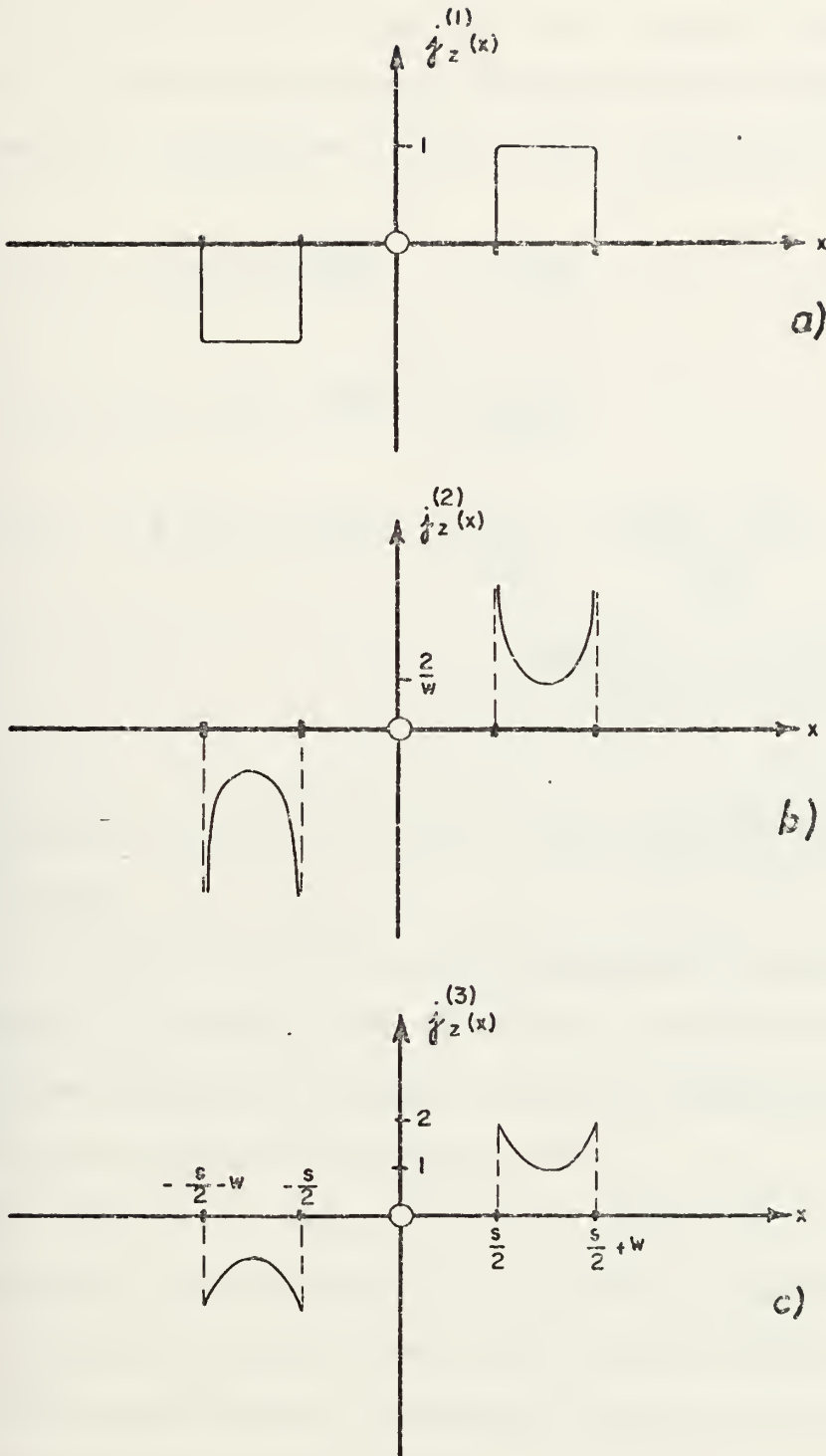


Figure 2.3/1 Assumed Current Density Component in z-Direction
 v_x . x for Coplanar Strip Line
 a) equation (2-33a)
 b) equation (2-34a)
 c) equation 2-35a)

The Fourier transforms can now be easily found by using again the shifting property of the Fourier transformation indicated in equations (2-28). The transforms are given as

$$J_z^{(1)}(\alpha) = j \frac{4}{\alpha} \sin\left[\alpha \frac{S+W}{2}\right] \cdot \sin\left(\frac{\alpha W}{2}\right) \quad (2-33b)$$

$$J_z^{(2)}(\alpha) = j 2\pi \sin\left[\alpha \frac{S+W}{2}\right] \cdot B_0\left(\frac{\alpha W}{2}\right) \quad (2-34b)$$

$$J_z^{(3)}(\alpha) = j \frac{8}{\alpha} \sin\left[\alpha \frac{S+W}{2}\right] \cdot \left[\frac{24}{(\alpha W)^3} + \frac{(\alpha W)^2 - 12}{(\alpha W)^2} \sin\left(\frac{\alpha W}{2}\right) \right. \\ \left. + 3 \frac{(\alpha W)^2 - 8}{(\alpha W)^3} \cos\left(\frac{\alpha W}{2}\right) \right] \quad (2-35b)$$

respectively. (B_0 is the zero order Bessel function of the first kind.)

It is obvious now that the theory and the numerical analysis of the slot line dispersion characteristic needs only minor changes to adapt a solution scheme for a coplanar strip line dispersion characteristic.

To compute the characteristic impedance of this transmission line a reformulation of (2-24) is necessary since the voltage between the two strips is not explicitly known. Again this definition is somewhat arbitrary because of the non-TEM nature of the problem.

Define

$$Z_0 = \frac{2 P_{avg}}{I_0^2} \quad (2-36)$$

where I_0 is the total current on one strip and can be found analytically through an integration of the current densities (2-33a) through (2-35a) with respect to the variable x , yielding

$$I_0^{(1)} = W \quad (2-37)$$

$$I_0^{(2)} = \pi \quad (2-38)$$

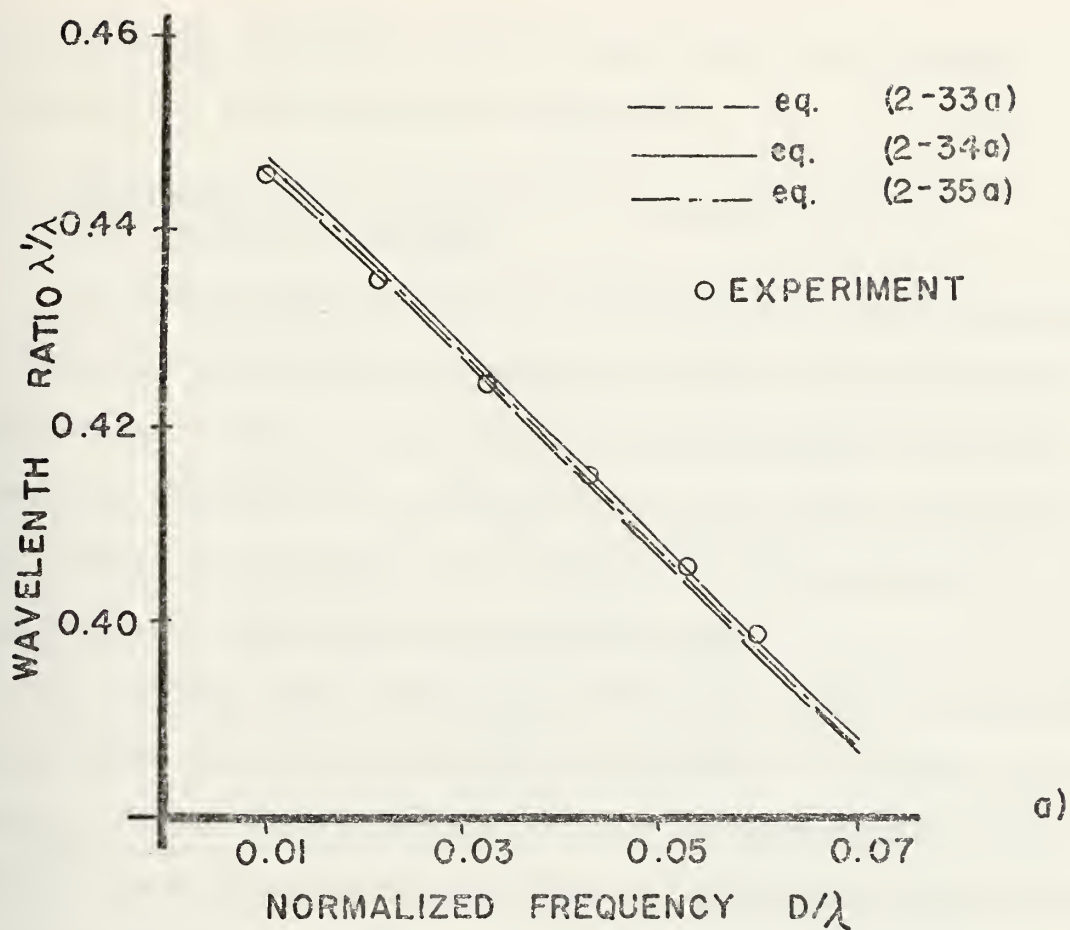
$$I_0^{(3)} = \frac{5}{4} W \quad (2-39)$$

The computation of the time average power flow follows in general the method outlined in Section 2.1.2. Some modifications are necessary, however, and are shown in detail in Appendix B.

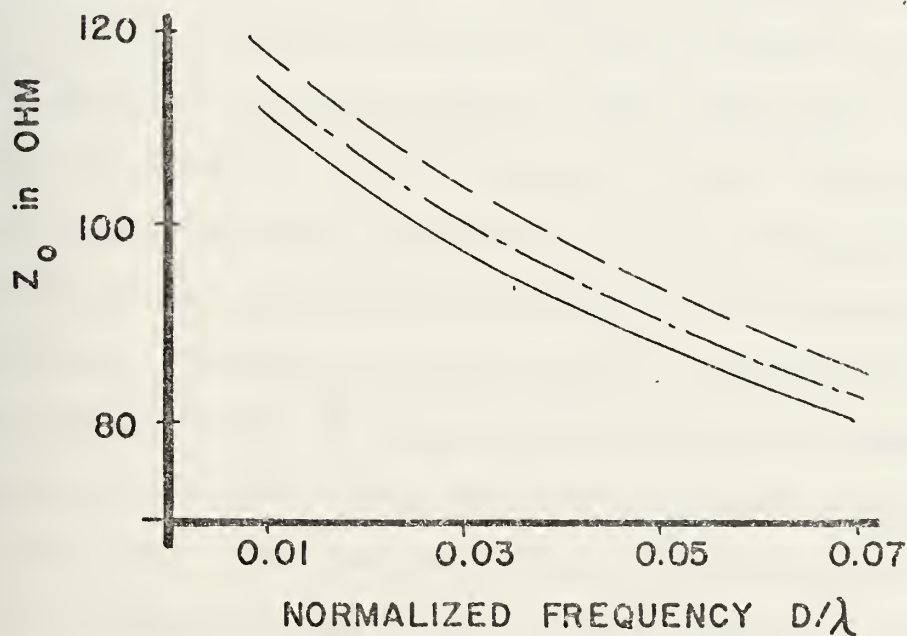
The results for the dispersion characteristic and characteristic impedance with these three different approximations are shown in Figure 2.3/2a-b.

These line parameters are basically new. The wavelength ratio λ'/λ was measured by Luna [Ref. 10] and good agreement is found between the present theory and the experimental data. Preliminary measurements on the characteristic impedance with a time domain reflectometer indicated good agreement with the theory using the current density distribution (2-34a). This work should be extended in the future.

Reasonable agreement for the impedances may be found by comparing the present values with the quasi-static results by Wen [Ref. 4]. As one might expect, however, the present



a)



b)

Figure 2.3/2 a) Dispersion Characteristic and b) Characteristic Impedance for Coplanar Strip Line with $S/D = W/D = 1.0$ and $\epsilon_r = 12$

method yields somewhat larger values due to the finite thickness of the dielectric substrate.

2.4 PERTURBATIONAL ANALYSIS OF A SINGLE SLOT LINE ON A FERRITE SUBSTRATE

The hybrid mode analysis presented so far has been applied to coplanar transmission lines on a dielectric substrate. Since these lines are new and only one complete frequency dependent analysis has been proposed it is not surprising that almost no analysis has appeared yet for coplanar transmission lines on ferrite substrates.

The reasons why these lines offer interesting properties are obvious and will be shortly given here. Ferrites are magnetic oxides with high resistivity, a scalar dielectric constant and a tensor permeability at microwave frequencies. Electromagnetic fields within these ferrites will interact with the precession of electron spins, where this precession is related to the magnetization vector which also precesses about the constant biasing magnetic field. The magnetic bias field determines the orientation and the frequency of the precession and thus can be adjusted to any desired microwave frequency. Depending on the relative polarization and orientation of the RF magnetic field and the magnetization precession to each other, stronger or weaker interaction is obtained. Since the amplitude of the precession decreases due to damping the amount of energy absorption can be quite large for resonance. A simple example of the use of this

phenomenon in ferrites is the isolator. If the RF magnetic field is circularly polarized and has the same orientation as the electron spin, strong interaction is obtained and a maximum of energy is absorbed. This attenuation would be a maximum for a wave travelling in one direction – where the orientation of RF field and electron spin is aligned – and smaller for a wave travelling in the opposite direction. Thus, the amount of absorption is dependent on the propagation direction which provides non reciprocal attenuation. Other non-reciprocal devices are switches, phase shifters, filters, and circulators [Ref. 19, 20].

It is then seen that coplanar transmission such as single or coupled slot lines – or CPW – are bound to be used in ferrite applications since these lines possess a region of elliptically or circularly polarized magnetic RF field, much more pronounced than the quasi TEM microstrip structure. A schematic representation of the fields on a slot line are shown in Figure 2.4/1. For these reasons and the fact that coplanar transmission lines offer advantages over the microstrip line as stated in Section 1, it can be foreseen that nonreciprocal devices for integrated circuits will be demanded. The need for an analysis of these structures becomes apparent. Furthermore, since the coplanar transmission lines as well as the properties of the ferrites are highly frequency dependent any analysis of these structures must be also frequency dependent. In this section an attempt is made to analyze the

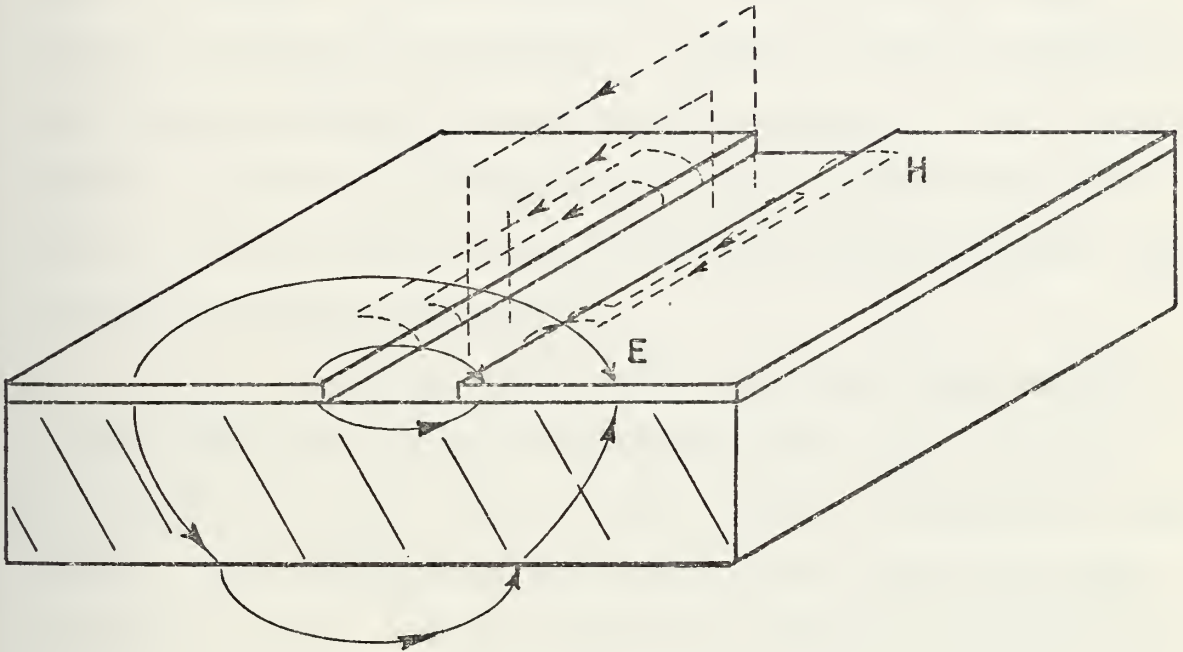


Figure 2.4/1 Field Configuration on Slot Line

slot line on a ferrite substrate by a perturbational method for the propagation constant in the spectral domain. This method can then be easily extended for the analysis of coupled slots and coplanar strip lines by the means described in Sections 2.1-2.3.

2.4.1 Perturbation Expression for the Propagation Constant

Perturbational analyses are useful for the calculation of changes in some quantity, if the problem itself is slightly changed or perturbed. Usually a solution for the unperturbed problem is known and the solution of the perturbed problem is found by assuming that these disturbances are small. Examples for the use of the perturbation theory are given in References 19 and 21.

In the present application the unperturbed problem is the computation of the wavelength ratio λ'/λ — or the propagation constant — of the slot line on a dielectric substrate. The solutions to this problem are known and given in Section 2.1.1. For the perturbed problem the dielectric substrate is replaced by a ferrite substrate with the same dielectric constant. It is assumed that this change in the structure is small enough to allow a perturbational analysis of the change in the propagation constant.

The perturbational expression for the propagation constant due to small changes in the type of material within the guidance structure is given by Helsenajn in Reference 19 as

$$\gamma' + \gamma^* = \frac{j\omega \iint_{\Delta S} [(\epsilon_0 [\Delta\chi_e^e] \cdot \vec{E} \cdot \vec{E}^*) + (\mu_0 [\Delta\chi^e] \cdot \vec{H} \cdot \vec{H}^*)] ds}{\iint_S (\vec{E}^* \times \vec{H} + \vec{E} \times \vec{H}^*) \cdot \vec{a}_z ds} \quad (2-40)$$

where the following nomenclature is used

S total cross section of waveguide

ΔS cross section of waveguide which is perturbed by a change in type of material

\vec{E} and \vec{H} are the electric and magnetic field of the unperturbed structure

$[\Delta\chi^e]$ change in magnetic susceptibility tensor

$[\Delta\chi_e^e]$ change in electric susceptibility tensor

$\gamma' = \alpha' + j\beta'$ propagation constant of perturbed problem

$\gamma = \alpha + j\beta$ propagation constant of unperturbed problem.

Although (2-40) applies in Reference 19 strictly to a closed boundary waveguide it can be shown that this expression also holds for an open boundary structure such as the slot line. This derivation is shown in Appendix C. A particular application of (2-40) for the slot line is now possible and is derived in the next section.

2.4.2 Computation of Perturbation Expression in the Spectral Domain

From the field configurations on the slot line it is seen that the magnetic field is elliptically polarized within the y-z plane. The strongest interaction between the RF magnetic field and the magnetization of the ferrite can then be expected for a magnetic biasing field in the x-direction.

From the discussion of the susceptibility tensor in an ellipsoidal medium in Reference 19 it is seen that the present configuration is similar to that of a thin disk. Since the biasing magnetic field is along the x-axis no demagnetization for this field has to be considered.

However, a demagnetization for the y-component of the RF magnetic field is to be noted. This was the deciding factor in using the external rather than internal susceptibility tensor, where the demagnetization enters into the formulation of the tensor rather than the fields and was found to be much easier to use in the following derivation. According to the small signal approximation of the equation of motion in Reference 19 two radian frequencies can be defined where

$$\omega_y = \omega_0 - N_x \omega_m + N_y \omega_m$$

$$\omega_z = \omega_0 - N_x \omega_m + N_z \omega_m$$

$$\text{with } \omega_0 = -\gamma H_{x0} \quad , \quad \omega_m = -\gamma \frac{M_S}{\mu_0} = 2.8 \cdot 10^6 \frac{M_S}{\text{G}}$$

$$\gamma = -1.4 \cdot g \cdot 10^6 \text{ [Hz/Oe]}$$

g Landé factor

H_{x0} magnetic biasing field in x direction

M_S saturation magnetization

N demagnetization factor (in this application $N_x = N_z = 0$, $N_y = 1$)

Furthermore, define the ellipticity of the normal modes of the uniform precession as $e_o = \sqrt{\frac{\omega_z}{\omega_y}}$ and note that $\omega_r = \sqrt{\omega_y \cdot \omega_z}$ is the Kittel resonance relation. According to the Landau-Lifshitz phenomenological damping formulation [Refs. 19,22] the damping can be defined as $a\omega = -\frac{\gamma\Delta H}{2}$ where ΔH is the linewidth of the ferrite material. The external susceptibility tensor is then

$$[\chi^e] = \begin{bmatrix} 0 & 0 & 0 \\ 0 & \chi_{yy} & \chi_{yz} \\ 0 & \chi_{zy} & \chi_{zz} \end{bmatrix}^e \quad (2-41)$$

where $\chi = \chi' - j\chi''$ and $\chi_{yz} = -\chi_{zy}$.

$$\chi'_{yy} = e_o \frac{\omega_m \omega_r (\omega_r^2 - \omega^2) + \omega_m \omega_r \omega^2 a^2}{DN} \quad (2-41a)$$

$$\chi''_{yy} = e_o \frac{\omega_m \omega_a [\omega_r^2 + \omega^2 (1+a^2)]}{DN} \quad (2-41b)$$

$$\chi'_{zz} = \frac{1}{e_o} \chi'_{yy} \quad (2-41c)$$

$$\chi''_{zz} = \frac{1}{e_o} \chi''_{yy} \quad (2-41d)$$

$$\chi'_{yz} = \frac{j\omega_m \omega [\omega_r^2 - \omega^2 (1+a^2)]}{DN} \quad (2-41e)$$

$$\chi''_{yz} = \frac{j 2\omega_m \omega_r \omega^2 a}{DN} \quad (2-41f)$$

with $DN = [\omega_r^2 - \omega^2 (1+a^2)]^2 + 4\omega_r^2 \omega^2 a^2$.

Equation (2-40) can now be evaluated. Note that the denominator can be expressed as $4 \cdot P_{avg}$ (see also Section 2.1.2) and that $[\Delta\chi_e^e] = 0$ due to the assumption that the dielectric constant remains unchanged, $[\Delta\chi^e]$ is obviously identical to equation (2-41). To evaluate the remainder of the numerator note that the product $[\Delta\chi^e] \cdot \vec{H} \cdot \vec{H}^*$ has to be integrated in the crosssectional area ΔS which extends such that $-\infty < x < \infty$ and $0 \leq y \leq D$. The RF magnetic field is given in terms of the scalar potentials in equations (2-2), (2-5) and (2-6). With these substitutions (2-40) becomes

$$\begin{aligned} \gamma' + \gamma^* = \frac{j\omega \mu_0}{4 P_{avg}} \int_{-\infty}^{\infty} \int_0^D & [\chi_{yy} (\pm \beta \frac{\partial \psi_2}{\partial y} - \omega \epsilon_2 \frac{\partial \phi_2}{\partial x})^2 \\ & + 2\chi_{yz} k \frac{\partial \psi_2}{\partial y} (\mp j\beta \frac{\partial \psi_2}{\partial y} + j\omega \epsilon_2 \frac{\partial \phi_2}{\partial x}) \\ & + \chi_{zz} k^2 (\psi_2)^2] dy dx \end{aligned} \quad (2-42)$$

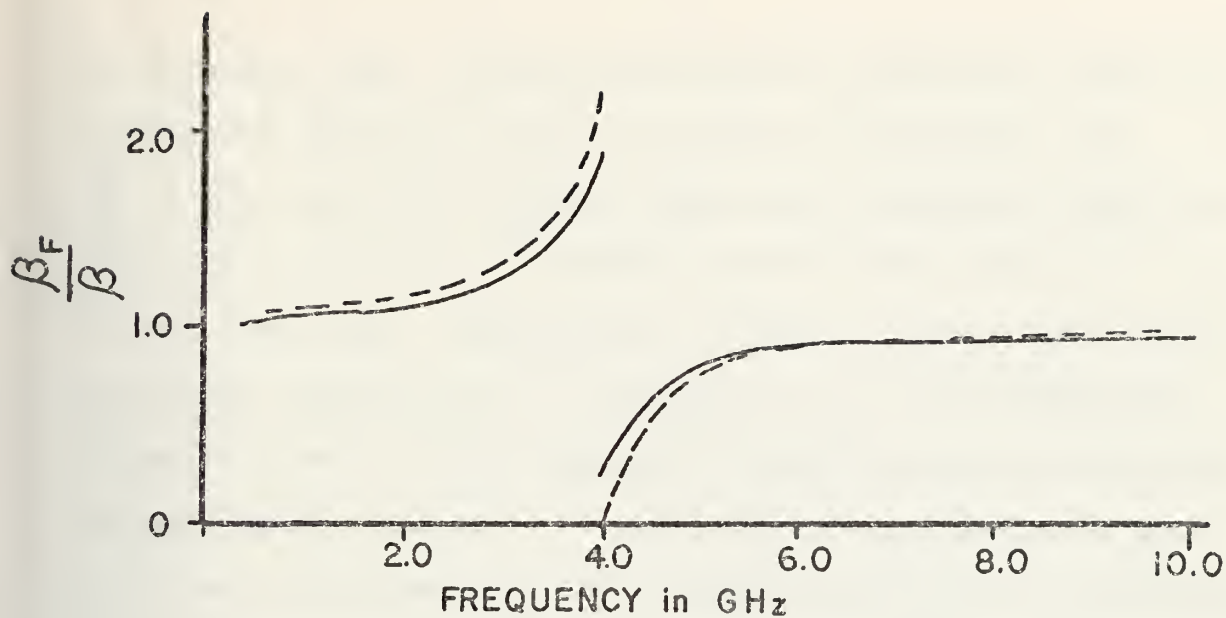
The upper and lower signs denote waves traveling in the negative and positive z-direction respectively.

This double integral is transformed via Parseval's relation [Ref. 15] into the spectral domain, the integration with respect to y computed analytically and the remaining single integration is performed numerically on a digital computer. Here again use is made of the fact that the

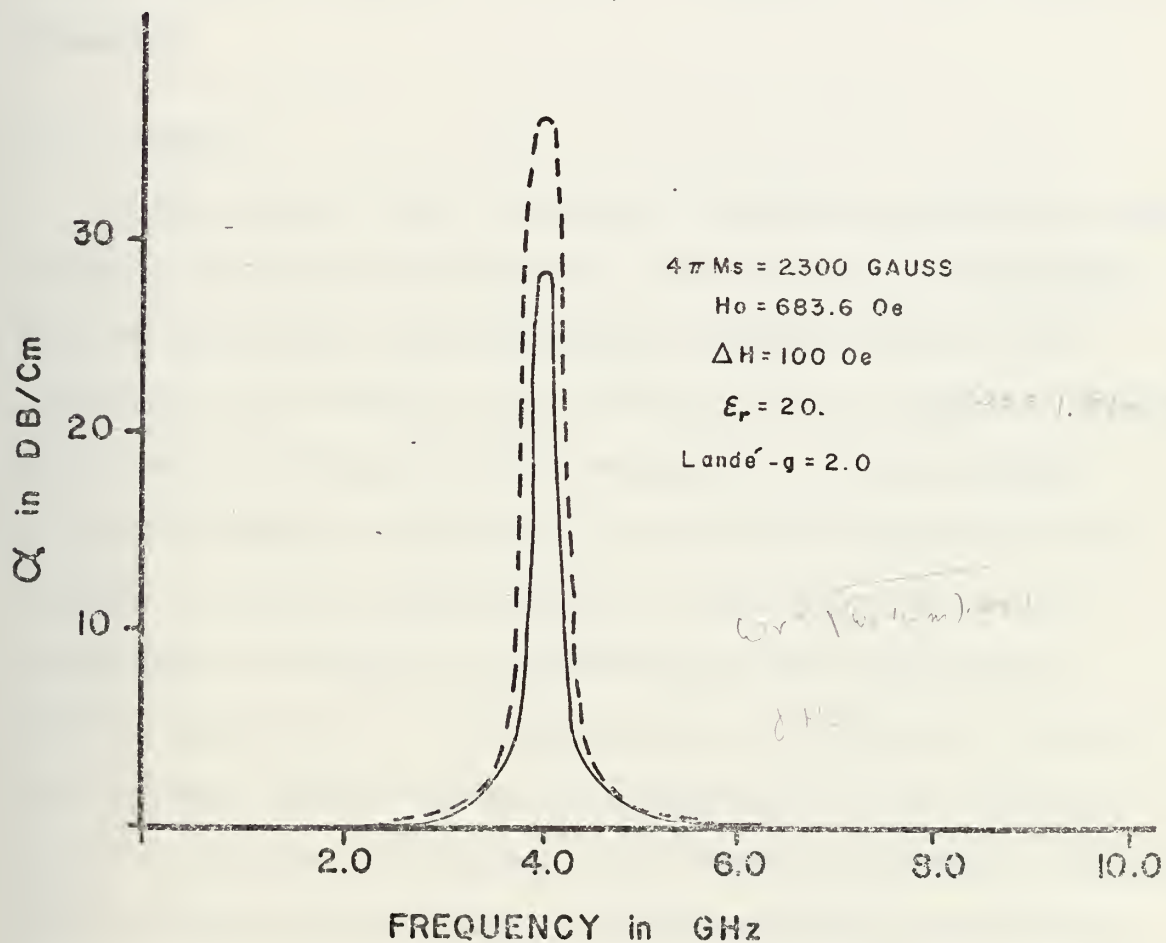
transforms of the scalar potentials are known after one has solved for the propagation constant β according to Section 2.1.1. The time average power flow P_{avg} is computed as explained in Section 2.1.2. Some details of the derivation leading to this single integral are shown in Appendix D, the method is the same as outlined in Sections 2.1 through 2.3.

This perturbational analysis was carried out for an arbitrarily chosen set of parameters, such that resonance occurred at 4 GHz. Figure 2.4/2 shows the result of this calculation where β_F/β represents the ferrite phase constant normalized by the pure dielectric phase constant. The magnetic biasing field of $H_{x0} = 683.6$ Oe was directed into the positive x direction. The material constants are $4\pi M_S = 2300$ Gauss, $\Delta H = 100$ Oe and $\epsilon_r = 20$.

This result in Figure 2.4/2 can be only qualitatively checked with results for similar structures for which a theory has been verified by experiment. Similar to the propagation constant for a ferrite filled parallel plane waveguide with transverse magnetization [Ref. 2] it is seen that there are two regions of propagation, below and above the resonance frequency, separated by a region of high attenuation. It is noted that this attenuation is dependent on the direction of propagation. Another qualitative comparison can be made here with the resonance isolator described in Reference 19. Both waves traveling in either direction are attenuated at resonance, although one not as much as the other. According



a)



b)

Figure 2.4/2 a) Propagation Constant Ratio and
b) Attenuation for Waves Traveling on a Slot
Line with Ferrite Substrate in +z and -z (dashed)
Direction

to Helszajn [Ref. 19] optimum forward attenuation does not correspond exactly to optimum reverse attenuation for $\chi_{yy}^e \neq \chi_{zz}^e$, since the normal modes are in general elliptically polarized. Due to the demagnetization described above this is the case here. Furthermore it must be noted that for the resonance isolator not to attenuate one of the propagating modes, the ferrite slab should be placed close to the center at some optimum position. But here the physical nature of the slot line determines an offcenter position of the ferrite if the conductor plane in $y = D$ is thought of as a line of symmetry.

2.5 SUMMARY

A new method for a frequency dependent analysis of open boundary coplanar transmission lines has been formulated. The two important line parameters, phase velocity and characteristic impedance, are derived from a complete hybrid mode analysis through scalar potential functions which satisfy Helmholtz's equation. This P.D.E. is solved by a Fourier transform technique and a matching of boundary conditions in terms of the electric field and current density components. The application of Galerkin's method in the spectral domain and an approximation of the electric field or current density by basis functions permits a solution for the phase velocity to any desired degree of accuracy. Through the application of Parseval's theorem to the integral of the complex Poynting vector in the space domain the evaluation of time average power flow on the waveguide

structure in the spectral domain is feasible and allows the computation of the characteristic impedance of the line. The often cumbersome inversion of a Fourier transform is thus avoided.

The only other existing analysis of a single slot line, Cohn [Ref. 3], has been numerically verified by a surprisingly close agreement between these two theories which are radically different. The present theory also provides new and more detailed information about the power density on the slot line structure.

The formulation of the problem is so general that a simple change in the assumed field distribution yielded a complete analysis of two coupled slot lines. The data obtained is new and will be of major importance for the microwave industry in the design of slot line filters and couplers. Wherever a comparison with related theories was possible excellent agreement was found. Another modification of the existing theory provided the complete analysis of the coplanar strip transmission line. To some extent a comparison with experimental data was possible and showed a very good agreement.

A perturbational spectral domain method for the analysis of the propagation constant of a coplanar transmission line on a ferrite substrate was developed and applied to the specific example of a slot line. An experimental verification was not performed.

The spectral domain technique is relatively straightforward in concept, but extensive algebraic manipulation is required to achieve computational efficiency. However, once the boundary value problems of Helmholtz's equation is solved in terms of electric fields and current densities at the air-metal-dielectric interface, any coplanar waveguide structure can be easily analyzed.

3. CLOSED BOUNDARY STRUCTURES

Lumped circuit elements are no longer of any practical use at microwave frequencies. Losses due to the increased resistance by the skin effect or due to radiation effectively terminates the use of such elements. A common alternative is the construction of circuit elements by sections of transmission lines of which the quarter wave transformer is one of the most important examples. Using standard transmission lines such as coaxial cables or rectangular waveguide these lines are mostly short circuited at one end to keep radiation losses to a minimum. The short circuit can be assumed in most cases to be ideal. This may be true and practical for closed boundary structures but is not easy to implement with an open boundary structure such as the slot-line. If a slot-line is simply terminated within the conducting plane by ending the slot it is found that a considerable amount of energy is stored behind this short circuit due to surface currents flowing around this end. This indicates that magnetic energy will be stored in this region so that the short circuit is not ideal but rather appears as an inductive reactance at a reference plane coincident with the end of the slot. This effect was first observed by Mariani and Agrios [Ref. 23] during their experimental investigation of slot line filters and later experimentally investigated by Knorr

and Saenz [Ref. 24] who also provided data curves of this so called "end-effect" for design purposes. No theory has appeared yet which describes this effect.

Another example of how lumped circuits are replaced by alternative circuits at microwave frequencies is the resonating circuit. Resonating structures are important in the design of filters and oscillators and have been constructed as cavities for rectangular or circular waveguides. For the slot-line to be an alternative transmission line to micro-strip line the use of resonating slots becomes evident for previously mentioned applications. Quarter wave coupled resonating slots and end coupled resonating slots have been presented on an experimental basis by Mariani and Agrios [Ref. 23], but again no theory exists to provide means for the design. The problem here is how to determine the dimensions of a resonating slot such that resonance at some desired frequency occurs which is often the lowest possible frequency. Using the wavelength ratio of the slot line computed in Section 2 for this half wavelength resonator will not yield this information because of the above described end-effect. The wavelength ratio was derived for a transmission line, which extends infinitely in the z -direction (see Figure 1.1/2).

An analysis of these kinds of problems is now proposed in this section. The hybrid mode analysis in the Fourier domain is used again as in Section 2 to provide a complete

frequency dependent solution. To minimize the losses due to radiation the resonating slot section is placed inside a shielding structure; this configuration is schematically shown in Figure 3.1/1.

As a byproduct of this analysis the above cited end effect is solved theoretically. Some further modifications in the derived theory of the resonating slot structure unveils that line parameters such as the dispersion characteristic and the characteristic impedance for shielded coplanar transmission lines can be obtained. As an example results for a single shielded slot line are provided.

An important result of Section 2 is that once the boundary value problem of Helmholtz's equation is solved in terms of the electric fields and surface currents in the plane between the air-conductor-dielectric interface any similar structure can be easily analyzed by minor modifications. This result holds also for the closed boundary structures in this section and will be demonstrated with the example of end coupled resonating slot-lines. This structure can be described by a circuit model, where the elements of this model can be solved for. The result is a solution to an inductive coupling between two serial slot-lines.

Throughout the following analyses in this section it is assumed that the two rectangular waveguides formed by the shielding structures have dimensions such that rectangular waveguide modes are kept below cutoff. The cutoff condition

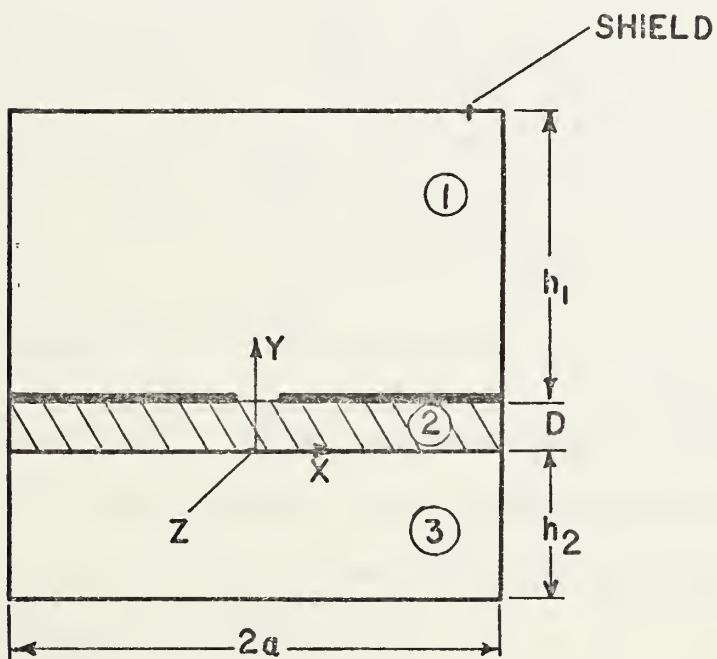
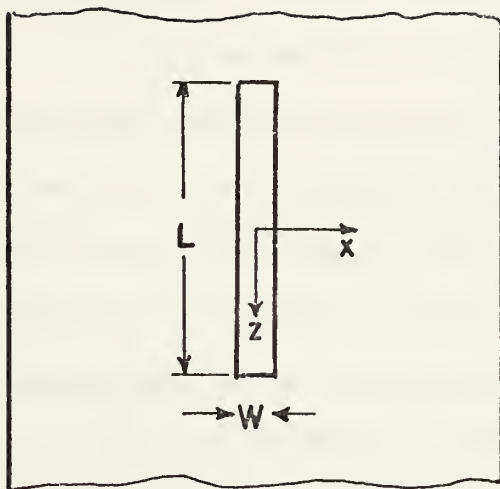


Figure 3.1/1 Shielded Slot Line Resonator

for the waveguide formed by region 1 in Figure 3.1/1 is well known. Besides, if dimensions h_1 and h_2 are kept such that only a TE_{10} limit mode (E field in y direction) could be excited, the lower waveguide formed by regions 2 and 3 will have the lower cutoff frequency due to the dielectric loading and has to be considered only. A cutoff condition was derived by Harrington [Ref. 21] for instance for a partially dielectric-filled rectangular waveguide. A solution is required for a transcendental equation given according to Reference 21 for the lowest possible mode as

$$\frac{k_{x2}}{\epsilon_2} \tan(k_{x2}D) = - \frac{k_{x3}}{\epsilon_3} \tan(k_{x3}h_2) \quad (3-1)$$

$$\text{where } k_{x2}^2 = \omega^2 \epsilon_2 \mu_2 - \left(\frac{\pi}{2a}\right)^2 \quad (3-2a)$$

$$k_{x3}^2 = \omega^2 \epsilon_3 \mu_3 - \left(\frac{\pi}{2a}\right)^2 \quad (3-2b)$$

The subscripts 2 and 3 refer to the regions 2 and 3 in Figure 3.1/1. This equation (3-1) is given here only for completeness and is solved numerically within the computer program described in Section 5.2.

3.1 SINGLE RESONANT SLOT LINE

The schematic of the resonating structure to be analyzed is shown in Figure 3.1/1 where it is assumed that the shielding structure extends for z such that $-\infty < z < \infty$.

The conducting material on top of the dielectric and the surrounding shield is assumed to be perfect and the dielectric material is lossless and isotropic.

Similar to the beginning in Section 2.1 a full mode analysis will require two linearly independent scalar potential functions. The z directed electric and magnetic field components in terms of these potentials may then be written according to References 13 or 21 as

$$E_{zi}(x,y,z) = \left(\frac{\partial^2}{\partial z^2} + k_i^2\right)\phi_i(x,y,z) \quad (3-3)$$

$$H_{zi}(x,y,z) = \left(\frac{\partial^2}{\partial z^2} + k_i^2\right)\psi_i(x,y,z) \quad (3-4)$$

$i=1,2,3$ defining the spatial region according to Figure 3.1/1

$$k_3^2 = k_1^2 = k_0^2 = \omega^2 \mu_0 \epsilon_0 \quad \text{and} \quad k_2^2 = \epsilon_r \cdot k_0^2$$

The transverse field components of the hybrid mode can then be derived through an application of Maxwell's curl equations to (3-3) and (3-4).

Then

$$E_{xi} = \frac{\partial^2 \phi_i}{\partial x \partial z} - j\omega \mu_0 \frac{\partial \psi_i}{\partial y} \quad (3-5a)$$

$$E_{yi} = \frac{\partial^2 \phi_i}{\partial y \partial z} + j\omega \mu_0 \frac{\partial \psi_i}{\partial x} \quad (3-5b)$$

$$H_{xi} = j\omega\epsilon_i \frac{\partial \phi_i}{\partial y} + \frac{\partial^2 \psi_i}{\partial x \partial z} \quad (3-6a)$$

$$H_{yi} = -j\omega\epsilon_i \frac{\partial \phi_i}{\partial x} + \frac{\partial^2 \psi_i}{\partial y \partial z} \quad (3-6b)$$

The scalar potential functions satisfy Helmholtz's equation in the three spatial regions [Ref. 21], thus

$$\nabla^2 \phi_i + k_i^2 \phi_i = 0 \quad (3-7)$$

$$\nabla^2 \psi_i + k_i^2 \psi_i = 0 \quad (3-8)$$

where ∇^2 denotes the three dimensional Laplacian operator in x, y, z coordinates. Two Fourier transforms are now used to transform these three-dimensional partial differential equations into ordinary differential equations which can be readily solved in terms of the boundary conditions.

Define a two dimensional Fourier transform as

$$G(\alpha_n, y, \xi) = \int_{-\infty}^{\infty} \int_{-a}^a g(x, y, z) e^{j(\alpha_n x + \xi z)} dx dz \quad (3-9)$$

Note that the transform with respect to x is a finite transform [Ref. 25], also widely known as a complex Fourier series coefficient.

Some physical reasoning must be used here to determine the discrete transform variable α_n . For the lowest order mode in this resonant slot structure the fields of the

standing waves inside the slot in the z direction are similar to the z directed fields of a traveling wave shown in Figure 2.4/1. Thus, the z directed magnetic field component H_z will be an even function with respect to x and from Section 2.1.1 and the second order approximation it is known that the z directed electric field component E_z is an odd function with respect to x . A distinction in equation (3-9) in sine- and cosine-transforms aids in the following discussion. It is easily seen that if

$$F(n) = \int_{-\pi}^{\pi} f(x) \begin{cases} \cos \\ \sin \end{cases} (nx) dx$$

then

$$\int_{-\pi}^{\pi} f''(x) \cos(nx) dx = -n^2 F(n) + (-1)^n f'(\pi) - f'(-\pi)$$

and

$$\int_{-\pi}^{\pi} g''(x) \sin(nx) dx = -n^2 G(n) + n[g(-\pi) - (-1)^n g(\pi)]$$

So these transforms are expedient for problems in which either the function to be transformed or its derivative is prescribed at the endpoints of the interval. But note that for the above problem at the endpoints $x = -a$ and $x = a$ the tangential electric fields must be zero due to the conducting shield, hence E_{zi} and E_{yi} , or as seen from equations (3-3) and (3-5) ϕ_i and $\frac{\partial \psi_i}{\partial x}$ vanish at these boundaries since $E_{zi} \sim \phi_i$ and $H_{zi} \sim \psi_i$. The transform

variable α_n in (3-9) is thus determined to be

$$\alpha_n = \frac{n\pi}{a} \quad \text{for } n = 0, \pm 1, \pm 2, \dots$$

With these considerations the two dimensional transform of equations (3-3) and (3-4) via (3-9) can be accomplished to obtain

$$E_{zi}(\alpha_n, y, \xi) = (k_i^2 - \xi^2) \phi_i(\alpha_n, y, \xi) \quad (3-10)$$

$$H_{zi}(\alpha_n, y, \xi) = (k_i^2 - \xi^2) \psi_i(\alpha_n, y, \xi) \quad (3-11)$$

Similarly equations (3-5a) and (3-6a) are transformed into

$$E_{xi} = -\alpha_n \xi \phi_i - j\omega\mu_0 \frac{\partial \psi_i}{\partial y} \quad (3-12)$$

$$H_{xi} = j\omega\epsilon_i \frac{\partial \phi_i}{\partial y} - \alpha_n \xi \psi_i \quad (3-13)$$

The y directed components are of no concern in the development.

Define

$$\alpha_n^2 + \xi^2 - k_i^2 = \gamma_i^2 \quad (3-14)$$

then the two Helmholtz's equations in (3-7) and (3-8) are transformed into

$$\left(\frac{\partial^2}{\partial y^2} - \gamma_i^2\right) \phi_i(\alpha_n, y, \xi) = 0 \quad (3-15)$$

$$\left(\frac{\partial^2}{\partial y^2} - \gamma_i^2\right) \psi_i(\alpha_n, y, \xi) = 0 \quad (3-16)$$

It is observed, that the boundary conditions for the tangential electric fields of $y = D + h_1$ and at $y = -h_2$ require $E_x = 0$ and $E_z = 0$, so that certain solutions to (3-15) and (3-16) are eliminated. These conditions are independent of x and z and may be applied in the transform domain as well. The solutions to (3-15) and (3-16) are then

$$\phi_1(\alpha_n, y, \xi) = A^e(\alpha_n, \xi) \sinh \gamma_1(D+h_1-y)$$

$$\phi_2(\alpha_n, y, \xi) = B^e(\alpha_n, \xi) \sinh \gamma_2 y + C^e(\alpha_n, \xi) \cosh \gamma_2 y \quad (3-17)$$

$$\phi_3(\alpha_n, y, \xi) = D^e(\alpha_n, \xi) \sinh \gamma_1(h_2+y)$$

$$\psi_1(\alpha_n, y, \xi) = A^h(\alpha_n, \xi) \cosh \gamma_1(D+h_1-y)$$

$$\psi_2(\alpha_n, y, \xi) = B^h(\alpha_n, \xi) \sinh \gamma_2 y + C^h(\alpha_n, \xi) \cosh \gamma_2 y \quad (3-18)$$

$$\psi_3(\alpha_n, y, \xi) = D^h(\alpha_n, \xi) \cosh \gamma_1(h_2+y)$$

It is to be noted at this point that n may assume the value zero and $-\infty < \xi < \infty$. γ_1^2 may therefore be less than zero for certain values of ξ . Furthermore, since $k_2^2 > k_1^2$ there will be three sets of solutions in equations (3-17) and (3-18) for $n = 0$, namely $\gamma_1^2 < 0$, $\gamma_2^2 < 0$ where trigonometric functions replace all hyperbolic functions; $\gamma_1^2 > 0$, $\gamma_2^2 < 0$ where trigonometric functions replace the hyperbolic functions in spatial region 2 and $\gamma_1^2 > 0$, $\gamma_2^2 > 0$ for which

the solutions are as given above. It can furthermore be seen that these three types of solutions will exist only for $n = 0$. Assume $n = 1$ and ξ^2 assumes its lowest value of $\xi = 0$. For $\gamma_i^2 < 0$ then $\frac{\pi}{a} < k_i$ or $\frac{\lambda_i}{2} < a$. However, to avoid rectangular waveguide modes it is assumed that $\frac{\lambda}{2} > 2a$, thus $\gamma_i^2 > 0$ for $n \pm 1, \pm 2, \dots$ at all frequencies of interest. According to the method of solution outlined in Section 2 the next step is the application of the continuity or boundary conditions at the interfaces between the three spatial regions. These conditions are given in equations (2-14) and (2-15) and apply for this closed boundary structure as well with a minor modification. The last four equations of (2-15) must now include a general dependence on the variable z for the electric field and current density components. A z dependence of $e^{\gamma z}$ is sufficient for a transmission line only. For instance, the current density component in the x direction would now be of the form $j_x(x, z)$, the other components are changed similarly in (2-15). Denote the transforms of these components at $y = D$ as

$$\begin{aligned} E_x(\alpha_n, \xi) &= F\{E_x(x, z)\} & E_z(\alpha_n, \xi) &= F\{E_z(x, z)\} \\ J_x(\alpha_n, \xi) &= F\{j_x(x, z)\} & J_z(\alpha_n, \xi) &= F\{j_z(x, z)\} \quad (3-19) \end{aligned}$$

If these components and the transforms of (2-14) and (2-15) are used with the substitution of the scalar potential

transforms through the solutions to Helmholtz's equations (3-17) and (3-18) it is possible to eliminate again the unknown coefficients A^e through D^h . Details of this extensive algebraic manipulation are shown in Appendix E, the result of which is

$$\begin{bmatrix} M_1(\alpha_n, \xi) & M_2(\alpha_n, \xi) \\ M_3(\alpha_n, \xi) & M_4(\alpha_n, \xi) \end{bmatrix} \begin{bmatrix} E_x(\alpha_n, \xi) \\ E_z(\alpha_n, \xi) \end{bmatrix} = \begin{bmatrix} J_x(\alpha_n, \xi) \\ J_z(\alpha_n, \xi) \end{bmatrix} \quad (3-20)$$

To apply here again the method of moments by Galerkin's method [Ref. 16] in the spectral domain the following definition of the scalar product is used [Ref. 15]

$$\langle f(\alpha_n, \xi), g(\alpha_n, \xi) \rangle = \sum_{n=-\infty}^{\infty} \int_{-\infty}^{\infty} f(\alpha_n, \xi) g^*(\alpha_n, \xi) d\xi \quad (3-21)$$

For the application of Galerkin's method the suitable set of weighting functions is $(E_x(\alpha_n, \xi), E_z(\alpha_n, \xi))$. With this set and through equations (3-21), (3-20) becomes

$$\langle M_1(\alpha_n, \xi) E_x(\alpha_n, \xi), E_x(\alpha_n, \xi) \rangle + \langle M_2(\alpha_n, \xi) E_z(\alpha_n, \xi), E_x(\alpha_n, \xi) \rangle = 0 \quad (3-22)$$

$$\langle M_3(\alpha_n, \xi) E_x(\alpha_n, \xi), E_z(\alpha_n, \xi) \rangle + \langle M_4(\alpha_n, \xi) E_z(\alpha_n, \xi), E_z(\alpha_n, \xi) \rangle = 0$$

The transforms of the field components are not known but can be expanded in terms of basis functions such that

$$E_x(\alpha_n, \xi) = \sum_{i=1}^{\infty} a_i E_{xi}(\alpha_n, \xi) \quad (3-23a)$$

$$E_z(\alpha_n, \xi) = \sum_{i=1}^{\infty} b_i E_{zi}(\alpha_n, \xi) \quad (3-23b)$$

Equation (3-22) can then be written explicitly as

$$\begin{aligned} & \sum_{i=1}^{\infty} a_i \sum_{n=-\infty}^{\infty} \int_{-\infty}^{\infty} M_1(\alpha_n, \xi) E_{xi}(\alpha_n, \xi) E_{xm}^*(\alpha_n, \xi) d\xi \\ & + \sum_{i=1}^{\infty} b_i \sum_{n=-\infty}^{\infty} \int_{-\infty}^{\infty} M_2(\alpha_n, \xi) E_{zi}(\alpha_n, \xi) E_{xm}^*(\alpha_n, \xi) d\xi = 0 \\ & m = 1, 2, 3, \dots \end{aligned} \quad (3-24)$$

$$\begin{aligned} & \sum_{i=1}^{\infty} a_i \sum_{n=-\infty}^{\infty} \int_{-\infty}^{\infty} M_3(\alpha_n, \xi) E_{xi}(\alpha_n, \xi) E_{zm}^*(\alpha_n, \xi) d\xi \\ & + \sum_{i=1}^{\infty} b_i \sum_{n=-\infty}^{\infty} \int_{-\infty}^{\infty} M_4(\alpha_n, \xi) E_{zi}(\alpha_n, \xi) E_{zm}^*(\alpha_n, \xi) d\xi = 0 \\ & m = 1, 2, 3, \dots \end{aligned}$$

Equation (3-24) is still an exact formulation of the resonant problem to which a solution could be found in the following fashion. The coefficients M_1 to M_4 are besides other factors functions of the operating frequency, while the geometry of the structure and therefore the slot length enters through the

basis functions into the calculations. Given a desired frequency of operation the slot length L is changed until the determinant of the coefficient matrix of (3-24) is equal to zero. This still is a rather theoretical way of solving this problem since in (3-24) two infinite sets of basis functions are implied. Any solution will involve the numerical evaluations of the various coefficients, the integrations and other algebraic manipulations so that an approximate solution seems desirable. In Section 2 it was found for the open boundary structure that good agreement between this theory and others or experiments could be obtained if a good choice for a one term expansion of the electric field components was made. If the slot is relatively narrow the experience with the different approximations in Section 2.1.1 suggests the z directed electric field component at $y = D$ may be neglected while the x directed field component at $y = D$ may be approximated such that

$$E_x(x, D, z) = E_x(x, z) \approx e_{x1}(x, z) = e_{x1}^{(1)}(x) \cdot e_{x1}^{(2)}(z) \quad (3-25)$$

where

$$e_{x1}^{(1)}(x) = \begin{cases} \frac{1}{\sqrt{\left(\frac{W}{2}\right)^2 - x^2}} & |x| < \frac{W}{2} \\ 0 & \text{elsewhere} \end{cases} \quad (3-26a)$$

$$e_{x1}^{(2)}(z) = \begin{cases} \frac{1}{2L} \cos \frac{\pi z}{L} & |z| < \frac{L}{2} \\ 0 & \text{elsewhere} \end{cases} \quad (3-26b)$$

The Fourier transform of (3-26a) was already given in equation (2-23a) but is presented here for completeness for the finite transform. The transform of (3-26b) can be found analytically.

The transforms of (3-26) are then

$$E_{x1}^{(1)}(\alpha_n) = \pi B_0\left(\frac{\alpha_n W}{2}\right) \quad (3-27a)$$

$$E_{x1}^{(2)}(\xi) = \frac{\pi \cos\left(\frac{\xi L}{2}\right)}{\pi^2 - (\xi L)^2} \quad (3-27b)$$

where B_0 denotes the zero order Bessel function of the first kind.

It is now possible to obtain a solution for the resonant slot length by varying L such that

$$\sum_{n=-\infty}^{\infty} \int_{-\infty}^{\infty} M_1(\alpha_n, \xi) |E_{x1}^{(1)}(\alpha_n) \cdot E_{x1}^{(2)}(\xi)|^2 d\xi = 0 \quad (3-28)$$

This root finding can be accomplished now by a numerical solution on a digital computer, the details of which are given in Section 5.

A representative graph of a result of this computation is shown in Figure 3.1/2 where the resonant length versus frequency for the lowest resonant mode is displayed. All quantities are scaled by the thickness D of the dielectric

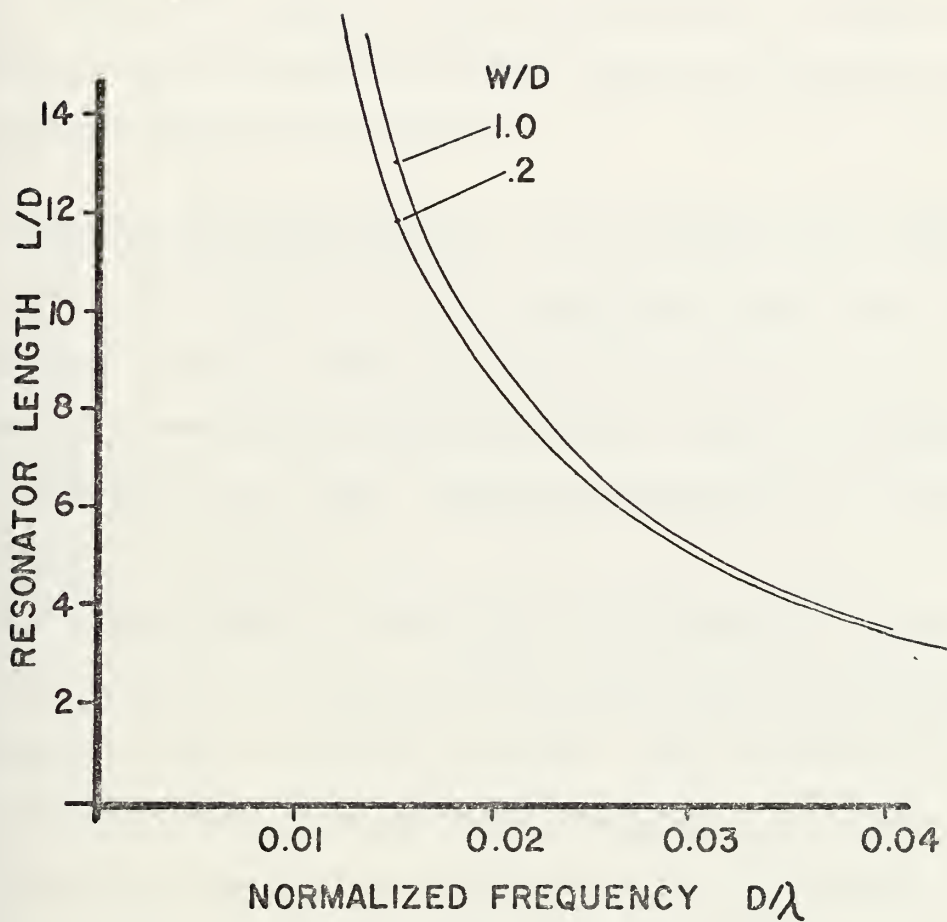


Figure 3.1/2 Resonant Slot Length vs. Normalized Frequency for a Halfwave Slot Line Resonator with $a/D = 5.5$, $h_1/D = h_2/D = 8.0$ and $\epsilon_r = 20$

substrate which makes these results more versatile for any applications. These results are new and cannot be compared with any values resulting from other theories. However, values for the resonant length by this method are used to compute, theoretically, the end effect of a shorted slot line. Very good agreement with experiments is found which substantiates the validity of the theory and suffices as an experimental verification.

3.2 DISPERSION CHARACTERISTIC AND CHARACTERISTIC IMPEDANCE

After the results for the resonating slots were obtained a thorough review of the involved formulas led to the following investigation which analyzes the line parameters for a shielded slot line. These parameters are of importance for mainly two reasons.

The first reason is that for a theoretical analysis of the end effect of a single shorted slot-line the propagation constant of this line must be known. But so far only the open boundary slot line has been analyzed. An approximation could certainly be made in assuming that the boundary walls are far enough removed so that their effect on the slot line is negligible allowing the calculation of the end effect with the open boundary propagation constant. But for reasons of completeness line parameters for the shielded line should be involved to provide for studies on the effect of shields on the line parameters.

This effect now provides the second reason. If the slot-line is to be used in integrated microwave circuits physical dimensions will in general be small. Cohn noted in Reference 3 that the permittivity of the dielectric substrate must be sufficiently large to confine the wave to the slot and to minimize radiation losses. However, from the graph of the power density in the neighborhood of the slot shown in Figure 2.1/4b it is seen that even for $\epsilon_r = 16$ a substantial amount of power is found for distances of some multiples of slot width away from the center. Hence, it can be anticipated that a shielding structure around the slot line seems desirable in some applications to comply with the miniaturization of microwave circuits. Since no analysis of a shielded slot-line has appeared yet in the literature the following study is another contribution towards a complete investigation of coplanar transmission lines. The method used follows exactly the one described in Sections 2.1.1 and 2.1.2.

A careful comparison of the equations used in Section 3.1 for the resonant slot and those used in Section 2.1 for the open boundary slot line reveals that only slight modifications are necessary to adapt the theory in Section 3.1 for an analysis of shielded coplanar transmission lines, shown by the example of a single slot-line.

If the general scalar potential function $\phi(x,y,z)$ in equation (3-3) is replaced by $\phi(x,y)e^{+\gamma z}$ which accounts for a traveling wave in the negative z direction it is found

that equations (2-1) to (2-8) are equivalent to (3-3) to (3-8) if the partial differentiation with respect to z is accomplished, provided a similar replacement for $\psi(x,y,z)$ of course. Now define the finite Fourier transform

$$F_n\{\phi(x,y)\} = \phi(\alpha_n,y) = \int_{-a}^a \phi(x,y) e^{j\alpha_n x} dx \quad (3-29)$$

where α_n is determined by the same considerations stated in Section 3.1.

The Helmholtz's equations for the scalar potential functions are then

$$\left(\frac{\partial^2}{\partial y^2} - \gamma_i^2\right) \phi_i(\alpha_n,y) = 0 \quad (3-30)$$

$$\left(\frac{\partial^2}{\partial y^2} - \gamma_i^2\right) \psi_i(\alpha_n,y) = 0 \quad (3-31)$$

$$i=1,2,3$$

where for the lossless case $\gamma = j\beta$ and $\gamma_i^2 = \alpha_n^2 + \beta^2 - k_i^2$. Hence equations (2-10) and (2-11) are obtained from (3-15) and (3-16) if ξ is replaced by β . Similarly equations (3-10) through (3-13) hold for the transmission line problem if this replacement is carried out there. But then it is observed that an extensive algebraic manipulation towards a solution like that of Section 2.1 can be avoided since all equations derived in Section 3.1 up to equation (3-20) and all of Appendix E hold.

The final part of the formulation is then obvious. To solve for β Galerkin's method is applied again, which requires the scalar product to be defined as

$$\langle f(\alpha_n), g(\alpha_n) \rangle = \sum_{n=-\infty}^{\infty} f(\alpha_n) \cdot g^*(\alpha_n) . \quad (3-32)$$

As in Section 2.1, the electric field components at $y = D$ are approximated by basis functions and used in connection with the above scalar product definition on equation (3-20) to obtain the set of simultaneous equations. The zero of the determinant of the associated coefficient matrix will provide the desired propagation constant β . The details are by now familiar and given in Section 2.1.1.

A first order approximation was used to obtain a solution where $E_z(x,D) \approx 0$ and $E_x(x,D) = E_x(x)$ was given by equation (2-22a). A representative result and comparison with an open boundary slot line is given at the end of this section.

Inspired by the experience that only minor modifications were necessary to adapt equations from Section 3.1 for a solution of the shielded slot line, the following investigation is determined to evaluate the second line parameter, the characteristic impedance, whose definition is given in equation (2-24). The time average power flow on the shielded slot line can be computed according to equation (2-26) as

$$P_{avg} = \frac{1}{2} \operatorname{Re} \int_{-h_2}^{h_1+D} \int_{-a}^a \{ \omega \mu_0 \beta [(\frac{\partial \psi}{\partial x})^2 + (\frac{\partial \psi}{\partial y})^2] + \omega \epsilon \beta [(\frac{\partial \phi}{\partial x})^2 + (\frac{\partial \phi}{\partial y})^2] + (\beta^2 + k^2) (\frac{\partial \phi}{\partial y} \frac{\partial \psi}{\partial x} - \frac{\partial \phi}{\partial x} \frac{\partial \psi}{\partial y}) \} dx dy . \quad (3-33)$$

This formulation applies to the spatial domain and cannot be computed since the scalar potential functions are not known in this domain. Through the use of Parseval's relation [Ref. 15] it is possible, however, to transform this expression into the spectral domain where the scalar potentials are known after the propagation constant β is solved for.

Due to the finite transform in equation (3-29) the integration with respect to x is transformed via Parseval's relation into an infinite summation, thus (3-33) becomes

$$P_{avg} = \frac{1}{4a} \operatorname{Re} \sum_{n=-\infty}^{\infty} \int_{-h_2}^{h_1+D} \{ -\alpha_n^2 \beta \omega \epsilon |\Phi|^2 - \alpha_n^2 \beta \omega \mu_0 |\Psi|^2 - \beta \omega \mu_0 \left| \frac{\partial \Psi}{\partial y} \right|^2 - \beta \omega \epsilon \left| \frac{\partial \Phi}{\partial y} \right|^2 - j \alpha_n \beta^2 \left(\Phi \frac{\partial \Psi^*}{\partial y} + \frac{\partial \Phi}{\partial y} \Psi^* \right) + j \alpha_n k^2 \left(\Phi^* \frac{\partial \Psi}{\partial y} + \frac{\partial \Psi^*}{\partial y} \Psi \right) \} dy . \quad (3-34)$$

According to the general procedure outlined in Section 2.1.2 each coefficient of this series can be evaluated. The transforms of the scalar potential functions are given by

equations (3-17) and (3-18) where again the transform variable ξ is replaced by the propagation constant β . The simple functional dependence on the variable y allows one to perform the integration in equation (3-34) analytically. Note that each coefficient of the series in (3-34) is actually the sum of three further coefficients which present the power carried in each of the three spatial regions. The details about these are shown in Appendix F.

The final part in the evaluation of the characteristic impedance is shown in Section 2.1.2 and involves only the computation of the slot voltage to obtain the characteristic impedance according to equation (2-24). For programming purposes it should be noted that the computation for the shielded line is easier to perform since a numerical integration is avoided and replaced by a summation. The coefficients in the infinite series of equation (3-34) were found to decay rapidly so that a finite approximation yields good results.

A representative set of curves from this calculation is displayed in Figure 3.2/1a-b where the wavelength ratio λ'/λ and the characteristic impedance Z_0 of the shielded slot-line is compared with the line parameters of an equivalent open boundary slot line for two different slot widths. The cutoff frequency for the lowest order waveguide mode was computed according to equation (3-1) and is in this example in normalized form $D/\lambda_c = 0.0421$.

Several facts can be learned from this comparison.

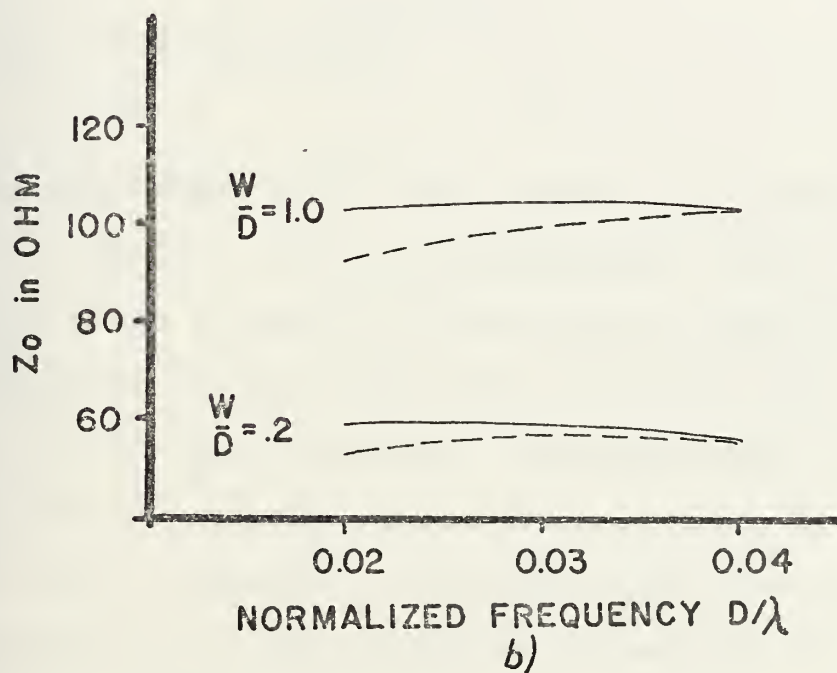
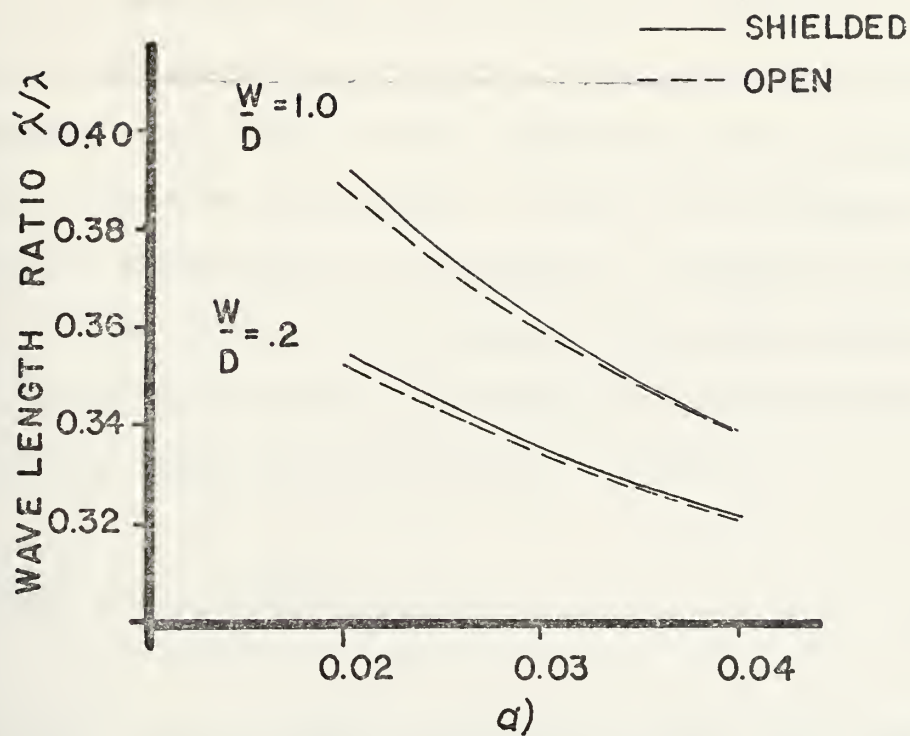


Figure 3.2/1 a) Dispersion Characteristic and b) Characteristic Impedance of a Shielded Slot Line vs. Normalized Frequency with $a/D = 5.5$, $h_1/D = h_2/D = 8.0$ and $\epsilon_r = 20$

It is observed that the difference between the parameters of open and shielded structures differ more for the lower frequency range than for the higher one, where the parameters of both lines merge together. This is no surprise if the following computation is performed. According to Cohn [Ref. 3] the ratio of the voltage $V(r)$ along a semicircular path of constant radius r in region 1 divided by the voltage V directly across the slot can be given as

$$\frac{V(r)}{V} = \frac{\pi}{2} k_c r |H_1^{(1)}(k_c r)| \quad (3-35)$$

where $H_1^{(1)}$ is the Hankel function of first kind and first order and

$$k_c r = j 2\pi \frac{D}{\lambda} \frac{r}{D} \sqrt{\left(\frac{\lambda}{\lambda_r}\right)^2 - 1} \quad (3-36)$$

The Hankel function $H_1^{(1)}(jx)$ asymptotically approaches e^{-x}/x for $x \rightarrow \infty$ so that an approximate result for the voltage ratio in equation (3-35) may be easily obtained. In the above stated example the waveguide walls are at $r/D = 5.5$ in the x direction. Then for $W/D = 0.2$ a voltage ratio of 0.34 is computed for $D/\lambda = 0.02$ and of 0.05 for $D/\lambda = 0.04$. Similarly, the voltage ratio for $W/D = 1.0$ is 0.39 and 0.07 for the normalized frequencies 0.02 and 0.04 respectively at the position of the sidewalls. One may now conjecture that at the lower frequencies a considerable

amount of surface current flows on the sidewalls of the shields at $|x/D| = 5.5$. This in turn means that due to these surface currents more power flow is distributed in the air regions 1 and 3 than is the case for the open boundary line. This conjecture is verified and can be seen in Figure 3.2/1 where the shielded slot line shows a larger wavelength ratio and a larger impedance for the lower frequency range due to this larger amount of power flow in air. The above calculation shows furthermore that the shields will effect a wider slot-line slightly more than a narrow one, due to the closer confinement to the slot region of the latter. Again, this is verified by investigating Figure 3.2/1.

As the frequency increases, the shields have less effect and the line parameters approach those for the open boundary line. However, the upper limit on the frequency of operation is the onset of a rectangular TE_{10} mode in the lower waveguide formed by regions 2 and 3.

3.3 END EFFECT OF SHORTED SLOT LINE

With the results of the preceding sections the end effect of a short circuited slot-line can now be computed analytically. A convenient description of this effect is based upon transmission line theory and can be performed in terms of a normalized reactance. This method was used by Knorr and Saenz [Ref. 24] in their experimental investigation of this effect and is accepted here to provide for a comparison between theory and experiment.

Consider a slot-line which is shorted at one end by ending the slot in the conductor plane. The slot voltage would not only be zero at this short but also at multiples of $\lambda'/2$ along the line if the short were perfect, thus forming a standing wave pattern. Any section on this line between two voltage nulls could be considered then as being a half wave resonator described and analyzed in Section 3.1. If the half wavelength $\lambda'/2$ of a wave on this line is compared with the resonating length L of the resonator for comparable physical dimensions at the same frequency, however, it is found that $\lambda'/2 > L$. This could be expected since merely ending the slot in the plane of the conductor does not provide a perfect short circuit. Surface currents on the conductor beyond the extension of the slot-line increase the electrical length of the line so that the virtual short circuit appears at a distance $\lambda'/4 - L/2$ behind the physical short at the end of the line.

The reactance caused by this effect is then computed as follows. The input impedance of a short circuited transmission line is

$$Z_i = j Z_0 \tan \beta \ell \quad (3-37)$$

where $\beta = 2\pi/\lambda'$ and $\ell = \lambda'/4 - L/2$. The normalized reactance can then be given as

$$X_s = \tan[\pi(1/2 - L/\lambda')] \quad (3-38)$$

where the necessary data is provided by the analytic/numerical methods developed in Sections 3.1 and 3.2. Results of this calculation are shown in Figure 3.3/1a-b and are compared with the experimental data from Reference 24. Although actually the theoretical result for a shielded line is compared with the experiment from an open boundary line, excellent agreement can be seen. It should be noted, however, that the data presented was obtained by assuming that the z-directed electric field component could be neglected. It was found in Section 2.1.1 that this component becomes significant for normalized frequencies above 0.03. This fact may explain why there is a slight discrepancy between theory and experiment in Figure 3.3/1b for $W/D = 0.541$. A solution which accounts for the z-directed field component can be easily established since all necessary computations are given in Appendix E. This work was not performed here, since the amount of computation time on the digital computer increases substantially. The good agreement between theory and experiment adequately verifies the method.

The resulting data from this section are the basis for the theoretical design of microstrip to slot-line transitions which are based so far on the experimental data from Knorr and Saenz [Ref. 24]. Furthermore these results are used in the analysis of the following section.

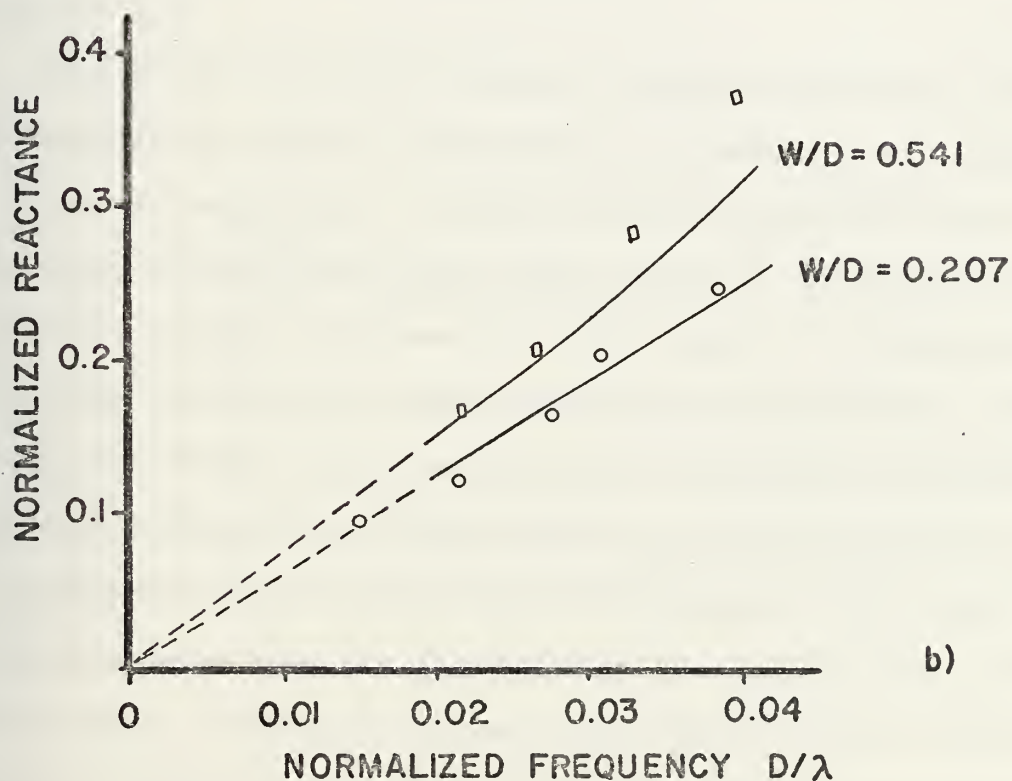
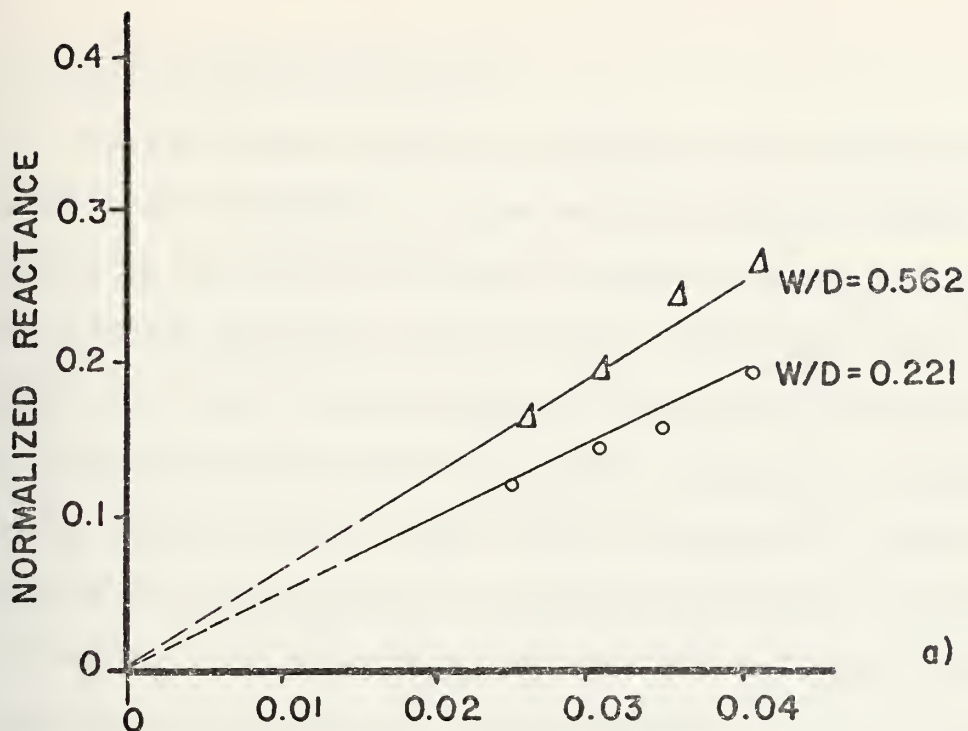


Figure 3.3/1 Short-Circuit Reactance Referred to a Plane Coincident with End of Slot Line for
a) $\epsilon_r = 12$, b) $\epsilon_r = 20$
with $a/D = 5.5$ and $h_1/D = h_2/D = 8.0$

3.4 END COUPLED SLOT-LINES

An important results of Section 2 is that once the Helmholtz's equations in the various spatial regions are solved by the noted boundary matching technique in terms of the surface currents and electric field components in the plane $y = D$ any configuration of conductors in this plane may be solved for the line or resonant parameters by approximating either one of these field quantities. While in Section 2 this feature was demonstrated with the analysis of coupled slot lines and coplanar strip lines, the example presented here shows how still another slot-line configuration may be analyzed by a modification of the theory derived in Section 3.1.

The coupling effect between transmission lines and resonators is used in the design of couplers and filters at microwave frequencies. This fact was mentioned before and is shown theoretically and experimentally in Section 4 for parallel coupling between two slot-lines. An analysis of parallel coupled slot line resonators for instance would basically follow the same procedure outlined in Section 2.2. Another configuration which has not yet been studied is investigated here: end coupled slot-lines. This end coupling effect between the two lines can be described easily in terms of a mutual inductance since it was found in the previous section that a simple short circuited slot line could be represented by an inductance at the end of the line.

The following analysis studies this coupling effect between two end coupled slot resonators in terms of odd and even mode resonant lengths. A simple application of transmission line theory unveils the coupling effect in terms of network parameters such as end inductances and mutual inductance. A physical layout of two end coupled slot resonators is shown in Figure 3.4/1a where the shielding structure is not displayed since the same configuration as in Figure 3.1/1 applies. A circuit model of the two slots with their mutual inductance can then be thought of as given in Figure 3.4/2. The analysis is then as follows.

The impedance of an ideal transmission at any point on this line in terms of the load impedance Z_L , the characteristic impedance Z_0 of the line and the electrical length $\beta\ell$ is given as

$$Z = Z_0 \frac{Z_L + jZ_0 \tan \beta\ell}{Z_0 + jZ_L \tan \beta\ell} \quad (3-39)$$

where β is the propagation constant and ℓ is the length of the line from the load impedance to the point of interest. In this problem the load impedance Z_L is $Z_S = jX_S$, the short circuit reactance due to the end effect which is given as a normalized quantity in equation (3-38). Normalize (3-39) to obtain

$$z = \frac{jx_s + j \tan \beta\ell}{1 - x_s \tan \beta\ell} \quad (3-40)$$

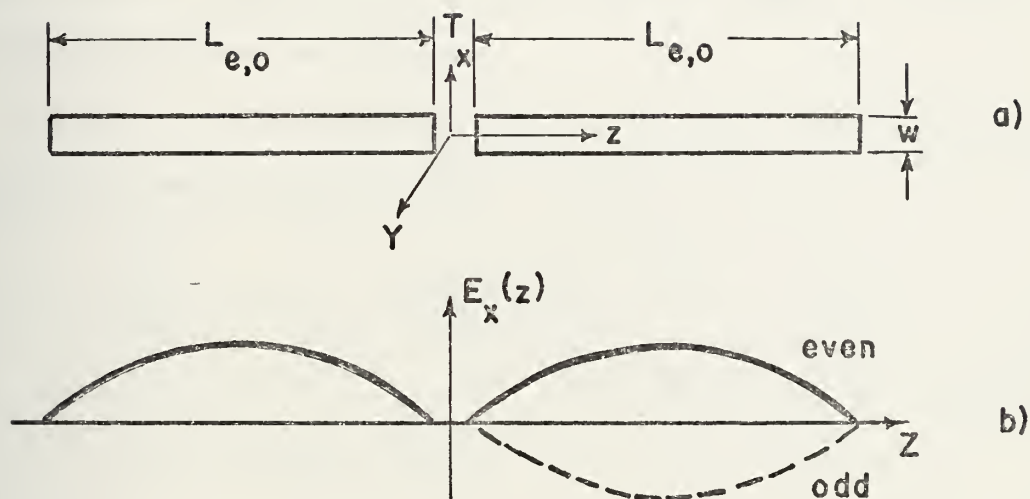


Figure 3.4/1 End Coupled Slot Line Resonators
 a) Physical Layout and Dimensions
 b) Electric Field Component in x -Direction
 vs. z for Even and Odd Mode of Excitation

Since $x_s = \tan(\arctan x_s)$

$$x = \frac{\tan(\arctan x_s) + \tan \beta l}{1 - \tan(\arctan x_s) \cdot \tan \beta l} \quad (3-41)$$

or with the angle-sum relation of the tangent function

$$x = \tan(\arctan x_s + \beta l) \quad (3-42)$$

The network description of the circuit model in Figure 3.4/2 is accomplished as follows.

Using the two current loops in Figure 3.4/2 the corresponding loop equations are

$$ZI_1 + j\omega L_C I_1 \pm j\omega M I_2 = 0 \quad (3-43)$$

$$ZI_2 + j\omega L_C I_2 \pm j\omega M I_1 = 0$$

or after normalizing with respect to Z_0 , the characteristic impedance of the line

$$(jx + jx_c)I_1 \pm jm I_2 = 0 \quad (3-44)$$

$$\pm jm I_1 + (jx + jx_c)I_2 = 0$$

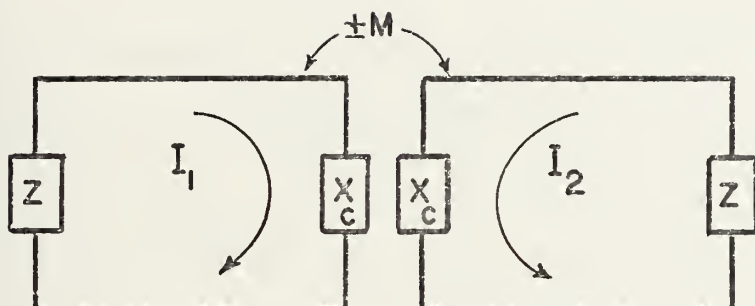


Figure 3.4/2 Circuit Model for End Coupled Slot Resonators

Nontrivial solutions to this set of equations can be obtained for

$$(x+x_c)^2 - m^2 = 0$$

or

$$x = \pm m - x_c \quad (3-45)$$

$$\text{Define } x_e = -m - x_c \quad (3-46a)$$

$$x_o = m - x_c \quad (3-46b)$$

Then the inductances of each circuit loop and the mutual inductance of the coupling region are

$$x_c = - \frac{x_e + x_o}{2} \quad (3-47a)$$

$$\text{and } m = \frac{x_o - x_e}{2} \quad (3-47b)$$

Equations (3-47) could be solved now if x_e and x_o are known. These can be computed with the aid of equation (3-42) using the procedure outlined in Section 3.1 as follows.

Let the even mode of operation be defined as

$$E_x(x, z) = E_x(x, -z) \quad \text{and similarly the odd mode as}$$

$$E_x(x, z) = -E_x(x, -z). \quad \text{A plot of these functions is shown in}$$

Figure 3.4/lb. Given a set of physical parameters and a frequency of operation one computes the resonant lengths

L_e and L_o for the even and odd mode of operation respectively

where the same method for obtaining these applies as outlined in Section 3.1 with equation (3-28) in general. However, due to the different geometry of this problem the approximating transforms of the electric field components in equation (3-27b) are now changed to

$$E_{x1}^{(2)} = 2 \frac{\pi \cos \frac{\xi L_e}{2}}{\pi^2 - (\xi L_e)^2} \cdot \cos(\xi \frac{T+L_e}{2}) \quad (3-46a)$$

$$E_{x1}^{(2)} = j 2 \frac{\pi \cos \frac{\xi L_o}{2}}{\pi^2 - (\xi L_o)^2} \cdot \sin(\xi \frac{T+L_o}{2}) \quad (3-46b)$$

for the even and odd mode respectively while equation (3-27a) remains unchanged. The shifting property of the Fourier transform was used as previously described in detail in Section 2.2.

Once the two quantities L_e and L_o are solved for by a numerical root seeking procedure the even and odd mode reactances are then

$$x_e = \tan(2\pi \frac{L_e}{\lambda} + \arctan x_s) \quad (3-47a)$$

$$x_o = \tan(2\pi \frac{L_o}{\lambda} + \arctan x_s) \quad (3-47b)$$

The final computation for the reactances in the coupling region with equations (3-47) completes this analysis.

A representative set of curves resulting from this calculation is shown in Figure 3.4/3 where the following dimensions of the shielding structure were assumed: $a/D = 5.5$, $h_1/D = h_2/D = 8.0$, $\epsilon_r = 20$ and the normalized frequency of operation is $D/\lambda = 0.0159$, which corresponds for the commercially available thickness of the dielectric $D = 1/16"$ to a frequency of 3 GHz. As one expects, the normalized reactance in the coupling region is essentially that computed for the end effect of a single short circuited slot line, while the mutual inductance describing the coupling effect rapidly decreases as the separation T between the ends of the two lines increases.

Although these results are not confirmed yet by experiment, it is believed that sufficient experimental verification exists in the comparisons of Section 3.3. The analysis of this section is nothing but a simple extension of the same method and the results should again be accurate.

3.5 SUMMARY

The theory developed in Section 2 has been extended for the analysis of shielded coplanar transmission lines and resonators. An exact formulation of the problem via a full or hybrid mode analysis is carried out in the Fourier transform domain where the transforms of dyadic Green's function components are derived. With the application of Galerkin's method in the transform domain and a finite approximation of the electric fields in the conductor plane

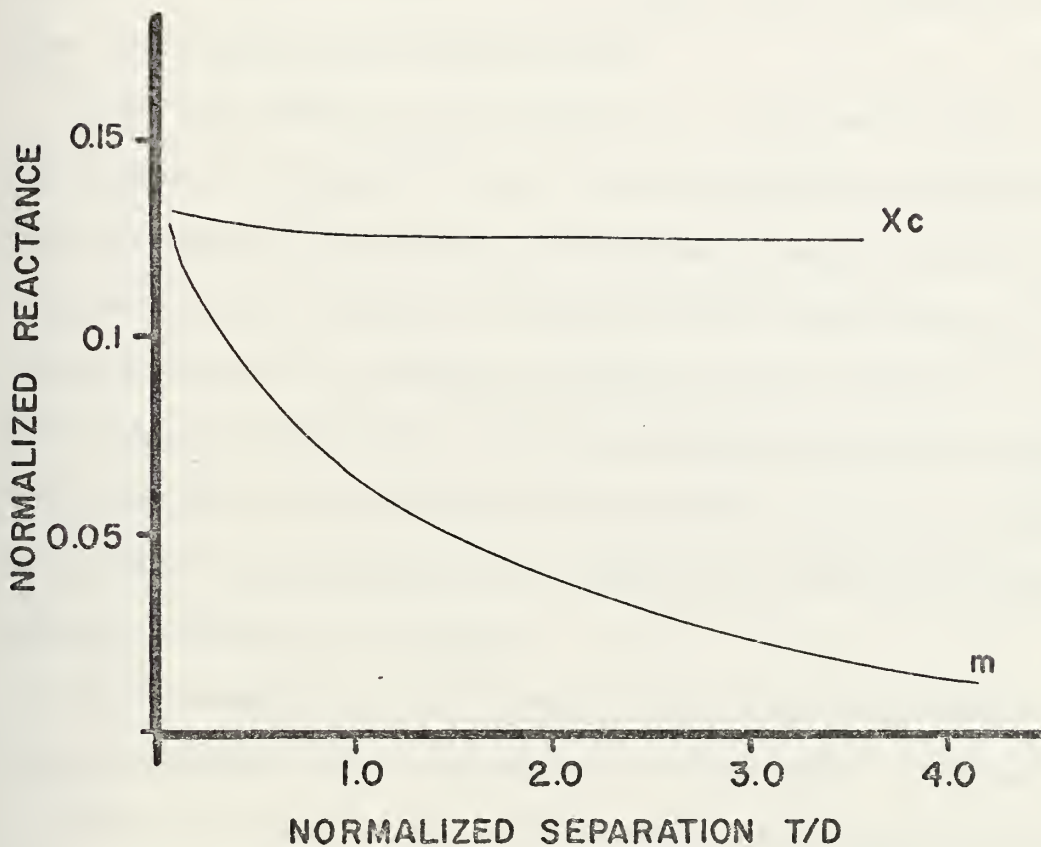


Figure 3.4/3 Reactances x_c and m for Two End Coupled Slot Lines vs. Varying Separation with $a/D = 5.5$, $h_1/D = h_2/D = 8.0$, $W/D = 0.5$, $D/\lambda = 0.0159$ and $\epsilon_r = 20$

above the dielectric substrate a numerical solution to the slot line resonator problem is obtained. Although the primary intention was the analysis of a halfwave resonator an easy modification of the theory unveiled the line parameters of a shielded slot-line. Furthermore, with this data available the end effect of a single short circuited slot-line is theoretically determined.

Once the Helmholtz's equations of the two scalar potential functions are solved for this inhomogeneous boundary value problem through a matching of boundary conditions in the various spatial domains in terms of the transforms of the current density or electric fields at the conductor plane above the dielectric any other configuration may be analyzed. The geometry of the problem encountered enters into the calculation only through the functional behavior of the assumed currents or fields.

As an example of this result the coupling effect between two end coupled slot resonators was analyzed. Furthermore it is by now clear that any coplanar transmission line within the shielding structure may be investigated by simple modifications of the assumed distributions similar to the methods employed in Section 2 for coupled slot-lines and coplanar strip lines.

The theoretical results of this section are new and provide important design information. An experimental verification is always desirable. Therefore, experimental

data for the end effect of a shorted open boundary slot line [Ref. 24] is used in a comparison with the theory developed here for a closed boundary structure. If the shielding walls are moved far enough from the slot it is intuitively clear that this comparison is valid. Excellent agreement is found for various parameters. Since the resonating length of the halfwave resonator as well as the wavelength ratio of the transmission line are involved in this computation, this experimental verification of the theory is quite thorough. Furthermore, shielded transmission line parameters tend to approach the values of the open boundary structure if the shields are further removed or similarly if the frequency of operation is increased. This also justifies the validity of the comparison.

Since modification of this theory for the analysis of the end coupling effect between two slot lines is of a simple nature, further experimental verifications were not believed to be necessary.

Unfortunately design curves for any of the configurations discussed in this section cannot be given for various reasons. Depending on a specific application the dimensions of the shielding structure can vary and hence will influence the line parameters. Line parameters are not only frequency dependent but depend on various considerations in specific applications, for instance in transitions to microstrip lines. So the parameters D/λ , W/D , T/D and ϵ_r are determined by

other constraints. Hence, the computer program proves to be more versatile than design curves and can be used in any specific application.

4. SLOT LINE DIRECTIONAL COUPLER DESIGN

The design of passive components such as filters and couplers in the upper UHF and SHF frequency bands is based on electrical coupling between two or more transmission lines. (Some examples are bandpass filters, comb-line filters, interdigital filters and directional couplers.) The following analysis and experiments will be confined to the study of directional couplers, which are used as attenuators, power splitters or hybrid junctions. However, most commonly directional couplers are used as a sampling device to measure separately the forward and backward waves on a transmission line, where a fraction of the energy traveling in either direction is coupled out such that the energy flow on the main line is not disturbed. Measurements of the reflection can be used in matching loads to a transmission line while the differences between forward and backward sampled power indicates the net power transfer. The most often used structure for the realization of a directional coupler is a four-part network formed by placing two transmission lines close enough to each other so that their fields interact [Ref. 18]. Numerous authors investigated these parallel line couplers with strip or microstrip lines. Although only recently the interest in the studies of these shifted from TEM analyses to frequency dependent solutions, one may say that the design and performance is well understood and known.

Since the introduction of the slot line as an alternative transmission line in 1969 by Cohn [Ref. 3] there has appeared only one publication in the literature about a slot line coupler. An experimental investigation by Mariani and Agrios [Ref. 23] points out that co-directional coupling can be achieved with two parallel slot lines. This fact is no longer surprising since Oliver in Reference 26 showed that contra-directional coupling is possible only for TEM lines, but co-directional coupling occurs if the phase constants for the two natural modes is different. That this is the case for the slot line is clearly seen now in Section 2.2.

Since this thesis provides for the first time the analytical data necessary to describe the coupling effect between these two lines the objective of this section is not only a verification of the theoretical results obtained in Section 2.2 by experiment but is also the first presentation of a co-directional as well as a contra-directional coupler using slot transmission lines.

4.1 THEORETICAL METHODS FOR ANALYSIS

A schematic diagram of the directional coupler to be analyzed is presented in Figure 4.1/1. Two of the terminals of this four-port network are in general connected to a main transmission line while the other two provide the sampled output.

This four port may be described mathematically by either the scattering matrix or the impedance matrix where the

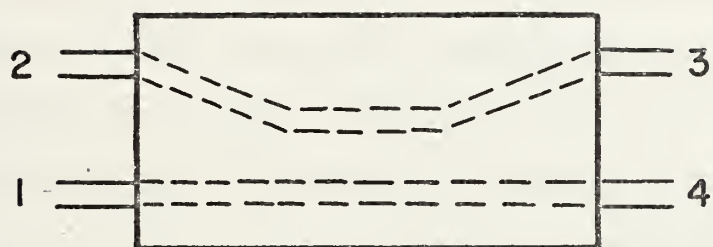


Figure 4.1/1 Schematic of Directional Coupler

elements of the matrices may be found from basic transmission line theory. Both matrix formulations will require in general that the line parameters such as the characteristic impedances and the phase velocities for the two natural modes be known. Since in the design of directional couplers the ratios of power at the various ports are important to determine coupler parameters such as coupling coefficient and directivity, a more explicit formulation in terms of the ratios of the voltages at the various ports seems desirable. All four ports in general will be matched by the characteristic impedances of the connecting transmission lines, thus the load impedances for the four-port network are given by design considerations and the ratios of power can be calculated from the voltage ratios. In the following sections two mathematical methods are derived, an impedance matrix method and a method which explicitly provides the voltage ratios at the various parts as well as the input impedance at port 1. The latter is used for computing the theoretical response of the coupler while the first method has been used as a numerical check by an alternative method.

4.1.1 Impedance Matrix Formulation

According to Zysman and Johnson [Ref. 27] the impedance matrix description of the four-port network is

$$[V] = [Z][I] \qquad (4-1)$$

where $[Z]$ is a 4×4 matrix whose elements are given as

$$Z_{11} = Z_{22} = Z_{33} = Z_{44} = -j \frac{1}{2} (Z_{0e} \cot \theta_e + Z_{0o} \cot \theta_o)$$

$$Z_{12} = Z_{21} = Z_{34} = Z_{43} = -j \frac{1}{2} (Z_{0e} \cot \theta_e - Z_{0o} \cot \theta_o)$$

$$Z_{13} = Z_{31} = Z_{24} = Z_{42} = -j \frac{1}{2} (Z_{0e} \csc \theta_e - Z_{0o} \csc \theta_o)$$

$$Z_{14} = Z_{41} = Z_{23} = Z_{32} = -j \frac{1}{2} (Z_{0e} \csc \theta_e + Z_{0o} \csc \theta_o)$$

where θ_e and θ_o are the even and odd mode electrical lengths of the coupling region.

Assume now that ports 2, 3 and 4 are terminated with some known impedance Z_o and a known test voltage V_1 is supplied to port 1. Let the input admittance at port 1 be denoted by Y_{in} . Then a substitution of these values in (4-1) and a reordering yields

$$\begin{bmatrix} Z_{11}V_1 & -\frac{Z_{12}}{Z_o} & -\frac{Z_{13}}{Z_o} & -\frac{Z_{14}}{Z_o} \\ Z_{12}V_1 & -(\frac{Z_{12}}{Z_o}+1) & -\frac{Z_{14}}{Z_o} & -\frac{Z_{13}}{Z_o} \\ Z_{13}V_1 & -\frac{Z_{14}}{Z_o} & -(\frac{Z_{11}}{Z_o}+1) & -\frac{Z_{12}}{Z_o} \\ Z_{14}V_1 & -\frac{Z_{13}}{Z_o} & -\frac{Z_{12}}{Z_o} & -(\frac{Z_{11}}{Z_o}+1) \end{bmatrix} \begin{bmatrix} Y_{in} \\ V_2 \\ V_3 \\ V_4 \end{bmatrix} = \begin{bmatrix} V_1 \\ 0 \\ 0 \\ 0 \end{bmatrix} \quad (4-2)$$

or in a shorthand notation

$$[A][x] = [y] \quad (4-3)$$

The unknown vector $[x]$ can now be found by standard means for solving a set of simultaneous linear equations. It is seen that the matrices are in general complex. To avoid this complex arithmetic an isomorphism between this system of four complex unknowns and a system of eight real unknowns given by Zurmühl in Reference 28 was used. The imaginary quantities of (4-2) are then treated as real numbers.

However, this method of describing the directional coupler is not very useful for design purposes, since not enough explicit information about the voltage ratios or the input impedance at port 1 is provided by analytical means. A more suitable formulation is given in the next section.

4.1.2 Explicit Coupler Equations

An explicit form of coupler equations was given by Jones and Bolljahn [Ref. 29], where the superposition principle was used. The input at port 1 is considered as the superposition of the two modes of excitation, odd and even. The analysis presented in Reference 29 is restricted in that it applies only for equal phase velocities of the two natural modes. By some algebraic manipulation it is possible to derive a more general form for unequal phase velocities. This calculation follows the general approach outlined in [Ref. 29] and details are not presented here.

Assume that ports 2 to 4 are terminated with

$$Z_0 = \sqrt{Z_{0e} \cdot Z_{0o}} \quad (4-4)$$

Then the ratio of the three voltages at these ports with respect to port 1 are given as

$$\frac{V_2}{V_1} = \frac{\cos \theta_e + j \frac{1}{R} \sin \theta_e}{DE} - \frac{\cos \theta_o + j R \sin \theta_o}{DO} \quad (4-5)$$

$$\frac{V_3}{V_1} = \frac{1}{DE} - \frac{1}{DO} \quad (4-6)$$

$$\frac{V_4}{V_1} = \frac{1}{DE} + \frac{1}{DO} \quad (4-7)$$

where $R = \sqrt{Z_{0o}/Z_{0e}}$

$$DE = 2\cos \theta_e + j(R + 1/R) \sin \theta_e$$

$$DO = 2\cos \theta_o + j(R + 1/R) \sin \theta_o$$

The input impedance at port 1 is given by

$$Z_{in} = Z_0 \frac{1 - A \tan \theta_e \tan \theta_o + j(B \tan \theta_e + C \tan \theta_o)}{1 - A \tan \theta_e \tan \theta_o + j(C \tan \theta_e + B \tan \theta_o)} \quad (4-8)$$

where

$$A = \left(\frac{Z_{0e} + Z_{0o}}{2Z_o} \right)^2$$

$$B = \frac{3Z_{0e} + Z_{0o}}{4Z_o}$$

$$C = \frac{Z_{0e} + 3Z_{0o}}{4Z_o}$$

The necessary data for an evaluation of these equations is provided by the analysis in Section 2.2. The investigation of several configurations of directional couplers is now possible.

4.2 THEORETICAL RESPONSE OF SEVERAL COUPLERS

Some basic design considerations and the theoretical performance of several slot line couplers designed using data from Section 2.2 are discussed in this section. The analysis of the first coupler follows a similar investigation by Dalley [Ref. 30] for strip-line directional couplers. It is seen from equation (4-8) that a perfect impedance match at port 1 will be obtained if $Z_{in} = Z_o$. If any coupling between the lines is assumed then $Z_{0e} \neq Z_{0o}$ and $\theta_e \neq \theta_o$ and an impedance match is obtained only for $\tan \theta_e = \tan \theta_o$ or

$$\theta_o = \theta_e + n\pi \quad , \quad n = 1, 2, 3, \dots$$

A realistic example shows, however, that this design would be almost impractical even for $n = 1$ since a 10 dB coupler at 3 GHz should require a coupling length of approximately 5" for $\epsilon_r = 16$. Such a coupler shows the interesting property of power flowing mainly from port 1 to port 3 while a tenth of the input power is diverted to port 2; port 4 is essentially isolated at the center frequency. This theoretical response is shown in Figure 4.2/1. It can also be seen that this coupler is much narrower in its bandwidth response than a conventional TEM line coupler.

Another coupler design could be based on the fact that the phase velocities of the two natural modes do not differ very much. An examination of equations (4-5) to (4-8) with the assumption $\theta_e + \theta_o = \pi$ for $\theta_e \approx \theta_o$ unveils that one could indeed expect a similar performance for this coupler as for a contra-directional TEM-line coupler, though not an infinite directivity.

A digital computer simulation was performed and the characteristics of this simulated coupler are shown in Figure 4.2/2. This coupler has a wider bandwidth characteristic than the previous one and exhibits directivity of better than 6 dB. Due to the loose coupling the assumption $Z_0 = \sqrt{Z_{0e} \cdot Z_{0o}}$ is still valid and the mismatch at port 1 causes a VSWR of less than 1.08.

Since the objective of this study is an experimental verification rather than an optimum coupler design no attempt to obtain a perfect match was made.

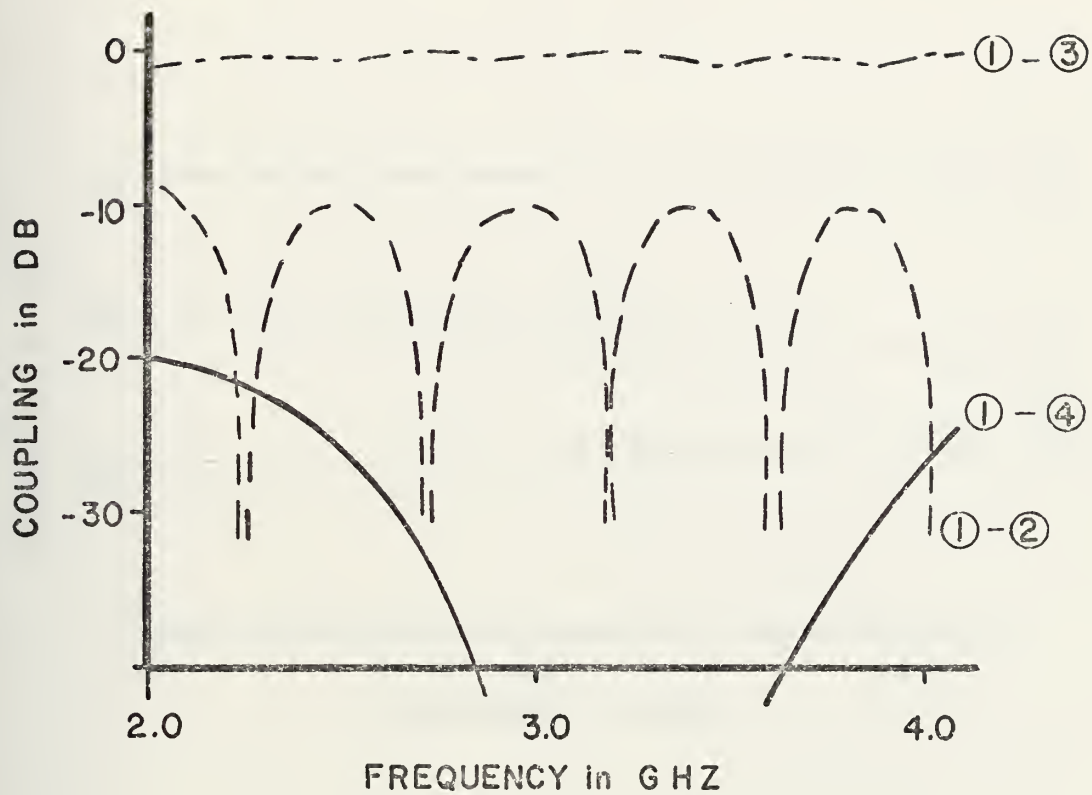


Figure 4.2/1 Theoretical Response of Coupler with $\theta_o = \theta_e + \pi$, $W/D = 0.5$, $S/D = 0.3$ and $\epsilon_r = 16$

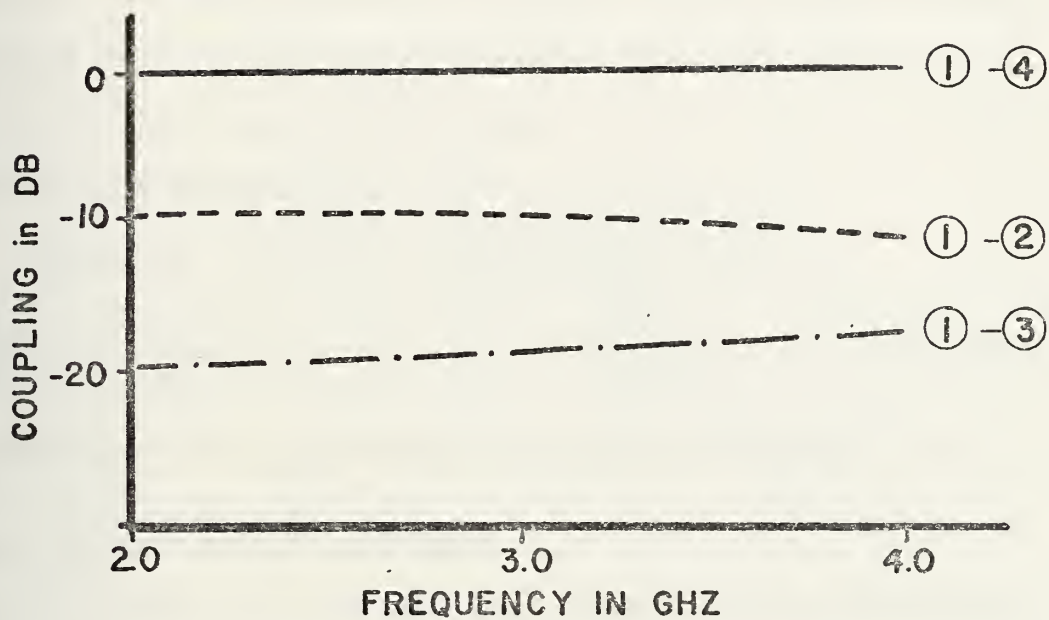


Figure 4.2/2 Theoretical Response of Contra-Directional Coupler with $S/D = 0.3$, $W/D = 0.5$ and $\epsilon_r = 16$

A third possible choice of design is one where $\theta_e + \theta_o = 2\pi$. This coupler will perform as a co-directional coupler with high directivity as can be seen if the following approximations are made. Assume loose coupling, then $(Z_{oe} + Z_{oo}) / \sqrt{Z_{oe} \cdot Z_{oo}} \approx 2$ with $Z_{oe} \approx Z_{oo}$. $\theta_e + \theta_o = 2\pi$ and θ_o is slightly larger than π while θ_e is slightly less than π . Let $\theta_o = \pi + \alpha$ and $\theta_e = \pi - \alpha$ where α is the difference between the electrical lengths for either even or odd mode and the electrical length of a single slot line. The physical length of the coupling region is still computed from $\theta_o + \theta_e = 2\pi$.

Equation (4-6) can then be simplified to

$$\left| \frac{V_3}{V_1} \right| \approx \alpha \text{ and equation (4-5) to } \left| \frac{V_2}{V_1} \right| \approx 0. \text{ The theoretical}$$

performance of this coupler is shown in Figure 4.3/2.

4.3 DESIGN OF TWO COUPLERS

A comparison between the previously derived theory of a dispersive line coupler and its actual performance was made by designing two slot line couplers. A general layout for a coupler is shown in Figure 4.3/1. It was decided to use a microstrip to slot line transition to couple energy into and out of the coupler. The theory of this transition is well understood because Knorr in Reference 5 derived a circuit model for this transition and developed a computer program by which an iterative scheme yields the values of the various parameters required to achieve minimum VSWR.

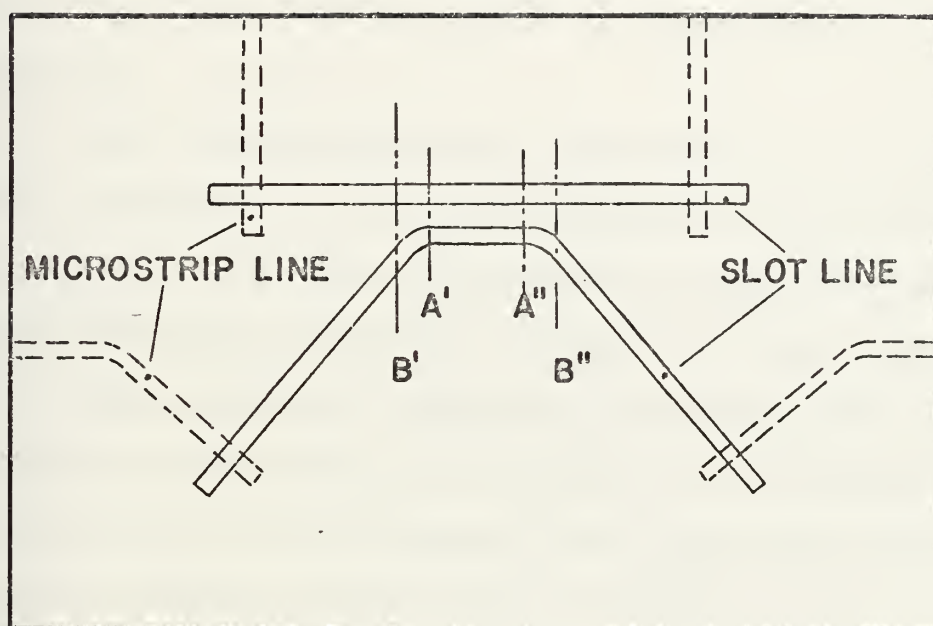


Figure 4.3/1 Geometry of Experimental Slot Line Coupler with Microstrip-Slot Transitions

This program was readily available and used in this study. The theory is given in detail in Reference 5 and therefore not reiterated here.

The following design steps were taken before the actual physical construction could be made.

a) It was decided to use standard miniature coaxial cable with an impedance of 50 Ohm to connect the coupler to the test equipment. This implied the use of a 50 Ohm microstrip line, thus the width of the microstrip was determined.

b) The iterative procedure described in Reference 5 was used to determine the physical dimensions of the slot and microstrip line stubs and the width of the slot line at the desired operating frequency of 3 GHz for lowest VSWR.

c) With the known dimension of the slot line the digital computer program described in Section 5.2.1 computed the line characteristics of two coupled slot lines for varying spacing (varying coupling) between the two lines.

d) The data from step c) were used in another computer program which evaluated the performance of the slot line coupler but did not include the microstrip to slot line transitions. The coupling length could be varied. Both mathematical formulations of Sections 4.1.1 and 4.1.2 were used in this design step.

e) After the desired theoretical performance was obtained the lines were photo-etched onto the dielectric substrate.

Several iterations through steps c) and d) are in general necessary until the requirements for the coupler are met.

In the two experiments the coupled slots were etched onto one side of a 1 oz. copper surface on a dielectric substrate with thickness $D = 0.125"$ and permittivity $\epsilon_r = 16$, dimensions $4.5" \times 6.5"$, while the four microstrip lines were etched onto the opposite side, to make all four ports accessible. OSM 248-4 adapters performed the transition from microstrip to the miniature coaxial cable of the test equipment. A network analyzer was used for the recording of the coupler characteristic.

The first coupler designed was the co-directional coupler shown in Figure 4.3/2. The discrete points in this graph indicate the experimentally measured coupler response. The slot width was $0.0625"$ and the separation between the parallel slots $0.135"$. It was originally thought that the coupling length could be defined to be the length between the points A' and A" shown in Figure 4.3/1. This length was $0.375"$ and was found not to match the experimental with the theoretical results. It was learned, however, that good agreement could be obtained if the coupling length was taken between points B' and B", in this case $0.75"$ which corresponds to $\theta_e + \theta_o = 2\pi$. The waves on the two transmission lines do obviously not decouple abruptly in this particular design so that the coupling region is somewhat extended to an "effective" coupling length. The sidearms to ports 2 and 3, however, could not be bent further or the waves on these arms would interfere with each other.

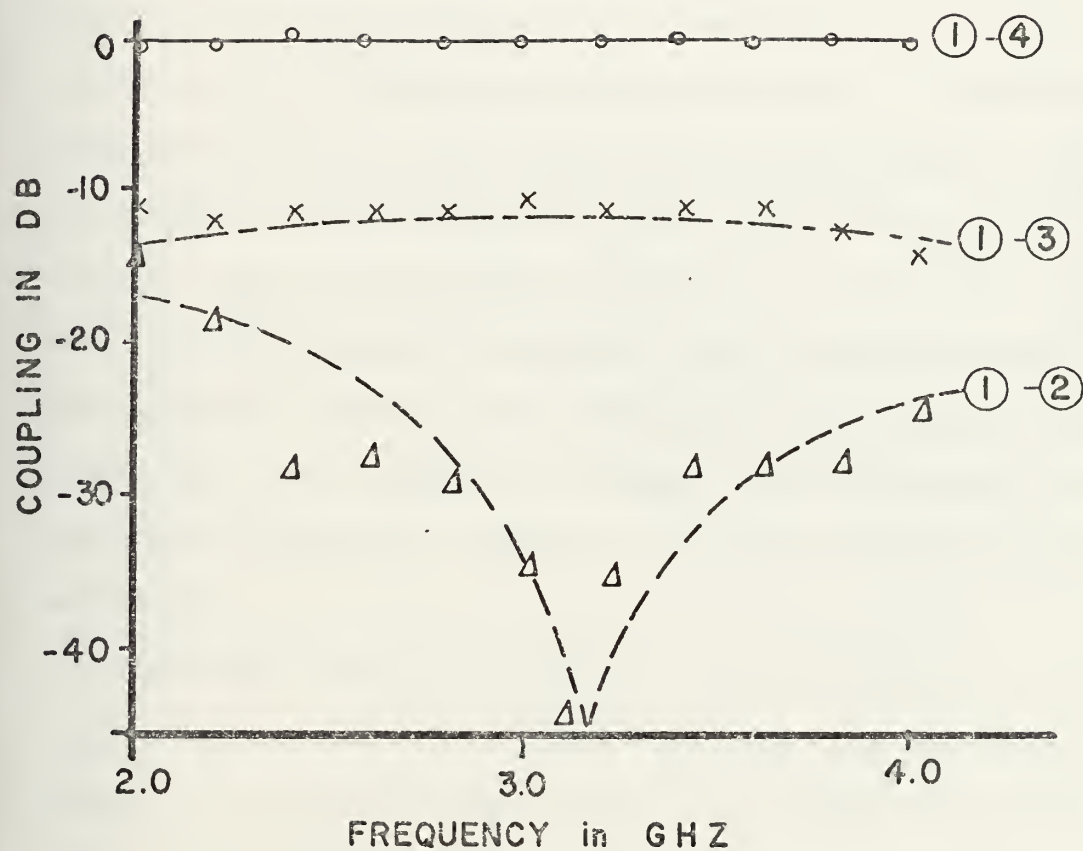


Figure 4.3/2 Theoretical and Experimental Response of Co-directional Coupler with $S/D = 1.08$, $W/D = 0.5$ and $\epsilon_r = 16$

The second experiment was the design of a contra-directional 10 dB coupler. The slot width was again 0.0625", but the separation between the slots was decreased to 0.0375". The coupling length was taken between points B' and B" to be 0.371". The result of this experiment, shown by the discrete points in Figure 4.3/3 revealed some disagreement with the theoretical performance in Figure 4.2/2. Although the experimental curves include the micro-strip to slot line transition, these transitions had a return loss of better than 10 dB over most of the frequency band and could not have caused this disagreement. Again it was found that the critical design parameter was the coupling length. Due to the closer coupling in this second coupler design, the coupling length had to be extended by 20% beyond the length B' - B" to match experiment and theory. Figure 4.3/3 shows the comparison between the experimental and the adjusted theoretical response, where now better agreement is achieved.

Although initially intended, design curves for slot line couplers cannot be presented since the slot line, single or coupled configuration, is a dispersive transmission line with frequency dependent characteristics. Thus any set of design parameters would be valid for a narrow frequency band only.

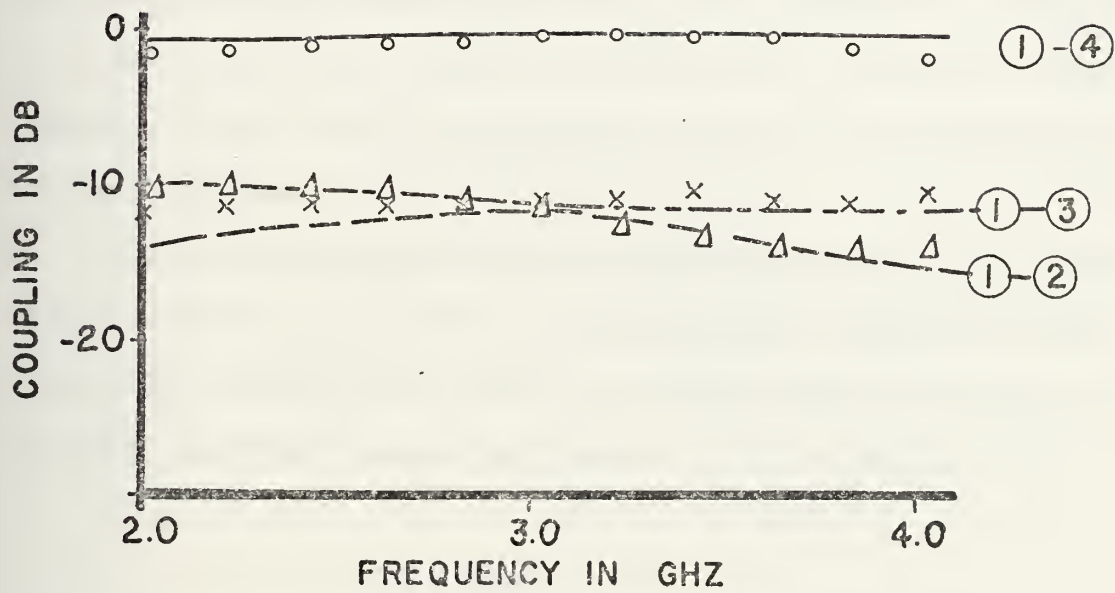


Figure 4.3/3 Theoretical and Experimental Response of a Coupler with $S/D = 0.3$, $W/D = 0.5$ and $\epsilon_r = 16$

4.4 SUMMARY

An analytical evaluation of slot line directional couplers has been presented. Due to the different phase velocities of the even and odd modes, co- or contra-directional coupling can be achieved. Theoretical results were compared with experimental data by the design of two couplers. It was found that the coupling length is a critical parameter in this design. Coupled lines were assumed to extend infinitely in the computation of the line parameters in Section 2.2. However, in a coupler, abrupt decoupling of the two lines does not occur due to surface currents on the metal and this tends to increase the effective coupling length. This result is also new and will be important in future designs.

With an adjustment of the coupling length good agreement between the theoretical and experimental results further verifies the spectral domain technique used in Section 2 in general and the results of Section 2.2 in particular.

5. COMPUTER PROGRAMMING

In Sections 2 and 3 the theoretical background of the analyses were provided together with some examples of the results obtained. By no means do these examples furnish enough information for any design purposes. Since this study presents the first extensive investigation of coplanar transmission lines, data aiding in the design are needed. Extensive design curves would not only be beyond the scope of this thesis but are even sometimes impossible to provide as stated before. For instance, for parallel and end coupled slot lines, not all applications can be foreseen at this point. Hence, a great effort was devoted to the development of two versatile computer programs which offer a variety of choices for the analysis of open and shielded boundary coplanar transmission lines. It is believed that these will be of more value to the microwave industry than any design curves could be. Before the two programs are described some general considerations which led to their development are necessary for the understanding of the numerical methods used.

5.1 REMARKS ON NUMERICAL ANALYSIS

The computation of the characteristic impedance and the perturbational analysis in Section 2 is based upon the solution to the dispersion characteristic problem for the transmission

line under consideration. In other words, the wave propagation constant or wavelength ratio λ'/λ must be known before any other investigations can be started since only in this case are the scalar potential functions in the transform domain known. These are necessary for the evaluation of the power distribution and for the perturbational analysis for a ferrite substrate. Hence, in the analysis of slot lines the starting point is a solution for the propagation constant β to equation (2-19), while for coplanar strip lines equation (2-32) applies.

In general a β is sought such that

$$-\int_{-\infty}^{\infty} G(\alpha, \beta) |T(\alpha)|^2 d\alpha = 0 \quad (5-1)$$

where $G(\alpha, \beta)$ is a component of the transform of the dyadic Green's function $N_1(\alpha, \beta)$ or $M_4(\alpha, \beta)$ with equations (2-19) and (2-32) respectively and $T(\alpha)$ is the Fourier transform of the electric field or current density assumed in the plane $y = D$ for slot or coplanar strip line respectively. A first order approximation is assumed here; if a second or higher order approximation is desired the zero of the determinant of the appropriate coefficient matrix must be found.

It is obvious that an analytic solution in closed form for β cannot be obtained due to the algebraic complexity leading to the quantity $G(\alpha, \beta)$ as shown in Appendix A. Thus a numerical solution is mandatory and must be obtained by programming a digital computer.

Several observations must be made to adapt the theoretical formulations in Section 2 to this numerical solution via a digital computer.

It is shown in Appendix A that the transforms of the dyadic Green's function components $M_1 - M_4$ or $N_1 - N_4$ are given in terms of coefficients F_1 through L_4 which are obtained by definitions during the application of the boundary matching technique. These coefficients are either real or imaginary so that in general a complex computation on the computer seems to be necessary. Furthermore, it is shown in Section 2.1.1 that for all values of the transform variable $|\alpha| < \sqrt{k_2^2 - \beta^2}$ the nature of the solutions in equations (2-12) and (2-13) changes from hyperbolic to trigonometric functions. For example, $\sinh \gamma_2 D$ changes to $j \sin \gamma_2'' D$. Since these functions enter into the computation of the quantities F_1 to N_4 it is found that these quantities are not only pure real or pure imaginary but change from real to imaginary or vice versa for the two cases $\gamma_2^2 > 0$ and $\gamma_2^2 < 0$.

This fact furthermore seems to suggest a complex analysis on the computer. However, on the other hand, the disadvantages of a complex arithmetic with digital computation are well known. Not only is the required amount of memory storage twice as large as for a real computation; a fundamental setback is that the computation times for instructions like multiplications, divisions, and evaluations of trigonometric and hyperbolic functions with complex arguments are on the

average four to five times longer than in real arithmetic. An avoidance of digital complex computation is therefore highly desirable and can be obtained if some algebraic manipulations with the quantities F_1 to N_4 of Appendix A are performed prior to the computer programming.

Before the details of this manipulation are shown a remark with regard to a scaling technique implied in the following derivation must be made. Dielectric substrates are commercially available for various thicknesses D so that in general the line parameters should be computed for each thickness and varying frequency. A more generalized method of analysis is simply to scale the various geometric quantities involved with respect to this thickness to obtain more versatile parameters for a varying normalized frequency D/λ . The resulting design curves are then applicable for any geometry independent of the specific dielectric thickness. A manipulation of equations (A-13) to (A-24) including this scaling technique is given in Appendix G, where it is shown that the avoidance of complex arithmetic on the computer and thus long computation times can be traded against a somewhat lengthy but straightforward algebraic computation by hand before the programming is attempted.

With this formulation of the dyadic Green's function the further steps to obtain the wavelength ratio λ'/λ are as follows. For a first order approximation equation (5-1) has to be solved where now due to the scaling technique the

variable of integration is αD . The transform of the assumed electric field (or current density) for the geometry of transmission line to be analyzed is given in Section 2. Since in (5-1) the absolute value squared of these functions is to be taken, this part of the integrand will be in general a real and even function of αD . Preliminary numerical investigations showed that the components M_1 , M_4 , N_1 and N_4 are also even functions of αD so that the whole integrand in (5-1) is even, a fact which allows further savings in computation time since a numerical integration over a half interval between the integration limits is sufficient. Two representative examples of the real parts of the components M_4 and N_1 and their dependence on αD are displayed in Figures 5.1/1 and 5.1/2 respectively. Although these components according to the derivation in Appendix G are imaginary, this fact is immaterial if a first order approximation is used.

For a second order approximation, however, the following observation must be made as explained here for instance with reference to equation (2-19). According to equations (2-21) or (2-23) $E_x(\alpha)$ is an even and real function of α while $E_z(\alpha)$ is odd and imaginary. N_1 and N_4 are found to be even functions while N_2 and N_3 are odd functions; all are imaginary. Equation (2-19) can be rewritten in a simplified form after the integration with respect to α is performed as

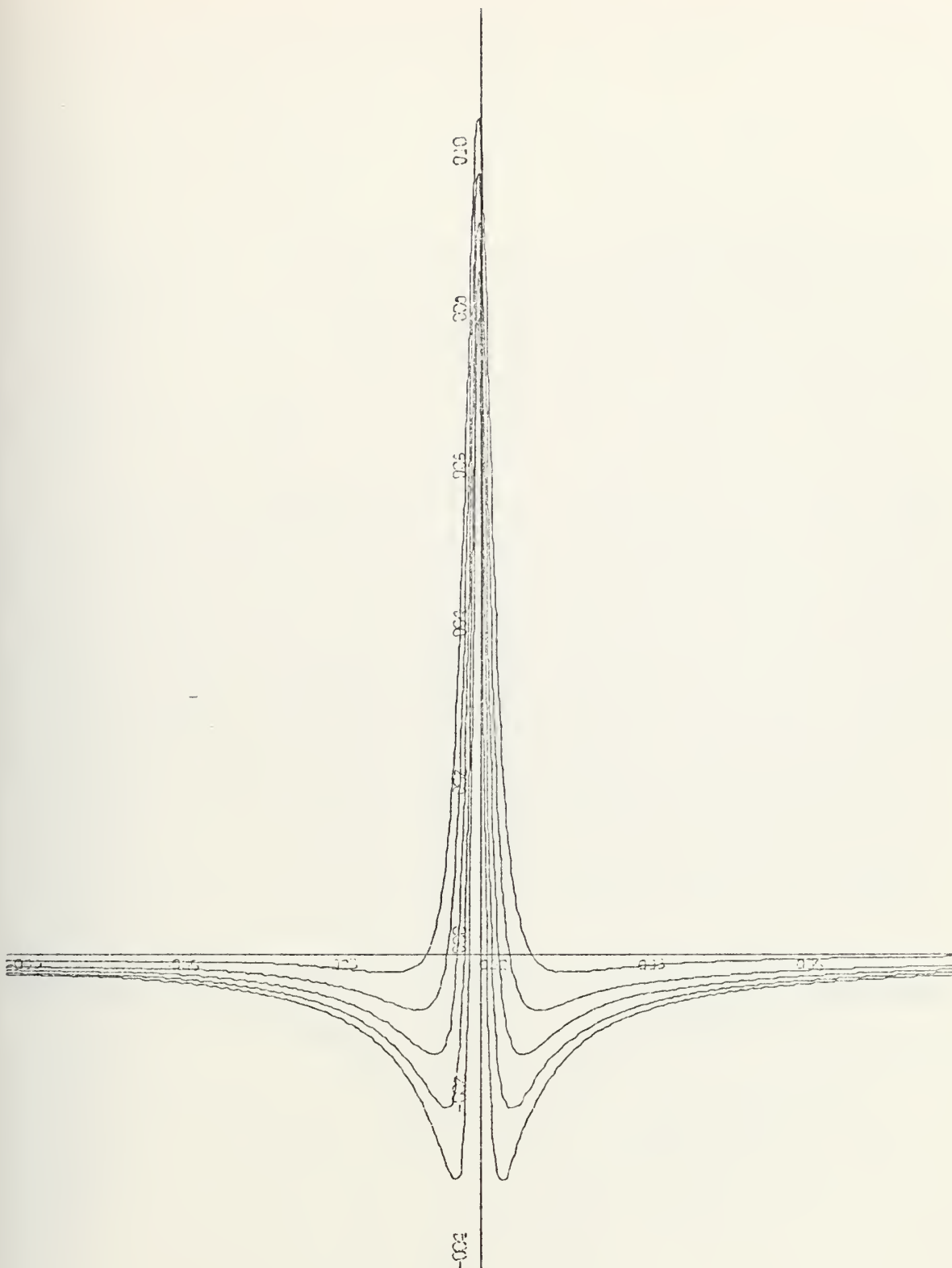


Figure 5.1/1 $M_4''(\alpha D, \lambda'/\lambda)$ vs. αD with $\epsilon_r = 12$ and $D/\lambda = 0.03$
for Five Arbitrary Values λ'/λ

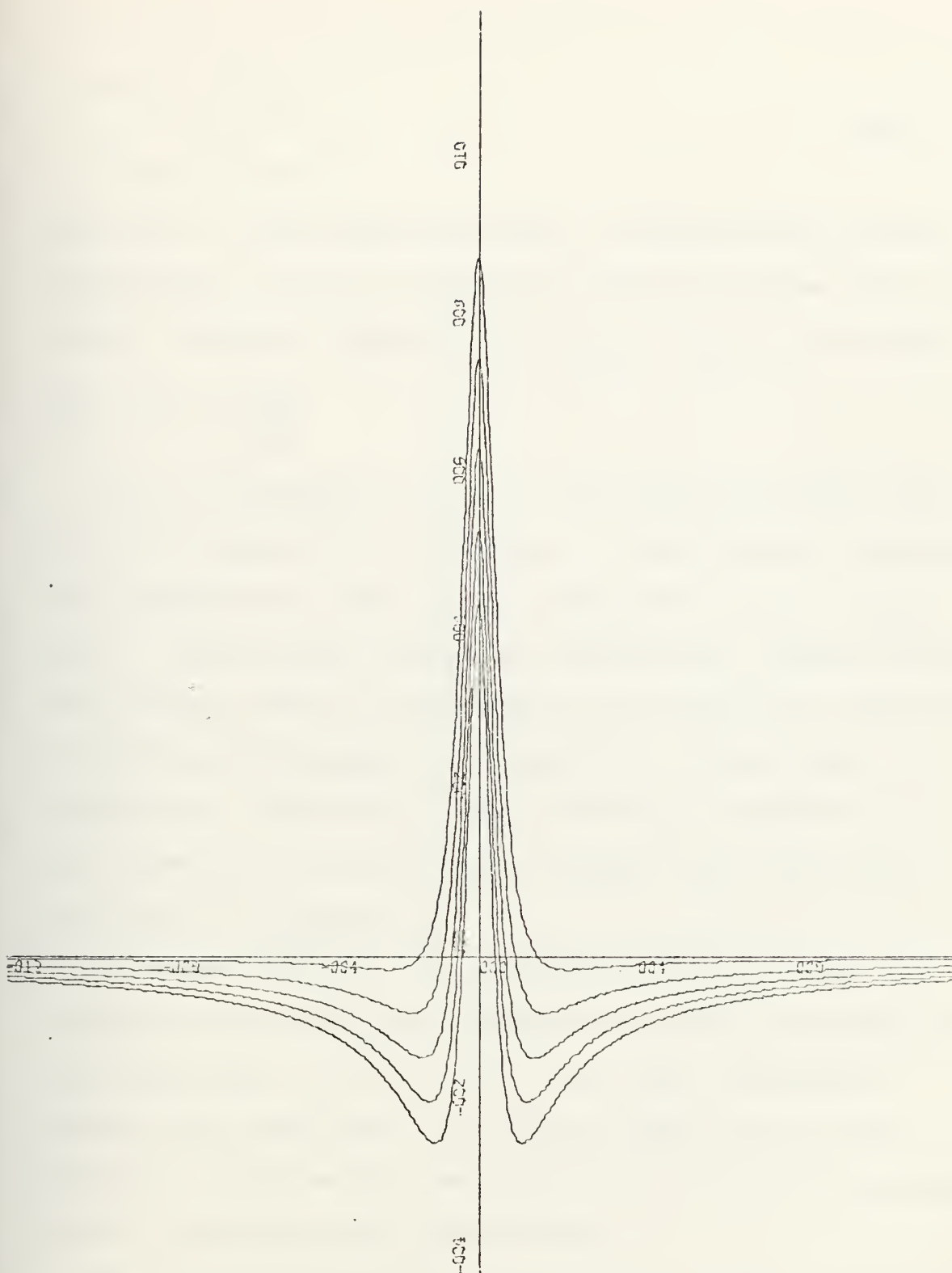


Figure 5.1/2 $N_1''(\alpha D, \lambda'/\lambda)$ vs. αD with $\epsilon_r = 16$ and $D/\lambda = 0.03$
 For Five Arbitrary Values λ'/λ

$$ja\eta_{11} - b\eta_{12} = 0$$

(5-2)

$$ja\eta_{21} - b\eta_{22} = 0$$

where the η_{ij} are real quantities. A solution for the two coefficients a and b of the basis functions (other than the trivial solution) does exist if $\eta_{11}\eta_{22} = \eta_{12}\eta_{21}$ in which case $ja = b \frac{\eta_{12}}{\eta_{11}}$.

If b is assumed to be real this clearly indicates that a must be imaginary or vice versa, in other words, the electric field components in the x and z directions are 90° out of phase. Although this result is automatically implied through the notation used in the dispersion characteristic calculations it should receive special consideration in the power calculation. Since only a first order approximation for this computation is used in the present work, this phase shift was of no concern.

A desired solution for equation (5-1) can now be found by assigning an arbitrary numerical value for the wavelength ratio such that $1 < \lambda/\lambda' < \epsilon_r$ and then iteratively changing this until the integration yields zero or more precisely a small enough value so that a prescribed accuracy for the wavelength ratio is realized.

Several representative graphs of integrands for equation (5-1) are shown in Figures 5.1/3-6 where the coefficients displayed in Figures 5.1/1-2 are used. Figure 5.1/3 shows

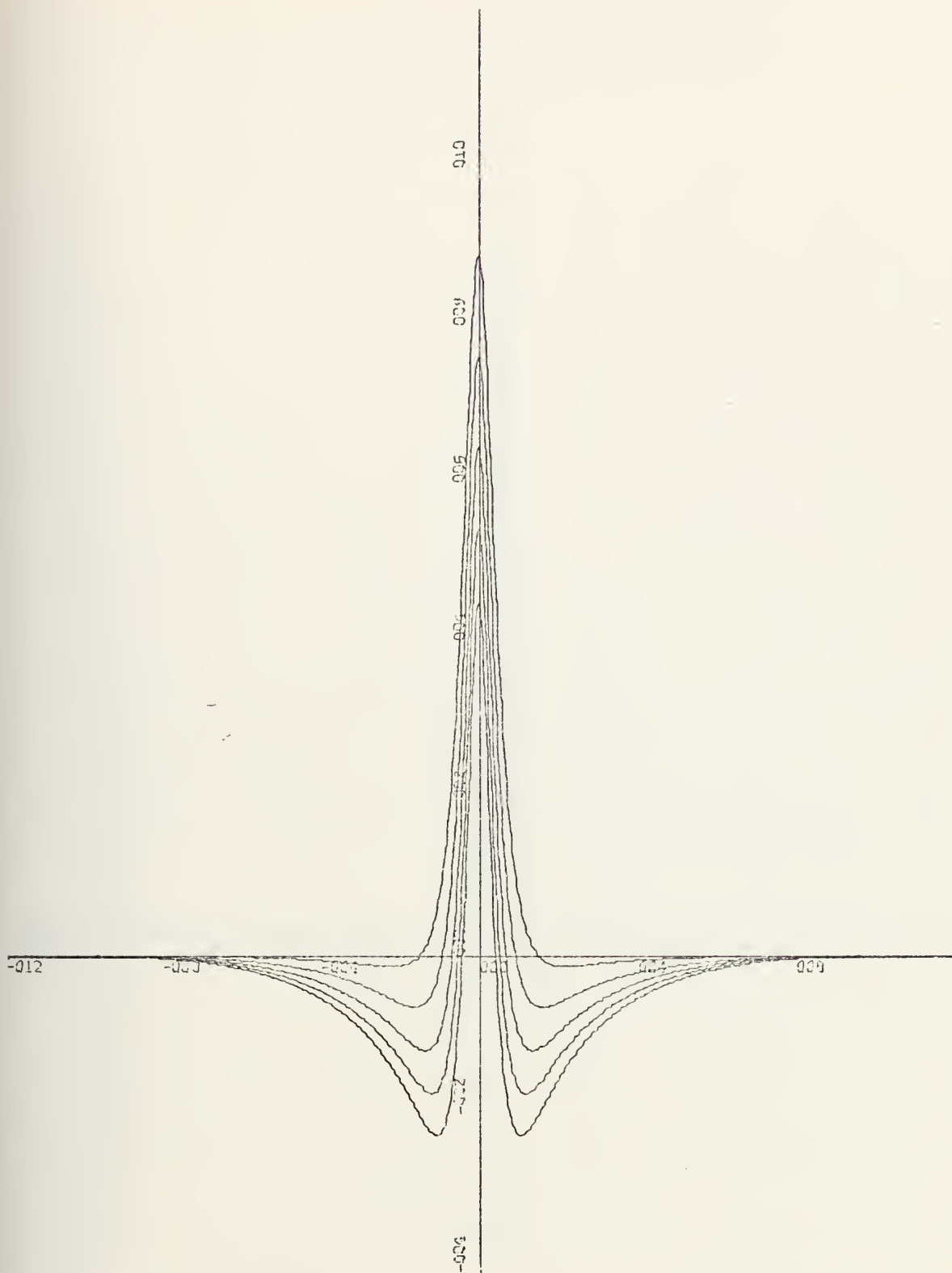


Figure 5.1/3 $N_1''(\alpha D, \lambda'/\lambda) |E_x(\alpha D)|^2$ vs. αD with $W/D = 0.5$,
 $D/\lambda = 0.03$ and $\epsilon_r = 16$ (single slot) for
several values of λ'/λ

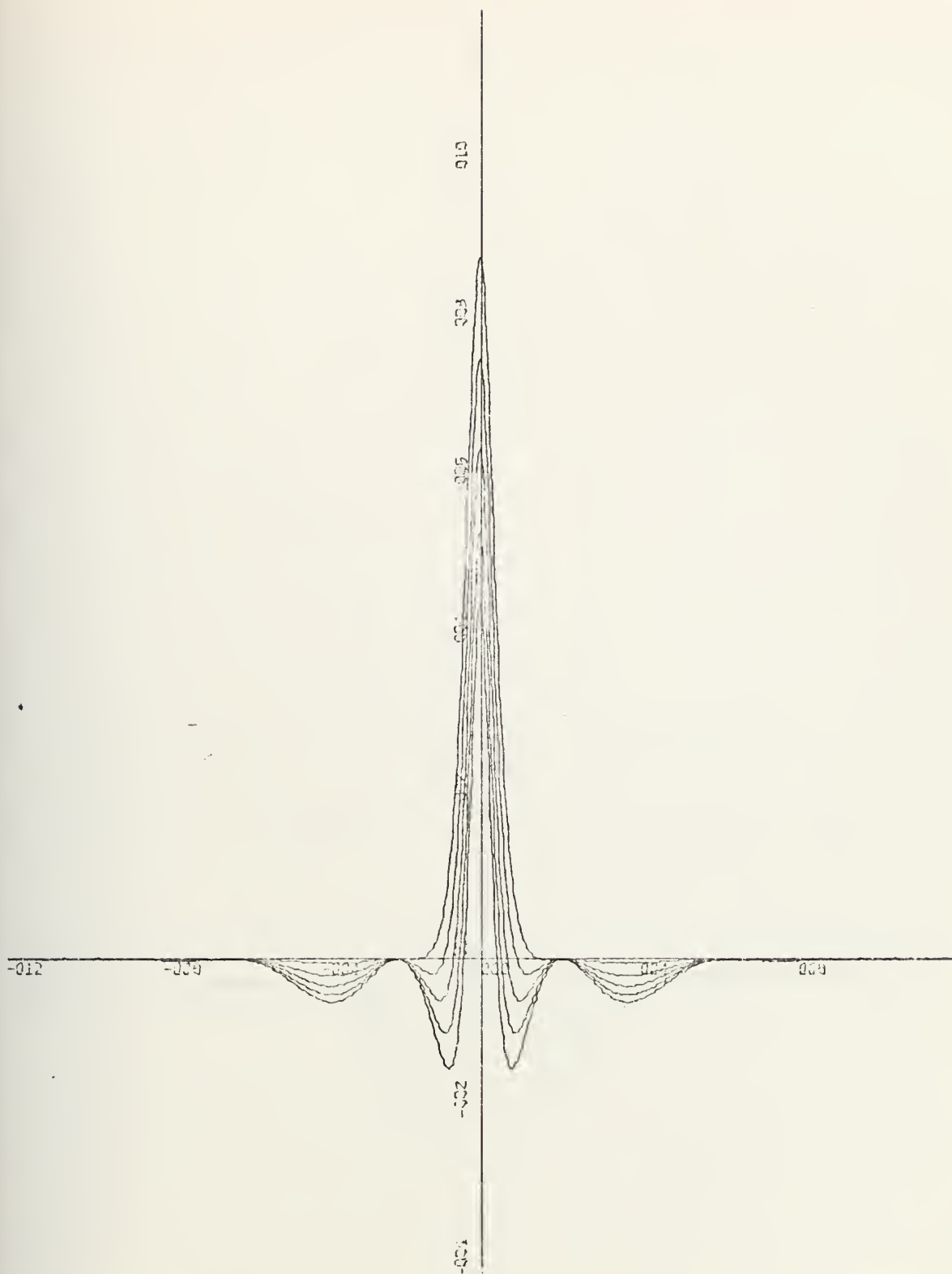


Figure 5.1/4 $N_1''(\alpha D, \lambda'/\lambda) |E_x(\alpha D)|^2$ vs. αD with $W/D = 0.5$, $D/\lambda = 0.03$, $S/D = 1.0$ and $\epsilon_r = 16$ (coupled slots, even mode) for several values of λ'/λ

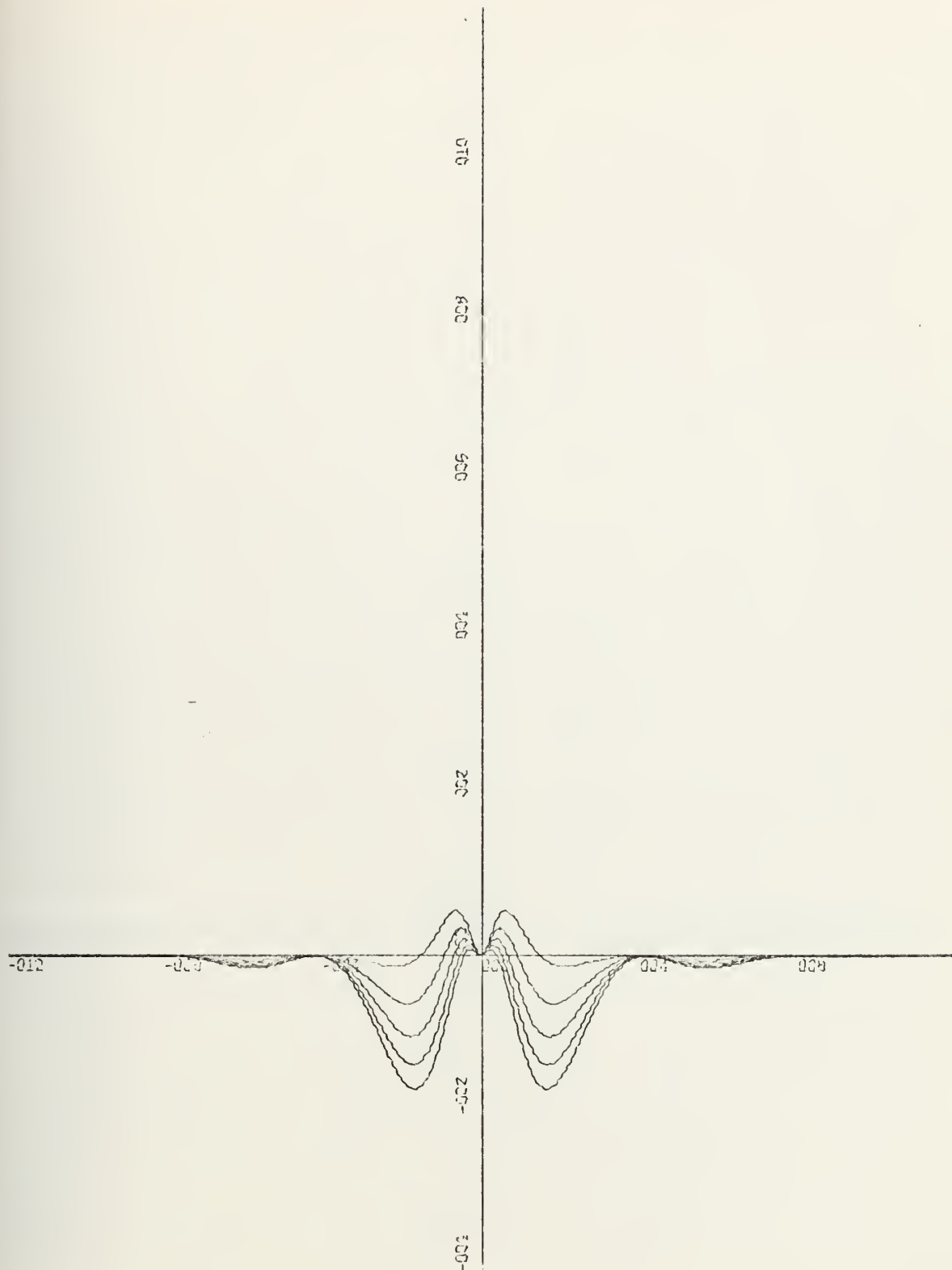


Figure 5.1/5 $N_1''(\alpha D, \lambda'/\lambda) |E_x(\alpha D)|^2$ vs. αD with $W/D = 0.5$, $D/\lambda = 0.03$, $S/D = 1.0$ and $\epsilon_r = 16$ (coupled slots, odd mode) for several values of λ'/λ

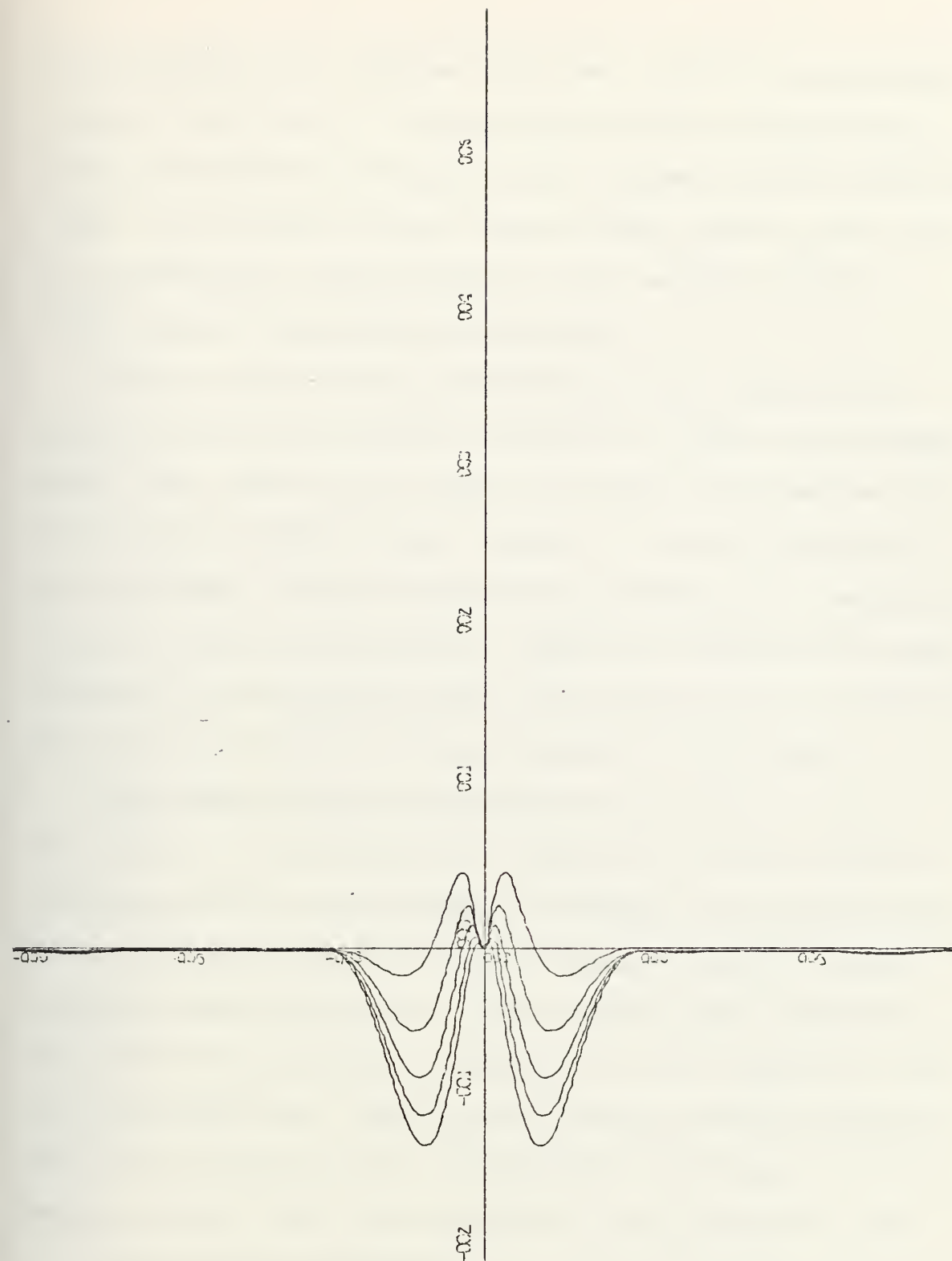


Figure 5.1/6 $M_4''(\alpha D, \lambda'/\lambda) |J_z(\alpha D)|^2$ vs. αD with
 $W/D = S/D = 1.0$, $D/\lambda = 0.03$ and $\epsilon_r = 12$
(coplanar strip line) for several values
of λ'/λ

the integrand for a single slot line, 5.1/4-5 two parallel coupled slot lines in the even and odd mode respectively, and 5.1/6 shows the integrand for a coplanar strip configuration. In all cases the zero order Bessel function was used as the basis for the transform of the assumed electric field (current density) distribution.

The next task is the preparation of the appropriate equations for the numerical evaluation of the time average power flow. Here again complex arithmetic expressions can be avoided if manipulations similar to those in Appendix G are performed. General expressions for the time average power flow are given in Appendix B. Appendix H shows, how a real arithmetic evaluation of these expressions can be accomplished for the open boundary slot and coplanar strip lines.

The normalization of equations with respect to the thickness D of the dielectric (ferrite) substrate and the technique used to avoid complex arithmetic are given by now, with sufficient explanation and detail so that no further expansion seems necessary. The perturbational expression for the ferrite analysis in Appendix D, for instance, need only be normalized. Appropriate remarks have already been made with regard to real and imaginary quantities involved. Hence equation (D-2) will require a real arithmetic only.

Furthermore, although so far details are given for open boundary lines only, the manipulations described obviously apply for the shielded coplanar lines as well. The details

of the preparation of these equations for programming are given in Appendix J. It is observed that for the dispersion characteristic computations the infinite integration in equation (5-1) is replaced by an infinite series due to the discrete nature of the transform variable α_n . This remark holds also for the computation of time average power flow.

Preliminary numerical investigations of the coefficients of these series indicated an even distribution with respect to the variable α_n so that computation time can be saved by summing over a half interval only.

This result even holds for computations concerning the length of a halfwave resonating slot, where equation (3-28) given in a simplified form as

$$\sum_{n=-\infty}^{\infty} \int_{-\infty}^{\infty} M_1(\alpha_n, \xi) |T(\alpha_n, \xi)|^2 d\xi = 0 \quad (5-3)$$

has to be evaluated. Instead, due to the even behavior of the integrand with respect to ξ and α_n the following computation suffices:

$$\int_0^{\infty} M_1(0, \xi) |T(0, \xi)|^2 d\xi + 2 \sum_{n=1}^{\infty} \int_0^{\infty} M_1(\alpha_n, \xi) |T(\alpha_n, \xi)|^2 d\xi = 0 \quad (5-4)$$

After this preparation of the equations for computer programming the only remaining task is to investigate the numerical integration with regard to its limits and the procedure to be used. One of the limits of the integrals

discussed so far extends to infinity so that due to the finite presentation of numbers on a digital computer a finite approximation has to be used instead. From the representative examples shown in Figures 5.1/1-6 it is seen that the integrands will decay very rapidly in general. Although no analytic method can be applied to estimate the order of magnitude of a finite and adequate upper limit, a trial and error procedure by numerical means showed that for the open boundary lines a limit of $\alpha D = 55$ and for the shielded lines $\xi D = 9$ is sufficiently large to be considered infinite for all practical purposes since the integrands are at least down by a factor of 10^{-5} relative to their largest value close to the origin. Several different investigations showed that these limits guarantee at least a three digit accuracy for any practical set of line parameters.

After establishing appropriate limits of integration the remaining problem of which numerical integration scheme to use must be considered. Many schemes are supplied through the standard literature on numerical analysis. In this study only three methods were investigated seriously. Two integration subroutines are supplied as part of 'IMSL' Library [Ref. 31] with names 'DRMBIU' and 'DCADRE' where both use a repeated interval-halving technique, also referred to as a Romberg integration. 'DCADRE' is an improved version of 'DRMBIU' since it provides for an adaptive method and thus may save computation time. This routine is quite new and became available only very recently. It is used for comparative purposes in this discussion.

An alternate integration scheme is the Gaussian-quadrature method. According to Reference 32 the Gauss-Legendre formulas are significantly more accurate than the equal-interval formulas such as the Romberg-method for a comparable number of sub-intervals between the integration limits with the condition that the magnitudes of higher order derivatives of the integrand decrease or at least do not increase. In other words, an equal-interval formula will in general need more divisions into sub-intervals to acquire the same accuracy which results in a greater computation time. Since the computer programs presented here are intended to be used very often for design purposes, the computation time is an important factor. Considerable effort was devoted therefore to finding the optimum numerical integration scheme where "optimum" means the shortest possible computation time for a prescribed accuracy of the result.

Due to the algebraic complexity of the integrands the behavior of its higher order derivatives cannot be studied on an analytical basis. It is observed, however, that these integrands will partly consist of the transforms of the dyadic Green's function components. The examples shown in Figures 5.1/1 and 5.1/2 indicate a smooth and continuous behavior with at most one zero for αD in the interval $[0, \infty)$. The other part of the integrand will consist of the transform of the assumed field (current density) distribution. If, for instance, coupled slots in the odd mode are considered,

this function will be in the form of

$$\sin\left(\frac{S/D + W/D}{2}\right) \alpha D) \cdot B_0\left(\frac{W/D \cdot \alpha D}{2}\right) . \quad \text{Let } y = E(x) \text{ where } y \text{ is}$$

the largest integer less than or equal to x . Then the first term above has $E\left(\frac{55}{2\pi}(S/D + W/D)\right)$ zeros for αD in the interval $(0, 55]$. The second term has approximately $E\left(\frac{55}{2\pi} W/D\right)$ zeros since for large arguments s , $B_0(x) \sim \cos(x)$. These zeros are not necessarily coincident with any of the first ones so that the total number of zeros of the integrand is the sum of both.

For resonant slot length computations that part of the integrand involving the transform variable ξD is proportional to $\cos\left(\frac{\xi D \cdot L/D}{2}\right)$ (see equation (3-27b)), a function which will have $E\left(\frac{9 \cdot L/D - \pi}{2\pi}\right)$ zeros for ξD in the interval $(0, 9]$.

Since in general the integrands will be basically in the form of a product of a trigonometric and a zero order Bessel function the following test was performed to find an efficient numerical integration scheme for the specific needs in this analysis.

A test function to be integrated in the interval $[0, 30]$ was chosen to be $f(x) = \sin(5x) \cdot B_0(2x)$ which has 68 zeros within this interval. If a three digit accuracy is desired a numerical Romberg integration with 'DRMBIU' needs approximately 6 seconds computation time while the cautious adaptive Romberg method in 'DCADRE' needs only 4 seconds. On the other hand, a Gaussian-quadrature 80 points integration requires only 0.5 seconds to guarantee the same result.

The advantage of this integration scheme becomes obvious then. However, in contrast to the Romberg integrations, where the user can simply specify the accuracy of the result, this is not possible with a Gaussian-quadrature routine. Here the user must have advance knowledge of the general behavior of the integrand to select the number of quadrature points. Still, no estimate of the integration error can be obtained.

But from the numerical example above it was conjectured, that in the present applications a quadrature integration of sufficient accuracy can be achieved, if the number of quadrature points is at least twice the number of zeros of the integrand within the limits of integration.

This number depends on the parameters such as slot width, separation between slots or strips and for the resonator analysis on the frequency of operation and will usually vary over a wide range. A basic feature in the first program 'COPLAN' is therefore a short computation which estimates the number of zeros of the integrand according to which the selection of an appropriate quadrature routine is made. It was found by several test runs and comparisons that a substantial amount of computation time could be saved without any sacrifice in accuracy.

5.2 COMPUTER PROGRAM 'COPLAN' FOR OPEN BOUNDARY COPLANAR TRANSMISSION LINES

A numerical analysis of open boundary coplanar transmission lines is provided by the digital computer program

'COPLAN' and its accompanying subroutines 'COMBO' and 'GAUSQ', all shown in Appendix M, written in the FORTRAN IV programming language. The Gaussian-quadrature integration routines are not shown.

Although during the development of the theory in Section 2 of this thesis separate programs were written for different line configurations, this program 'COPLAN' is a combination of all of them and offers a high degree in versatility. Dispersion characteristic and characteristic impedance may be computed for single or coupled slot lines, for coplanar waveguides or for coplanar strip lines. Except for the latter the perturbational analysis for phase shift and attenuation may be applied as well for ferrite substrates.

The necessary input data and some further information about the use of this program are described in the preceeding commentary section of the main program. Input and output formats are chosen such that design curves may be easily generated if so desired.

After the input data is read in and printed in an echo check, preliminary computations and initializations of the various computation loops are performed. The first computation inside the inner loop is a check whether the operating frequency is above the cut-off-frequency of the lowest order surface wave mode; if so the job is terminated. The next step is to obtain an estimate of the number of zeros to be encountered in the interval of integration, according to

which a numerical value is assigned to an integer variable to be used in the selection of the appropriate Gaussian-quadrature integration routine. This selection and the actual integration are performed in the subfunction 'GAUSQ' whose use is self-evident.

The program proceeds with a zero finding procedure to find the wavelength ratio λ'/λ , according to equations (2-19) and (2-31), where $1 < \lambda/\lambda' < \epsilon_r$. Integration limits are computed to determine for which values of αD the trigonometric and hyperbolic functions in the solutions to Helmholtz's equation apply (Section 2.1.1). For hyperbolic functions ($k_{c2}D < |\alpha D| < 55$) the appropriate numerical integration is performed via the subroutine 'GAUSQ' while for $0 \leq |\alpha D| < k_{c2}D$ it was found that a 24 point Gaussian-quadrature routine is accurate enough for all practical parameters. The subroutine COMBO provides the appropriate integrands via several identifiers or flags.

After the integration is carried out the result is used to select a new value for λ'/λ through a bisectional zero finding to improve the result and the procedure starts over again. The computation is terminated when the absolute value of the difference between the new and the old value for λ/λ' is less than $5 \cdot 10^{-4}$ and thus a three digit accuracy after the decimal point is guaranteed.

Preliminary computations follow for the determination of the characteristic impedance. Depending on the transmission line configuration, mode of operation and the spatial

region the appropriate integrands are provided again through the subroutine 'COMBO' in accordance to the equations of Section 2. The numerical integration of the power density in the spectral domain follows the same considerations given above for the dispersion calculations. The proper definition of the characteristic impedance for the transmission line to be analyzed is then used to evaluate this line parameter. A three digit accuracy is guaranteed in this computation.

The two line parameters for a dielectric substrate are thus determined and are printed into a tabulated output. If a perturbational analysis for a ferrite substrate is desired, however, the computer program proceeds with preliminary computations to evaluate the external susceptibility tensor components. These are then provided to the subroutine 'COMBO' which computes the appropriate integrands for the perturbational analysis of the attenuation and the phase shift for waves travelling in either direction. After the numerical integration is performed some further manipulations are necessary to allow the attenuation to be printed in the unit [dB/cm] and the phase shift as a ratio of the ferrite phase constant over the dielectric phase constant. These results are printed together with the results for a dielectric substrate. The procedure is then reiterated for the next set of parameters.

The subroutine 'COMBO' provides the integrands for the dispersion characteristic and power density computations as

well as for the perturbation analysis. The entry variable of this routine is the normalized transform variable αD while other coefficients are exchanged in common storage areas (COMMON statement) with the main program. Depending on the transmission line configuration the appropriate transform of the assumed electric field (current density) is computed by the use of a Bessel-function subroutine. The further evaluations of the respective integrands follows the general theoretical outline of Section 2. Variable names are chosen such that these equations can be easily compared with the derivations of equations in the appropriate appendices so that no further explanations are necessary.

Representative computer outputs are given in Tables I through VII. Waves travelling on a ferrite substrate show a nonreciprocal behavior. It is therefore pertinent to cite the orientation of the coordinate system and the biasing field. Following the convention of Section 2.4 the direction of the coordinates are given in Figure 1/2 and the biasing magnetic field is in the positive x-direction. A forward wave then travels into the positive z direction.

Finally some statistics about this program seem to be apt. The total program including all subroutines requires 182 K bytes storage space and 78 K bytes for the execution step. To obtain a fast execution time the program was compiled with the FORTRAN H compiler which applies an optimization code. The computation time for execution vary greatly

DISP. AND CHARACT. IMPEDANCE OF SINGLE SLOT LINE				
W/D	EPSILON	D/L	LP/L	Z0
0.100	11.0	0.020	0.4572	57.6
0.100	11.0	0.030	0.4446	59.9
0.100	11.0	0.040	0.4347	61.3
0.100	11.0	0.050	0.4264	61.9
0.100	11.0	0.060	0.4191	61.7
2.000	11.0	0.020	0.5599	153.6
2.000	11.0	0.030	0.5244	173.6
2.000	11.0	0.040	0.4958	187.6
2.000	11.0	0.050	0.4718	195.7
2.000	11.0	0.060	0.4512	197.9

TABLE I. Single Slot Line on a Dielectric Substrate

COUPLED SLOTS ON DIELECTRIC SUBSTRATE				EVEN MODE		ODD MODE	
W/D	S/D	EPSILON	D/L	LP/L	Z0	LP/L	Z0
0.400	0.300	16.0	0.010	0.4754	44.2	0.3496	111.2
0.400	0.300	16.0	0.030	0.4065	55.6	0.3458	111.7
0.500	0.300	16.0	0.010	0.4861	47.3	0.3519	118.1
0.500	0.300	16.0	0.030	0.4125	50.6	0.3472	118.9
0.400	0.600	16.0	0.010	0.4844	47.5	0.3537	93.8
0.400	0.600	16.0	0.030	0.4113	61.0	0.3484	94.7
0.500	0.600	16.0	0.010	0.4951	50.6	0.3565	100.5
0.500	0.600	16.0	0.030	0.4172	56.1	0.3501	101.9

TABLE II. Coupled Slot Lines on a Dielectric Substrate

DISPERSION AND CHARACT. IMPEDANCE OF CO-PLANAR WAVEGUIDE					
W/D	S/D	EPSILON	D/L	LP/L	Z ₀
1.500	0.500	20.0	0.010	0.3497	68.5
1.500	0.500	20.0	0.020	0.3412	71.1
1.500	0.500	20.0	0.030	0.3313	72.7
1.500	0.500	20.0	0.040	0.3208	72.8
1.500	1.000	20.0	0.010	0.3599	61.2
1.500	1.000	20.0	0.020	0.3495	64.1
1.500	1.000	20.0	0.030	0.3376	66.1
1.500	1.000	20.0	0.040	0.3252	66.4

TABLE III. Coplanar Waveguide on a Dielectric Substrate

DISPERSION AND CHARACT. IMPEDANCE OF CO-PLANAR STRIPS					
W/D	S/D	EPSILON	D/L	LP/L	Z ₀
1.500	0.200	20.0	0.010	0.3582	58.4
1.500	0.200	20.0	0.030	0.3332	49.0
2.000	0.200	20.0	0.010	0.3794	59.8
2.000	0.200	20.0	0.030	0.3455	47.1
1.500	0.400	20.0	0.010	0.3626	65.4
1.500	0.400	20.0	0.030	0.3359	54.2
2.000	0.400	20.0	0.010	0.3835	65.8
2.000	0.400	20.0	0.030	0.3479	51.3

TABLE IV. Coplanar Strip Line on a Dielectric Substrate

SINGLE SLOT LINE ON FERRITE SUBSTRATE

THICKNESS OF DIELECTRIC = 0.100 CM W/D = 0.500 S/D = 0.0

PERMITTIVITY = 20.0

SATURATION MAGNETISATION = 2300.00 GAUSS

MAGNETIC BIASING FIELD = 683.60 OERSTED

LINEWIDTH = 100.00 OERSTED LANDÉ-G FACTOR = 2.0

GENERAL DATA FOR DIELECTRIC SUBSTRATE				FERRITE SUBSTRATE WAVE TRAVELING			
				FORWARD	REVERSE		
FREQ GHZ	D LAMBDA	LAMBDA P LAMBDA	Z0	ALPHA DB/CM	BETA=FF BETA-DI	ALPHA DB/CM	BETA=FF BETA-DI
2.500	0.0083	0.4043	61.9	0.122	1.136	0.182	1.202
2.700	0.0090	0.4011	62.6	0.180	1.157	0.265	1.232
2.900	0.0097	0.3981	63.4	0.278	1.186	0.402	1.271
3.100	0.0103	0.3952	64.1	0.454	1.226	0.649	1.326
3.300	0.0110	0.3925	64.7	0.814	1.288	1.144	1.409
3.500	0.0117	0.3900	65.4	1.688	1.391	2.336	1.547
3.700	0.0123	0.3875	66.0	4.551	1.582	6.197	1.799
3.900	0.0130	0.3852	66.6	18.403	1.729	24.646	1.984
4.100	0.0137	0.3830	67.1	19.693	0.293	25.956	0.077
4.300	0.0143	0.3809	67.7	5.780	0.419	7.434	0.256
4.500	0.0150	0.3788	68.2	2.549	0.602	3.254	0.503
4.700	0.0157	0.3769	68.7	1.458	0.703	1.832	0.639
4.900	0.0163	0.3748	69.1	0.966	0.763	1.197	0.721
5.100	0.0170	0.3731	69.6	0.701	0.803	0.855	0.775
5.300	0.0177	0.3713	70.0	0.542	0.831	0.651	0.813
5.500	0.0183	0.3696	70.4	0.437	0.852	0.518	0.842

TABLE V. Single Slot Line on a Ferrite Substrate

COUPLED SLOT LINES ON FERRITE SUBSTRATE

THICKNESS OF DIELECTRIC = 0.100 CM W/D = 1.000 S/D = 0.500
 PERMITTIVITY = 20.0
 SATURATION MAGNETISATION = 2300.00 GAUSS
 MAGNETIC BIASING FIELD = 683.60 OERSTED
 LINEWIDTH = 100.00 OERSTED LANDE-G FACTOR = 2.0

GENERAL DATA FOR DIELECTRIC SUBSTRATE				FERRITE SUBSTRATE WAVE TRAVELING			
EREG CHZ	MODE LAMBDA	LAMBDA LAMBDA	Z0	ALPHA DB/CM	BETA=EF BETA=DI	ALPHA DB/CM	BETA=EF BETA=DI
EVEN 2.900 ODD	MODE 0.0097	0.4864 0.3339	59.0 118.3	0.185 0.423	1.151 1.226	0.251 0.555	1.209 1.324
EVEN 3.100 ODD	MODE 0.0103	0.4817 0.3336	60.1 118.5	0.307 0.682	1.186 1.275	0.410 0.866	1.254 1.378
EVEN 3.300 ODD	MODE 0.0110	0.4770 0.3332	61.2 118.6	0.557 1.204	1.240 1.350	0.734 1.485	1.322 1.462
EVEN 3.500 ODD	MODE 0.0117	0.4726 0.3329	62.3 118.8	1.170 2.467	1.329 1.476	1.520 2.951	1.434 1.601
EVEN 3.700 ODD	MODE 0.0123	0.4683 0.3326	63.3 119.0	3.193 6.565	1.495 1.708	4.089 7.640	1.641 1.858
EVEN 3.900 ODD	MODE 0.0130	0.4642 0.3322	64.3 119.2	13.064 26.226	1.625 1.882	16.491 29.736	1.797 2.036
EVEN 4.100 ODD	MODE 0.0137	0.4602 0.3319	65.3 119.4	14.136 27.744	0.392 0.123	17.609 30.656	0.252 0.068
EVEN 4.300 ODD	MODE 0.0143	0.4563 0.3315	66.3 119.5	4.193 8.052	0.497 0.281	5.160 8.693	0.391 0.262
EVEN 4.500 ODD	MODE 0.0150	0.4526 0.3312	67.2 119.7	1.868 3.513	0.654 0.506	2.270 3.710	0.591 0.518
EVEN 4.700 ODD	MODE 0.0157	0.4490 0.3308	68.1 119.9	1.079 1.989	0.741 0.629	1.296 2.058	0.701 0.658
EVEN 4.900 ODD	MODE 0.0163	0.4455 0.3304	69.0 120.0	0.722 1.305	0.793 0.703	0.858 1.324	0.767 0.741
EVEN 5.100 ODD	MODE 0.0170	0.4421 0.3300	69.8 120.2	0.529 0.938	0.828 0.752	0.621 0.936	0.812 0.796

TABLE VI. Coupled Slot Lines on a Ferrite Substrate

CO-PLANAR WAVEGUIDE ON FERRITE SUBSTRATE

THICKNESS OF DIELECTRIC = 0.100 CM W/D = 1.000 S/D = 0.500

PERMITTIVITY = 20.0

SATURATION MAGNETISATION = 2300.00 GAUSS

MAGNETIC BIASING FIELD = 683.60 OERSTED

LINEWIDTH = 100.00 OERSTED LANDÉ-G FACTOR = 2.0

GENERAL DATA FOR DIELECTRIC SUBSTRATE				FERRITE SUBSTRATE WAVE TRAVELING			
FREQ GHZ	D LAMBDA	LAMBDA P LAMBDA	Z0	FORWARD		REVERSE	
				ALPHA DB/CM	BETA=FF BETA-DI	ALPHA DB/CM	BETA=FF BETA-DI
2.500	0.0083	0.3345	58.9	0.192	1.167	0.269	1.257
2.700	0.0090	0.3342	59.0	0.279	1.192	0.378	1.285
2.900	0.0097	0.3339	59.1	0.423	1.226	0.555	1.324
3.100	0.0103	0.3336	59.2	0.682	1.275	0.866	1.378
3.300	0.0110	0.3332	59.3	1.204	1.350	1.485	1.462
3.500	0.0117	0.3329	59.4	2.467	1.476	2.951	1.601
3.700	0.0123	0.3326	59.5	6.565	1.708	7.640	1.858
3.900	0.0130	0.3322	59.6	26.226	1.882	29.736	2.036
4.100	0.0137	0.3319	59.7	27.744	0.123	30.656	0.068
4.300	0.0143	0.3315	59.8	8.052	0.281	8.693	0.262
4.500	0.0150	0.3312	59.9	3.513	0.506	3.710	0.518
4.700	0.0157	0.3308	59.9	1.989	0.629	2.058	0.658
4.900	0.0163	0.3304	60.0	1.305	0.703	1.324	0.741
5.100	0.0170	0.3300	60.1	0.938	0.752	0.936	0.796
5.300	0.0177	0.3296	60.2	0.718	0.786	0.705	0.835
5.500	0.0183	0.3292	60.3	0.574	0.811	0.555	0.863

TABLE VI. Coplanar Waveguide on a Ferrite Substrate

with the line configuration and the physical parameters so that only some typical examples are given here. To generate the Tables I through VII the respective computation times are 60, 65, 95, 45, 55, 300 and 145 seconds.

For a comparison of accuracy, storage and computation time the Gaussian-quadrature integration was replaced by the adaptive Romberg integration routine 'DCADRE'. The total program length was found to be 215 K bytes while the computation time increased at least fivefold to guarantee the same numerical accuracy. The detailed and involved investigations of the numerical methods are thus justified since with the here presented program an efficient numerical application of the theory of Section 2 is presented and can be used by future users.

5.3 COMPUTER PROGRAM 'RESO' FOR RESONATING SLOT LINE AND TRANSMISSION LINE PARAMETERS FOR SHIELDED CONFIGURATIONS

A computer program which provides a numerical analysis of shielded slot lines and halfwave slot resonators is shown in Appendix N with the main program called 'RESO' and its accompanying subroutines 'COMBC' and 'DET', all written in the FORTRAN IV programming language. The preceeding commentary section of the main program describes the use, the necessary input data and explains some of the variable names which are important for input/output operations.

After the input data is read the program computes the lowest order mode cut-off frequency for a rectangular waveguide mode in the guide formed by the shielding walls and

the metal above the dielectric substrate, thus including the latter. The determining equation is given by (3-1) and can be easily programmed, shown in the subroutine 'DET'. The result is printed and is subsequently compared with the operating frequency where any further computation is terminated if the operating frequency can cause an onset of a rectangular waveguide mode. Initialization of computation loops for varying normalized frequency and slot width follow.

The first major computation is to find the wavelength ratio λ'/λ . The necessary coefficients for the determining series are provided by the subroutine 'COMBC'. Similar to the procedure described in Section 5.2 a bisectional search to find the zero of the determining functional is used to improve subsequently the accuracy of the result through several iterations. The computation stops when an accuracy of three digits after the decimal point is guaranteed for the ratio λ/λ' . The program proceeds with the computation of the characteristic impedance. The coefficients for this computation (equation 3-34) are provided again by the subroutine 'COMBC'.

Finally the computation of a halfwave slot resonator is started. Similar to the iterative procedure for the dispersion characteristic, the halfwave resonating length is found by a bisectional zero finding procedure. The result from the dispersion characteristic is used to ensure that the correct zero is found since the slot resonator would not

only resonate at a halfwave length but also at multiples thereof. For a halfwave length resonator the normalized resonating length $L/D < \frac{\lambda'/\lambda}{2D/\lambda}$. A first guess is subsequently improved until a one digit accuracy after the decimal point for L/D is obtained. The necessary integrands for equation (3-28) are provided by the subroutine 'COMBC'. It was mentioned in the general considerations to the numerical methods employed, that an estimate of the number of zeros of the integrands could improve the computational efficiency. By investigating various choices of input parameters it was found, however, that the following number of points of Gaussian quadrature integration schemes guarantee a three digit accuracy for the integration:

$$\gamma_1^2 < 0, \quad \gamma_2^2 < 0 \quad 12 \text{ points}$$

$$\gamma_1^2 > 0, \quad \gamma_2^2 < 0 \quad 24 \text{ points}$$

$$\gamma_1^2 > 0, \quad \gamma_2^2 > 0 \quad 56 \text{ points}$$

After finding the resonating length the program proceeds with the computation of the end effect of a simple short circuited slot line by evaluating the equations for the normalized short circuit reactance. All results are printed together with some of the input data. If no analysis of end coupled slot lines is desired the total procedure is reiterated for the next set of parameters of frequency and slot width.

The analysis for end coupled slot lines is performed in the same manner as the single slot resonator length is computed. Normalized reactance and mutual reactance of the coupling region are derived from the resonating length in the odd and even excitation of two resonating slots. For a given operating frequency and slot width these parameters are computed for the desired number of different separations between slots and are printed. The program starts for another set of input data from the beginning.

The subroutine 'COMBC' provides the coefficients and integrands for the various computations. The entry variable is βD for dispersion and impedance computation and is ξD for the resonator analysis. All variable names have been chosen such that the coded statements can be readily compared with the respective equations of the appropriate appendices. The transform of the assumed electric field distribution is chosen as follows. It was learned, that for the dispersion characteristic and resonator analysis a distribution

$$e_{xl}^{(1)} = \begin{cases} 1 + \left| \frac{x}{w/2} \right|^3 & |x| \leq w/2 \\ 0 & \text{elsewhere} \end{cases} \quad (5-5)$$

which is mathematically similar to (2-35a) gives almost identical results as if a distribution according to (3-26a) is chosen; both analyses seem to be relatively insensitive to

the choice of basis functions while the characteristic impedance computation is more sensitive. Furthermore, observe that the largest computation time in this program is needed for the iterative procedures for dispersion and resonator analyses. The numerical evaluation of the transform of (3-26a) given in (3-27a) requires the use of another subroutine -- a Bessel function routine -- while the transform of (5-5) simply involves algebraic manipulations of trigonometric functions as can be seen in equation (2-35b) and thus is faster on the computer. This aspect is observed in the subroutine 'COMBC' which uses the Bessel function for the power density computation only.

The total program length including all subroutines is 54 K bytes in storage. The program was compiled with the FORTRAN H compiler. A sample output is shown in Table VIII, where 23 minutes computation was needed.

SLOT-TRANSMISSION LINE AND HALF-WAVE SLOT-RESONATOR
ON A DIELECTRIC SUBSTRATE WITH SHIELDING WALLS

DIMENSIONS: $A/D = 5.50$ $H1/D = 8.00$ $H2/D = 8.00$ $EPSR = 20.0$

THE NORMALIZED LOWEST CUT-OFF FREQUENCY $D/LC = 0.0421$

$W/D = 0.200$	$D/L = 0.0200$	$LP/L = 0.3549$	$Z_0 = 59.0$	$L/D = 8.1$	$XSC = 0.129$
$T/D = 0.100$	$L-ODD/D = 8.5$	$L-EVEN/D = 7.8$	$XS = 0.134$	$MS = 0.113$	
$T/D = 0.200$	$L-ODD/D = 8.4$	$L-EVEN/D = 7.9$	$XS = 0.133$	$MS = 0.100$	
$W/D = 0.200$	$D/L = 0.0300$	$LP/L = 0.3366$	$Z_0 = 59.1$	$L/D = 5.0$	$XSC = 0.173$
$T/D = 0.100$	$L-ODD/D = 5.3$	$L-EVEN/D = 4.7$	$XS = 0.182$	$MS = 0.161$	
$T/D = 0.200$	$L-ODD/D = 5.2$	$L-EVEN/D = 4.8$	$XS = 0.179$	$MS = 0.137$	
$W/D = 0.200$	$D/L = 0.0400$	$LP/L = 0.3245$	$Z_0 = 58.5$	$L/D = 3.4$	$XSC = 0.239$
$T/D = 0.100$	$L-ODD/D = 3.7$	$L-EVEN/D = 3.2$	$XS = 0.248$	$MS = 0.234$	
$T/D = 0.200$	$L-ODD/D = 3.7$	$L-EVEN/D = 3.2$	$XS = 0.245$	$MS = 0.200$	
$W/D = 0.500$	$D/L = 0.0200$	$LP/L = 0.3684$	$Z_0 = 77.0$	$L/D = 8.4$	$XSC = 0.148$
$T/D = 0.100$	$L-ODD/D = 8.7$	$L-EVEN/D = 7.9$	$XS = 0.154$	$MS = 0.142$	
$T/D = 0.200$	$L-ODD/D = 8.7$	$L-EVEN/D = 8.0$	$XS = 0.151$	$MS = 0.128$	
$W/D = 0.500$	$D/L = 0.0300$	$LP/L = 0.3454$	$Z_0 = 77.2$	$L/D = 5.0$	$XSC = 0.209$
$T/D = 0.100$	$L-ODD/D = 5.3$	$L-EVEN/D = 4.6$	$XS = 0.225$	$MS = 0.209$	
$T/D = 0.200$	$L-ODD/D = 5.3$	$L-EVEN/D = 4.7$	$XS = 0.219$	$MS = 0.182$	
$W/D = 0.500$	$D/L = 0.0400$	$LP/L = 0.3299$	$Z_0 = 76.1$	$L/D = 3.4$	$XSC = 0.295$
$T/D = 0.100$	$L-ODD/D = 3.7$	$L-EVEN/D = 3.0$	$XS = 0.317$	$MS = 0.306$	
$T/D = 0.200$	$L-ODD/D = 3.7$	$L-EVEN/D = 3.1$	$XS = 0.311$	$MS = 0.270$	

TABLE VIII. Shielded Slot Line, Halfwave Resonator and
End Coupled Slot Lines on a Dielectric Substrate

6. SUGGESTIONS FOR FURTHER RESEARCH

Although an extensive analysis of slot lines and coplanar strip lines has been presented, several problems still remain which could be the subject of further investigation. The intention at this point of the thesis is to simply list a few of these and to provide some guidelines for their possible analysis.

The transforms of the dyadic Green's function components which were derived here are general and could be used in the analysis of different coplanar configurations. For instance, Mariani and Agrios presented in Reference 23 some preliminary experimental results for quarter wave coupled slot line resonators in a shielding box. This configuration could be useful in the design of microwave filters. To obtain numerical results for this type of line all one has to do is to approximate the anticipated electric field distribution. This approximation has to be Fourier transformed and is then applied in equation (3-28) where it replaces the transform of the assumed electric field for a single halfwave slot line resonator.

Coplanar transmission lines on a ferrite substrate have been analyzed in this thesis by a perturbational expression for the propagation constant only. These results still need an experimental verification. Furthermore, an exact analysis for these configurations seems highly desirable and is still

missing in the literature. It seems that this formulation can be easily obtained in the following manner. The transforms of the dyadic Green's function components should be derived for a ferrite substrate. The derivation would follow exactly the general concept shown in Appendix A where the permeability tensor characteristics would be implied in a general formulation from the start. Although this method would result in a higher degree of algebraic complexity it should be by now a straightforward procedure. This work would be more general and complete than any of the two analyses reported so far [Ref. 11, this thesis].

Circular apertures are used in antenna engineering and their analyses are described by various authors in the literature. But nothing has been reported so far about a circular aperture on a dielectric substrate and hence specific properties are unknown. An attempt was made to apply the Fourier transform method derived in this thesis to an analysis of this configuration. The steps of this analysis are briefly outlined in Appendix K and indicate that various and difficult problems are encountered. It cannot be predicted whether this formulation is feasible at all.

A final suggestion is the analysis of sandwich slot or coplanar strip lines. These line configurations will be similar to the one described in this thesis where another dielectric slab is placed on top of the conductor. This configuration was first suggested by Mariani and Agrios

[Ref. 23] since it offers the advantages of shorter wavelength and greater confinement of the electromagnetic fields and thus can reduce radiation losses or perturbing effects from nearby obstacles. A possible analysis would be started by developing the transforms of the dyadic Green's function components for this geometry where perhaps some simplifications could be made due to the symmetry with respect to the conductor plane.

7. CONCLUSION

A complete hybrid mode formulation has been presented for the analysis of coplanar transmission lines. The analytical methods are applied in the Fourier transform domain where dyadic Green's function components have been derived for open boundary and shielded transmission lines. These components are very general and do not depend on the specific geometry of any particular line configuration. Using these in connection with Galerkin's method, exact equations are obtained from which line parameters such as the length of a resonator and dispersion characteristics of transmission lines can be computed. Approximations by the use of a finite set of basis functions yield good numerical results.

Using the results of the dispersion problem the theory was extended to a formulation of the characteristic impedance in the Fourier transform domain. In still another extension a perturbational expression in the spectral domain was applied for the analysis of the propagation coefficient of coplanar transmission lines on a ferrite substrate. Both of these applications show the flexibility of the formulation in the Fourier domain since all necessary computations can be performed in this domain. Inversion of the transforms, a task which quite often is difficult to accomplish, is thus avoided.

Some design curves and two computer programs have been derived and are provided within this thesis. Various new information for the design of coplanar transmission lines is therefore available.

Where applicable, results were compared with other existing theories and good agreement was found in all cases.

Comparisons with experiments were also performed. In particular the numerical line parameters for coupled slot lines were used in the design of slot line directional couplers of which several different types were investigated theoretically. Due to the dispersive character of a slot line co- and contra-directional coupler design is feasible. Two directional couplers were built and their actual performances measured. Good agreement between theory and experiment further verified the validity of the analyses.

In this thesis particular interest was devoted to the analysis of specific coplanar transmission lines such as slot lines and coplanar strip lines. However, the method employed is completely versatile since it is a general formulation of an inhomogeneous transmission line problem where metal conductors of any shape are placed upon one side of a dielectric substrate.

APPENDIX A

Derivation of Spectral Domain Dyadic Green's Function Components (Open Boundary)

Equations (2-3) and (2-5) are substituted into the continuity conditions (2-14) and (2-15) and the result is transformed into the Fourier domain which yields

at $y = 0$

$$k_{c2}^2 \phi_2(\alpha, 0) = k_{c0}^2 \phi_3(\alpha, 0)$$

$$-j\alpha\gamma\phi_2(\alpha, 0) - j\omega\mu \frac{\partial}{\partial y} \psi_2(\alpha, 0) = -j\alpha\gamma\phi_3(\alpha, 0) - j\omega\mu \frac{\partial}{\partial y} \phi_3(\alpha, 0)$$

$$k_{c2}^2 \psi_2(\alpha, 0) = k_{c0}^2 \psi_3(\alpha, 0) \quad (A-1)$$

$$-j\alpha\gamma\psi_2(\alpha, 0) + j\omega\epsilon_2 \frac{\partial}{\partial y} \phi_2(\alpha, 0) = -j\alpha\gamma\psi_3(\alpha, 0) + j\omega\epsilon_0 \frac{\partial}{\partial y} \phi_3(\alpha, 0)$$

at $y = D$

$$k_{c0}^2 \phi_1(\alpha, D) = k_{c2}^2 \phi_2(\alpha, D)$$

$$-j\alpha\gamma\phi_1(\alpha, D) - j\omega\mu \frac{\partial}{\partial y} \psi_1(\alpha, D) = -j\alpha\gamma\phi_2(\alpha, D) - j\omega\mu \frac{\partial}{\partial y} \psi_2(\alpha, D)$$

$$k_{c0}^2 \phi_1(\alpha, D) = E_z(\alpha)$$

$$-j\alpha\gamma\phi_1(\alpha, D) - j\omega\mu \frac{\partial}{\partial y} \psi_1(\alpha, D) = E_x(\alpha) \quad (A-2)$$

$$k_{c0}^2 \psi_1(\alpha, D) - k_{c2}^2 \psi_2(\alpha, D) = J_x(\alpha)$$

$$-j\alpha\gamma\psi_1(\alpha, D) + j\omega\epsilon_0 \frac{\partial}{\partial y} \phi_1(\alpha, D) + j\alpha\gamma\psi_2(\alpha, D) - j\omega\epsilon_2 \frac{\partial}{\partial y} \phi_2(\alpha, D) = J_z(\alpha)$$

where $\mu_1 = \mu_2 = \mu_3 = \mu$, and $\epsilon_1 = \epsilon_3 = \epsilon_0$ so that

$$k_{c1} = k_{c3} = k_{c0}$$

The solutions to the two Helmholtz equations given by equations (2-12) and (2-13) are now substituted; the dependence of the coefficients A^e through D^h on α is understood and from here on is not shown explicitly.

$$k_{c2}^2 C^e = k_{c0}^2 D^e \quad (A-3)$$

$$-j\alpha\gamma C^e - j\omega\mu\gamma_2 B^h = -j\alpha\gamma D^e - j\omega\mu\gamma_3 D^h \quad (A-4)$$

$$k_{c2}^2 C^h = k_{c0}^2 D^h \quad (A-5)$$

$$-j\alpha\gamma C^h + j\omega\epsilon_2\gamma_2 B^e = -j\alpha\gamma D^h + j\omega\epsilon_0\gamma_3 D^e \quad (A-6)$$

$$k_{c0}^2 A^e = k_{c2}^2 B^e \sinh \gamma_2 D + k_{c2}^2 C^e \cosh \gamma_2 D \quad (A-7)$$

$$-j\alpha\gamma A^e + j\omega\mu\gamma_1 A^h = -j\alpha\gamma B^e \sinh \gamma_2 D - j\alpha\gamma C^e \cosh \gamma_2 D$$

$$-j\omega\mu\gamma_2 B^h \cosh \gamma_2 D - j\omega\mu\gamma_2 C^h \sinh \gamma_2 D \quad (A-8)$$

$$k_{c0}^2 A^e = E_z(\alpha) \quad (A-9)$$

$$-j\alpha\gamma A^e + j\omega\mu\gamma_1 A^h = E_x(\alpha) \quad (A-10)$$

$$k_{c0}^2 A^h - k_{c2}^2 B^h \sinh \gamma_2 D - k_{c2}^2 C^h \cosh \gamma_2 D = J_x(\alpha) \quad (A-11)$$

$$-j\alpha\gamma A^h - j\omega\epsilon_0\gamma_1 A^e + j\alpha\gamma B^h \sinh \gamma_2 D + j\alpha\gamma C^h \cosh \gamma_2 D$$

$$-j\omega\epsilon_2\gamma_2 B^e \cosh \gamma_2 D - j\omega\epsilon_2\gamma_2 C^e \sinh \gamma_2 D = J_z(\alpha) \quad (A-12)$$

The objective at this point is to replace the unknown coefficients A^e through D^h to obtain a direct relation between the current density and electric field components.

From equation (A-3)

$$D^e = \left(\frac{k_{c2}}{k_{c0}}\right)^2 C^e$$

and (A-5)

$$D^h = \left(\frac{k_{c2}}{k_{c0}}\right)^2 C^h$$

Substitute these in (A-4) and (A-6). Define the coefficients such that

$$F_1 = \frac{\alpha\gamma}{\omega\mu\gamma_2} \left[\left(\frac{k_{c2}}{k_{c0}}\right)^2 - 1 \right] \quad (A-13a)$$

$$F_2 = \frac{\gamma_3}{\gamma_2} \left(\frac{k_{c2}}{k_{c3}}\right)^2 \quad (A-13b)$$

$$\text{then } B^h = F_1 C^e + F_2 C^h \quad (A-14a)$$

$$\text{and } B^e = \frac{\epsilon_0}{\epsilon_2} F_2 C^e - \frac{\mu}{\epsilon_2} F_1 C^h \quad (A-14b)$$

Substitute (A-14) in (A-7) and define

$$G_1 = \left(\frac{k_{c2}}{k_{c0}}\right)^2 \left(\frac{\epsilon_0}{\epsilon_2} F_2 \sinh \gamma_2 D + \cosh \gamma_2 D\right) \quad (A-15a)$$

$$G_2 = - \left(\frac{k_{c2}}{k_{c1}}\right)^2 \frac{\mu}{\epsilon_2} F_1 \sinh \gamma_2 D \quad (A-15b)$$

$$\text{then } A^e = G_1 C^e + G_2 C^h \quad (A-16a)$$

Likewise (A-8) can be rewritten if the following definition is used.

$$G_3 = \frac{\alpha \gamma}{\omega \mu \gamma_1} \left(G_1 - \frac{\epsilon_0}{\epsilon_2} F_2 \sinh \gamma_2 D - \cosh \gamma_2 D\right) - \frac{\gamma_2}{\gamma_1} F_1 \cosh \gamma_2 D \quad (A-15c)$$

$$G_4 = \frac{\alpha \gamma}{\omega \mu \gamma_1} \left(G_2 + \frac{\mu}{\epsilon_2} F_1 \sinh \gamma_2 D\right) - \frac{\gamma_2}{\gamma_1} (F_2 \cosh \gamma_2 D + \sinh \gamma_2 D) \quad (A-15d)$$

then

$$A^h = G_3 C^e + G_4 C^h \quad (A-16b)$$

Now solve for B^e through C^h in terms of A^e and A^h .

Inversion of (A-16) yields

$$C^e = J_1 A^e + J_2 A^h \quad (A-17a)$$

$$C^h = J_3 A^e + J_4 A^h \quad (A-17b)$$

where

$$J_1 = \frac{G_4}{\det G}$$

$$J_2 = \frac{-G_2}{\det G}$$

$$J_3 = \frac{-G_3}{\det G}$$

$$J_4 = \frac{G_1}{\det G}$$

$$\text{with } \det G = G_1 G_4 - G_2 G_3$$

Substitute (A-17) in (A-14) and define

$$K_1 = \frac{\epsilon_0}{\epsilon_2} F_2 J_1 - \frac{\mu}{\epsilon_2} F_1 J_3$$

$$K_2 = \frac{\epsilon_0}{\epsilon_2} F_2 J_2 - \frac{\mu}{\epsilon_2} F_1 J_4$$

$$K_3 = F_1 J_1 + F_2 J_3$$

$$K_4 = F_1 J_2 + F_2 J_4$$

then

$$B^e = K_1 A^e + K_2 A^h \quad (\text{A-19a})$$

$$B^h = K_3 A^e + K_4 A^h \quad (\text{A-19b})$$

The next substitution is (A-17) and (A-19) in (A-11) and (A-12).

Define

$$L_1 = -(K_3 \sinh \gamma_2 D + J_3 \cosh \gamma_2 D)$$

$$L_2 = 1 - \left(\frac{k_{c2}}{k_{c0}}\right)^2 (K_4 \sinh \gamma_2 D + J_4 \cosh \gamma_2 D)$$

$$L_3 = \frac{\alpha \gamma}{\omega \epsilon_0 \gamma_1} (K_3 \sinh \gamma_2 D + J_3 \cosh \gamma_2 D) \\ - \frac{\epsilon_2 \gamma_2}{\epsilon_1 \gamma_1} (K_1 \cosh \gamma_2 D + J_1 \sinh \gamma_2 D) - 1$$

$$L_4 = \frac{\alpha \gamma}{\omega \epsilon_2 \gamma_2} (K_4 \sinh \gamma_2 D + J_4 \cosh \gamma_2 D - 1) \\ - K_2 \cosh \gamma_2 D - J_2 \sinh \gamma_2 D$$

then

$$k_{c2}^2 L_1 A^e + k_{c0}^2 L_2 A^h = J_x(\alpha) \quad (A-20a)$$

$$j \omega \epsilon_0 \gamma_1 L_3 A^e + j \omega \epsilon_2 \gamma_2 L_4 A^h = J_z(\alpha) \quad (A-20b)$$

Equations (A-20) may be solved for A^e and A^h in terms of the current density components. The result substituted in (A-9) and (A-10) will eliminate all unknown coefficients and express the electric field components in terms of the current density components with the following definition.

$$DM = \left(\frac{k_{c2}}{k_{c1}}\right)^2 L_1 L_4 - \frac{\epsilon_1 \gamma_1}{\epsilon_2 \gamma_2} L_2 L_3$$

$$M_1 = \left(-\frac{j\alpha\gamma}{k_{c0}^2} L_4 - \frac{j\omega\mu\epsilon_0\gamma_1^2}{k_{c0}^2 \epsilon_2 \gamma_2} L_3\right) \frac{1}{DM}$$

$$M_2 = \left(\frac{\alpha\gamma}{\omega\epsilon_2\gamma_2} L_2 + \frac{\mu\gamma_1}{\epsilon_2\gamma_2} \left(\frac{k_{c2}}{k_{c1}}\right)^2 L_1\right) \frac{1}{DM} \quad (A-21)$$

$$M_3 = \frac{L_4}{DM}$$

$$M_4 = j \frac{k_{c0}^2}{\omega\epsilon_2\gamma_2} \frac{L_2}{DM}$$

Then

$$\begin{bmatrix} M_1 & M_2 \\ M_3 & M_4 \end{bmatrix} \begin{bmatrix} J_x \\ J_z \end{bmatrix} = \begin{bmatrix} E_x \\ E_z \end{bmatrix} \quad (A-22)$$

If the M-matrix is inverted another set of coupled equations is obtained in the form

$$\begin{bmatrix} N_1 & N_2 \\ N_3 & N_4 \end{bmatrix} \begin{bmatrix} E_x \\ E_z \end{bmatrix} = \begin{bmatrix} J_x \\ J_z \end{bmatrix} \quad (A-23)$$

where with

$$\det M = M_1 M_4 - M_2 M_3$$

$$N_1 = \frac{M_4}{\det M}$$

$$N_2 = \frac{-M_2}{\det M}$$

(A-24)

$$N_3 = \frac{-M_3}{\det M}$$

$$N_4 = \frac{M_1}{\det M}$$

Note that the use of hyperbolic functions applies only if $\gamma_2^2 > 0$. For $\gamma_2^2 < 0$ the trigonometric solutions for ϕ_2 and ψ_2 apply since $\gamma_2 = j\gamma_2''$ for $\gamma_2'' = \sqrt{k_c^2 - \alpha^2}$.

APPENDIX B

Time Average Power Flow in the Spectral Domain (Open Boundary)

The following expressions for the time average power flow in the three spatial regions are derived from equation (2-26). The solutions to Helmholtz's equations given in (2-12) and (2-13) are substituted in the transformed scalar potentials of (2-27). Although the detailed derivation would be quite lengthy and therefore prohibits a presentation here, the algebraic manipulation and the analytic integration with respect to y is routine. In the following derivation the dependence of the coefficients A^e through D^h on the variable α is understood. Note also that $\gamma_1 = \gamma_3$ since regions 1 and 3 are assumed air filled.

In region 1

$$P_{avg} = - \frac{1}{8\pi} \operatorname{Re} \int_{-\infty}^{\infty} \left[\beta \omega \frac{\alpha^{2+\gamma_1^2}}{\gamma_1} (\epsilon_0 |A^e|^2 + \mu |A^h|^2) \right. \\ \left. + j2\alpha(k_0^2 A^{e*} A^h - \beta^2 A^e A^{h*}) \right] d\alpha \quad (B-1)$$

In region 2 for $\gamma_2^2 > 0$, γ_2 real

$$\begin{aligned}
 P_{\text{avg}} = & -\frac{1}{4\pi} \operatorname{Re} \int_{-\infty}^{\infty} \left\{ \left\{ \frac{\omega\beta}{2} \left[\sinh 2\gamma_2 D \left[\frac{\alpha^2 + \gamma_2^2}{2\gamma_2} (\epsilon_2 (|B^e|^2 + |C^e|^2) \right. \right. \right. \right. \right. \\
 & \left. \left. \left. + \mu (|B^h|^2 + |C^h|^2) \right) \right] \right. \right. \\
 & + D(\alpha^2 - \gamma_2^2) [\epsilon_2 (|C^e|^2 - |B^e|^2) + \mu (|C^h|^2 - |B^h|^2)] \\
 & + (\cosh 2\gamma_2 D - 1) \frac{\alpha^2 + \gamma_2^2}{2\gamma_2} (\epsilon_2 (B^e C^{e*} + B^{e*} C^e) \\
 & \left. \left. + \mu (B^h C^{h*} + B^{h*} C^h) \right) \right\} \\
 & + j \frac{\alpha}{4} \sinh 2\gamma_2 D [\beta^2 (B^e C^{h*} + B^{h*} C^e) \\
 & - k_2^2 (B^{e*} C^h + B^h C^{e*})] \\
 & + (\cosh 2\gamma_2 D - 1) [\beta^2 (B^e B^{h*} + C^e C^{h*}) \\
 & - k_2^2 (B^{e*} B^h + C^{e*} C^h)] \} \} d\alpha \\
 & \hspace{15em} (B-2)
 \end{aligned}$$

In region 2 for $\gamma_2^2 < 0$, $\gamma_2 = j\gamma_2''$, γ_2'' real

$$\begin{aligned}
 P_{\text{avg}} = & -\frac{1}{4\pi} \operatorname{Re} \int_{-\infty}^{\infty} \left\{ \frac{\omega\beta}{2} \sin 2\gamma_2'' D \left[\frac{\gamma_2''^2 - \alpha^2}{2\gamma_2''} (\epsilon_2 (|B^e|^2 - |C^e|^2) \right. \right. \\
 & \left. \left. + \mu (|B^h|^2 - |C^h|^2)) \right] \right. \\
 & + D(\alpha^2 + \gamma_2''^2) [\epsilon_2 (|B^e|^2 + |C^e|^2) + \mu (|B^h|^2 + |C^h|^2)] \\
 & + 2(1 - \cos 2\gamma_2'' D) \frac{\gamma_2''^2 - \alpha^2}{2\gamma_2''} [\epsilon_2 \operatorname{Im}(B^e C^{e*}) + \mu \operatorname{Im}(B^h C^{h*})] \} \\
 & + \frac{\alpha}{2} \sin 2\gamma_2'' D [\beta^2 (B^{h*} C^e - B^e C^{h*}) - k_2^2 (B^{e*} C^h - B^h C^{e*})] \\
 & + j \frac{\alpha}{2} (1 - \cos 2\gamma_2'' D) [\beta^2 (B^e B^{h*} - C^e C^{h*}) - k_2^2 (B^{e*} B^h - C^{e*} C^h)] \} d\alpha
 \end{aligned}$$

(B-3)

where $\operatorname{Im}(\) \rightarrow$ "imaginary part of ()"

In region 3

$$\begin{aligned}
 P_{\text{avg}} = & -\frac{1}{8\pi} \operatorname{Re} \int_{-\infty}^{\infty} \left[\omega\beta \frac{\alpha^2 + \gamma_1^2}{\gamma_1} (\epsilon_0 |D^e|^2 + \mu |D^h|^2) \right. \\
 & \left. + j2\alpha (\beta^2 D^e D^{h*} - k_0^2 D^{e*} D^h) \right] d\alpha
 \end{aligned}$$

(B-4)

The minus sign in front of all these integrals appears since a wave traveling into the $-z$ -direction was assumed.

For slot transmission lines

Observe that the coefficients B^e through D^h are expressed in terms of A^e and A^h with equations (A-19), (A-17), (A-5) and (A-3).

But A^e and A^h are expressed with (A-9) and (A-10) in terms of the transforms of the electric field components and are therefore known.

For coplanar strip transmission line

As for the slot line the coefficients B^e through D^h are expressed in terms of A^e and A^h . (See above.)

Since for this line the current densities are approximated, an explicit dependence of these two coefficients on the transform of the current density basis functions is required.

This means equations (A-20) in Appendix A have to be inverted which yields

$$A^e = \frac{M_3}{k_{c1}^2} J_x(\alpha) + \frac{M_4}{k_{c1}^2} J_z(\alpha) \quad (B-5)$$

$$A^h = - \frac{\epsilon_0 \gamma_1 L_3}{k_{c1}^2 \epsilon_2 \gamma_2 DM} J_x(\alpha) - j \frac{k_{c2}^2 L_1}{\omega \epsilon_2 \gamma_2 k_{c1}^2 DM} J_z(\alpha) \quad (B-6)$$

where all coefficients are as given in Appendix A.

With this modification the expressions for the time average power (B-1) to (B-4) apply for the coplanar strip line as well as the slot line.

APPENDIX C

Perturbation Theory for Open Boundary Waveguides

In this appendix a perturbational expression for the propagation constant of a wave traveling on an open boundary waveguide structure is obtained. It is assumed the wave travels into the z direction and that the perturbation is a small change in the type of material within this structure.

Let \vec{E} and \vec{H} represent the fields in the unperturbed structure where the z dependence as $e^{-\gamma z}$ is implied; then

$$\vec{\nabla} \times \vec{E} = -j\omega[\mu] \vec{H} \quad (C-1)$$

$$\vec{\nabla} \times \vec{H} = j\omega[\epsilon] \vec{E} \quad (C-2)$$

and for the perturbed guide (z dependence $e^{-\gamma' z}$ implied)

$$\nabla \times \vec{E}' = -j\omega[\mu + \Delta\mu] \vec{H}' \quad (C-3)$$

$$\nabla \times \vec{H}' = j\omega[\epsilon + \Delta\epsilon] \vec{E}' \quad (C-4)$$

where "[]" denotes a tensor quantity.

The last two equations are scalarly multiplied by \vec{H}^* and \vec{E}^* while the conjugates of the first two are scalarly multiplied by \vec{H}' and \vec{E}' respectively, which yields

$$\vec{H}' \cdot \vec{\nabla} \times \vec{E}^* = j\omega[\mu]^* \vec{H}^* \cdot \vec{H}' \quad (C-5)$$

$$\vec{E}' \cdot \vec{\nabla} \times \vec{H}^* = -j\omega[\epsilon]^* \vec{E}^* \cdot \vec{E}' \quad (C-6)$$

$$\vec{H}^* \cdot \vec{\nabla} \times \vec{E}' = -j\omega[\mu+\Delta\mu] \vec{H}' \cdot \vec{H}^* \quad (C-7)$$

$$\vec{E}^* \cdot \vec{\nabla} \times \vec{H}' = j\omega[\epsilon+\Delta\epsilon] \vec{E}' \cdot \vec{E}^* \quad (C-8)$$

Equations (C-5) through (C-8) are now combined to obtain

$$\vec{\nabla} \cdot (\vec{H}' \times \vec{E}^*) = j\omega[\epsilon+\Delta\epsilon] \vec{E}' \cdot \vec{E}^* - j\omega[\mu]^* \vec{H}^* \cdot \vec{H}' \quad (C-9)$$

$$\vec{\nabla} \cdot (\vec{H}^* \times \vec{E}') = -j\omega[\epsilon]^* \vec{E}^* \cdot \vec{E}' + j\omega[\mu+\Delta\mu] \vec{H}' \cdot \vec{H}^* \quad (C-10)$$

where use of a vector identity is made:

$$\text{namely} \quad \vec{\nabla} \cdot (\vec{A} \times \vec{B}) = \vec{B} \cdot \vec{\nabla} \times \vec{A} - \vec{A} \cdot \vec{\nabla} \times \vec{B}$$

Now add (C-9) and (C-10) and integrate over some volume V

$$\begin{aligned} \iiint_V [\vec{\nabla} \cdot (\vec{H}' \times \vec{E}^*) + \vec{\nabla} \cdot (\vec{H}^* \times \vec{E}')] dv = \\ j\omega \iiint_V [[\epsilon+\Delta\epsilon] \vec{E}' \cdot \vec{E}^* - [\epsilon]^* \vec{E}^* \cdot \vec{E}'] dv \\ -j\omega \iiint_V [[\mu]^* \vec{H}^* \cdot \vec{H}' - [\mu+\Delta\mu] \vec{H}' \cdot \vec{H}^*] dv \end{aligned} \quad (C-11)$$

The restriction is now imposed that the material of the unperturbed structure is isotropic so that

$$[\epsilon] = \epsilon[1] = [\epsilon]^* \quad \text{and similarly for} \quad [\mu] = [\mu]^*$$

With this assumption some simplifications are possible. A further simplification of (C-11) is possible through an application of the divergence theorem. Then

$$\oint_S (\vec{H}' \times \vec{E}^* + \vec{H}^* \times \vec{E}') \cdot \vec{n} \, ds =$$

$$j\omega \iiint_V [[\Delta\epsilon] \cdot \vec{E}' \cdot \vec{E}^* + [\Delta\mu] \vec{H}' \cdot \vec{H}^*] \, dv \quad (C-12)$$

This equation is still exact and may be applied to any region V. Choose this volume such that a differential cylinder surrounds it, where the three sides are

$$S_1 \quad z = a$$

$$S_2 \quad z = b = a+dz$$

$$S_3 \quad \text{wall of cylinder at } r = \sqrt{x^2 + y^2}$$

Note that

$$\vec{H}' \times \vec{E}^* \cdot \vec{n} = -\vec{H}' \cdot \vec{n} \times \vec{E}^*$$

and $\vec{H}^* \times \vec{E}' \cdot \vec{n} = -\vec{H}^* \cdot \vec{n} \times \vec{E}'$

For an open boundary structure and r very large the outward unit normal vector $\vec{n} \rightarrow \vec{r}$

But $\lim_{r \rightarrow \infty} |\vec{H}' \times \vec{E}^* + \vec{H}^* \times \vec{E}'| \cdot \vec{r} \rightarrow 0$ since the fields

finally vanish exponentially for large r.

This means that the surface integral over S_3 is equal to zero. Denote the surface integration over S_1 as $F(a)$ and the surface integration over S_2 as $F(b)$. Then

$$F(b) = -[F(a) + \frac{\partial}{\partial z} F(z) \Big|_a \cdot dz] .$$

Since $H' \times E^* \propto e^{-(\gamma' + \gamma^*)z}$

and $H^* \times E' \propto e^{-(\gamma' + \gamma^*)z}$

then

$$\frac{\partial}{\partial z} F(z) \Big|_{z=a} = -(\gamma' + \gamma^*) F(a) .$$

This derivation applies for any a along the z axis.

Equation (C-12) can then be written as

$$\begin{aligned} & -(\gamma' + \gamma^*) dz \iint_S (\vec{H}' \times \vec{E}^* + \vec{H}^* \times \vec{E}') \cdot \vec{n} \, ds \\ & = j\omega \iiint_V [[\Delta\epsilon] \vec{E}' \cdot \vec{E}^* + [\Delta\mu] \vec{H}' \cdot \vec{H}^*] \, dv \quad (C-13) \end{aligned}$$

where S is the cross-section of the structure and extends to infinity.

The right hand side of equation (C-13) remains essentially constant for a small enough variation in z so that the volume integral can be replaced by

$$j\omega \, dz \iint_S [[\Delta\epsilon] \vec{E}' \cdot \vec{E}^* + [\Delta\mu] \vec{H}' \cdot \vec{H}^*] \, dS .$$

Noting that $[\Delta\epsilon] = [\epsilon'] - [\epsilon]$ and $[\Delta\mu] = [\mu'] - [\mu]$

$$\text{where } [\epsilon] = \epsilon_0 ([1] + [\chi_e])$$

$$\text{and } [\mu] = \mu_0 ([1] + [\chi])$$

the difference between the perturbed and unperturbed susceptibility tensors is found to be

$$[\Delta\chi_e] = [\chi'_e] - [\chi_e]$$

$$[\Delta\chi] = [\chi'] - [\chi] \quad .$$

(C-13) can then be brought into the final form of

$$\gamma' + \gamma^* = \frac{j\omega \iint_{\Delta S} (\epsilon_0 [\Delta\chi_e] \cdot \vec{E}' \cdot \vec{E}^* + \mu_0 [\Delta\chi] \cdot \vec{H}' \cdot \vec{H}^*) \, ds}{\iint_S (\vec{E}^* \times \vec{H}' + \vec{E}' \times \vec{H}^*) \cdot \vec{a}_z \, ds}$$

The susceptibility tensors are internal tensors and therefore apply to the internal fields only. As it can be seen in Section 2.4.2 it is more convenient to use the external fields and external tensors if due to the physical shape of the ferrite demagnetization must be taken into account.

$$[\chi_e] \vec{E}' = [\chi_e^e] \vec{E}$$

$$\text{and } [\chi] \vec{H}' = [\chi^e] \vec{H}$$

where the superscript "e" denotes external.

Equation (2-40) is now obtained. This detailed perturbational analysis of an open boundary waveguide could not be found in the literature and hence was rigorously carried out to prove its application for the slot line.

APPENDIX D

Perturbational Expression for the Propagation Constant in the Spectral Domain

Apply Parseval's relation to equation (2-42) which is then

$$\begin{aligned}
 \gamma' + \gamma^* = & \frac{j\omega\mu_0}{8\pi P_{avg}} \int_{-\infty}^{\infty} \int_0^D \left\{ \chi_{yy} [\beta^2 \left| \frac{\partial \Psi_2}{\partial y} \right|^2 + (\alpha\omega\epsilon_2)^2 |\Phi_2|^2 \right. \\
 & \left. \pm j\alpha\omega\epsilon_2 \beta (\Phi_2 \frac{\partial \Psi_2^*}{\partial y} - \Phi_2^* \frac{\partial \Psi_2}{\partial y}) \right. \\
 & \left. + 2k_{c2}^2 \chi_{yz} [\mp j\beta \frac{\partial \Psi_2}{\partial y} \Psi_2^* + \alpha\omega\epsilon_2 \Phi_2 \Psi_2^*] \right. \\
 & \left. + \chi_{zz} k_{c2}^4 |\Psi_2|^2 \right\} dy d\alpha \quad (D-1)
 \end{aligned}$$

The transforms of the scalar potentials are known through equations (2-12) and (2-13) and the dependence of the coefficients B^e through C^h on the assumed electric field distribution is derived in Appendix A. The integration with respect to y may be carried out analytically. Since this integration is performed in the spatial region 2, the two different solutions in this region for $\gamma_2^2 > 0$ and $\gamma_2^2 < 0$ have to be considered. The amount of algebraic manipulation is quite lengthy to obtain the final form of the integrand and will not be shown here, because it contains no new information. Note that in the lossless case the lefthand side of equation (D-1) is

$$\gamma' + \gamma^* = \alpha' + j\beta' - j\beta = \alpha' + j\Delta\beta \quad .$$

A shorthand notation for the final form of equation (D-1) is then given by

$$\begin{aligned} \alpha'^{\pm} = & \frac{\omega\mu_0}{8\pi P_{avg}} \int_{-\infty}^{\infty} \left\{ \chi''_{YY} [(\beta\gamma_2)^2 (B^h)^2 + (\alpha\omega\epsilon_2)^2 (C^e)^2 \right. \\ & \left. \pm 2\omega\epsilon_2\alpha\beta\gamma_2 B^h C^e \right] \\ & + 2\hat{\chi}''_{YZ} k_{c2}^2 [\pm\beta\gamma_2 B^h C^h + \alpha\omega\epsilon_2 C^e C^h] \\ & + \chi''_{ZZ} k_{c2}^4 (C^h)^2 \} \cdot C_1 \\ & + \{ \chi''_{YY} [(\beta\gamma_2)^2 (C^h)^2 + (\alpha\omega\epsilon_2)^2 (B^e)^2 \pm 2\omega\epsilon_2\alpha\beta\gamma_2 B^e C^h] \\ & + \delta \cdot 2\hat{\chi}''_{YZ} k_{c2}^2 [\pm\beta\gamma_2 B^h C^h + \alpha\omega\epsilon_2 B^e C^h] + \chi''_{ZZ} k_{c2}^4 (B^h)^2 \} \cdot C_2 \\ & + \{ \delta \cdot \chi''_{YY} [(\beta\gamma_2)^2 B^h C^h + (\alpha\omega\epsilon_2)^2 B^e C^e \\ & \pm \omega\epsilon_2\alpha\beta\gamma_2 (B^e C^h + C^e C^h)] \\ & + \hat{\chi}''_{YZ} k_{c2}^2 [\pm\beta\gamma_2 ((B^h)^2 + \delta(C^h)^2) + \alpha\omega\epsilon_2 (\delta B^e C^h + B^h C^e)] \\ & + \chi''_{ZZ} k_{c2}^4 B^h C^h \} \cdot C_3 \} d\alpha \end{aligned} \quad (D-2)$$

where the following notation is used:

The coefficients B^e through C^h are either pure real or pure imaginary; if pure imaginary take the real part (see also Section 5)

$$\underline{\text{for } \gamma_2^2 > 0}$$

$$\delta = +1$$

$$C_1 = \frac{\sinh 2\gamma_2 D}{4\gamma_2} + \frac{D}{2}$$

$$C_2 = \frac{\sinh 2\gamma_2 D}{4\gamma_2} - \frac{D}{2}$$

$$C_3 = \frac{\cosh 2\gamma_2 D - 1}{2\gamma_2}$$

$$\underline{\text{for } \gamma_2^2 < 0, \quad \gamma_2 = j\gamma_2''} \quad (\text{replace } \gamma_2 \text{ by } \gamma_2'' \text{ in (D-2)})$$

$$\delta = -1$$

$$C_1 = \frac{\sin 2\gamma_2'' D}{4\gamma_2''} + \frac{D}{2}$$

$$C_2 = \frac{D}{2} - \frac{\sin 2\gamma_2'' D}{4\gamma_2''}$$

$$C_3 = \frac{1 - \cos 2\gamma_2'' D}{2\gamma_2''}$$

furthermore,

$$\hat{\chi}_{yz}'' = \text{Re}\{\chi_{yz}''\}$$

If the expression for $\Delta\beta^{\mp}$ is desired, the following replacements have to be made:

replace χ''_{yy} by χ'_{yy}

χ''_{zz} by χ'_{zz}

and $\hat{\chi}''_{yz}$ by χ'_{yz}

The superscript "+" on α' and $\Delta\beta$ denotes that these parameters refer to a wave traveling in the positive z direction, so that the lower signs in the integrand have to be taken wherever a double sign appears; the superscript "-" refers similarly to a wave traveling in the negative z direction where upper signs in the integrand have to be taken.

APPENDIX E

Derivation of Spectral Domain Dyadic Green's Function Components (Closed Boundary)

The continuity conditions given in equations (2-14) and (2-15) are transformed via (3-9) into the two dimensional Fourier domain. Transformed field quantities can be expressed through the solutions to the two Helmholtz's equations in equations (3-14) and (3-15) in forms of the coefficients A^e through D^h , whose dependence on α_n and ξ is understood from here on and is not shown explicitly.

at $y = 0$

$$-\alpha_n \xi C^e - j\omega\mu\gamma_2 B^h = -\alpha_n \xi D^e \sinh \gamma_1 h_2 - j\omega\mu\gamma_1 D^h \sinh \gamma_1 h_2 \quad (E-1)$$

$$C^e(k_2^2 - \xi^2) = D^e(k_0^2 - \xi^2) \sinh \gamma_1 h_2 \quad (E-2)$$

$$j\omega\epsilon_2 \gamma_2 B^e - \alpha_n \xi C^h = j\omega\epsilon_0 \gamma_1 D^e \cosh \gamma_1 h_2 - \alpha_n \xi D^h \cosh \gamma_1 h_2 \quad (E-3)$$

$$C^h(k_2^2 - \xi^2) = D^h(k_0^2 - \xi^2) \cosh \gamma_1 h_2 \quad (E-4)$$

at $y = D$

$$\begin{aligned} -\alpha_n \xi A^e \sinh \gamma_1 h_1 + j\omega\mu\gamma_1 A^h \sinh \gamma_1 h_1 = \\ -\alpha_n \xi B^e \sinh \gamma_2 D - \alpha_n \xi C^e \cosh \gamma_2 D - j\omega\mu\gamma_2 B^h \cosh \gamma_2 D \\ - j\omega\mu\gamma_2 C^h \sinh \gamma_2 D \end{aligned} \quad (E-5)$$

$$A^e(k_0^2 - \xi^2) \sinh \gamma_1 h_1 = B^e(k_2^2 - \xi^2) \sinh \gamma_2 D + C^e(k_2^2 - \alpha_z^2) \cosh \gamma_2 D \quad (E-6)$$

$$-\alpha_n \xi A^e \sinh \gamma_1 h_1 + j\omega \mu \gamma_1 A^h \sinh \gamma_1 h_1 = E_x(\alpha_n, \xi) \quad (E-7)$$

$$A^e(k_0^2 - \xi^2) \sinh \gamma_1 h_1 = E_z(\alpha_n, \xi) \quad (E-8)$$

$$\begin{aligned} & -j\omega \epsilon_0 \gamma_1 A^e \cosh \gamma_1 h_1 - \alpha_n \xi A^h \cosh \gamma_1 h_1 - j\omega \epsilon_2 \gamma_2 B^e \cosh \gamma_2 D \\ & -j\omega \epsilon_2 \gamma_2 C^e \sinh \gamma_2 D + \alpha_n \xi B^h \sinh \gamma_2 D + \alpha_n \xi C^h \cosh \gamma_2 D \\ & = J_z(\alpha_n, \xi) \end{aligned} \quad (E-9)$$

$$\begin{aligned} & A^h(k_0^2 - \xi^2) \cosh \gamma_1 h_1 - B^h(k_2^2 - \xi^2) \sinh \gamma_2 D \\ & - C^h(k_2^2 - \xi^2) \cosh \gamma_2 D = J_x(\alpha_n, \xi) \end{aligned} \quad (E-10)$$

Define

$$F_1 = \frac{k_2^2 - \xi^2}{(k_0^2 - \xi^2) \sinh \gamma_1 h_2} \quad (E-11a)$$

and

$$F_2 = \frac{k_2^2 - \xi^2}{(k_0^2 - \xi^2) \cosh \gamma_1 h_2} \quad (E-11b)$$

then (E-2) and (E-4) can be rewritten as

$$D^e = F_1 C^e \quad (E-12a)$$

$$D^h = F_2 C^h$$

The further objective is to express B^e through C^h in terms of A^e and A^h which are related to the transforms of the electric field and current density components at $y = D$. Substitute (E-12) into (E-1) and (E-3) and use the following definition:

$$\begin{aligned}
 G_1 &= \alpha_n \xi (F_1 \sinh \gamma_1 h_2 - 1) \\
 G_2 &= j\omega\mu\gamma_1 F_2 \sinh \gamma_1 h_2 \\
 G_3 &= j\omega\epsilon_0 \gamma_1 F_1 \cosh \gamma_1 h_2 \\
 G_4 &= -\alpha_n \xi (F_2 \cosh \gamma_1 h_2 - 1) \quad .
 \end{aligned}
 \tag{E-13}$$

Then

$$\begin{aligned}
 G_1 C^e + G_2 C^h &= j\omega\mu\gamma_2 B^h \\
 G_3 C^e + G_4 C^h &= j\omega\epsilon_2 \gamma_2 B^e \quad .
 \end{aligned}
 \tag{E-14}$$

(E-14) can be solved for C^e and C^h in terms of B^e and B^h to yield

$$\begin{aligned}
 C^e &= H_1 B^e + H_2 B^h \\
 C^h &= H_3 B^e + H_4 B^h
 \end{aligned}
 \tag{E-16a}$$

with

$$\begin{aligned}
 H_1 &= \frac{-j\omega\epsilon_2\gamma_2 G_2}{\det G} \\
 H_2 &= \frac{j\omega\mu\gamma_2 G_4}{\det G} \\
 H_3 &= \frac{j\omega\epsilon_2\gamma_2 G_1}{\det G} \\
 H_4 &= \frac{-j\omega\mu\gamma_2 G_3}{\det G}
 \end{aligned} \tag{E-15}$$

$$\det G = G_1 G_4 - G_2 G_3 .$$

With (E-16) now substituted into (E-5) and (E-6) and the definition of

$$\begin{aligned}
 J_1 &= -\alpha_n \xi (\sinh \gamma_2 D + H_1 \cosh \gamma_2 D) - j\omega\mu\gamma_2 H_3 \sinh \gamma_2 D \\
 J_2 &= -j\omega\mu\gamma_2 (\cosh \gamma_2 D + H_4 \sinh \gamma_2 D) - \alpha_n \xi H_2 \cosh \gamma_2 D \\
 J_3 &= (k_2^2 - \xi^2) (\sinh \gamma_2 D + H_1 \cosh \gamma_2 D) \\
 J_4 &= H_2 (k_2^2 - \xi^2) \cosh \gamma_2 D
 \end{aligned} \tag{E-17}$$

these are rewritten as

$$\begin{aligned}
 J_1 B^e + J_2 B^h &= -A^e \alpha_n \xi \sinh \gamma_1 h_1 + jA^h \omega\mu\gamma_1 \sinh \gamma_1 h_1 \\
 J_3 B^e + J_4 B^h &= A^e (k_0^2 - \xi^2) \sinh \gamma_1 h_1
 \end{aligned}$$

where now B^e and B^h can be solved for in terms of A^e and A^h .

Define

$$\begin{aligned} K_1 &= \frac{[-\alpha_n \xi J_4 - (k_0^2 - \xi^2) J_2] \sinh \gamma_1 h_1}{\det J} \\ K_2 &= \frac{j\omega\mu\gamma_1 J_4 \sinh \gamma_1 h_1}{\det J} \\ K_3 &= \frac{[\alpha_n \xi J_3 + (k_0^2 - \xi^2) J_1] \sinh \gamma_1 h_1}{\det J} \\ K_4 &= \frac{-j\omega\mu\gamma_1 J_3 \sinh \gamma_1 h_1}{\det J} \end{aligned} \quad (E-18)$$

$$\det J = J_1 J_4 - J_2 J_3 \quad .$$

Then

$$B^e = K_1 A^e + K_2 A^h \quad (E-19a)$$

$$B^h = K_3 A^e + K_4 A^h \quad (E-19b)$$

Now (E-16) and (E-19) are substituted into (E-9) and (E-10).

Define

$$\begin{aligned} L_1 &= -j\omega\epsilon_0\gamma_1 \cos \gamma_1 h_1 - j\omega\epsilon_2\gamma_2 K_1 \cosh \gamma_2 D - j\omega\epsilon_2\gamma_2 (H_1 K_1 + H_2 K_3) \cdot \\ &\quad \cdot \sinh \gamma_2 D \\ &\quad + \alpha_n \xi K_3 \sinh \gamma_2 D + \alpha_n \xi (H_3 K_1 + H_4 K_3) \cosh \gamma_2 D \end{aligned}$$

$$\begin{aligned}
L_2 = & -\alpha_n \xi \cosh \gamma_1 h_1 - j\omega \epsilon_2 \gamma_2 K_2 \cosh \gamma_2 D - j\omega \epsilon_2 \gamma_2 (H_1 K_2 + H_2 K_4) \sinh \gamma_2 D \\
& + \alpha_n \xi K_4 \sinh \gamma_2 D + \alpha_n \xi (H_3 K_2 + H_4 K_4) \cosh \gamma_2 D
\end{aligned} \tag{E-20}$$

$$L_3 = -(k_2^2 - \xi^2) K_3 \sinh \gamma_2 D - (k_2^2 - \xi^2) (H_3 K_1 + H_4 K_3) \cosh \gamma_2 D$$

$$\begin{aligned}
L_4 = & (k_0^2 - \xi^2) \cosh \gamma_1 h_1 - (k_2^2 - \xi^2) K_4 \sinh \gamma_2 D \\
& - (k_2^2 - \xi^2) (H_3 K_2 + H_4 K_4) \cosh \gamma_2 D .
\end{aligned}$$

Then

$$L_1 A^e + L_2 A^h = J_z \tag{E-21a}$$

$$L_3 A^e + L_4 A^h = J_x . \tag{E-21b}$$

Equations (E-7) and (E-8) can be solved for A^e and A^h yielding

$$A^e = \frac{E_z}{(k_0^2 - \xi^2) \sinh \gamma_1 h_1} \tag{E-22a}$$

$$A^h = \frac{E_x}{j\omega \mu \gamma_1 \sinh \gamma_1 h_1} + \frac{\alpha_n \xi E_z}{j\omega \mu \gamma_1 (k_0^2 - \xi^2) \sinh \gamma_1 h_1} . \tag{E-22b}$$

Substitute (E-22) in (E-21) and define

$$M_3 = \frac{L_2}{j\omega \mu \gamma_1 \sinh \gamma_1 h_1}$$

$$\begin{aligned}
 M_4 &= \frac{L_1}{(k_0^2 - \xi^2) \sinh \gamma_1 h_1} + \frac{\alpha_n \xi L_2}{j\omega\mu\gamma_1 (k_0^2 - \xi^2) \sinh \gamma_1 h_1} \\
 M_1 &= \frac{L_4}{j\omega\mu\gamma_1 \sinh \gamma_1 h_1} \\
 M_2 &= \frac{L_3}{(k_0^2 - \xi^2) \sinh \gamma_1 h_1} + \frac{\alpha_n \xi L_4}{j\omega\mu\gamma_1 (k_0^2 - \xi^2) \sinh \gamma_1 h_1}
 \end{aligned}
 \tag{E-22}$$

Then

$$M_1 E_x + M_2 E_z = J_x \tag{E-23a}$$

$$M_3 E_x + M_4 E_z = J_z \tag{E-23b}$$

APPENDIX F

Time Average Power Flow in the Spectral Domain (Closed Boundary)

A short hand notation for equation (3-34) is

$$P_{avg} = \frac{1}{4a} \operatorname{Re} \sum_{n=-\infty}^{\infty} (P_{1n} + P_{2n} + P_{3n}) \quad (F-1)$$

where the first subscript denotes the spatial region 1 to 3. These terms P_{in} are then found by substitution of (3-17) and (3-18) into (3-34) where the variable ξ is replaced by the constant β . The integration with respect to y can be performed analytically since (3-17) and (3-18) show a simple dependence on this variable. Without showing the details of this rather lengthy but straightforward algebraic manipulation the single terms for equation (F-1) are given below with the following implication. Only a first order approximation will be used, hence $E_z(\alpha_n) = 0$ and through (E-22a) $A^e(\alpha_n) = 0$.

Then

$$P_{1n} = \frac{\omega \mu_0 \beta}{2} \left[\frac{\alpha_n^2 + \gamma_1^2}{2\gamma_1} \sinh(2\gamma_1 h_1) + (\alpha_n^2 - \gamma_1^2) h_1 \right] |A^h(\alpha_n)|^2 \quad (F-2)$$

$$\begin{aligned}
P_{3n} = & \frac{\omega \mu_0 \beta}{2} \left[\frac{\alpha_n^2 + \gamma_1^2}{2\gamma_1} \sinh(2\gamma_1 h_2) - (\alpha_n^2 - \gamma_1^2) h_2 \right] |D^e(\alpha_n)|^2 \\
& + \frac{\omega \mu_0 \beta}{2} \left[\frac{\alpha_n^2 + \gamma_1^2}{2\gamma_1} \sinh(2\gamma_1 h_2) + (\alpha_n^2 - \gamma_1^2) h_2 \right] |D^h(\alpha_n)|^2 \\
& + \alpha_n (k_0^2 + \beta^2) D^e(\alpha_n) D^h(\alpha_n) \sinh(2\gamma_1 h_2) \quad (F-3)
\end{aligned}$$

For P_{2n} it is not necessary to go through this cumbersome algebraic work if one observes that equations (3-17) and (3-18) are written according to the nomenclature used for the solutions for the open boundary Helmholtz's equations in the spectral domain given in equations (2-12) and (2-13). Therefore the derivations for region 2 in Appendix B hold if only the integrand is considered in equations (B-2) and (B-3) and α is replaced by α_n .

So for $\gamma_2^2 > 0$

$$P_{2n} \text{ given by integrand of (B-2) where } \alpha_n \text{ replaces } \alpha \quad (F-4)$$

and for $\gamma_2^2 < 0$

$$P_{2n} \text{ given by integrand of (B-3) where } \alpha_n \text{ replaces } \alpha \quad (F-5)$$

The coefficients A^h through D^h for the above equations are related to the assumed transform of the electric field component E_x as given in Appendix E with coefficients F_1 to

K_4 and equation (E-22). All terms of (F-1) are then known and can be evaluated on the computer after a normalization technique has been applied which is described in Section 5.

APPENDIX G

Normalized Equations for Open Boundary Lines

In this appendix the equations of Appendix A leading to the dyadic Green's function components are rewritten such that quantities are scaled with respect to the thickness D of the dielectric substrate. The equations are first written out for the two cases where $\gamma_2^2 > 0$ and $\gamma_2^2 < 0$ and are then combined in a form which lends itself towards a computer programming application.

In the following notation an imaginary quantity u is written as ju where u is then real. The normalization of the frequency with respect to D leads to

$$\omega \epsilon_0 D = \frac{1}{60} \frac{D}{\lambda}$$

$$\omega \epsilon_2 D = \frac{\epsilon_r}{60} \frac{D}{\lambda}$$

$$\omega \mu_0 D = 60 \frac{D}{\lambda} (2\pi)^2$$

where now D/λ is the normalized frequency and

$$\beta D = 2\pi \frac{D}{\lambda} \frac{\lambda}{\lambda_T}$$

From equations (2-1) and (2-2) then

$$(k_{c1}D)^2 = - (2\pi \frac{D}{\lambda})^2 [(\frac{\lambda}{\lambda_T})^2 - 1]$$

$$(k_{c2}D)^2 = (2\pi \frac{D}{\lambda})^2 [\epsilon_r - (\frac{\lambda}{\lambda_T})^2]$$

$$\gamma_1 D = [(\alpha D)^2 - (k_{c1}D)^2]^{\frac{1}{2}} \text{ which is a real quantity}$$

for αD since $1 \leq \frac{\lambda}{\lambda_T} \leq \epsilon_r$.

a) Case 1, $\gamma_2^2 > 0$

According to equation (2-11) the above condition is equivalent to $(\alpha D)^2 > (2\pi \frac{D}{\lambda})^2 [\epsilon_r - (\frac{\lambda}{\lambda_T})^2]$ so that

$$\gamma_2 D = [(\alpha D)^2 - (k_{c2}D)^2]^{\frac{1}{2}} \text{ is real.}$$

The coefficients F_1 through N_4 from Appendix A are then

$$F_1 = j F_1''$$

$$F_1'' = \frac{\alpha D}{\omega \mu D} \frac{\beta D}{\gamma_2 D} [(\frac{k_{c2}D}{k_{c1}D})^2 - 1]$$

$$F_2 = \frac{\gamma_1 D}{\gamma_2 D} (\frac{k_{c2}D}{k_{c1}D})^2$$

$$G_1 = (\frac{k_{c2}D}{k_{c1}D})^2 (\frac{F_2}{\epsilon_r} \sinh \gamma_2 D + \cosh \gamma_2 D)$$

$$G_2 = j G_2''$$

$$G_2'' = - \left(\frac{k_{c2D}}{k_{c1D}} \right)^2 \frac{(120\pi)^2}{\epsilon_r} F_1'' \sinh \gamma_2 D$$

$$G_3 = j G_3''$$

$$G_3'' = \frac{\alpha D}{\omega \mu D} \frac{\beta D}{\gamma_1 D} (G_1 - \frac{F_2}{\epsilon_r} \sinh \gamma_2 D - \cosh \gamma_2 D) - \frac{\gamma_2 D}{\gamma_1 D} F_1'' \cosh \gamma_2 D$$

$$G_4 = - \frac{\alpha D}{\omega \mu D} \frac{\beta D}{\gamma_1 D} (G_2'' + \frac{(120\pi)^2}{\epsilon_r} F_1'' \sinh \gamma_2 D) - \frac{\gamma_2 D}{\gamma_1 D} (F_2 \cosh \gamma_2 D + \sinh \gamma_2 D)$$

$$\det G = G_1 G_4 - G_2 G_3 = G_1 G_4 + G_2'' G_3''$$

$$J_1 = G_4 / \det G$$

$$J_2 = j J_2''$$

$$J_2'' = - G_2'' / \det G$$

$$J_3 = j J_3''$$

$$J_3'' = - G_3'' / \det G$$

$$J_4 = G_1 / \det G$$

$$K_1 = \frac{1}{\epsilon_r} (F_2 J_1 + (120\pi)^2 F_1'' J_3'')$$

$$K_2 = j K_2''$$

$$K_2'' = \frac{1}{\epsilon_r} (F_2 J_2'' - (120\pi)^2 F_1'' J_4)$$

$$K_3 = j K_3''$$

$$K_4 = - F_1'' J_2'' + F_2 J_4$$

$$L_1 = j L_1''$$

$$L_1'' = - (K_3'' \sinh \gamma_2 D + J_3'' \cosh \gamma_2 D)$$

$$L_2 = 1 - \frac{k_{c2} D}{k_{c1} D} (K_4 \sinh \gamma_2 D + J_4 \cosh \gamma_2 D)$$

$$L_3 = - \frac{\alpha D}{\omega \epsilon_0 D} \frac{\beta D}{\gamma_1 D} (K_3'' \sinh \gamma_2 D + J_3'' \cosh \gamma_2 D) \\ - \epsilon_r \frac{\gamma_2 D}{\gamma_1 D} (K_1 \cosh \gamma_2 D + J_1 \sinh \gamma_2 D) - 1$$

$$L_4 = j L_4''$$

$$L_4'' = \frac{\alpha D}{\omega \epsilon_2 D} \frac{\beta D}{\gamma_2 D} (K_4 \sinh \gamma_2 D + J_4 \cosh \gamma_2 D - 1) \\ - (K_2'' \cosh \gamma_2 D + J_2'' \sinh \gamma_2 D)$$

$$DM = - \left(\frac{k_{c2} D}{k_{c1} D} \right)^2 L_1'' L_4'' - \frac{1}{\epsilon_r} \frac{\gamma_1 D}{\gamma_2 D} L_2 L_3$$

$$M_1 = j M_1''$$

$$M_1'' = \left[\frac{\alpha D \beta D}{(k_{c1} D)^2} L_4'' - \frac{\omega \mu_0 D}{\epsilon_r \gamma_2 D} \left(\frac{\gamma_1 D}{k_{c1} D} \right)^2 L_3 \right] \frac{1}{DM}$$

$$M_2 = j M_2''$$

$$M_2'' = \left[\frac{\alpha D \beta D}{\omega \epsilon_2 D \gamma_2 D} L_2 + \frac{(120 \pi)^2}{\epsilon_r} \frac{\gamma_1 D}{\gamma_2 D} \left(\frac{k_{c2} D}{k_{c1} D} \right)^2 L_1'' \right] \frac{1}{DM}$$

$$M_3 = j M_3''$$

$$M_3'' = L_4''/DM$$

$$M_4 = j M_4''$$

$$M_4'' = \frac{(k_{c1}D)^2}{\omega\epsilon_2 D \gamma_2 D} \frac{L_2}{DM}$$

$$\det M = M_2'' M_3'' - M_1'' M_4''$$

$$N_1 = j N_1''$$

$$N_1'' = M_4''/\det M$$

$$N_2 = j N_2''$$

$$N_2'' = -M_2''/\det M$$

$$N_3 = j N_3''$$

$$N_3'' = -M_3''/\det M$$

$$N_4 = j N_4''$$

$$N_4'' = M_1''/\det M$$

$$b) \quad \underline{\text{Case 2, } \gamma_2^2 < 0}$$

This condition implies that the normalized transform variable $(\alpha D)^2 < (2\pi \frac{D}{\lambda})^2 [\epsilon_e - (\frac{\lambda}{\lambda_1})^2]$ so that

$$\gamma_2 = j \gamma_2''$$

$$\gamma_2'' = [(k_{c2}D)^2 - (\alpha D)^2]^{1/2}$$

The coefficients F_1 through N_4 are then

$$F_1 = \frac{\alpha D}{\omega \mu D} \frac{\beta D}{\gamma_2'' D} \left[\left(\frac{k_{c2} D}{k_{c1} D} \right)^2 - 1 \right]$$

$$F_2 = j F_2''$$

$$F_2'' = - \frac{\gamma_1 D}{\gamma_2'' D} \left(\frac{k_{c2} D}{k_{c1} D} \right)^2$$

$$G_1 = \left(\frac{k_{c2} D}{k_{c1} D} \right)^2 \left(- \frac{F_2''}{\epsilon_r} \sin \gamma_2'' D + \cos \gamma_2'' D \right)$$

$$G_2 = j G_2''$$

$$G_2'' = - \left(\frac{k_{c2} D}{k_{c1} D} \right)^2 \frac{(120\pi)^2}{\epsilon_r} F_1 \sin \gamma_2'' D$$

$$G_3 = j G_3''$$

$$G_3'' = \frac{\alpha D}{\omega \mu_0 D} \frac{\beta D}{\gamma_1 D} \left(G_1 + \frac{F_2''}{\epsilon_r} \sin \gamma_2'' D - \cos \gamma_2'' D \right) - \frac{\gamma_2'' D}{\gamma_1 D} F_1 \cos \gamma_2'' D$$

$$G_4 = - \frac{\alpha D}{\omega \mu_0 D} \frac{\beta D}{\gamma_1 D} \left(G_2'' + \frac{(120\pi)^2}{\epsilon_r} F_1 \sin \gamma_2'' D \right) + \frac{\gamma_2'' D}{\gamma_1 D} (F_2'' \cos \gamma_2'' D + \sin \gamma_2'' D)$$

$$\det G = G_1 G_4 + G_2'' G_3''$$

$$J_1 = G_4 / \det G$$

$$J_2 = j J_2''$$

$$J_2'' = -G_2''/\det G$$

$$J_3 = j J_3''$$

$$J_3'' = -G_3''/\det G$$

$$J_4 = G_1/\det G$$

$$K_1 = j K_1''$$

$$K_1'' = \frac{1}{\epsilon_r} (F_2'' J_1 - (120\pi)^2 F_1 J_3'')$$

$$K_2 = \frac{1}{\epsilon_r} (-F_2'' J_2'' - (120\pi)^2 F_1 J_4)$$

$$K_3 = F_1 J_1 - F_2'' J_3''$$

$$K_4 = j K_4''$$

$$K_4'' = F_1 J_2'' + F_2'' J_4$$

$$L_1 = j L_1''$$

$$L_1'' = - (K_3 \sin \gamma_2'' D + J_3'' \cos \gamma_2'' D)$$

$$L_2 = 1 - \left(\frac{k_{c2} D}{k_{c1} D}\right)^2 (-K_4'' \sin \gamma_2'' D + J_4 \cos \gamma_2'' D)$$

$$L_3 = - \frac{\alpha D}{\omega \epsilon_0 D} \frac{\beta D}{\gamma_1 D} (K_3 \sin \gamma_2'' D + J_3'' \cos \gamma_2'' D) \\ + \epsilon_r \frac{\gamma_2 D}{\gamma_1 D} (K_1'' \cos \gamma_2'' D + J_1 \sin \gamma_2'' D) - 1$$

$$L_4 = \frac{\alpha D}{\omega \epsilon_2 D} \frac{\beta D}{\gamma_2 D} (-K_4'' \sin \gamma_2'' D + J_4 \cos \gamma_2'' D - 1) \\ - (K_2 \cos \gamma_2'' D - J_2'' \sin \gamma_2'' D)$$

$$DM = j \, DM''$$

$$DM'' = - \left(\frac{k_{c2}^D}{k_{c1}^D} \right)^2 L_1'' L_4 - \frac{1}{\epsilon_r} \frac{\gamma_1^D}{\gamma_2''^D} L_2 L_3$$

$$M_1 = j \, M_1''$$

$$M_1'' = \left[\frac{\alpha^D \beta^D}{(k_{c1}^D)^2} L_4 - \frac{\omega \mu_0^D}{\epsilon_r \gamma_2''^D} \left(\frac{\gamma_1^D}{k_{c1}^D} \right)^2 L_3 \right] \frac{1}{DM''}$$

$$M_2 = j \, M_2''$$

$$M_2'' = \left[\frac{\alpha^D \beta^D}{\omega \epsilon_2^D \gamma_2''^D} L_2 + \frac{(120\pi)^2}{\epsilon_r} \frac{\gamma_1^D}{\gamma_2''^D} \left(\frac{k_{c2}^D}{k_{c1}^D} \right)^2 L_1'' \right] \frac{1}{DM''}$$

$$M_3 = j \, M_3''$$

$$M_3'' = L_4 / DM''$$

$$M_4 = j \, M_4''$$

$$M_4'' = \frac{(k_{c1}^D)^2}{\omega \epsilon_2^D \gamma_2''^D} \frac{L_2}{DM''} \quad .$$

The equations for N_1 through N_4 are identical with those listed above for $\gamma_2^2 > 0$ and need not be reiterated here.

For programming purposes it is now important to notice that indeed a complex arithmetic on the computer can be avoided since only a real arithmetic is necessary for the evaluation of the dyadic Green's function components M_1 through N_4 . A further simplification is even possible by

comparing the two sets of equations for the two cases $\gamma_2^2 > 0$ and $\gamma_2^2 < 0$ where it can be seen that some of the equations differ only by the hyperbolic or trigonometric sine and cosine function and some algebraic signs; the double prime superscript is immaterial for the further computation since it is only used to distinguish between real and imaginary quantities in the above derivation. It is then possible to reduce the two sets of equations above to one set where depending on whether γ_2^2 is greater or less than zero the proper signs and functions are applied.

The procedure is self evident and needs no further development in this appendix. The result can easily be seen in the subroutine named "COMBO" of the attached computer program "COPLAN" where a consistent notation with the one used above is found.

APPENDIX H

Normalized Power Flow Equations

The equations for the time average power flow of open boundary coplanar transmission lines are given in Appendix B. To accomplish a formulation which allows a numerical evaluation on the digital computer the following steps are to be taken.

The coefficients A^e through D^h depend on the assumed field distribution at $y = D$ as stated in Appendix A. These dependences are given for the two cases where γ_2^2 is greater or less than zero as follows in normalized form for slot lines:

$$\underline{\gamma_2^2 > 0}$$

$$\frac{A^h}{D^2} = j \frac{A^{h''}}{D^2}$$

$$\frac{A^{h''}}{D^2} = - \frac{E_x(\alpha D)}{\omega \mu D \gamma_1 D}$$

$$\frac{B^e}{D^2} = - K_2'' \frac{A^{h''}}{D^2}$$

$$\frac{B^h}{D^2} = j \frac{B^{h''}}{D^2}$$

$$\frac{B^{h''}}{D^2} = K_4 \frac{A^{h''}}{D^2}$$

$$\frac{C^e}{D^2} = - J_2'' \frac{A^{h''}}{D^2}$$

$$\frac{C^h}{D^2} = j \frac{C^{h''}}{D^2}$$

$$\frac{C^{h''}}{D^2} = J_4 \frac{A^{h''}}{D^2}$$

$$\frac{D^e}{D^2} = \left(\frac{k_{c2D}}{k_{c1D}} \right)^2 \frac{C^e}{D^2}$$

$$\frac{D^h}{D^2} = j \frac{D^{h''}}{D^2}$$

$$\frac{D^{h''}}{D^2} = \left(\frac{k_{c2D}}{k_{c1D}} \right)^2 \frac{C^{h''}}{D^2} ,$$

$$\text{and for } \gamma_2^2 < 0$$

as above except

$$\frac{B^e}{D^2} = j \frac{B^{e''}}{D^2}$$

$$\frac{B^e}{D^2} = j \frac{B^{e''}}{D^2}$$

$$\frac{B^{e''}}{D^2} = K_2 \frac{A^{h''}}{D^2}$$

$$\frac{B^h}{D^2} = - K_4'' \frac{A^{h''}}{D^2} .$$

With the assumption $E_z(x) \approx 0$ it follows that $A^e = 0$.
The normalized equations for the power flow then become

For region 1

$$P_1 = -\frac{1}{4\pi} \int_{-\infty}^{\infty} \frac{\beta D}{2} \omega \mu D \frac{(\alpha D)^2 + (\gamma_1 D)^2}{\gamma_1 D} \left(\frac{A^{h''}}{D^2}\right)^2 d(\alpha D) \quad (H-1)$$

For region 2, $\gamma_2^2 > 0$

$$\begin{aligned} P_2 = & -\frac{1}{4\pi} \int_{-k_{c2} D}^{k_{c2} D} \left\{ \frac{\beta D}{2} \left\{ \frac{\sinh 2\gamma_2 D}{2} \left[\frac{(\alpha D)^2 + (\gamma_2 D)^2}{\gamma_2 D} \right. \right. \right. \\ & \cdot \left. \left. \left(\omega \epsilon_2 D \left(\left(\frac{B^e}{D^2}\right)^2 + \left(\frac{C^e}{D^2}\right)^2 \right) + \omega \mu D \left(\left(\frac{B^{h''}}{D^2}\right)^2 + \left(\frac{C^{h''}}{D^2}\right)^2 \right) \right) \right] \right. \\ & + \left. \left[(\alpha D)^2 - (\gamma_2 D)^2 \right] \left[\omega \epsilon_2 D \left(\left(\frac{C^e}{D^2}\right)^2 - \left(\frac{B^e}{D^2}\right)^2 \right) + \omega \mu D \left(\left(\frac{C^{h''}}{D^2}\right)^2 - \left(\frac{B^{h''}}{D^2}\right)^2 \right) \right] \right. \\ & + \left. \left(\cosh 2\gamma_2 D - 1 \right) \frac{(\alpha D)^2 + (\gamma_2 D)^2}{\gamma_2 D} \left(\omega \epsilon_2 D \frac{B^e}{D^2} \frac{C^e}{D^2} + \omega \mu D \frac{B^{h''}}{D^2} \frac{C^{h''}}{D^2} \right) \right\} \\ & + \alpha D \left[(\beta D)^2 + (k_2 D)^2 \right] \left\{ \frac{\sinh 2\gamma_2 D}{2} \left(\frac{B^e}{D^2} \frac{C^{h''}}{D^2} + \frac{C^e}{D^2} \frac{B^{h''}}{D^2} \right) \right. \\ & + \left. \frac{\cosh 2\gamma_2 D - 1}{2} \left(\frac{B^e}{D^2} \frac{B^{h''}}{D^2} + \frac{C^e}{D^2} \frac{C^{h''}}{D^2} \right) \right\} d(\alpha D) \quad (H-2a) \end{aligned}$$

For region 2, $\gamma_2^2 < 0$

$$\begin{aligned}
 P_2 = & -\frac{1}{4\pi} \int_{-\infty}^{-k_{c2}D} \frac{d(\alpha D)}{d(\alpha D)} \left\{ \frac{\beta D}{2} \left\{ \frac{\sin 2\gamma_2''D}{2} \left[\frac{(\alpha D)^2 - (\gamma_2''D)^2}{\gamma_2''D} \right. \right. \right. \\
 & \left. \left. \left. (\omega\epsilon_2 D \left(\left(\frac{C^e}{D^2} \right)^2 - \left(\frac{B^{e''}}{D^2} \right)^2 \right) + \omega\mu D \left(\left(\frac{C^h}{D^2} \right)^2 - \left(\frac{B^h}{D^2} \right)^2 \right) \right] \right. \right. \\
 & + \left. \left. \left. ((\alpha D)^2 + (\gamma_2''D)^2) \left[\omega\epsilon_2 D \left(\left(\frac{B^{e''}}{D^2} \right)^2 + \left(\frac{C^e}{D^2} \right)^2 \right) + \omega\mu D \left(\left(\frac{B^h}{D^2} \right)^2 + \left(\frac{C^{h''}}{D^2} \right)^2 \right) \right] \right. \right. \\
 & + \left. \left. \left. (\cos 2\gamma_2''D - 1) \frac{(\alpha D)^2 - (\gamma_2''D)^2}{\gamma_2''D} \left(\omega\epsilon_2 D \frac{B^{e''}}{D^2} \frac{C^e}{D^2} - \omega\mu D \frac{B^h}{D^2} \frac{C^{h''}}{D^2} \right) \right\} \right. \\
 & + \left. \left. \left. \alpha D [(\beta D)^2 + (k_2 D)^2] \left[-\frac{\sin 2\gamma_2''D}{2} \left(\frac{B^h}{D^2} \frac{C^e}{D^2} - \frac{B^{e''}}{D^2} \frac{C^{h''}}{D^2} \right) \right. \right. \right. \\
 & + \left. \left. \left. \frac{\cos 2\gamma_2''D - 1}{2} \left(\frac{B^{e''}}{D^2} \frac{B^h}{D^2} + \frac{C^e}{D^2} \frac{C^{h''}}{D^2} \right) \right] \right\} d(\alpha D) \quad (H-2b)
 \end{aligned}$$

For region 3

$$\begin{aligned}
 P_3 = & -\frac{1}{4\pi} \int_{-\infty}^{-k_{c2}D} \frac{d(\alpha D)}{d(\alpha D)} \left\{ \frac{\beta D}{2} \frac{(\alpha D)^2 + (\gamma_1 D)^2}{\gamma_1 D} \right. \\
 & \left. \left[\omega\epsilon_1 D \left(\frac{C^e}{D^2} \right)^2 + \omega\mu D \left(\frac{C^{h''}}{D^2} \right)^2 \right] + \alpha D [(\beta D)^2 + (k_0 D)^2] \frac{C^e}{D^2} \frac{C^{h''}}{D^2} \right\} d(\alpha D) . \\
 & (H-3)
 \end{aligned}$$

All coefficients in these integrands are real quantities now and can be easily programmed into a digital computer language.

To accomplish an evaluation of the time average power flow for the coplanar strip line with real coefficients, equations (B-5) and (B-6) in Appendix B have to be written explicitly for the two cases $\gamma_2^2 > 0$ and $\gamma_2^2 < 0$.

Note that in the equations given here $j_x(x) \approx 0$ is assumed. Furthermore, from equations (2-33) to (2-35) it is seen that the transform of the assumed current density $J_z(\alpha)$ is imaginary so that

$$J_z(\alpha) = j J_z''(\alpha) \quad .$$

Following the guidelines above and those in Appendix G, the coefficients A^e to D^h are then derived in terms of the assumed current density.

For $\gamma_2^2 > 0$

$$\frac{A^e}{D^2} = - \frac{M_4''}{(k_{cl} D)^2} J_z''$$

$$\frac{A^h}{D^2} = j \frac{A^{h''}}{D^2}$$

$$\frac{A^{h''}}{D^2} = - \frac{L_1''}{\omega \epsilon_2^D \gamma_2^D} \left(\frac{k_{c2}^D}{k_{c1}^D} \right)^2 \frac{J_z''}{DM}$$

$$\frac{B^e}{D^2} = K_1 \frac{A^e}{D^2} - K_2'' \frac{A^{h''}}{D^2}$$

$$\frac{B^h}{D^2} = j \frac{B^{h''}}{D^2}$$

$$\frac{B^{h''}}{D^2} = K_3'' \frac{A^e}{D^2} + K_4 \frac{A^{h''}}{D^2}$$

$$\frac{C^e}{D^2} = J_1 \frac{A^e}{D^2} - J_2'' \frac{A^{h''}}{D^2}$$

$$\frac{C^h}{D^2} = j \frac{C^{h''}}{D^2}$$

$$\frac{C^{h''}}{D^2} = J_3'' \frac{A^e}{D^2} + J_4 \frac{A^{h''}}{D^2}$$

$$\frac{D^e}{D^2} = \left(\frac{k_{c2}^D}{k_{c1}^D} \right)^2 \frac{C^e}{D^2}$$

$$\frac{D^h}{D^2} = j \frac{D^{h''}}{D^2}$$

$$\frac{D^{h''}}{D^2} = \left(\frac{k_{c2}^D}{k_{c1}^D} \right)^2 \frac{C^{h''}}{D^2} .$$

For $\gamma_2^2 < 0$

$$\frac{A^e}{D^2} = - \frac{M_4''}{(k_{c1}D)^2} J_z''$$

$$\frac{A^h}{D^2} = j \frac{A^{h''}}{D^2}$$

$$\frac{A^{h''}}{D^2} = - \frac{L_1''}{\omega \epsilon_2 D \gamma_2'' D} \left(\frac{k_{c2} D}{k_{c1} D} \right)^2 \frac{J_z''}{DM''}$$

$$\frac{B^e}{D^2} = j \frac{B^{e''}}{D^2}$$

$$\frac{B^{e''}}{D^2} = K_1'' \frac{A^e}{D^2} + K_2 \frac{A^{h''}}{D^2}$$

$$\frac{B^h}{D^2} = K_3 \frac{A^e}{D^2} - K_4'' \frac{A^{h''}}{D^2}$$

and the rest of the coefficients are as given above for $\gamma_2^2 > 0$.

The normalized equations for the power flow are then, in region 1

$$P_1 = - \frac{1}{4\pi} \int_{-\infty}^{\infty} \left\{ \frac{\beta D}{2} \frac{(\alpha D) + (\gamma_1 D)^2}{\gamma_1 D} [\omega \epsilon_0 D \left(\frac{A^e}{D^2} \right)^2 + \omega \mu D \left(\frac{A^{h''}}{D^2} \right)^2] \right. \\ \left. + \alpha D [(\beta D)^2 + (k_0 D)^2] \frac{A^e}{D^2} \frac{A^{h''}}{D^2} \right\} d(\alpha D) \quad H-4)$$

For regions 2 and 3 equations (H-2) and (H-3) apply without any further change so that here again a formulation with real quantities only can be achieved.

The further translation into a computer language is then routine.

APPENDIX J

Normalized Equations for Closed Boundary Lines

Similar to the detailed manipulation of the various coefficients for the open boundary structures shown in Appendix G, a complex arithmetic for the closed boundary coplanar lines can be avoided. The equations leading to the transforms of the dyadic Green's function components are derived in Appendix E in a general form. It must be observed that the smallest value the discrete transform variable α_n can attain is zero. For the computation of the dispersion characteristic and subsequently for the line average power flow the transform variable ξ is replaced by the propagation constant β as stated in Section 3.2 where $k_1 < \beta < k_2$, so that for computations concerning these two line parameters γ_1^2 will always be positive but γ_2^2 may be positive or negative depending on the value of α_n .

In the computation for the resonant slot length, however, the transform variable ξ extends such that $-\infty < \xi < \infty$, thus in general three possible solutions for the transformed Helmholtz's equations (3-15), (3-16) must be considered, namely

$$a) \quad \gamma_1^2 > 0 \quad , \quad \gamma_2^2 > 0$$

$$b) \quad \gamma_1^2 > 0 \quad , \quad \gamma_2^2 < 0$$

$$c) \quad \gamma_1^2 < 0 \quad , \quad \gamma_2^2 < 0$$

where a) and b) apply for the dispersion and characteristic impedance calculations as well.

The coefficients in Appendix E for these three possible sets of solutions can then be derived in normalized form, where an imaginary quantity is written as $u = j u''$. It is found that the transform of the dyadic Green's function component matrix $[M]$ is imaginary and that the evaluation of each single component can be based upon an evaluation of real quantities only for the three cases mentioned above.

Similar to the derivation indicated in Appendix G it is now possible to reduce these three sets of equations to one set, where the following notation is used for the three types of solutions:

Case a) upper signs apply

Case b) middle signs apply, ' $\sinh \gamma_2 D$ ' should be replaced by ' $\sin \gamma_2'' D$ ' and ' $\cosh \gamma_2 D$ ' by ' $\cos \gamma_2'' D$ ', furthermore ' $\gamma_2'' D$ ' replaces ' $\gamma_2 D$ '.

Case c) lower signs apply, replacements as indicated in b) above. Furthermore replace ' $\sinh \gamma_1 h$ ' by ' $\sin \gamma_1'' h$ ', ' $\cosh \gamma_1 h$ ' by ' $\cos \gamma_1'' h$ ' and ' $\gamma_1 D$ ' by ' $\gamma_1'' D$ '.

The coefficients are then

$$F_1 = + \frac{(k_2 D)^2 - (\xi D)^2}{- [(k_0 D)^2 - (\xi D)^2] \sinh \gamma_1 h_2}$$

$$F_2 = \frac{(k_2 D)^2 - (\xi D)^2}{[(k_0 D)^2 - (\xi D)^2] \cosh \gamma_1 h_2}$$

$$G_1 = \alpha_n D \xi D \left(+ F_1 \sinh \gamma_1 h_2 - 1 \right)$$

$$G_2 = + \omega \mu D \gamma_1 D F_2 \sinh \gamma_1 h_2$$

$$G_3 = + \omega \epsilon_0 D \gamma_1 D F_1 \cosh \gamma_1 h_2$$

$$G_4 = - \alpha_n D \xi D (F_2 \cosh \gamma_1 h_2 - 1)$$

$$\det G = G_1 G_4 + G_2 G_3$$

$$H_1 = \omega \epsilon_2 D \gamma_2 D G_2 / \det G$$

$$H_2 = + \omega \mu D \gamma_2 D G_4 / \det G$$

$$H_3 = + \omega \epsilon_2 D \gamma_2 D G_1 / \det G$$

$$H_4 = \omega \mu D \gamma_2 D G_3 / \det G$$

$$J_1 = - \alpha_n D \xi D (\sinh \gamma_2 D + H_1 \cosh \gamma_2 D) + \omega \mu D \gamma_2 D H_3 \sinh \gamma_2 D$$

$$J_2 = + \omega \mu D \gamma_2 D (\cosh \gamma_2 D - H_4 \sinh \gamma_2 D) - \alpha_n D \xi D H_2 \cosh \gamma_2 D$$

$$J_3 = [(k_2 D)^2 - (\xi D)^2] (\sinh \gamma_2 D + H_1 \cosh \gamma_2 D)$$

$$J_4 = H_2 [(k_2 D)^2 - (\xi D)^2] \cosh \gamma_2 D$$

$$\det J = J_1 J_4 - J_2 J_3$$

$$K_1 = \left\{ \begin{matrix} - \\ + \end{matrix} \alpha_n D \xi D J_4 + \begin{matrix} - \\ - \end{matrix} [(k_0 D)^2 - (\xi D)^2] J_2 \right\} \sinh \gamma_1 h_1 / \det J$$

$$K_2 = \begin{matrix} + \\ - \end{matrix} \omega \mu D \gamma_1 D J_4 \sinh \gamma_1 h_1 / \det J$$

$$K_3 = \begin{matrix} - \\ + \end{matrix} \left\{ \alpha_n D \xi D J_3 + [(k_0 D)^2 - (\xi D)^2] J_1 \right\} \sinh \gamma_1 h_1 / \det J$$

$$K_4 = \begin{matrix} - \\ + \end{matrix} \omega \mu D \gamma_1 D J_3 \sinh \gamma_1 h_1 / \det J$$

$$\begin{aligned} L_1 = & \begin{matrix} - \\ + \end{matrix} \omega \epsilon_0 D \gamma_1 D \cosh \gamma_1 h_1 + \begin{matrix} - \\ + \end{matrix} \omega \epsilon_2 D \gamma_2 D K_1 \cosh \gamma_2 D \\ & - \omega \epsilon_2 D \gamma_2 D (H_1 K_1 - H_2 K_3) \sinh \gamma_2 D + \begin{matrix} + \\ - \end{matrix} \alpha_n D \xi D K_3 \sinh \gamma_2 D \\ & + \alpha_n D \xi D (H_3 K_1 + \begin{matrix} + \\ - \end{matrix} H_4 K_3) \cosh \gamma_2 D \end{aligned}$$

$$\begin{aligned} L_2 = & - \alpha_n D \xi D \cosh \gamma_1 h_1 + \omega \epsilon_2 D \gamma_2 D K_2 \cosh \gamma_2 D \\ & + \begin{matrix} + \\ - \end{matrix} \omega \epsilon_2 D \gamma_2 D (H_1 K_2 + H_2 K_4) \sinh \gamma_2 D + \begin{matrix} + \\ - \end{matrix} \alpha_n D \xi D K_4 \sinh \gamma_2 D \\ & + \begin{matrix} - \\ + \end{matrix} \alpha_n D \xi D (H_3 K_2 - H_4 K_4) \cosh \gamma_2 D \end{aligned}$$

$$\begin{aligned} L_3 = & \begin{matrix} - \\ + \end{matrix} [(k_2 D)^2 - (\xi D)^2] K_3 \sinh \gamma_2 D \\ & - [(k_2 D)^2 - (\xi D)^2] (H_3 K_1 + \begin{matrix} + \\ - \end{matrix} H_4 K_3) \cosh \gamma_2 D \end{aligned}$$

$$L_4 = [(k_0 D)^2 - (\xi D)^2] \cosh \gamma_1 h_1 + [(k_2 D)^2 - (\xi D)^2] K_4 \sinh \gamma_2 D \\ + [(k_2 D)^2 - (\xi D)^2] (H_3 K_2 - H_4 K_4) \cosh \gamma_2 D$$

$$M_1 = - L_2 / \omega \mu D \gamma_1 D \sinh \gamma_1 h_1$$

$$M_2 = + [L_1 - \alpha_n D \xi D L_2 / \omega \mu D \gamma_1 D] / [(k_0 D)^2 - (\xi D)^2] \sinh \gamma_1 h_1$$

$$M_3 = - L_4 / \omega \mu D \gamma_1 D \sinh \gamma_1 h_1$$

$$M_4 = + [L_3 - \alpha_n D \xi D L_4 / \omega \mu D \gamma_1 D] / [(k_0 D)^2 - (\xi D)^2] \sinh \gamma_1 h_1 .$$

While the above equations are applicable for the dispersion characteristic calculation of shielded slot lines and slot line resonator lengths, some further manipulations are necessary to provide means for a numerical evaluation of the time average power flow computation for slot lines.

The dependence of the coefficients A^e through D^h on the assumed electric field distribution is given in Appendix E. Rewriting these equations in the normalized form and combining the two sets of equations for the two possible solutions as above where $\gamma_2^2 > 0$ and $\gamma_2^2 < 0$ then leads to the following expressions.

$$\frac{A^e}{D^2} = 0 \quad \text{since in the first order approximation it is assumed} \\ \text{that } E_z \approx 0 .$$

$$\frac{A^h}{D^2} = - \frac{E_x}{\omega \mu D \gamma_1 D \sinh \gamma_1 D h_1 / D}$$

$$\frac{B^e}{D^2} = + K_2 \frac{A^h}{D^2}$$

$$\frac{B^h}{D^2} = - K_4 \frac{A^h}{D^2}$$

$$\frac{C^e}{D^2} = + H_1 \frac{B^e}{D^2} - H_2 \frac{B^h}{D^2}$$

$$\frac{C^h}{D^2} = H_3 \frac{B^e}{D^2} + H_4 \frac{B^h}{D^2}$$

$$\frac{D^e}{D^2} = F_1 \frac{C^e}{D^2}$$

$$\frac{D^h}{D^2} = F_2 \frac{C^h}{D^2}$$

where the upper sign applies for $\gamma_2^2 > 0$ and the lower sign for $\gamma_2^2 < 0$. (Note that a quite similar notation was used for the expressions in Appendix H for the open boundary transmission lines, written there separately for $\gamma_2^2 > 0$ and $\gamma_2^2 < 0$ while the above form shows the advantage of a more composite form.)

The final step for a preparation for numerical analysis is then the normalization of the expressions for the discrete Fourier transformed power density terms given in Appendix F.

For region 1,

$$P_{1n} = \omega \mu D \frac{\beta D}{2} \left(\frac{A^h}{D^2} \right)^2 \left\{ [(\alpha_n D)^2 + (\gamma_1 D)^2] \frac{\sinh 2\gamma_1 D h_1 / D}{2\gamma_1 D} + \frac{h_1}{D} [(\alpha_n D)^2 - (\gamma_1 D)^2] \right\}$$

and for region 3,

$$P_{3n} = \omega \epsilon_0 D \frac{\beta D}{2} \left(\frac{D^e}{D^2} \right) \left\{ [(\alpha_n D)^2 + (\gamma_1 D)^2] \frac{\sinh 2\gamma_1 D h_2 / D}{2\gamma_1 D} - \frac{h_2}{D} [(\alpha_n D)^2 - (\gamma_1 D)^2] \right\} \\ + \omega \mu D \frac{\beta D}{2} \left(\frac{D^h}{D^2} \right) \left\{ [(\alpha_n D)^2 + (\gamma_1 D)^2] \frac{\sinh 2\gamma_1 D h_2 / D}{2\gamma_1 D} + \frac{h_2}{D} [(\alpha_n D)^2 - (\gamma_1 D)^2] \right\} \\ + \alpha_n D [(\beta D)^2 + (k_0 D)^2] \frac{D^e}{D^2} \frac{D^h}{D^2} \sinh 2\gamma_1 D h_2 / D .$$

The two expressions for region 2 for $\gamma_2^2 > 0$ and $\gamma_2^2 < 0$ are readily available with the integrands of equations (H-2a) and (H-2b) in Appendix H due to the same nomenclature used for the solutions to the Helmholtz equations for open and closed boundary slot lines in equations (2-12, 2-13) and (3-17, 3-18) where the continuous variable αD is replaced by the discrete variable $\alpha_n D$.

The necessary translation into a digital computer language is then routine and can be easily seen in the subroutine "COMBC" of the attached computer program "RESO" which computes parameters for shielded slot lines and resonators. A consistent nomenclature with the one used above has been used.

APPENDIX K

Circular Resonating Aperture on a Dielectric Substrate

This appendix presents an attempt to analyze a circular slot on a dielectric substrate enclosed with conducting cylindrical walls of a circular waveguide closed at both ends by conductors across the cross-sections of this guide. A schematic of this configuration is shown in Figure K/1.

This geometry is considered to be analyzed if depending on the assumed field mode of operation for a certain set of geometric parameters the resonant frequency can be found.

The following derivation is not meant to be complete and rigorous but is merely intended to outline possible problems an investigator may encounter. For analytical purposes the conductors and the dielectric are assumed to be ideal and the dimensions of the surrounding walls are such that a regular circular cavity mode cannot exist.

It is a well known fact that the scalar potential functions satisfy the Helmholtz equation which is in cylindrical coordinates

$$\frac{1}{r} \frac{\partial}{\partial r} \left(r \frac{\partial \phi}{\partial r} \right) + \frac{1}{r^2} \frac{\partial^2 \phi}{\partial \theta^2} + \frac{\partial^2 \phi}{\partial z^2} + k^2 \phi = 0 \quad . \quad (K-1)$$

If a general formulation of the resonating problem via a transformation is sought — following the guidelines in Section 2 and 3 — the partial differential equation (K-1)

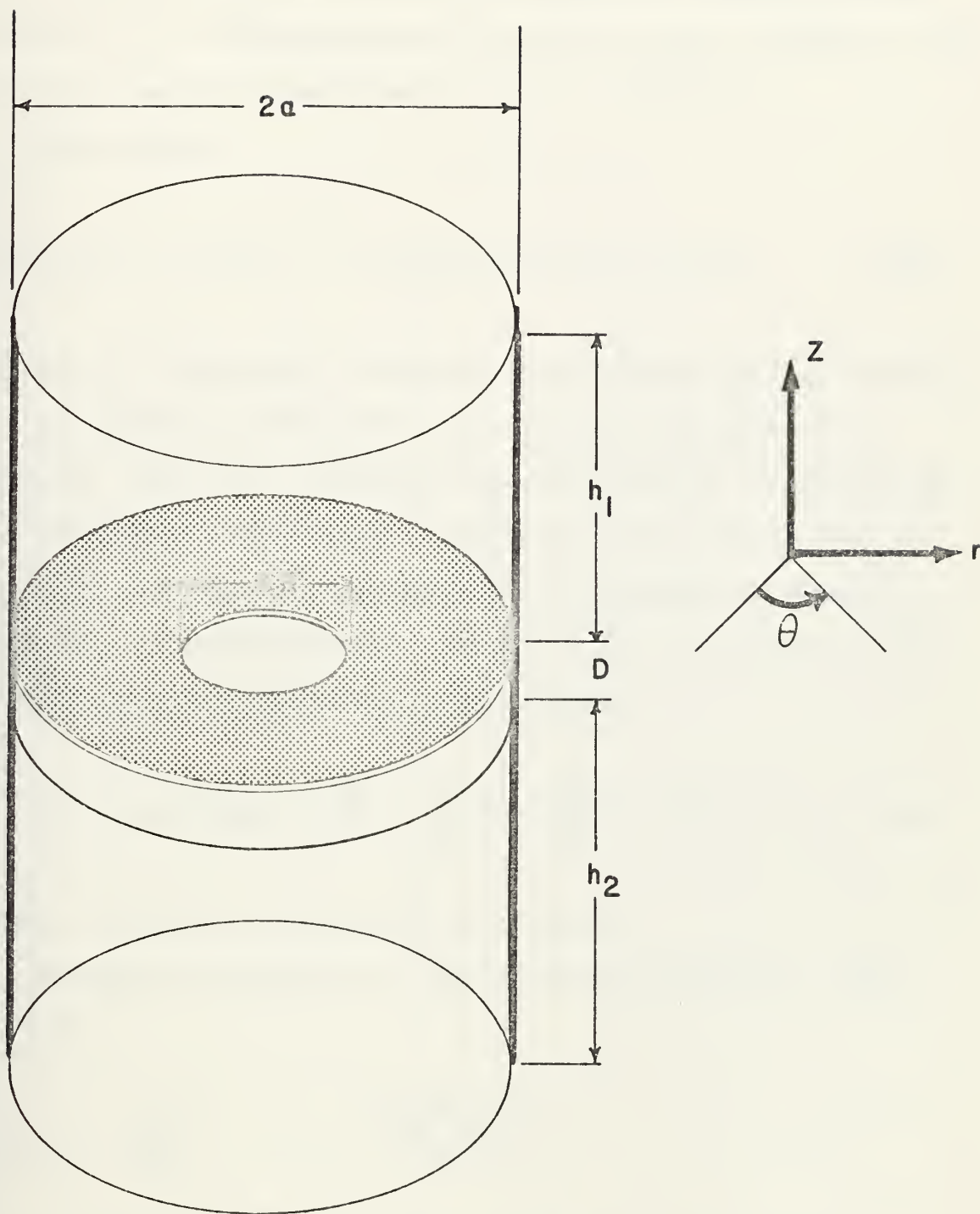


Figure K/1 Circular Resonant Aperture on a Dielectric in a Closed Cylinder

is to be transformed into an ordinary differential equation. This suggests the use of a two dimensional transform which consists of a finite Fourier transform in the variable θ and a finite Hankel transformation in the variable r .

Thus define

$$H(n, \xi_m, z) = \int_{-\pi}^{\pi} e^{jn\theta} \int_0^a r B_n(\xi_m r) h(\theta, r, z) dr d\theta \quad (K-2)$$

where B_n is the Bessel function of the first kind of order n .

It is easily shown that this transform applied to equation (K-1) will transform the differential operators of the variables θ and r into algebraic operations so that an ordinary differential equation in the variable z remains. Obviously the differential operator $\frac{\partial^2}{\partial \theta^2}$ is replaced by $-n^2$ so that equation (K-1) via (K-2) becomes

$$\int_0^a r B_n(\xi_m r) \left\{ \frac{1}{r} \frac{\partial}{\partial r} \left(r \frac{\partial h}{\partial r} \right) - \frac{n^2}{r^2} h + \frac{\partial^2 h}{\partial z^2} + k^2 h \right\} dr = 0 \quad (K-3)$$

where h is now a function of n , r and z .

Integration by parts of the first two terms will then lead to

$$\begin{aligned} & B_n(\xi_m r) r \frac{\partial h}{\partial r} \Big|_0^a - h \cdot r \frac{\partial B_n(\xi_m r)}{\partial r} \Big|_0^a \\ & + \int_0^a \frac{\partial}{\partial r} \left(r \frac{\partial B_n(\xi_m r)}{\partial r} \right) h dr - n^2 \int_0^a \frac{1}{r} B_n(\xi_m r) h dr \\ & \left(\frac{\partial^2}{\partial z^2} + k^2 \right) \int_0^a r B_n(\xi_m r) h dr = 0 \end{aligned} \quad (K-4)$$

Bessel's equation is known as

$$\frac{\partial}{\partial r} \left(r \frac{\partial B_n(\xi_m r)}{\partial r} \right) = \left(\frac{n^2}{r} - \xi_m^2 r \right) B_n(\xi_m r)$$

so that equation (K-4) can be written as

$$\frac{\partial^2}{\partial z^2} H(n, \xi_m, z) = (\xi_m^2 - k^2) H(n, \xi_m, z) \quad (K-5)$$

which is the desired ordinary differential equation.

However, this only holds if the boundary terms in (K-4) vanish. These terms must now be investigated in more detail.

But first a sidestep is to be taken to formulate the behavior of the field components and their dependence on the scalar potential functions. The fields are contained within the circular waveguide cavity so that no energy is lost due to radiation. This fact makes the problem symmetrical in the θ , r and z coordinates because standing waves do exist in these three directions. But then the fields may be expressed as TE or TM to any one of these coordinates where a conventional choice suggests the use of the z coordinate, similar to cylindrical cavities.

According to Collin [Ref. 14] one may assume a magnetic Hertzian potential $\vec{\Pi}_h = \vec{a}_z \psi(\theta, r, z)$ and an electric Hertzian potential $\vec{\Pi}_e = \vec{a}_z \phi(\theta, r, z)$ for a full or hybrid mode analysis.

The field quantities in the three cylindrical coordinates can then be expanded by Maxwell's equations to yield

$$E_r = \frac{\partial^2 \phi}{\partial r \partial z} - j\omega\mu \frac{1}{r} \frac{\partial \psi}{\partial \theta}$$

$$E_\theta = \frac{1}{r} \frac{\partial^2 \phi}{\partial \theta \partial z} + j\omega\mu \frac{\partial \psi}{\partial r}$$

$$E_z = \left(\frac{\partial^2}{\partial z^2} + k^2 \right) \phi$$

(K-6)

$$H_r = \frac{\partial^2 \psi}{\partial r \partial z} + j\omega\epsilon \frac{1}{r} \frac{\partial \phi}{\partial \theta}$$

$$H_\theta = \frac{1}{r} \frac{\partial^2 \psi}{\partial \theta \partial z} - j\omega\epsilon \frac{\partial \phi}{\partial r}$$

$$H_z = \left(\frac{\partial^2}{\partial z^2} + k^2 \right) \psi .$$

Bessel functions of the first kind are finite at the origin and have finite derivatives; similarly the scalar potential functions for this configuration will be finite with finite derivatives so that the boundary terms in equation (K-4) vanish at the lower limit. At the upper limit $r=a$ where E_z and E_θ must vanish (tangential electric field vanishes at the surface of a conductor), one of the boundary conditions for the scalar potential by equation (K-6) is then $\phi(a, \theta, z) = 0$. This requires then that $B_n(\xi_m a) = 0$ so that a discrete set of transform variables ξ_m with $m = 1, 2, 3, \dots$ is obtained where $\xi_m \cdot a$ is the m -th zero of the n -th order Bessel function.

While this derivation holds for the transformation of the potential function ϕ it is not obvious that the same set of transform variables will apply for the transformation of the function ψ for which the boundary condition is $\frac{\partial \psi}{\partial r} = 0$.

A further complication in this analysis can be foreseen as follows. For the matching of the boundary conditions at the two interfaces at $z = 0$ and $z = D$ the field components in the r and the θ direction must be transformed where it is observed that the field components in the θ direction consists of partial derivatives of the scalar potential functions with respect to the variable r . The finite Hankel transform of a derivative of a function is given by Sneddon [Ref. 25]. For instance, if $n \neq 0$ and if

$$G_n(\xi_m) = \int_0^a r B_n(\xi_m r) g(r) dr$$

then

$$\int_0^a r B_n(\xi_m r) \frac{dg}{dr} dr = \frac{n+1}{2n} \xi_m G_{n-1}(\xi_m) - \frac{n-1}{2n} \xi_m G_{n+1}(\xi_m) .$$

It is seen that a derivative in the space domain is thus transformed into a algebraic operation in the transform domain but the order of the transforming Bessel function has to be changed which further complicates this analysis.

As one may observe at this point, the relatively straightforward transform method in a rectangular coordinate system is anything but simple in a problem of cylindrical geometry.

Finally, it should be mentioned that if the Hertzian potentials are assumed to be in the other directions the set of equations (K-6) is changed in such a way that the boundary conditions are even more difficult to handle.

This problem was abandoned here, since it was felt that if this method of analysis is applicable at all further study would more appropriately be the subject of new thesis work.

APPENDIX L

Design Curves

This appendix includes some design curves for single slot and coplanar strip transmission lines. The appropriate parameters can be found in the figure captions.

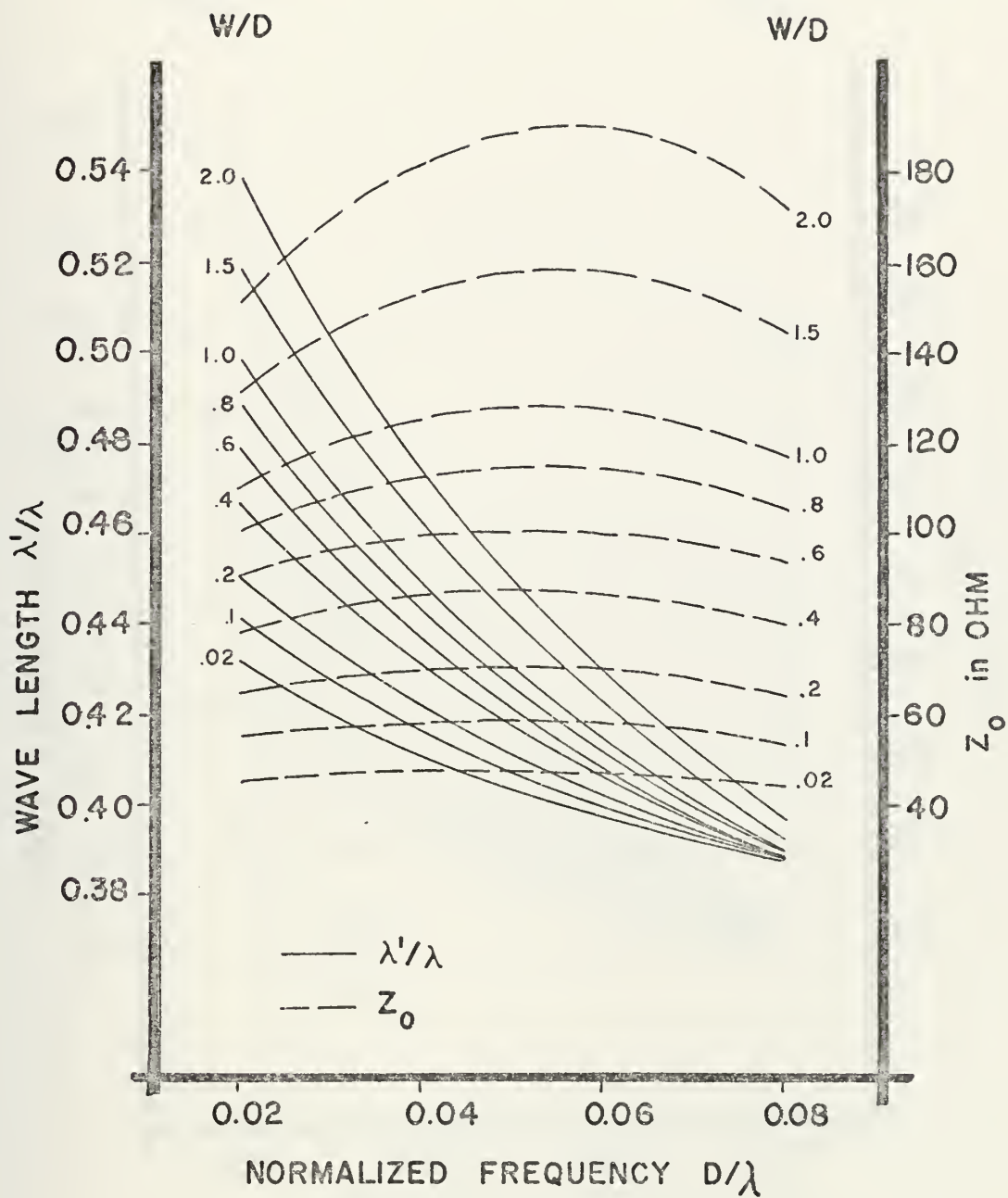


Figure L/1 Dispersion Characteristic and Characteristic Impedance of Single Slot Line with $\epsilon_r = 12$

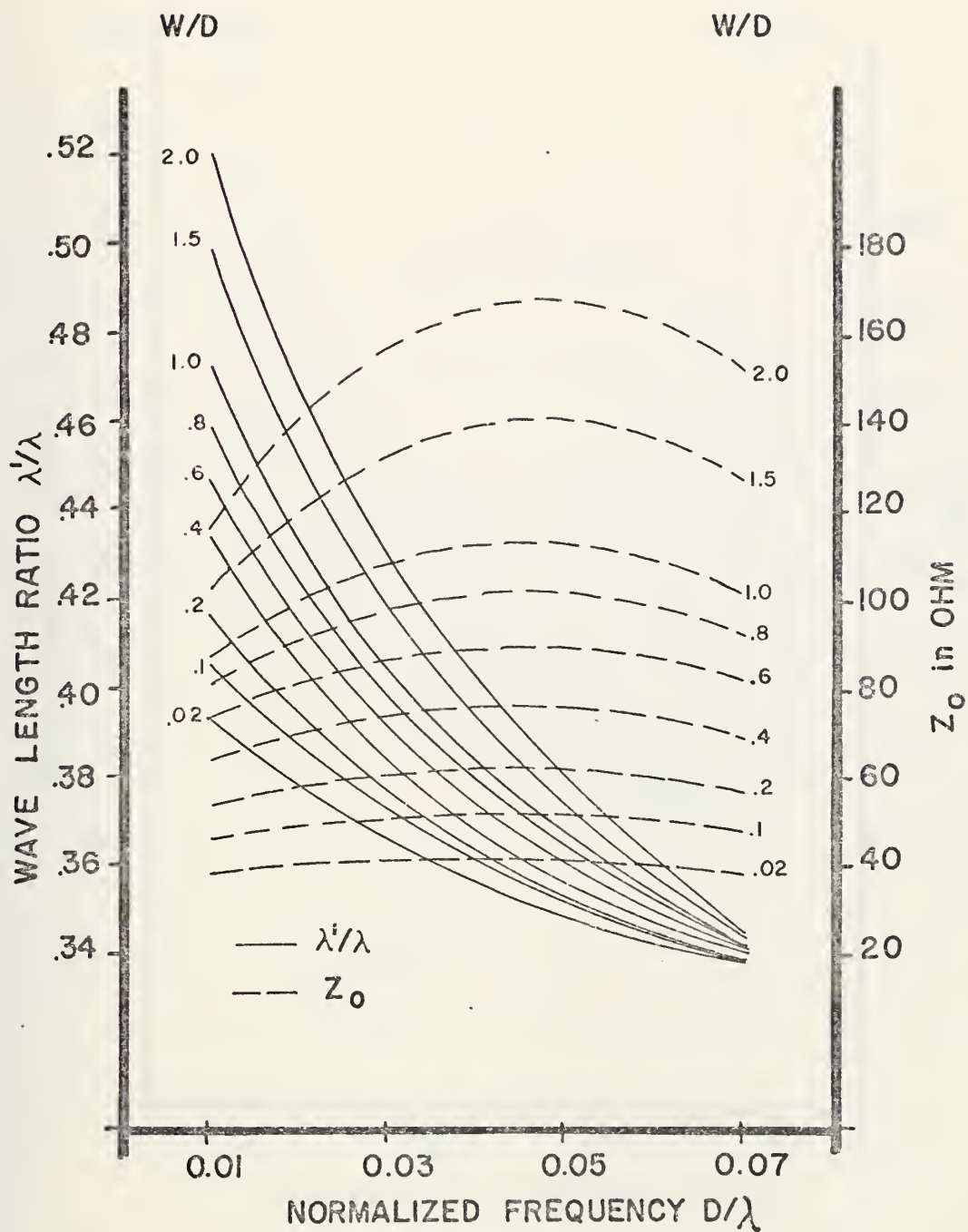


Figure L/2 Dispersion Characteristic and Characteristic Impedance of Single Slot Line with $\epsilon_r = 16$

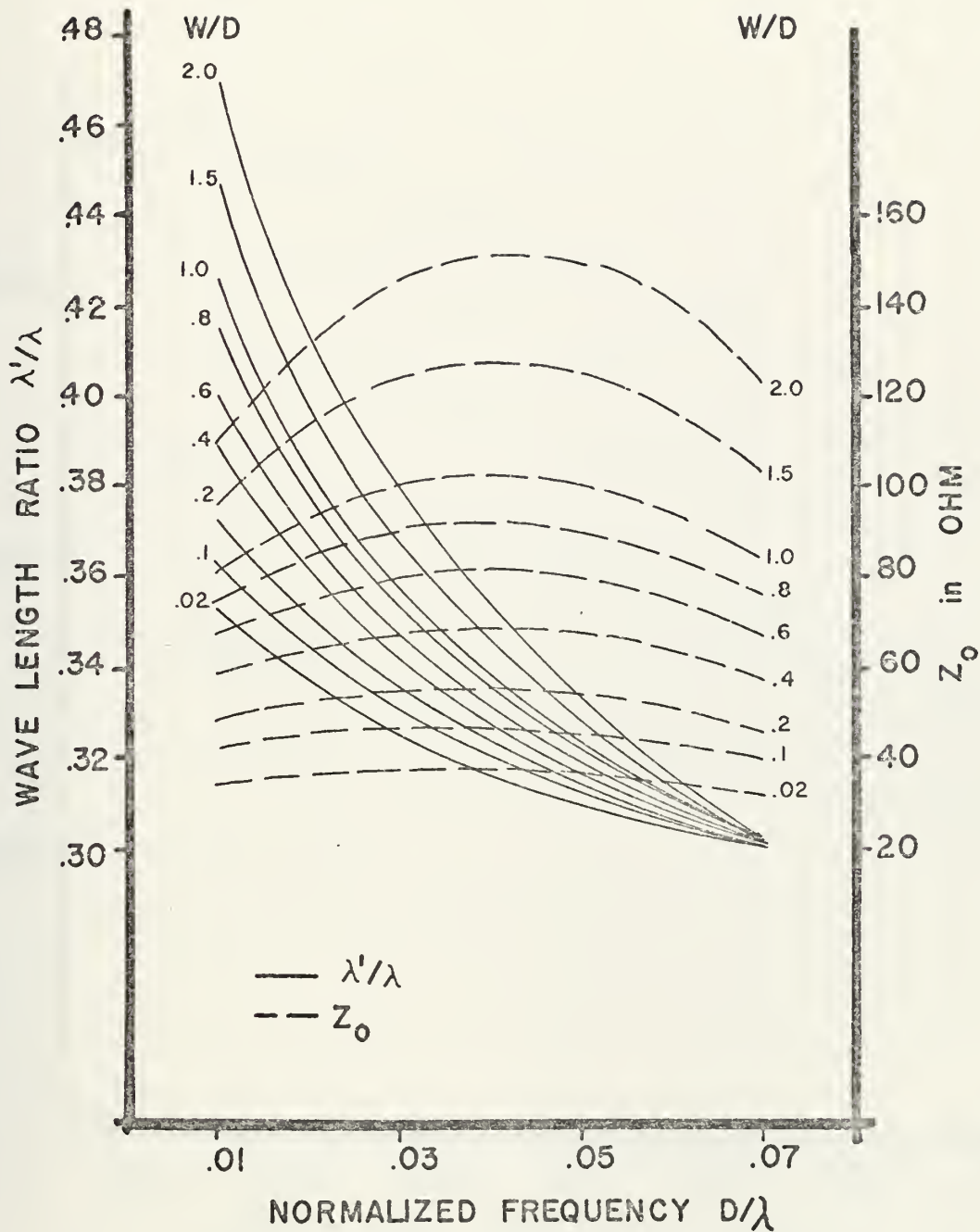


Figure L/3 Dispersion Characteristic and Characteristic Impedance of Single Slot Line with $\epsilon_r = 20$

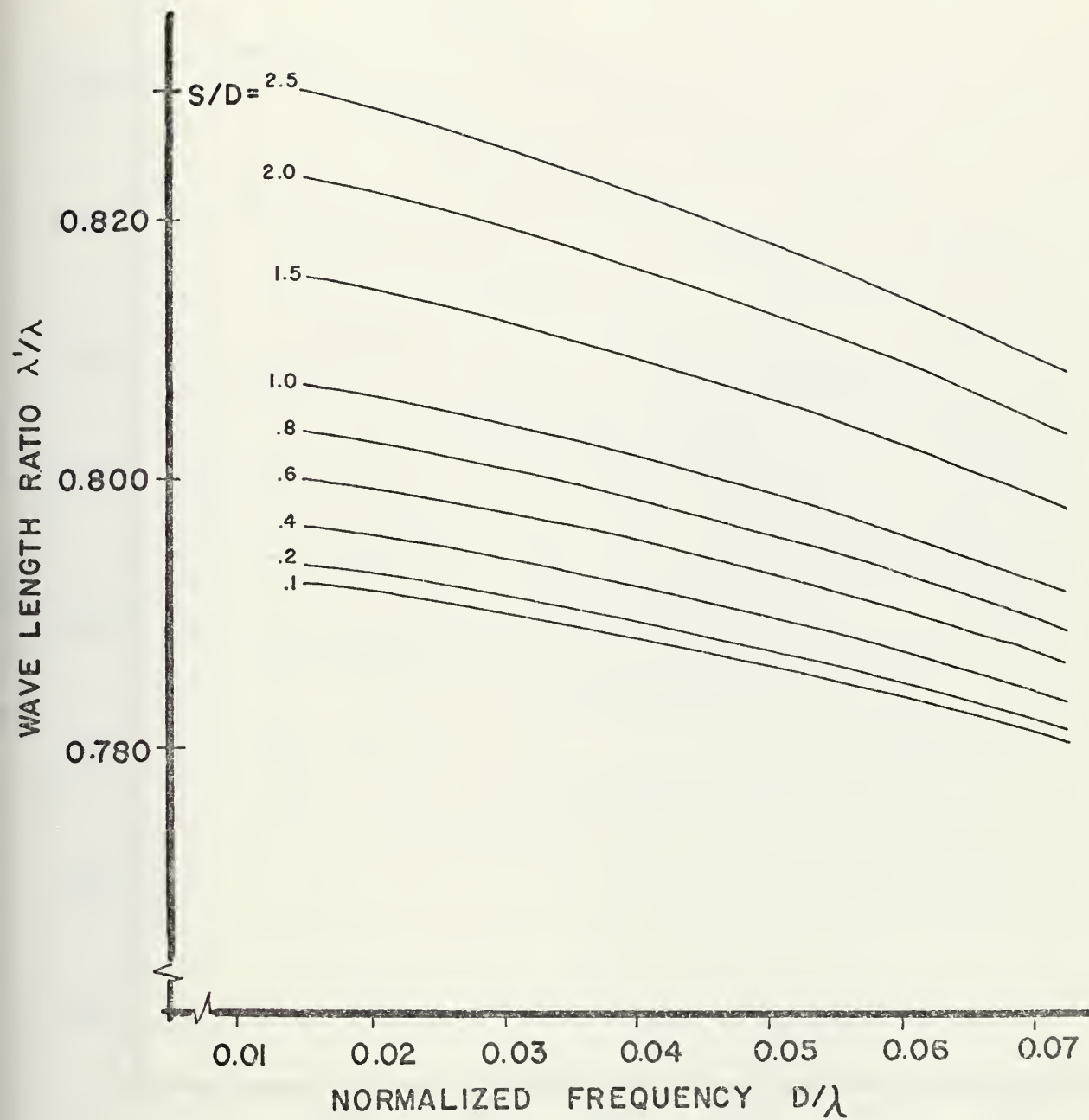


Figure L/4a Dispersion Characteristic of Coplanar Strip Line with $W/D = 1.5$ and $\epsilon_r = 2.5$

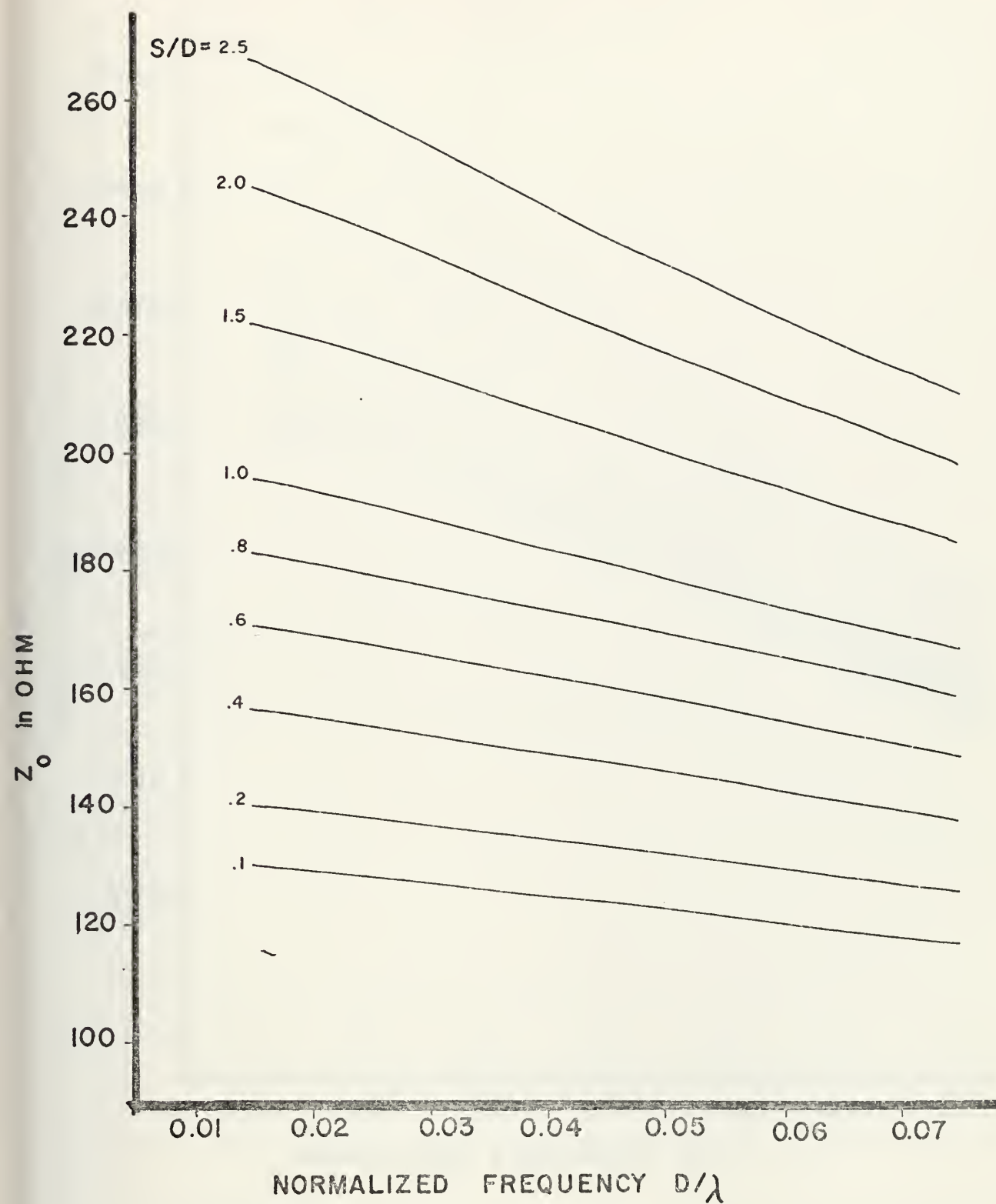


Figure L/4b Characteristic Impedance of Coplanar Strip Line with $W/D = 1.5$ and $\epsilon_r = 2.5$

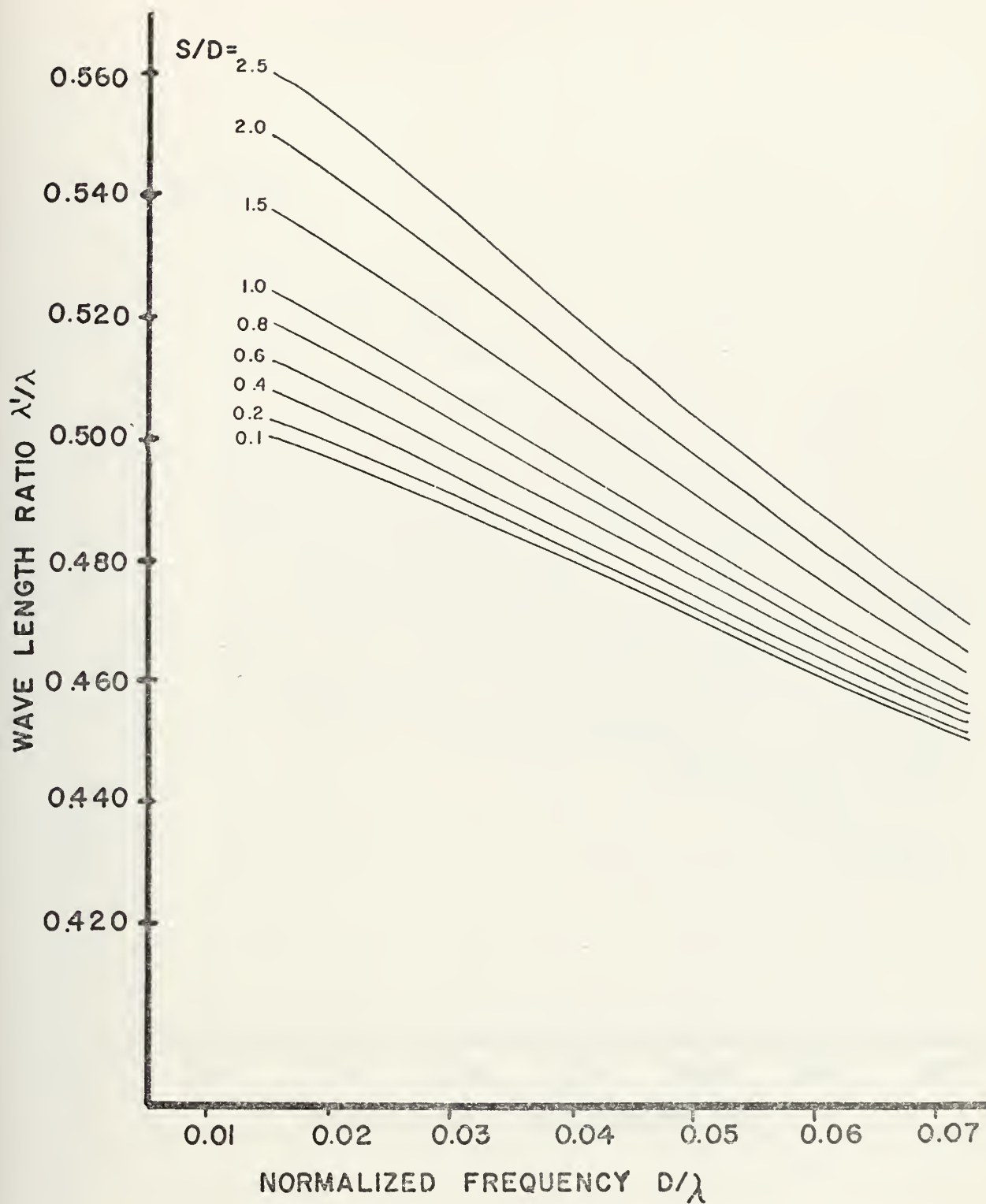


Figure L/5a Dispersion Characteristic of Coplanar Strip Line with $W/D = 1.5$ and $\epsilon_r = 9.0$

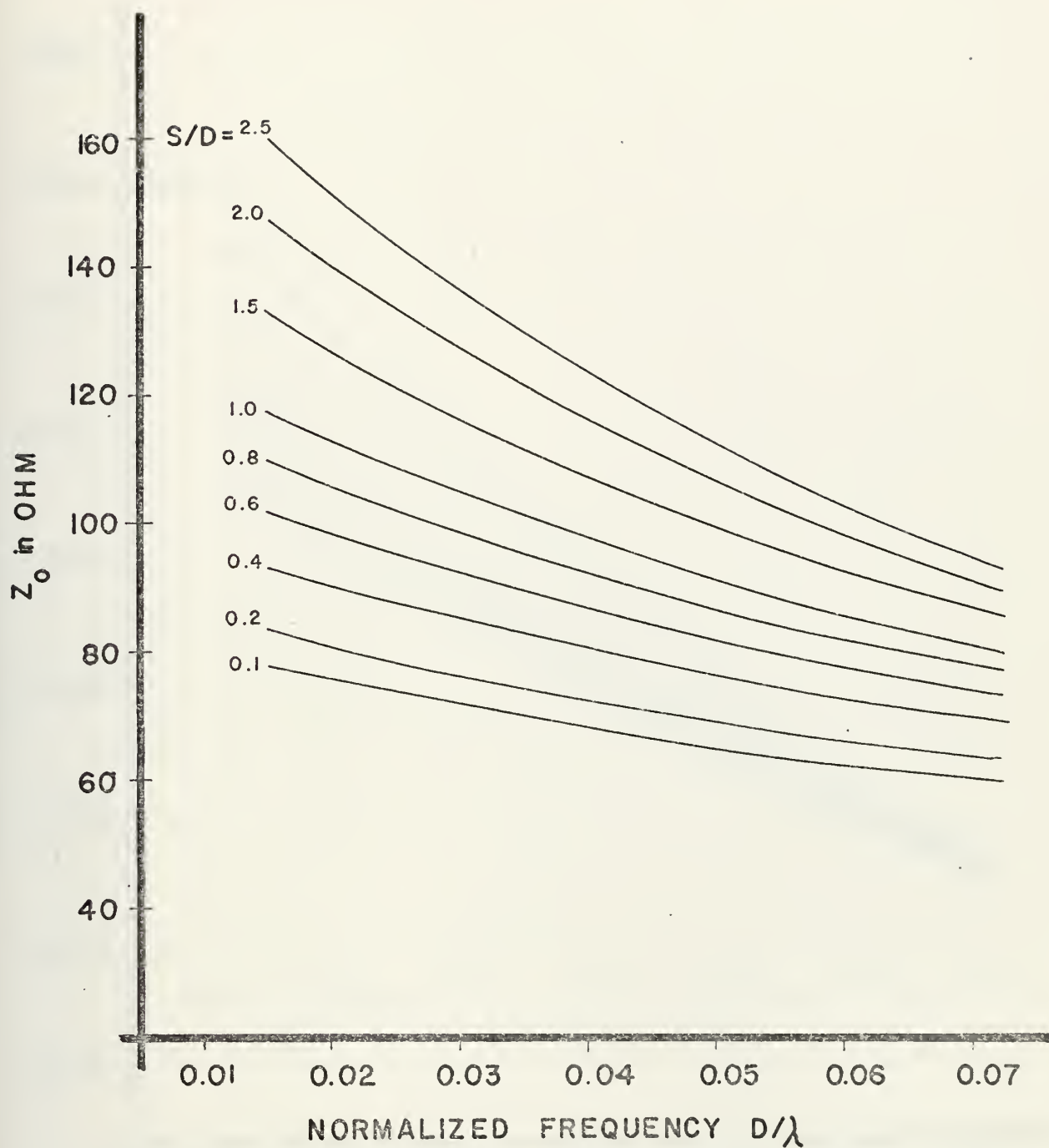


Figure L/5b Characteristic Impedance of Coplanar Strip Line with $W/D = 1.5$ and $\epsilon_r = 9.0$

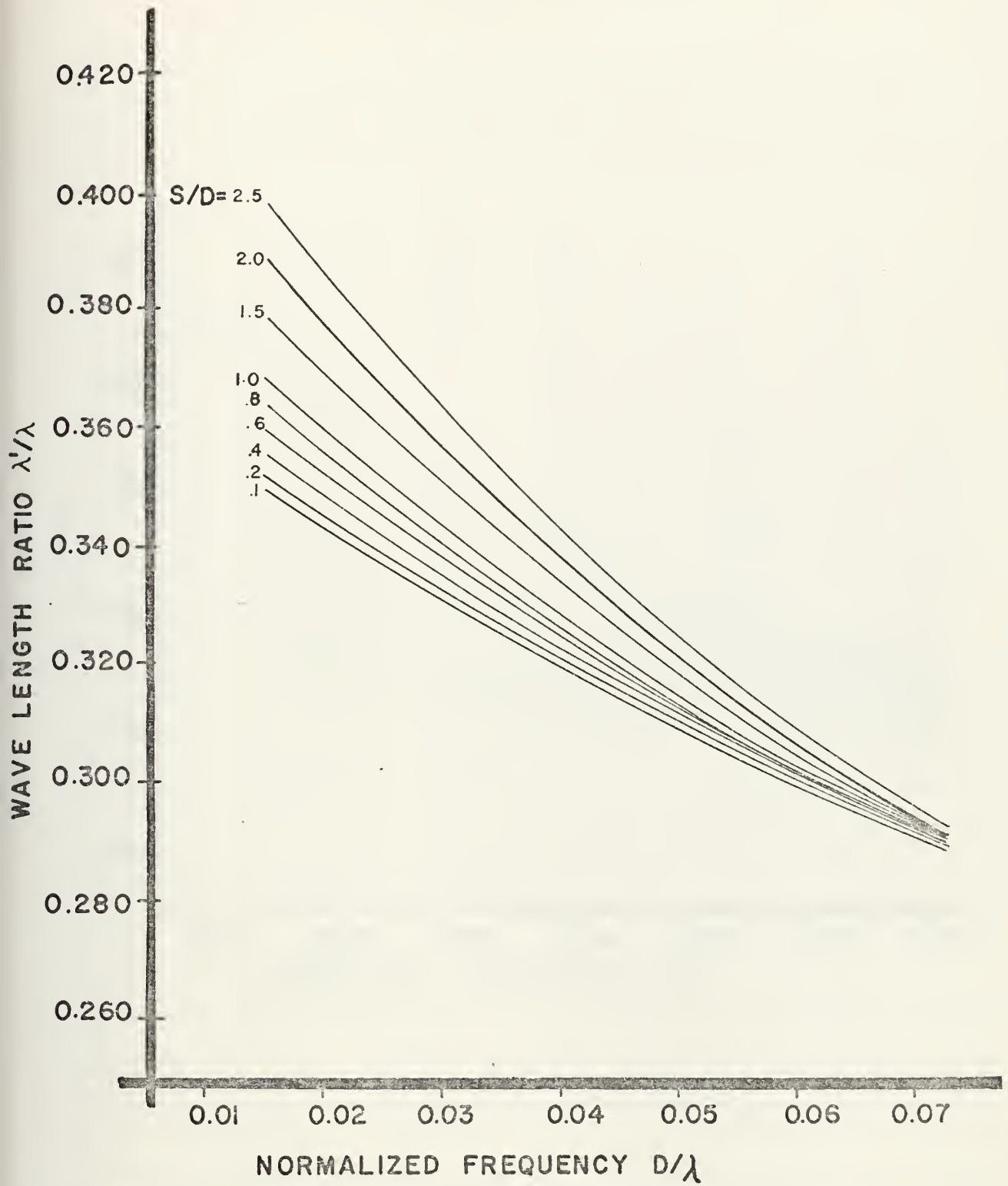


Figure L/6a Dispersion Characteristic for Coplanar Strip Line with $W/D = 1.5$ and $\epsilon_r = 20$

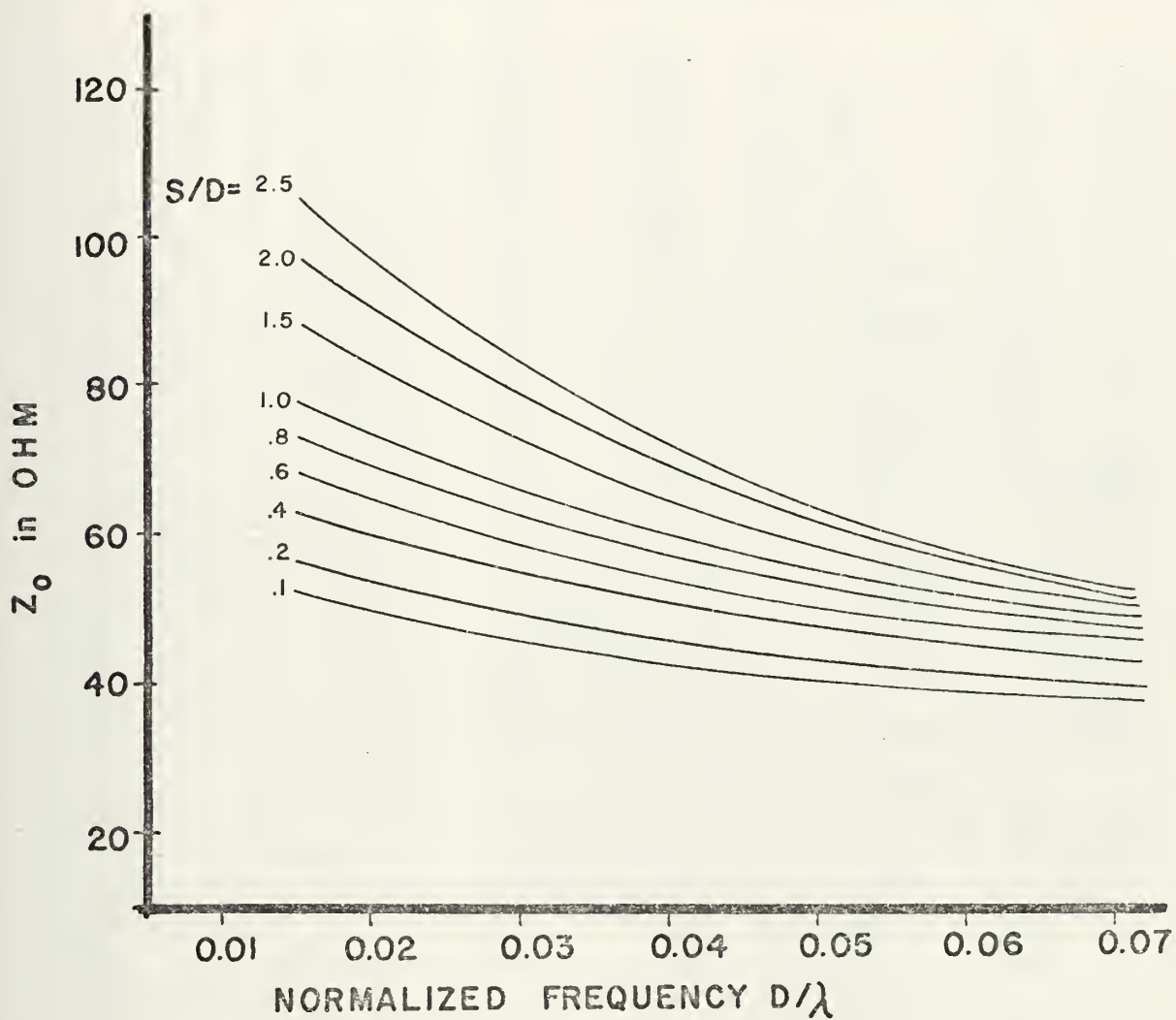


Figure L/6b Characteristic Impedance of Coplanar Strip Line with $W/D = 1.5$ and $\epsilon_r = 20$

APPENDIX M

Computer Program 'COPLAN'

```

.....
THIS PROGRAM COMPUTES THE WAVELENGTH RATIOS AND CHARACTERISTIC
IMPEDANCES OF VARIOUS OPEN BOUNDARY COPLANAR TRANSMISSION LINES
WITH A DIELECTRIC SUBSTRATE.
A PERTURBATION ANALYSIS OF THE PROPAGATION CONSTANT FOR SLOT CON-
FIGURATION IS INCLUDED FOR FERRITE SUBSTRATES WITH EQUAL PERMIT-
TIVITY. THE DIRECTION OF BIASING MAGNETIC FIELD IS IN THE PLANE OF
THE METAL AND PERPENDICULAR TO THE SLOT.
THE METHOD USED IN THESE COMPUTATIONS IS BASED UPON A SOLUTION TO
HELMHOLTZ'S EQUATION IN THE FOURIER TRANSFORM DOMAIN.
EXCEPT FOR FERRITE COMPUTATIONS ALL PARAMETERS ARE NORMALIZED WITH
RESPECT TO THE THICKNESS D OF THE SUBSTRATE WHERE IN THE FOLLOWING
NOTATION
  DL IS THE RATIO OF THICKNESS D OVER WAVELENGTH LAMBDA
  WD IS THE NORMALIZED SLOT (STRIP) WIDTH W/D
  SD IS THE NORMALIZED SEPARATION BETWEEN SLOTS (STRIPS)
      S/D

REQUIRED INPUT DATA :

FIRST CARD:  A DIGIT IN COLUMN 1 SPECIFIES THE CONFIGURATION
             VARIABLE ICON WHERE LINE PARAMETERS ARE COMPUTED FOR
             SINGLE SLOT LINES - 1
             COUPLED SLOT LINES - 2
             COPLANAR WAVEGUIDE - 3
             COPLANAR STRIPLINE - 4
             A SECOND DIGIT IN COLUMN 2 FOR THE VARIABLE IFER
             NOT EQUAL TO ZERO WILL COMPUTE THE CHANGES IN THE
             PROPAGATION CONSTANT FOR FERRITE SUBSTRATE (NOT
             APPLICABLE FOR COPLANAR STRIPLINE)
             INPUT FORMAT FOR COPLANAR ICON, IFER IN (211)

IF DIELECTRIC SUBSTRATE IS ASSUMED THE FOLLOWING 3 CARDS MUST BE
SUPPLIED (FOR FERRITE SEE BELOW)

SECOND CARD: THIS CARD SPECIFIES THE NUMBER OF POINTS TO BE
              COMPUTED. DIGITS MUST BE RIGHT JUSTIFIED.
              ID - NO. OF DIFFERENT VALUES FOR DL
              IW - NO. OF DIFFERENT VALUES FOR WD
              IS - NO. OF DIFFERENT VALUES FOR SD
              INPUT FORMAT ID,IW,IS IN (312)

THIRD CARD:  CONTAINS ACTUAL SIZE OF INCREMENTS FOR THE NORMAL-
              IZED QUANTITIES REFERRED TO ON CARD 2
              DELDL - INCREMENTS IN DL
              DELWD - INCREMENTS IN WD
              DELSD - INCREMENTS IN SD
              INPUT FORMAT DELDL,DELWD,DELS D IN (4F10.5)

```

CC

FOURTH CARD: SPECIFIES INITIAL VALUES FOR COMPUTATION AND THE PERMITTIVITY. INITIALS DL
 DLI - INITIALS WD
 WDI - INITIALS SD
 SDI - PERMITTIVITY
 EPSR - INPUT FORMAT DLI,WDI,SDI,EPSR IN (4F10.5)

IF A PERTURBATIONAL ANALYSIS FOR FERRITE SUBSTRATE IS DESIRED THE FOLLOWING 3 CARDS APPLY

SECOND CARD: SPECIFIES THE FOLLOWING PARAMETERS OF SUBSTRATE
 DDC - THICKNESS OF SUBSTRATE IN CENTIMETER
 WDI - WIDTH OVER THICKNESS RATIO
 SDI - SEPARATION OVER THICKNESS RATIO
 EPSR - PERMITTIVITY
 INPUT FORMAT DDC,WDI,SDI,EPSR IN (4F10.5)

THIRD CARD: SPECIFIES NUMBER OF POINTS, INCREMENT AND INITIAL VALUE OF FREQUENCY
 IFR - NO. OF POINTS OF FREQUENCY
 DELFR - SIZE OF INCREMENT IN GHZ
 STFR - INITIAL FREQUENCY IN GHZ
 INPUT FORMAT IFR,DEFR,STFR IN (12,F10,2F10.5)

FOURTH CARD: CONTAINS INFORMATION ABOUT BIASING MAGNETIC FIELD AND FERRITE MATERIAL CONSTANTS.
 DCHO - FIELD STRENGTH IN OERSTEDT
 DELH - LINEWIDTH OF FERRITE IN OERSTEDT
 MAGS - SATURATION MAGNETISATION IN GAUSS
 LANDEG - LANDE-G FACTOR OF FERRITE
 INPUT FORMAT DCHO,DELH,MAGS,LANDEG IN (4F10.2)

OUTPUT: THE OUTPUT CONSISTS OF AN ECHO-CHECK OF THE INPUT DATA
 COMPUTED LINE-PARAMETERS ARE PRINTED INTO A TABLE

ALL COMPUTATIONS ARE PERFORMED IN DOUBLE PRECISION

REQUIRED SUBROUTINES : A) GAUSSIAN QUADRATURE INTEGRATION ROUTINES
 USING THE FOLLOWING NUMBER OF POINTS -
 12,24,56,96,168,256,386 - (SUPPLIED WITH
 THIS PROGRAM)
 B) A SUBROUTINE WHICH COMPUTES THE ZERO
 ORDER BESSEL FUNCTION OF THE FIRST KIND
 C) SUBROUTINE 'COMBO', COMPUTES THE VARIOUS
 INTEGRANDS (SUPPLIED WITH THIS PROGRAM)

OCPL0490
 OCPL0500
 OCPL0510
 OCPL0520
 OCPL0530
 OCPL0540
 OCPL0550
 OCPL0560
 OCPL0570
 OCPL0580
 OCPL0590
 OCPL0600
 OCPL0610
 OCPL0620
 OCPL0630
 OCPL0640
 OCPL0650
 OCPL0660
 OCPL0670
 OCPL0680
 OCPL0690
 OCPL0700
 OCPL0710
 OCPL0720
 OCPL0730
 OCPL0740
 OCPL0750
 OCPL0760
 OCPL0770
 OCPL0780
 OCPL0790
 OCPL0800
 OCPL0810
 OCPL0820
 OCPL0830
 OCPL0840
 OCPL0850
 OCPL0860
 OCPL0870
 OCPL0880
 OCPL0890
 OCPL0900
 OCPL0910
 OCPL0920
 OCPL0930
 OCPL0940
 OCPL0950
 OCPL0960

CC


```

READ(5,1002) DL1,WDL,SDL,EPSP
IF(ICON.EQ.1) IS=1
IF(ICON.EQ.4) FLDI = ONE
WRITE(6,5100) ID,IW,IS,DELDL,DELWD,DELSO,DL1,WDL,SDL,EPSP
GO TO (11,12,13,14),ICON
11 WRITE(6,6100)
GO TO 30
12 WRITE(6,7100)
GO TO 30
13 WRITE(6,4100)
WRITE(6,9100)
WRITE(6,4200)
GO TO 30
14 WRITE(6,4100)
WRITE(6,8100)
WRITE(6,4200)
GC TO 30

```

C
C
C

INPUT DATA FOR FERRITE SUBSTRATE IS READ

```

20 READ(5,1002) DDC,WDL,SDL,EPSP
READ(5,1003) IFR,DELFR,STFR
READ(5,1004) DCHO,DELH,MAGS,LANDEG
STFR = STFR*1.D09
DELFR = DELFR*1.D09
DD = DDC*1.D-02
GO TO (21,22,23),ICON
21 WRITE(6,6500)
GO TO 24
22 WRITE(6,7500)
GO TO 24
23 WRITE(6,9500)
24 WRITE(6,2101)
WRITE(6,2102)
FREQ = STFR
DL1 = DD*STFR/CCL
DELDL = DD*DELFR/CCL
ID = IFR
DDC,WDL,SDL,EPSP,MAGS,DCHO,DELH,LANDEG

```

C
C
C

ITERATION FOR SD,WD, AND DL START

```

30 SD = SDL - DELSD
IF(ICON.EQ.2) ICC=2
DO 800 IIS=1,IS
SD = SD + DELSD
WD = WDL - DELWD
DO 700 IIW=1,IW

```

OCPL1450
OCPL1460
OCPL1470
OCPL1480
OCPL1490
OCPL1500
OCPL1510
OCPL1520
OCPL1530
OCPL1540
OCPL1550
OCPL1560
OCPL1570
OCPL1580
OCPL1590
OCPL1600
OCPL1610
OCPL1620
OCPL1630
OCPL1640
OCPL1650
OCPL1660
OCPL1670
OCPL1680
OCPL1690
OCPL1700
OCPL1710
OCPL1720
OCPL1730
OCPL1740
OCPL1750
OCPL1760
OCPL1770
OCPL1780
OCPL1790
OCPL1800
OCPL1810
OCPL1820
OCPL1830
OCPL1840
OCPL1850
OCPL1860
OCPL1870
OCPL1880
OCPL1890
OCPL1900
OCPL1910
OCPL1920


```

      = WD + DELWD
      = DL1 - DELDL
      DO 600 IID=1, ID
      A = -55.D0
      DL = DL + CELDL
      FREQ = FREQ + DELFR
      CHECK WHETHER SURFACE MODES START TO PROPAGATE
      DL CUT = DL*DSQRT(EPSR)
      IF(DLCUT.GT..25D0) GO TO 997
      WDH = WD*HALF
      IF(ICON.EQ.1) GO TO 41
      XO = (SD + WD)*HALF
      ESTIMATE NUMBER OF ZEROS OF INTEGRAND. IDENTIFIER IS ASSIGNED TO
      IGQ FOR A SELECTION OF PROPER GAUSSIAN-QUADRATURE INTEGRATION
      ROUTINE
      INULL = IDINT((SD + TWO*WD)*DABS(A)/TWOPI + TWO)
38 DO 40 IZ=1,7
      IEX = 8 - IZ
      ITP = 2**IEX
      IF(INULL.GT.ITP) GO TO 42
40 CONTINUE = 1
      IGQ = 1
      GO TO 43
41 INULL = IDINT(WD*DABS(A)/TWOPI + ONE)
42 IGC = IEX + 1
43 GMMUOD = 60.D0*TWOPI*SD
      OMEPRD = DL/60.D0
      EPSR*OMEPRD
      KIDS = GMMUOD*OMEPRD
      K2CS = GMMUOD*OMEPRD
      DLS = DL**2
      IN LOOP 200 ALL LINE PARAMETERS ARE COMPUTED FOR ONE SET OF
      DL, WD AND SD
      DO 200 IMODE=1, ICC
      A = -55.D0
      IDP = 0
      LLP1 = ONE
      LLP2 = DSQRT(EPSR)
      BISECTIONAL SEARCH LOOP FOR ZERO FOR DISPERSION CHARACTERISTIC

```



```

C C C POWER FLOW COMPUTATIONS FOR REGION 1,2 AND 3
C C C DO 150 INR=1,3
C C C HYPERBOLIC FUNCTIONS
C C C SW = ONE
C C C PHH = GAUSSQ(A,B)
C C C UPI = COMBO(B)
C C C TRIGONOMETRIC FUNCTIONS
C C C SW = -ONE
C C C CALL DGQ24(C,D,COMBO,PTH)
C C C LO2 = COMBO(C)
C C C PCWERTH(INR) = PHH + (UPI + LO2)*(C - B)*HALF
C C C PCWERTH(INR) = PTH
C C C 150 CONTINUE
C C C POWR1 = (POWERH(1) + POWER(1))/TWOPI
C C C POWR2 = (POWERH(2) + POWER(2))/TWOPI
C C C POWR3 = (POWERH(3) + POWER(3))/TWOPI
C C C PAVG = POWR1 + POWR2 + POWR3
C C C
C C C DEPENDING ON CONFIGURATION APPROPRIATE COMPUTATION OF
C C C CHARACTERISTIC IMPEDANCE
C C C
C C C GO TO (171,172,173,174),ICON
C C C 171 ZO(1) = HALF/PAVG
C C C GO TO 175
C C C 172 ZO(IMODE) = ONE/(PAVG*4.D0)
C C C GO TO 175
C C C 173 ZO(1) = ONE/(PAVG*8.D0)
C C C GO TO 175
C C C 174 ZO(1) = 8.D0*PAVG
C C C 175 LLC(IMODE) = ONE/LLP
C C C IF(IFER.EQ.0) GO TO 200
C C C
C C C COMPUTATION FOR MAGNETIC SUSCEPTIBILITY COMPONENTS
C C C
C C C CMG = TWOPI*FREQ
C C C GYRO = -1.4D06*LANDEG
C C C OMGR = -GYRO*MAGS*TWOPI
C C C OMGA = -PI*GYRO*DELH
C C C OMGO = -GYRO*DCCH0*TWOPI
C C C CMGY = OMGO + OMGM
C C C OMGZ = OMGO
C C C OMGRZ = DSQRT(OMGY*OMGZ)

```


210	WRITE(6,2104)	LLC(2),ZO(2),(AB(2,2,I),I=1,2),(AB(2,1,I),I=1,2)	OCPL3850
	WRITE(6,2105)	FREQSK,DL	OCPL3860
	WRITE(6,2106)	LLC(1),ZO(1),(AB(1,2,I),I=1,2),(AB(1,1,I),I=1,2)	OCPL3870
	WRITE(6,2107)		OCPL3880
	GO TO 600		OCPL3890
250	WRITE(6,2103)	FREQSK,DL,LLC(1),ZO(1),(AB(1,2,I),I=1,2), (AB(1,1,I),I=1,2)	OCPL3900
	GC TC 600		OCPL3920
300	GO TO (310,320,334,334),ICON		OCPL3930
310	WRITE(6,6300)	WD,EPSR,DL,LLC(1),ZO(1)	OCPL3940
	GO TO 600		OCPL3950
320	WRITE(6,7300)	WD,SD,EPSR,DL,LLC(2),ZO(2),LLC(1),ZO(1)	OCPL3960
	GO TO 600		OCPL3970
334	WRITE(6,8300)	WD,SD,EPSR,DL,LLC(1),ZO(1)	OCPL3980
600	CONTINUE		OCPL3990
700	CONTINUE		OCPL4000
800	CONTINUE		OCPL4010
	WRITE(6,9001)		OCPL4020
997	GO TO 999		OCPL4030
	WRITE(6,9970)		OCPL4040
998	GO TO 999		OCPL4050
	WRITE(6,9999)		OCPL4060
	WRITE(6,9001)		OCPL4070
999	STOP		OCPL4080


```

6300 FORMAT(' ',T11,' ',T14,F5.3,T21,' ',T24,F4.1,T31,' ',T34,F5.3,T41,OCPL4570
1,' ',T43,F6.4,T27,' ',T39,' ',T51,' ',T54,F5.3,T61,' ',T71,' ',T74,LP/L,T81,OCPL4580
6500 FORMAT(' ',T11,' ',T14,F5.3,T21,' ',T24,F4.1,T31,' ',T34,F5.3,T41,OCPL4590
7100 FORMAT(' ',T11,' ',T14,F5.3,T21,' ',T24,F4.1,T31,' ',T34,F5.3,T41,OCPL4600
1,T71,' ',T51,' ',T54,F5.3,T61,' ',T71,' ',T74,LP/L,T81,OCPL4610
2RATE,' ',T11,' ',T14,F5.3,T21,' ',T24,F4.1,T31,' ',T34,F5.3,T41,OCPL4620
3T11,' ',T15,' ',T18,' ',T21,' ',T24,F4.1,T31,' ',T34,F5.3,T41,OCPL4630
4,' ',T15,' ',T18,' ',T21,' ',T24,F4.1,T31,' ',T34,F5.3,T41,OCPL4640
5,D/L,T51,' ',T54,F5.3,T61,' ',T71,' ',T74,LP/L,T81,OCPL4650
6,' ',T85,' ',T11,' ',T14,F5.3,T21,' ',T24,F4.1,T31,' ',T34,F5.3,T41,OCPL4660
7300 FORMAT(' ',T11,' ',T14,F5.3,T21,' ',T24,F4.1,T31,' ',T34,F5.3,T41,OCPL4670
1,' ',T44,F5.3,T51,' ',T54,F5.3,T61,' ',T71,' ',T74,LP/L,T81,OCPL4680
2T81,' ',T11,' ',T14,F5.3,T21,' ',T24,F4.1,T31,' ',T34,F5.3,T41,OCPL4690
7500 FORMAT(' ',T11,' ',T14,F5.3,T21,' ',T24,F4.1,T31,' ',T34,F5.3,T41,OCPL4700
8100 FORMAT(' ',T11,' ',T14,F5.3,T21,' ',T24,F4.1,T31,' ',T34,F5.3,T41,OCPL4710
1AR STRIPS,' ',T11,' ',T14,F5.3,T21,' ',T24,F4.1,T31,' ',T34,F5.3,T41,OCPL4720
8300 FORMAT(' ',T11,' ',T14,F5.3,T21,' ',T24,F4.1,T31,' ',T34,F5.3,T41,OCPL4730
1,' ',T44,F5.3,T51,' ',T54,F5.3,T61,' ',T71,' ',T74,LP/L,T81,OCPL4740
9001 FORMAT(' ',T11,' ',T14,F5.3,T21,' ',T24,F4.1,T31,' ',T34,F5.3,T41,OCPL4750
9100 FORMAT(' ',T11,' ',T14,F5.3,T21,' ',T24,F4.1,T31,' ',T34,F5.3,T41,OCPL4760
1AR WAVEGUIDE,' ',T11,' ',T14,F5.3,T21,' ',T24,F4.1,T31,' ',T34,F5.3,T41,OCPL4770
9500 FORMAT(' ',T11,' ',T14,F5.3,T21,' ',T24,F4.1,T31,' ',T34,F5.3,T41,OCPL4780
9970 FORMAT(' ',T11,' ',T14,F5.3,T21,' ',T24,F4.1,T31,' ',T34,F5.3,T41,OCPL4790
1,COMPUTATION TERMINATED',T20,OCPL4800
9999 FORMAT(' ',INCORRECT INPUT DATA ',OCPL4810
ENDOCPL4820

```


TRI00010
TRI00020
TRI00030
TRI00040
TRI00050
TRI00060
TRI00070
TRI00080
TRI00090
TRI00100
TRI00110
TRI00120
TRI00130
TRI00140
TRI00150
TRI00160
TRI00170
TRI00180
TRI00190
TRI00200
TRI00210
TRI00220
TRI00230
TRI00240
TRI00250
TRI00260
TRI00270
TRI00280
TRI00290
TRI00300
TRI00310
TRI00320
TRI00330
TRI00340
TRI00350
TRI00360
TRI00370
TRI00380
TRI00390
TRI00400
TRI00410
TRI00420
TRI00430
TRI00440
TRI00450
TRI00460
TRI00470
TRI00480

```

FUNCTION COMBO(AD)
IMPLICIT REAL*8(A-H,K-Z)
DIMENSION T(400)
COMMON /FLOT/ BD,BDH,BK1,BK2,CH1,CH12,CH21,CH22,CH31,CH32,EP,SR,
1 KC1DS,KC2DS,OMEPGD,OMEPRD,OMMUOD,RKC21S,SW,WDH,XO
COMMON /INTG/ IAB,ICON,IDIR,IDP,IMODE,INR
DATA ETAOS/1.421223033756867D05/,HALF/.5D0/,ONE/1.D0/,TWO/2.D0/

ACCORDING TO LINE CONFIGURATION THE APPROPRIATE TRANSFORM OF
ELECTRIC FIELD OR CURRENT DENSITY IS COMPUTED

```

CCCC

```

11 CSF = BJO
12 GO TO (21,22),IMODE
21 CSF = BJO*DSIN(XO*AD)
22 GO TO 25
23 CSF = BJO*DCOS(XO*AD)
24 ADS = AD**2
25 GAM1DS = ADS - KC1DS
GAM2DS = ADS - KC2DS
GAM1D = DSQRT(GAM1DS)
GAM2D = DSQRT(DABS(GAM2DS))
RGAM21 = GAM2D/GAM1D
RGAM12 = GAM1D/GAM2D

```

```

IF GAMMA**2 IS GREATER THAN ZERO, HYPERBOLIC, ELSE TRIGONOMETRIC
FUNCTIONS, ARE COMPUTED

```

CCCC

```

30 ABG2 = DSIN(GAM2D)
ABG1 = DCOS(GAM2D)
TF1 = AD*BD/GAM1D
TF2 = ABG2/OMMUOD*(RKC21S-ONE)
TF3 = SW*RGAM12*RKC21S
TF4 = SW*TF2*(SIG2/EP,SR + COG2)
1 TG4 = -RKC21S*(SW*TF2*(SIG2/EP,SR - COG2)
1 TRNJ = -RKC21S*(SW*TF2*(SIG2/EP,SR - COG2)
TJ1 = ABG1/OMMUOD*(TG1 - SW*TF2*(SIG2/EP,SR - COG2) -
TJ2 = RGAM21*(TF1*COG2
TJ3 = -ABG1/OMMUOD*(TG2+ETAOS*TF1*(SIG2/EP,SR) -
TJ4 = SW*RGAM21*(TF2*COG2 + SIG2)
TJ5 = ONE/(TG1*TG4 + TG3*TG2)
TJ6 = TG4*TRNJ
TJ7 = -TG2*TRNJ
TJ8 = -TG3*TRNJ

```


TRI00490
TRI00500
TRI00510
TRI00520
TRI00530
TRI00540
TRI00550
TRI00560
TRI00570
TRI00580
TRI00590
TRI00600
TRI00610
TRI00620
TRI00630
TRI00640
TRI00650
TRI00660
TRI00670
TRI00680
TRI00690
TRI00700
TRI00710
TRI00720
TRI00730
TRI00740
TRI00750
TRI00760
TRI00770
TRI00780
TRI00790
TRI00800
TRI00810
TRI00820
TRI00830
TRI00840
TRI00850
TRI00860
TRI00870
TRI00880
TRI00890
TRI00900
TRI00910
TRI00920
TRI00930
TRI00940
TRI00950
TRI00960

```

TJ4      = TGI*TRNJ
TK1      = (TF2*TIJ1 + SW* ETAOS*TF1*TJ3)/EPSR
TK2      = (SW*TF2*TJ2 - ETAOS*TF1*TJ4)/EPSR
TK3      = TF1*TIJ1 + SW*TF2*TIJ3
TK4      = -SW*TF1*TIJ2 + TF2*TIJ4      GO TO 110
IF((ICON.NE.4).AND.(IDP.NE.0))
  TL1     = -((TK3*SIG2 + TJ3*COG2)
  TL2     = ONE - RKCPD*(SW*TK4*SIG2 + TJ4*COG2)
  TL3     = -ABG1/OMEPD*(TK3*SIG2 + TJ3*COG2) -
  TL4     = SW*EPSR*RGAM21*(TK1*COG2 + TJ1*SIG2) - ONE
  1 TL4   = ABG2/OMEPRD*(SW*TK4*SIG2 + TJ4*COG2 - ONE) -
  1       (TK2*COG2 + SW* TJ2*SIG2)
  TNM     = RKCPD*(TL1*TL4 + RGAM12*TL2*TL3/EPSR
  TM1     = -AD*BD*TL4/(KCIDS*TNM) + OMMUDD*GAM1D*TL3/(KCIDS*(
  1 TM2   = EPSR*RGAM21*(RKCPD*TL1*TL4 + TL2*TL3))
  1 TM2   = -ABG2*TL2/(OMEPRD*TNM) - ETAOS*RGAM12*TL1/(EPSR*(
  1       TL1*TL4 + RGAM12*TL2*TL3/(EPSR*RKC21S)))
  TM3     = -TL4/TNM
  TM4     = -KCIDS*TL2/(OMEPRD*GAM2D*TNM)
IF((ICON.EQ.4).AND.(IDP.EQ.1)) GO TO 100
IF((ICON.EQ.4)) GO TO 50
TINN     = ONE/(TM2*TM3 - TM1*TM4)
TN1      = TM4*TINN

COMBO    = TN1*CSF*CSF
RETURN

TRANSFORM OF DYADIC GREEN'S FUNCTION COMPONENT FOR SLOT
LINE CONFIGURATIONS (INCLUDED CPW)

COMBO    = TN1*CSF*CSF
RETURN

TRANSFORM OF DYADIC GREEN'S FUNCTION COMPONENT FOR COPLANAR STRIPS

50 COMBO  = TM4*CSF*CSF
RETURN

PRELIMINARY COMPUTATIONS FOR POWER DENSITY EVALUATION FOR
COPLANAR STRIPS

100 AE    = TM4*CSF/KCIDS
  AH      = TL1*RKC21S*CSF/(GAM2D*OMEPRD*TNM)
  BE      = TK1*AE - SW*TK2*AH
  BH      = TK3*AE + SW*TK4*AH
  CE      = TJ1*AE - TJ2*AH
  CH      = TJ3*AE + TJ4*AH
  AES     = AE*AE
GO TO 120

PRELIMINARY COMPUTATIONS FOR POWER OR PERTURBATION CALCULATIONS

```



```

C 110 AH = -CSF/(GAM1D*OMMUOD)
      BE = -SW*TK2*AH
      BH = SW*TK4*AH
      CE = -TJ2*AH
      CH = TJ4*AH
      BES2 = BE*BE
      BHS = BH*BH
      CES = CE*CE
      CHS = CH*CH
      IF(IDP.EQ.2) GO TO 300
      DE = RKC21S*CE
      DHS = RKC21S*CH
      AHS = AH*AH
      DSH = DE*DE
      DSH = DH*DH
      AGP2 = ADS - GAM2DS
      TGAM2D = GAM2D + GAM2D
      IF(SW.GT.0.00) GO TO 420
      SIG2H = DSIN(TGAM2D)*HALF
      COG21 = DCOS(TGAM2D) - ONE
      COG21H = COG21*HALF
      ADGD1 = (ADS + GAM1DS)/GAM1D
      ADGD2 = (ADS + GAM2DS)/GAM2D
      GO TO (210,220,230),INR
210 IF(ICON.EQ.4) GO TO 211

C TRANSFORM OF POWER DENSITY OF SLOT LINES IN REGION 1
C
C COMBO = BDH*OMMUOD*ADGD1*AH
C RETURN

C TRANSFORM OF POWER DENSITY OF COPLANAR STRIPS IN REGION 1
C
C211 COMBO = BDH*ADGD1*(OMEPOD*AES + OMMUOD*AH) + AD*BK1*AE*AH
C RETURN

C TRANSFORM OF POWER DENSITY IN REGION 2
C
C220 COMBO = BDH*(SIG2H*ADGD2*(OMEPRD*(CES + SW*BES2) +
1 OMMUOD*(CHS + SW*BHS)) +
2 AGP2*(OMEPRD*(-SW*BES2 + CES) +
3 OMMUOD*(-SW*BHS + CHS)) +
4 COG21*ADGD2*(OMEPRD*BE*CE + SW*OMMUOD*BH*CH) +
5 AD*BK2*(SIG2H*(BH*BE + CE*CH)
6 COG21H*(BH*BE + CE*CH))
C RETURN

```

```

TRI00970
TRI00980
TRI00990
TRI01000
TRI01010
TRI01020
TRI01030
TRI01040
TRI01050
TRI01060
TRI01070
TRI01080
TRI01090
TRI01100
TRI01110
TRI01120
TRI01130
TRI01140
TRI01150
TRI01160
TRI01170
TRI01180
TRI01190
TRI01200
TRI01210
TRI01220
TRI01230
TRI01240
TRI01250
TRI01260
TRI01270
TRI01280
TRI01290
TRI01300
TRI01310
TRI01320
TRI01330
TRI01340
TRI01350
TRI01360
TRI01370
TRI01380
TRI01390
TRI01400
TRI01410
TRI01420
TRI01430
TRI01440

```



```

C      TRANSFORM OF POWER DENSITY IN REGION 3
C
230  COMBO = BDH*AU6D1*(OMEPOD*DES+OMMUOD*DHS) + AD*BK1*DE*DH
      RETURN
300  SIGN = -ONE
C
C      PERTURBATIONAL EXPRESSION FOR PROPAGATION CONSTANT OF SLOT
C      LINE CONFIGURATIONS (CPW INCLUDED) IS COMPUTED
C
      IF(IDIR.EQ.2) SIGN = ONE
      C1 = BD*GAM2D
      C1S = C1**2
      D1 = SIGN*C1*BH*CH
      C2 = OMEPRD*AD
      C2S = C2**2
      C3 = OMEPRD*AD*BD*GAM2D
      D2 = TWO*KC2DS
      D3 = SIGN*TWO*C3
      D4 = KC2DS**2
      F1 = C1S*BHS + C2S*CES + D3*BH*CE
      F2 = D2*(D1 + C2*CE*CH)
      F3 = D4*CHS
      F4 = C1S*CHS + C2S*BES2 + D3*BE*CH
      F5 = D2*(D1 + SW*C2*BE*BH)*SW
      F6 = D4*BHS
      F7 = SW*C1S*BH*CH + SW*C2S*BE*CE +
1      SW*SIGN*C3*(BE*BH + CE*CH)
      F8 = KC2DS*(SIGN*C1*(BHS + SW*CHS) +
1      C2*(BH*CE + SW*BE*CH))
      F9 = D4*BH*CH
      ARGTR = TWO*GAM2D
      IF(SW.GT.0.D0) GO TO 440
      ST1 = DSIN(ARGTR)/(4.D0*GAM2D)
      ST1 = ST1 + HALF
      STM = HALF - ST1
      CTM = (ONE - DCOS(ARGTR))/ARGTR
340  IF(IAB.EQ.2) GO TO 350
      G1 = (CH12*F1 + CH22*F2 + CH32*F3)*STP
      G2 = (CH12*F4 + CH22*F5 + CH32*F6)*STM
      G3 = (CH12*F7 + CH22*F8 + CH32*F9)*CTM
C
C      PERTURBATION EXPRESSION FOR CHANGE IN ATTENUATION CONSTANT
C
      COMBO = G1 + G2 + G3
      RETURN
350  G4 = (CH11*F1 + CH21*F2 + CH31*F3)*STP
      G5 = (CH11*F4 + CH21*F5 + CH31*F6)*STM
      G6 = (CH11*F7 + CH21*F8 + CH31*F9)*CTM

```


C
C
C

```

PERTURBATION EXPRESSION FOR CHANGE IN PHASE CONSTANT

COMBO = G4 + G5 + G6
RETURN
400 SIG2 = DSINH(GAM2D)
COG2 = DCOSH(GAM2D)
GO TO 30
420 SIG2H = DSINH(TWO*GAM2D)*HALF
COG2H = DCOSH(TWO*GAM2D) - ONE
COG21H = COG21*HALF
GO TO 130
440 ST1 = DSINH(ARGTR)/(4.D0*GAM2D)
STP = ST1 + HALF
STM = ST1 - HALF
CTM = {DCOSH(ARGTR) - ONE}/ARGTR
GO TO 340
END

```

TRI01930
TRI01940
TRI01950
TRI01960
TRI01970
TRI01980
TRI01990
TRI02000
TRI02010
TRI02020
TRI02030
TRI02040
TRI02050
TRI02060
TRI02070
TRI02080
TRI02090
TRI02100


```

FUNCTION GAUSQ(A,B)
IMPLICIT REAL*8(A-H,K-Z)
COMMON /INTQ/IGQ
EXTERNAL COMBO

```

C
C
C
C
C

```

      DEPENDING ON IDENTIFIER FOR ZEROS OF INTEGRAND THE PROPER GUASSIAN-
      QUADRATURE INTEGRATION ROUTINE IS SELECTED AND INTEGRATION IS
      PERFORMED

```

```

      GO TO (20,20,30,40,50,60,70,80),IGQ
20  CALL DGQ12(A,B,COMBO,GAUSQ)
    RETURN
30  CALL DGQ24(A,B,COMBO,GAUSQ)
    RETURN
40  CALL DGQ56(A,B,COMBO,GAUSQ)
    RETURN
50  CALL DGQ96(A,B,COMBO,GAUSQ)
    RETURN
60  CALL DGQ168(A,B,COMBO,GAUSQ)
    RETURN
70  CALL DGQ256(A,B,COMBO,GAUSQ)
    RETURN
80  CALL DGQ384(A,B,COMBO,GAUSQ)
    RETURN
      END

```

```

GAUQ00010
GAUQ00020
GAUQ00030
GAUQ00040
GAUQ00050
GAUQ00060
GAUQ00070
GAUQ00080
GAUQ00090
GAUQ00100
GAUQ00110
GAUQ00120
GAUQ00130
GAUQ00140
GAUQ00150
GAUQ00160
GAUQ00170
GAUQ00180
GAUQ00190
GAUQ00200
GAUQ00210
GAUQ00220
GAUQ00230
GAUQ00240
GAUQ00250

```


APPENDIX N

Computer Program 'RESO'

```

.....
THIS PROGRAM PROVIDES A FREQUENCY DEPENDENT ANALYSIS OF SLOT CON-
FIGURATIONS ON A DIELECTRIC SUBSTRATE WITHIN A SHIELDED STRUCTURE.
THE COMPUTED DATA CONTAIN THE DISPERSION CHARACTERISTIC AND THE
CHARACTERISTIC IMPEDANCE OF A SINGLE SLOT TRANSMISSION LINE. FOR
RESONATOR CONFIGURATIONS THE LENGTH OF A HALF WAVE SLOT RESONATOR IS
COMPUTED. RESULTS ARE FURTHERMORE USED TO COMPUTE THE 'END-EFFECT'
OF A SIMPLE SHORT-CIRCUITED SLOT LINE. PARAMETERS FOR END COUPLED
SLOT LINES MAY BE EVALUATED TOO.
THE METHODS USED ARE BASED UPON A COMPLETE HYBRID MODE ANALYSIS IN
THE FOURIER TRANSFORM DOMAIN.
ALL PARAMETERS ARE NORMALIZED WITH RESPECT TO THE THICKNESS D OF
THE DIELECTRIC SUBSTRATE.
THE FOLLOWING NOMENCLATURE IS USED FOR INPUT VARIABLES AND OUTPUT
DATA:
DL - RATIO OF THICKNESS D OVER WAVELENGTH LAMBDA
WD - NORMALIZED WIDTH OF SLOT W/D
AD - NORMALIZED DISTANCE OF SIDEWALLS FROM CENTER OF SLOT
HD1 - NORMALIZED HEIGHT OF SIDEWALLS ABOVE METAL
HD2 - NORMALIZED HEIGHT OF SIDEWALLS ABOVE DIELECTRIC
LPL - WAVELENGTH RATIO LAMBDA-P/LAMBDA
ZO - CHARACTERISTIC IMPEDANCE
LD - NORMALIZED HALF WAVE RESONATOR LENGTH
TD - NORMALIZED SEPARATION BETWEEN TWO END COUPLED SLOT LINES
XSC - NORMALIZED SHORT CIRCUIT REACTANCE OF A SINGLE SLOT LINE
XS - NORMALIZED REACTANCE IN COUPLING REGION BETWEEN TWO END
      COUPLED LINES
MS - NORMALIZED MUTUAL REACTANCE IN COUPLING REGION

REQUIRED INPUT DATA:

FIRST CARD:  THE CHARACTER STRING 'INDC' IN COL. 1-4 PROVIDES AN
              ANALYSIS FOR END COUPLED SLOT LINES, ANY OTHER
              STRING(INCL. BLANKS) WILL OMIT THIS OPTION

SECOND CARD: SPECIFIES THE DIMENSIONS OF THE SHIELDING WALLS AND
              THE PERMITTIVITY
              INPUT FORMAT AD,HD1,HD2,EPSR IN (4F10.6)

THIRD CARD:  SPECIFIES THE NUMBER OF POINTS TO BE COMPUTED AND
              THE INCREMENTS BETWEEN THESE
              IDL - NO. OF DIFFERENT VALUES FOR DL
              IWD - NO. OF DIFFERENT VALUES FOR WD
              DELD - INCREMENT IN DL
              DELW - INCREMENT IN WD
              INPUT FORMAT IDL,IWD,DELD,DELW IN (2I1,8X,2F10.6)

```


FOURTH CARD: CONTAINS INITIAL VALUES FOR COMPUTATION
 DLI - INITIALS DL
 WDI - INITIALS WD
 INPUT FORMAT DLI,WDI IN (2F10.6)

IF THE END COUPLING IS TO BE ANALYSED A FIFTH CARD MUST BE PROVIDED WHICH CONTAINS DATA ABOUT THE SPACING BETWEEN THE SLOTS
 INTD - NO. OF DIFFERENT VALUES FOR TD
 TDI - INITIAL VALUE OF TD
 DELT - INCREMENT IN TD
 INPUT FORMAT INTD,TDI,DELT IN (I1,9X,2F10.6)

OUTPUT: THE OUTPUT CONSISTS OF THE DIMENSIONS OF THE SHIELDING STRUCTURE AND THE COMPUTED VALUES FOR THE VARIOUS PARAMETERS, THE LOWEST NORMALIZED CUT-OFF FREQUENCY OF THE RECTANGULAR WAVEGUIDE MODE IS ALSO PRINTED.

ALL COMPUTATIONS ARE PERFORMED IN DOUBLE PRECISION

REQUIRED SUBROUTINES: A) SUBROUTINE 'COMBC', COMPUTES THE VARIOUS COEFFICIENTS AND INTEGRANDS (SUPPLIED WITH THIS PROGRAM)

B) SUBROUTINE 'DET', COMPUTES THE CUT-OFF FREQUENCY OF RECTANGULAR WAVEGUIDE MODE (SUPPLIED WITH THIS PROGRAM)

C) A SUBROUTINE WHICH COMPUTES THE ZERO ORDER BESSEL FUNCTION OF THE FIRST KIND

D) GAUSSIAN-QUADRATURE INTEGRATION ROUTINES USING 12,24 AND 56 POINTS (SUPPLIED WITH THIS PROGRAM)

SPACE REQUIRED: 40K (NOT INCL. INTEG. AND BESSEL FUNCT. ROUTINES)

CAUTION: COMPUTATION IS TERMINATED IF THE OPERATING FREQUENCY IS ABOVE THE CUT-OFF FREQUENCY OF THE LOWEST ORDER WAVEGUIDE-MODE

EQUIPMENT CONFIGURATION: IBM/SYSTEM 360

LANGUAGE: FORTRAN

PROGRAMMER: LCDR K-D. KUCHLER, FEDERAL GERMAN NAVY

RES00490
 RES00500
 RES00510
 RES00520
 RES00530
 RES00540
 RES00550
 RES00560
 RES00570
 RES00580
 RES00590
 RES00600
 RES00610
 RES00620
 RES00630
 RES00640
 RES00650
 RES00660
 RES00670
 RES00680
 RES00690
 RES00700
 RES00710
 RES00720
 RES00730
 RES00740
 RES00750
 RES00760
 RES00770
 RES00780
 RES00790
 RES00800
 RES00810
 RES00820
 RES00830
 RES00840
 RES00850
 RES00860
 RES00870
 RES00880
 RES00890
 RES00900
 RES00910
 RES00920
 RES00930

CC

SUPERVISED BY PROF. DR. J. B. KNORR
 U.S. NAVAL POSTGRADUATE SCHOOL, MONTEREY, CALIFORNIA
 APRIL 1975

```

      IMPLICIT REAL*8(A-H,J-Z)
      DIMENSION LEO(2)
      INTEGER INDC/,INDC//
      COMMON AND,ANDS,HD1,HD2,KODS,K2DS,LD,LDH,OMEPOD,OMEPRD,OMMUOD,
1     SI,S2,S3,TD,WD,WDH,IDP,IMODE,IEO
      DATA ACC/.5D-.02/,ZERO/0.D0/,HALF/.5D0/,ONE/1.D0/,TWO/2.D0/,
1     PI/3.141592653589793/,TWOPI/6.2831853079586D0/,FLD1/1.D0/,
2     TWOPI3/3.947841760435743D01/,DELT/0.D0/,LOLI1/0.D0/,
3     UPLI3/9.D0/
      DATA IDL/1/,IWD/1/
      EXTERNAL COMBC
      WRITE(6,2000)
      READ(5,1010) ICC
      READ(5,1000) AD,HD1,HD2,EPSR
      WRITE(6,9001) AD,HD1,HD2,EPSR

```

THE CUT-OFF-FREQUENCY FOR THE LOWER WAVEGUIDE IS
 COMPUTED AND PRINTED

```

      PIAS = (PI/(TWO*AD))*2
      DL2 = ONE/(4.D0*AD)
      DDL = .1D0*DL2
      FRN = DET(DL2,PIAS,HD2,EPSR)
      DO 3 ID=1,9
      DDL = DL2 - DDL
      FRN = DET(DDL,PIAS,HD2,EPSR)
      IF(FR*FRN) 4,9,1
      DL2 = DDL
      CONTINUE
1     DO 8 IZZ=1,20
2     DL1 = (DDL + DL2)*HALF
3     IF(DABS(DLC - DL1).LT.5.D-05) GO TO 9
4     FLCL = DET(DLC,PIAS,HD2,EPSR)
5     IF(FDLC*FR) 6,9,5
6     DL2 = DLC
7     GO TO 8
8     DL1 = DLC
9     CONTINUE
      WRITE(6,8301) DLC

```

READ THE NUMBER OF ITERATIONS, STEP SIZE

RES00940
 RES00950
 RES00960
 RES00970
 RES00980
 RES00990
 RES01000
 RES01010
 RES01020
 RES01030
 RES01040
 RES01050
 RES01060
 RES01070
 RES01080
 RES01090
 RES01100
 RES01110
 RES01120
 RES01130
 RES01140
 RES01150
 RES01160
 RES01170
 RES01180
 RES01190
 RES01200
 RES01210
 RES01220
 RES01230
 RES01240
 RES01250
 RES01260
 RES01270
 RES01280
 RES01290
 RES01300
 RES01310
 RES01320
 RES01330
 RES01340
 RES01350
 RES01360
 RES01370
 RES01380
 RES01390
 RES01400
 RES01410


```

C      AND INITIAL VALUES
C      READ(5,1001) IDL,IWD,DELD,DELD
C      READ(5,1000) DLI,WDI
C      IF(ICC.EQ.INDC) READ(5,1011) INTD,TDI,DELT
C      WD = WDI - DELW
C      DO 950 I IW=1,IWD
C      WD = WD + DELW
C      WDH = WD*HALF
C      DLI = DLI - DELD
C      DO 900 IID=1,IDL
C      DL = DL + DELD
C      IF OPERATIONAL FREQUENCY LESS THAN CUTOFF-FREQUENCY
C      COMPUTATION TERMINATES
C
C      IF(DL*GE.DLC) GO TO 980
C      OMMUOD = 60.D0*TWOPI*DL
C      OMEPOD = DL/60.D0
C      OMEPRD = EPSR*OMEPOD
C      K2DS = OMEPOD*OMMUOD
C      LPL1 = OMEPRD*OMMUOD
C      LPL2 = DSQRT(TWO/(EPSR + ONE))
C      I MODE = 0
C      IDP = 1
C
C      ITERATION LOOP FOR DISPERSION CHARACTERISTIC
C
C      DC 100 IBD=1,30
C      LPL = (LPL1 + LPL2)*HALF
C      IF(OABS(LPL - LPL1).LT.5.D-04) GO TO 110
C      BD = TWOPI*DL/LPL
C      BDS = BD**2
C      SUM = ZERO
C      DO 30 II=1,20
C      IINN = II - 1
C      AND = DFLAT(IINN)*PI/AD
C      ANDS = AND**2
C      GAMIDS = ANDS + BDS - K2DS
C      GAM2DS = ANDS + BDS - K2DS
C      IF(GAM2DS.LT.ZERO) GO TO 10
C      GAMMA2**2 GREATER THAN ZERO
C      S1 = ONE
C      S2 = ONE
C      S3 = ONE
C      COEF = COMBC(BD)

```



```

C C C
GC TO 29
  GAMMA**2 LESS THAN ZERO
10 S1 = -ONE
   S2 = -ONE
   S3 = ONE
   COEF = COMBC(BD)
29 IF(II.EQ.1) COEF = COEF*HALF
   SUM = SUM + COEF
30 CONTINUE
   IF(FLDI*SUM) 31,110,32
31 LPL2 = LPL
   GO TO 100
32 LPL1 = LPL
100 CONTINUE

C C C
      COMPUTATION OF THE CHARACTERISTIC IMPEDANCE
110 CONTINUE
   IDP = 2
   SUM = ZERO
   BDS = TWOPI*DL/LPL
   KCIDS = BD**2
   KC2DS = KODS - BDS
   DC 130 II=1,19
   IINN = II - 1
   AND = DFLOAT(IINN)*PI/AD
   ANDS = AND**2
   GAMIDS = ANDS - KCIDS
   GAM2DS = ANDS - KC2DS
   IF(GAM2DS.LT.ZERO) GO TO 121
      GAMMA2**2 GREATER THAN ZERO
C C C
   S1 = ONE
   S2 = ONE
   S3 = ONE
   COEF = COMBC(BD)
   GO TO 129

C C C
      GAMMA2**2 LESS THAN ZERO
121 S1 = -ONE
   S2 = -ONE
   S3 = ONE
   COEF = COMBC(BD)

```

RES01900
RES01910
RES01920
RES01930
RES01940
RES01950
RES01960
RES01970
RES01980
RES01990
RES02000
RES02010
RES02020
RES02030
RES02040
RES02050
RES02060
RES02070
RES02080
RES02090
RES02100
RES02110
RES02120
RES02130
RES02140
RES02150
RES02160
RES02170
RES02180
RES02190
RES02200
RES02210
RES02220
RES02230
RES02240
RES02250
RES02260
RES02270
RES02280
RES02290
RES02300
RES02310
RES02320
RES02330
RES02340
RES02350
RES02360
RES02370


```

129 IF(II.EC.1) COEF = COEF*HALF
130 SUM = SUM + COEF
131 CCNTINUE = AD/SUM

```

CC

```

      ITERATION FOR THE RESONANCE STRUCTURES
      FIRST RESONANT LENGTH OF SINGLE SLOT IS COMPUTED
      IF DATA FOR END COUPLED RESONANT SLOTS REQUESTED
      ITERATIONS FOR THESE FOLLOW

```

```

150 IDP = 3
    ITD = 1
    IMCDE = 1
    GO TO 160
    IMODE = 2
    TD = TD1 - DELT
    ITD = INTD
    DO 760 IT=1,ITD
    TD = TD + DELT
170 DO 750 IEO=1,IMODE
    LD2 = HALF*LPL/DL
    LD1 = HALF*LD2
    DO 690 IRR=1,50
    LD = (LD1 + LD2)*HALF
    LDH = LD*HALF
    IF(DABS(LD2 - LD).LT.ACC) GO TO 695
    SUM = ZERO
    DO 500 II=1,24
    IINN = II - 1
    AND = DFLOAT(IINN)*PI/AD
    ANDS = AND**2
    AZD2S = K2DS - ANDS
    AZD1S = K0DS - ANDS
    IF(AZD2S.GT.ZERO) GO TO 221

```

CC

```

      GAMMA1**2 AND GAMMA2**2 ARE BOTH GREATER THAN ZERO

```

```

S1 = ONE
S2 = ONE
S3 = ONE
CALL DGC56(LOLI1,UPLI3,COMBC,COEF)
GO TO 490

```

CC

```

      GAMMA1**2 IS GREATER, GAMMA2**2 LESS THAN ZERO

```

```

221 IF(AZD1S.GT.ZERO) GO TO 222
    AZD2 = DSQRT(AZD2S)
    KAP = 0.01D0*AZD2

```

RES02380
RES02390
RES02400
RES02410
RES02420
RES02430
RES02440
RES02450
RES02460
RES02470
RES02480
RES02490
RES02500
RES02510
RES02520
RES02530
RES02540
RES02550
RES02560
RES02570
RES02580
RES02590
RES02600
RES02610
RES02620
RES02630
RES02640
RES02650
RES02660
RES02670
RES02680
RES02690
RES02700
RES02710
RES02720
RES02730
RES02740
RES02750
RES02760
RES02770
RES02780
RES02790
RES02800
RES02810
RES02820
RES02830
RES02840
RES02850


```

      UPLI1 = AZD2 - KAP
      LOLI2 = AZD2 + KAP
      S1 = -ONE
      S2 = -ONE
      S3 = ONE
      CALL DGG24(LOLI1,UPLI1,COMBC,AREA1)
      S1 = ONE
      S2 = ONE
      S3 = ONE
      CALL DGG56(LOLI2,UPLI3,COMBC,AREA2)
      COEF = AREA1 + AREA2
      GO TO 490
      GAMMA1**2 AND GAMMA2**2 ARE BOTH LESS THAN ZERO
222  AZD2 = DSQRT(AZD2S)
      AZD1 = DSQRT(AZD1S)
      KAP1 = 0.01D0*AZD1
      KAP2 = 0.01D0*AZD2
      UPLI1 = AZD1 - KAP1
      LOLI2 = AZD1 + KAP1
      UPLI2 = AZD2 - KAP2
      LOLI3 = AZD2 + KAP2
      S1 = -ONE
      S2 = ONE
      S3 = -ONE
      CALL DGG12(LOLI1,UPLI1,COMBC,AREA1)
      S1 = -ONE
      S2 = -ONE
      S3 = ONE
      CALL DGG24(LOLI2,UPLI2,COMBC,AREA2)
      S1 = ONE
      S2 = ONE
      S3 = ONE
      CALL DGG56(LOLI3,UPLI3,COMBC,AREA3)
      COEF = AREA1 + AREA2 + AREA3
      IF(II.EQ.1) COEF = COEF*HALF
      SUM = SUM + COEF
      CCNTINUE
      IF(SUM*FLD1) 610,695,620
      LD = LD
      GO TO 690
      LD1 = LD
      CCNTINUE
      IF(IMODE.EQ.2) GO TO 710
      COMPUTATION OF THE END EFFECT
C
C
C

```

```

RES02860
RES02870
RES02880
RES02890
RES02900
RES02910
RES02920
RES02930
RES02940
RES02950
RES02960
RES02970
RES02980
RES02990
RES03000
RES03010
RES03020
RES03030
RES03040
RES03050
RES03060
RES03070
RES03080
RES03090
RES03100
RES03110
RES03120
RES03130
RES03140
RES03150
RES03160
RES03170
RES03180
RES03190
RES03200
RES03210
RES03220
RES03230
RES03240
RES03250
RES03260
RES03270
RES03280
RES03290
RES03300
RES03310
RES03320
RES03330

```



```

LLP      = LD*DL/LPL
DLLP     = HALF*(HALF - LLP)
XSC      = DTAN(TWOPI*DLLP)
DATA FOR SINGLE SLOT LINE AND SINGLE RESONATOR IS
PRINTED
WRITE(6,9200) WD,DL,LPL,ZO,LD,XSC
IF(ICC.EQ.INDC) GO TO 150
GO TO 900
LEO(LEO) = LD
710 CONTINUE
750
COMPUTATION OF THE INDUCTIVE EFFECT ON END COUPLED
RESONATORS STARTS
TANE      = DTAN(TWOPI*LEO(2)*DL/LPL + DATAN(XSC))
TANO      = DTAN(TWOPI*LEO(1)*DL/LPL + DATAN(XSC))
XS        = -(TANE + TANO)*HALF
MS        = -(TANE - TANO)*HALF
DATA FOR END COUPLED SLOT RESONATORS IS PRINTED
WRITE(6,9250) TD,LEO(1),LEO(2),XS,MS
760 CONTINUE
900 CONTINUE
950 CONTINUE
GO TO 990
980 WRITE(6,9800)
990 STOP
1000 FCRMAT(4F10.6)
1001 FCRMAT(2I1,8X,2F10.6)
1010 FCRMAT(A4)
1011 FCRMAT(I1,9X,2F10.6)
2000 1//,T25,'ON A DIELECTRIC SUBSTRATE WITH SHIELDING WALLS',//,
8301 1//,T22,'THE NORMALIZED LOWEST CUT-OFF FREQUENCY D/LC=',
1F6.4/)
9001 FCRMAT(' ',T17,'DIMENSIONS: A/D=',F5.2,T44,'H1/D=',F5.2,T58,
1//,H2/D=',F5.2,T72,'EPSR=',F4.1//)
9200 1FCRMAT(' ',T11,'W/D=',F5.3,T24,'D/L=',F6.4,T38,'LP/L=',F6.4,T53,
1//,Z0=',F5.1,T65,'L/D=',F4.1,T77,'XSC=',F5.3)
9250 1FCRMAT(' ',T15,'T/D=',F5.3,T28,'L-ODD/D=',F4.1,T44,'L-EVEN/D=',
1//,F4.1,T61,'XS=',F5.3,T73,'MS=',F5.3)
9800 1FCRMAT(' ',T16,'X', '/4X',
1//,IN REGION 3
2000 1//,NORMALIZED CUTOFF-FREQUENCY
END

```

RES03340
RES03350
RES03360
RES03370
RES03380
RES03390
RES03400
RES03410
RES03420
RES03430
RES03440
RES03450
RES03460
RES03470
RES03480
RES03490
RES03500
RES03510
RES03520
RES03530
RES03540
RES03550
RES03560
RES03570
RES03580
RES03590
RES03600
RES03610
RES03620
RES03630
RES03640
RES03650
RES03660
RES03670
RES03680
RES03690
RES03700
RES03710
RES03720
RES03730
RES03740
RES03750
RES03760
RES03770
RES03780
RES03790
RES03800
RES03810


```

FUNCTION COMBC(AZD)
IMPLICIT REAL*8(A-H,J-Z)
DIMENSION T(200)
COMMON AND,ANDS,HD1,HD2,KODS,K2DS,LD,LDH,OMEPOD,OMEPRD,OMMUOD,
1 DATA PISQ/9.869600456298941D0/,ONE/1.D0/,TWC/2.D0/
AZDS = AZD*AZD
GAMIDS = ANDS + AZDS - KODS
GAM2DS = ANDS + AZDS - K2DS
GAMID = DSQRT(DABS(GAMIDS))
GAM2D = DSQRT(DABS(GAM2DS))
IF GAMMA1**2 LESS THAN ZERO TRIGONOM. FUNCT. APPLY

IF(S3.LT.0.D0) GO TO 300
SIG11 = DSINH(GAMID*HD1)
COG11 = DCOSH(GAMID*HD1)
SIG12 = DSINH(GAMID*HD2)
COG12 = DCOSH(GAMID*HD2)
IF GAMMA2**2 LESS THAN ZERO TRIGONOM. FUNCT. APPLY

IF(S2.LT.0.D0) GO TO 200
SIG2 = DSINH(GAM2D)
COG2 = DCOSH(GAM2D)
ANDZ = AND*AZD
OMG1 = OMMUOD*GAMID
OMEG1 = OMEPOD*GAMID
OMG2 = OMMUOD*GAM2D
OMERG2 = OMEPRD*GAM2D
FAC1 = KODS - AZDS
FAC2 = K2DS - AZDS
FAC3 = FAC2/FAC1
F1 = S3*FAC3/SIG12
F2 = FAC3/COG12
G1 = ANZ*(S3*F1*SIG12 - ONE)
G2 = S3*OMG1*F2*SIG12
G3 = S3*OMEG1*F1*COG12
G4 = -ANZ*(F2*COG12 - ONE)
RDETG = ONE/(G1*G4 + G2*G3)
H1 = OMERG2*G2*RDETG
H2 = S1*OMG2*G4*RDETG
H3 = S1*OMERG2*G1*RDETG
H4 = OMG2*G3*RDETG
J1 = -ANZ*(SIG2 + H1*COG2) + OMG2*H3*SIG2
J2 = -S1*OMG2*(COG2 + S1*H4*SIG2) - ANZ*H2*COG2
J3 = FAC2*(SIG2 + H1*COG2)
J4 = FAC2*H2*COG2

```


COM00970
COM00980
COM00990
COM01000
COM01010
COM01020
COM01030
COM01040
COM01050
COM01060
COM01070
COM01080
COM01090
COM01100
COM01110
COM01120
COM01130
COM01140
COM01150
COM01160
COM01170
COM01180
COM01190
COM01200
COM01210
COM01220
COM01230
COM01240
COM01250
COM01260
COM01270
COM01280
COM01290
COM01300
COM01310
COM01320
COM01330
COM01340
COM01350
COM01360
COM01370
COM01380
COM01390
COM01400
COM01410
COM01420

```

BE      = -S1*K2*AH
BH      = S1*K4*AH
CH      = S1*(H1*BE - H2*BH)
DE      = H3*BE + H4*BH
ES2     = F1*CE
BH      = F2*CH
CES     = BE**2
CHS     = CE**2
BCH     = CH**2
ADGD1   = .5D0*A2D
ADGD2   = ANDS + GAM1DS
AMG1    = ANDS - GAM1DS
AMG2    = ANDS - GAM2DS
BK1     = AZDS + KODS
PK2     = AZDS + K2DS
TGAM1D  = TWO*GAM1D
TGAM2D  = TWO*GAM2D
SH11    = DSINH(TGAM1D*HD1)/TGAM1D
SH12    = DSINH(TGAM1D*HD2)/TGAM1D

      IF GAMMA2**2 LESS THAN ZERO TRIGONOM. FUNCT. APPLY

      IF(S2.LT.0.D0) GO TO 600
      SH2 = DSINH(TGAM2D)/TGAM2D
      CCR = (DCOSH(TGAM2D) - ONE)/TGAM2D

      POWER DENSITY IN SPATIAL REGIONS 1 TO 3

550 P1   = OMMUOD*BDH*(ADGD1*AH*SH11 + HD1*AMG1*AH)*AH
      P2   = BDH*(SH2*ADGD2*(OMEPD*(CES + S1*BES2) +
1         OMMUOD*(CHS + S1*BHS)) +
2         AMG2*(OMEPD*(CES - S1*BES2) + OMMUOD*(CHS -
3         S1*BHS)) + TWO*CCR*ADGD2*(S1*OMEPD*BES2*CE +
4         OMMUOD*BH*CH) + AND*GAM2D*BK2*(SH2*(S1*BES2*CH
5         + BH*CE) + S1*CCR*(BE*BH + CE*CH))
      P3   = BDH*OMMUOD*(ADGD1*DE*SH12 + HD2*DE*AMG1)*DE +
1         BDH*OMEPD*(ADGD1*DE*SH12 - HD2*DE*AMG1)*DE +
2         AND*GAM1D*DE*BK1*SH12*DH
      CCMBC = P1 + P2 + P3
      RETURN
600 SH2  = DSIN(TGAM2D)/TGAM2D
      CCR = (ONE - DCOS(TGAM2D))/TGAM2D
      GO TO 550
      END

```


DET000010
 DET000020
 DET000030
 DET000040
 DET000050
 DET000060
 DET000070
 DET000080
 DET000090
 DET000100

```

FUNCTION DET(DL,PIAS,HD,EPSR)
  IMPLICIT REAL*8(A-H,K-Z)
  DATA PI/3.141592653589793/
  KODS = (2.00*PI*DL)**2
  K2DS = KODS*EPSR
  KX1D = DSQRT(DABS(K2DS - PIAS))
  KX2D = DSQRT(DABS(KODS - PIAS))
  DET = KX1D*DTAN(KX1D)/EPSR - KX2D*DTAN(KX2D*HD)
  RETURN
END
  
```


LIST OF REFERENCES

1. M. Arditi, "Characteristics and Applications of Microstrip for Microwave Wiring", IRE. Trans. Microwave Theory Techn., vol. MTT-3, pp. 31-56, March 1955.
2. L. Young and H. Sobol, Advances in Microwaves, Academic Press, New York, 1974.
3. S. B. Cohn, "Slot Line on a Dielectric Substrate", IEEE Trans. Microwave Theory Techn., vol. MTT-17, pp. 768-778, Oct. 1969.
4. C. P. Wen, "Coplanar Waveguide: A Surface Strip Transmission Line Suitable for Nonreciprocal Gyromagnetic Device Applications", IEEE Trans. Microwave Theory Techn., vol. MTT-17, pp. 1087-1090, Dec. 1969.
5. J. B. Knorr, "Slot Line Transitions", IEEE Trans. Microwave Theory Techn., vol. MTT-22, pp. 548-554, May 1974.
6. T. Itoh and R. Mittra, "Spectral Domain Approach for Calculating the Dispersion Characteristics of Microstrip Lines", IEEE Trans. Microwave Theory Techn., vol. MTT-21, pp. 496-499, July 1973.
7. M.E. Davis, E.W. Williams and A.C. Celestini, "Finite Boundary Corrections to the Coplanar Waveguide Analysis", IEEE Trans. Microwave Theory Techn., vol. MTT-21, pp. 594-596, Sept. 1973.
8. T. Itoh and R. Mittra, "Dispersion Characteristics of Slot Lines", Electron. Lett., vol. 7, pp. 364-365, July 1971.
9. D. S. Jones, The Theory of Electromagnetism, Pergamon Press, 1964.
10. A. E. Luna, "Parallel Coplanar Strips on a Dielectric Substrate", Eng. Thesis, Naval Postgraduate School, Monterey, Calif., 1973.
11. T. Kitasawa, Y. Tujiki, Y. Hayashi and M. Suzuki, "Slot Line on a Magnetized Ferrite Substrate", Electronics and Communications in Japan, vol. 56-B, No. 3, 1973.
12. E. A. Mariani, C.P. Heinsman, J.P. Agrios and S.B. Cohn, "Slot Line Characteristics", IEEE Trans. Microwave Theory Techn. (1969 Symposium Issue), vol. MTT-17, pp. 1091-1096, Dec. 1969.

13. R.W. Collin, Field Theory of Guided Waves, McGraw-Hill Book Company, Inc., 1960.
14. S.S. Attwood, "Surface-Wave Propagation Over a Coated Plane Conductor", J. Appl. Phys., Vol. 22, pp. 504-509, April 1954.
15. J.W. Dettman, Mathematical Methods in Physics and Engineering, McGraw-Hill Book Company, Inc., 1969.
16. R.F. Harrington, Field Computations by Moment Methods, The Macmillan Company, 1968.
17. Oberhettinger, Tabellen zur Fourier Transformation, Springer-Verlag, Berlin, 1957.
18. L. Young, Parallel Coupled Lines and Directional Couplers, Artech House, Inc. 1972.
19. J. Helszajn, Principles of Microwave Ferrite Engineering, John Wiley & Sons Ltd, 1969.
20. W. H. von Aulock and C.E. Fay, Linear Ferrite Devices for Microwave Applications, Academic Press, 1968.
21. R.F. Harrington, Time Harmonic Fields, McGraw-Hill Book Company, Inc., 1961.
22. R.A. Waldron, Ferrites, D. van Nostrand Co. Ltd., 1961.
23. E.A. Mariani and J.P. Agrios, "Slot Line Filters and Couplers", IEEE Trans. Microwave Theory Techn., Vol. MTT-18, pp. 1089-1095, Dec. 1970.
24. J.B. Knorr and J. Saenz, "End Effect in a Shorted Slot", IEEE Trans. Microwave Theory Techn., Vol. MTT-21, pp. 579-580, Sept. 1973.
25. T.N. Sneddon, The Use of Integral Transforms, McGraw-Hill Book Company, 1972.
26. B.M. Oliver, "Directional Electromagnetic Couplers", Proc. IRE, Vol. 42, pp. 1686-1692, Nov. 1954.
27. G.I. Zysman and A.K. Johnson, "Coupled Transmission Line Networks in an Inhomogeneous Dielectric Medium", IEEE Trans. Microwave Theory Techn., vol. MTT-17, pp. 753-759, Oct. 1969.
28. R. Zurmühl, Matrizen, Springer-Verlag, 1961.

29. E.M.T. Jones and J.T. Bolljahn, "Coupled-Strip-Transmission-Line Filters and Directional Couplers", IRE Trans. Microwave Theory Techn., vol. MTT-4, pp. 75-81, April 1956.
30. J.E. Dalley, "A Strip-Line Directional Coupler Utilizing a Non-Homogeneous Dielectric Medium", IEEE Trans. Microwave Theory Techn., vol. MTT-17, pp. 706-712, Sept. 1969.
31. The IMSL Library, International Mathematical and Statistical Libraries, Inc., 1974.
32. B. Carnahan, H.A. Luther and J.O. Wilkes, Applied Numerical Methods, John Wiley and Sons, Inc., 1969.

INITIAL DISTRIBUTION LIST

	Copies
1. Defense Documentation Center Cameron Station Alexandria, Virginia 22314	2
2. Library, Code 0212 Naval Postgraduate School Monterey, California 93940	2
3. Department Chairman, Code 52 Department of Electrical Engineering Naval Postgraduate School Monterey, California 93940	1
4. Department Chairman, Code 53 Department of Mathematics Naval Postgraduate School Monterey, California 93940	1
5. Assoc. Professor R.W. Adler, Code 52Ab Department of Electrical Engineering Naval Postgraduate School Monterey, California 93940	1
6. Assoc. Professor J.B. Knorr, Code 52Ko Department of Electrical Engineering Naval Postgraduate School Monterey, California 93940	1
7. Marineamt -Al- 294 Wilhelmshaven Federal Republic of Germany	1
8. Dokumentationszentrale der Bundeswehr (See) 53 Bonn Friedrich-Ebert-Allee 34 Federal Republic of Germany	1
9. LCDR K-D Kuchler, FGN Marine Flieger Geschwader 3, Elowa-Staffel 2851 Nordholz Federal Republic of Germany	2



14OCT75
29DEC75

23796
23593

Thesis 161196
K8763 Kuchler
c.1 Hybrid mode analysis
of coplanar transmission
lines.

14OCT75

23796

Thesis 161196
K8763 Kuchler
c.1 Hybrid mode analysis
of coplanar transmission
lines.

thesK8763

Hybrid mode analysis of coplanar transmi



3 2768 001 03006 7
DUDLEY KNOX LIBRARY